



HAL
open science

New syntheses of N-heterocyclic carbene-stabilized gold nanoparticles

Laura Hippolyte

► **To cite this version:**

Laura Hippolyte. New syntheses of N-heterocyclic carbene-stabilized gold nanoparticles. Material chemistry. Sorbonne Université, 2018. English. NNT : 2018SORUS148 . tel-03029247

HAL Id: tel-03029247

<https://theses.hal.science/tel-03029247v1>

Submitted on 28 Nov 2020

HAL is a multi-disciplinary open access archive for the deposit and dissemination of scientific research documents, whether they are published or not. The documents may come from teaching and research institutions in France or abroad, or from public or private research centers.

L'archive ouverte pluridisciplinaire **HAL**, est destinée au dépôt et à la diffusion de documents scientifiques de niveau recherche, publiés ou non, émanant des établissements d'enseignement et de recherche français ou étrangers, des laboratoires publics ou privés.



Thèse

Pour l'obtention du grade de

Docteur de Sorbonne Université

Spécialité : Chimie des Matériaux

Ecole Doctorale: ED 397

New syntheses of N-heterocyclic carbene-stabilized gold nanoparticles

Présentée par : **Laura HIPPOLYTE**

Soutenance prévue le 26 novembre 2018 devant un jury composé de :

Mme Mona TREGUER-DELAPIERRE	Professeur	Rapporteur
M. Stéphane BELLEMIN-LAPONNAZ	Directeur de Recherche	Rapporteur
Mme Souhir BOUJDAY	Professeur	Examineur
M. Bruno CHAUDRET	Directeur de Recherche	Examineur
M. François RIBOT	Directeur de Recherche	Directeur de thèse
M. Louis FENSTERBANK	Professeur	Co-directeur de thèse

Acknowledgments

First, I would like to sincerely thank Prof. Mona Treguer-Delapierre, Dr. Stéphane Bellemin-Laponnaz, Prof. Souhir Boudjay and Dr. Bruno Chaudret for accepting to review my thesis and be part of my Jury.

I would also like to thank Dr. Florence Babonneau and Dr. Corinne Aubert for allowing me to work within the Laboratoire de Chimie de la Matière Condensée de Paris and the Institut Parisien de Chimie Moléculaire these past three years.

I would like to thank my supervisors Dr. François Ribot and Prof. Louis Fensterbank, as well as Prof. Corinne Chanéac, Prof. Marine Desage-El Murr and Dr. David Portehault, for their good humour, their patience and their scientific guidance.

I would like to thank next all the people who collaborated with me on this project: Denis Lesage for the MS analyses, Dr. Yves Gimbert for the theoretical calculations, Dr. Sébastien Blanchard for the EPR measurements, and Dr. Xavier Frogneux for the experiments on copper. A special thank goes to Dr. Dimitri Mercier for the thorough XPS analyses which brought us many answers (as well as many questions) and his patience when explaining the results.

A big thank you goes to Dr. Nathalie Bridonneau who carried out most of the experiments on the synthesis of gold nanoparticles from imidazolium and triazolium salts and has helped me tremendously for the first two years of this project.

I would also like to thank Alexandre Porcheron for agreeing to continue this work for the next three years and wish him luck on this journey.

Finally, I would like to thank all the members of the LCMCP and the IPCM (especially the MACO team) whom I have worked with over the years as they have been nothing but warm and welcoming.

Abbreviations

9-BBN	9-borabicyclo[3.3.1]nonane
AcOEt	Ethyl acetate
AuNP	Gold nanoparticle
BDE	Bond dissociation energy
BE	Binding energy
Boc	<i>tert</i> -butoxycarbonyl
CAAC	Cyclic alkyl amino carbene
CTAB	Cetyltrimethylammonium bromide
DCM	Dichloromethane
DDS	Dodecylsulfide
DDT	Dodecanethiol
DFT	Density functional theory
Dipp	2,6-diisopropylphenyl
DMAP	4-dimethylaminopyridine
DMF	N,N-Dimethylformamide
DMSO	Dimethyl sulfoxide
DTPB	Ditertbutyl peroxide
EPR	Electron paramagnetic resonance
eq	Equivalent
ESI	Electrospray ionization
Et ₂ O	Diethyl ether
EtOH	Ethanol
HRMS	High resolution mass spectrometry
Imd	Imidazol-2-ylidene
IR	Infrared
KHMDS	Potassium bis(trimethylsilyl)amide
LB	Lewis base
LSPR	Localized surface plasmon resonance
MeCN	Acetonitrile
Mes	Mesityl
MIC	Mesoionic carbene
MNP	Metallic nanoparticle

MS	Mass spectrometry
NaHMDS	Sodium bis(trimethylsilyl)amide
NHC	N-heterocyclic carbene
NHO	N-heterocyclic olefin
NMR	Nuclear magnetic resonance
NP	Nanoparticle
OTs	p-toluenesulfonate
PEG	Polyethylene glycol
SAM	Self-assembled monolayer
TEG	Triethylene glycol
TEM	Transmission electron microscopy
TEMPO	(2,2,6,6-Tetramethylpiperidin-1-yl)oxyl
OTf	Trifluoromethane sulfonate
TGA	Thermogravimetric analysis
THF	Tetrahydrofuran
THIBO	Tetrahydroimidazobisoxazol
TS	Transition state
UV	Ultra-violet
UV-vis	UV-visible
XPS	X-ray photoelectron spectroscopy

Table of contents

Acknowledgments	3
Abbreviations	5
Table of contents	7
INTRODUCTION	11
Bibliography (Introduction)	13
CHAPTER I: STATE OF THE ART ON NHC-STABILIZED GOLD NANOPARTICLES	15
I.A. Gold nanoparticles	15
I.B. N-heterocyclic carbenes	18
I.C. Gold nanoparticles stabilized by N-heterocyclic carbenes	20
I.C.1. Ligand exchange	21
I.C.2. NHC-gold complex reduction	28
I.C.3. Imidazolium gold complex reduction	33
I.D. Conclusion	36
Bibliography (Chapter I)	37
CHAPTER II: SYNTHESIS OF N-HETEROCYCLIC CARBENE-CAPPED GOLD NANOPARTICLES FROM IMIDAZOLIUM SALTS	43
II.A. Nanoparticles from imidazolium haloaurate salts and NaBH ₄	43
II.A.1. Imidazolium haloaurate salts	43
II.A.1.a. Synthesis	43
II.A.1.b. Crystallographic analysis	44
II.A.2. Nanoparticles synthesis	46
II.A.2.a. Synthesis with NaH	46
II.A.2.a.i. Effect of the ligand	46
II.A.2.a.ii. Effect of the ligand to gold ratio	47
II.A.2.b. Synthesis without NaH	48
II.A.2.b.i. Effect of the ligand	48
II.A.2.b.ii. Effect of the ligand to gold ratio	49
II.A.3. Surface analysis	50
II.A.3.a. MS analysis	51
II.A.3.b. NMR analysis	52
II.A.3.b.i. Liquid state NMR	52
II.A.3.b.ii. Solid state NMR	52
II.A.3.c. IR analysis	53

II.A.3.d. XPS analysis	54
II.B. Nanoparticles from imidazolium haloaurate salts and tBuNH ₂ BH ₃	57
II.B.1. Synthesis of the nanoparticles.....	57
II.B.2. XPS analysis	59
II.C. Nanoparticles from AuCl and unfunctionalized imidazolium salts	60
II.C.1. Using NaBH ₄ as a reducing agent.....	60
II.C.2. Using tBuNH ₂ BH ₃ as a reducing agent.....	62
II.D. Nanoparticle synthesis from functionalized imidazoliums	63
II.D.1. Water-soluble imidazolium	63
II.D.2. Azide functionalized imidazolium.....	66
II.D.3. C2-functionalized imidazoliums	68
III.D.3.a. 2-methylimidazolium	69
II.D.3.b. 2-phenyl imidazolium.....	73
II.D.3.c. C2 functionalized imidazoliums and tBuNH ₂ BH ₃ as a reducing agent	74
II.E. Conclusion	76
Bibliography (Chapter II)	77
CHAPTER III: SYNTHESIS OF N-HETEROCYCLIC CARBENE-CAPPED GOLD NANOPARTICLES FROM NHC-BORANES.....	79
III.A. Bibliographic introduction on N-heterocyclic carbene boranes	79
III.A.1. Synthesis of NHC-boranes	79
III.A.2. Uses of NHC-boranes in molecular chemistry	81
III.A.2.a. Heterolytic rupture.....	81
III.A.2.b. Homolytic rupture.....	83
III.A.3. Uses of NHC-boranes beyond molecular chemistry	84
III.B. NHC-BH ₃ synthesis.....	88
III.C. Nanoparticles synthesis from gold precursor: AuClPPh ₃	88
III.C.1. First attempts	88
III.C.2. Solvent screening	92
III.D. Nanoparticles synthesis from gold precursor HAuCl ₄ .3H ₂ O	94
III.E. Nanoparticles synthesis from gold precursor AuClSMe ₂	96
III.E.1. Reaction conditions effect	97
III.E.1.a. Solvent	97
III.E.1.b. Water.....	97
III.E.1.c. Ligand to gold ratio	98
III.E.1.d. Concentration	99
III.E.1.e. Stirring	100

III.E.1.f. Temperature.....	101
III.E.2. Surface characterization	102
III.E.2.a. MS.....	103
III.E.2.b. NMR.....	103
III.E.2.c. XPS	104
III.E.3. Mechanistic study.....	106
III.E.3.a. NMR.....	106
III.E.3.c. Theoretical chemistry	109
III.E.3.c.i. Hydride transfer	110
III.E.3.c.ii. Radical mechanism.....	111
III.E.3.d. EPR.....	113
III.E.3.e. Discussion	115
III.E.4. Reproducibility issues	116
III.E.4.a. Silica.....	117
III.E.4.b. Byproduct from the NHC-BH ₃ synthesis.....	117
III.E.4.c. Byproduct from the imidazolium synthesis.....	118
III.E.5.d. Dimer	119
III.F. Conclusion	120
Bibliography (Chapter III)	121
CHAPTER IV: SYNTHESIS OF MESOIONIC CARBENE-CAPPED GOLD NANOPARTICLES FROM TRIAZOLIUM SALTS AND MIC-BH ₃	125
IV.A Mesoionic carbenes in the literature	125
IV.B. Gold nanoparticles stabilized by MICs from triazolium salts	126
IV.B.1. Synthesis of the triazolium salts precursors	126
IV.B.2. Gold nanoparticle synthesis from triazolium salts	129
IV.B.3. XPS analysis	131
IV.C. Gold nanoparticles stabilized by MICs from MIC-BH ₃	133
IV.C.1. MIC-BH ₃ in the literature.....	133
IV.C.2. Synthesis of MIC-BH ₃	134
IV.C.3. Gold nanoparticle synthesis using AuClSMe ₂ as a precursor	135
IV.C.4. Gold nanoparticle synthesis using HAuCl ₄ .3H ₂ O as a precursor	139
IV.C.5. XPS analysis	140
IV.D. Conclusion	141
Bibliography (Chapter IV)	143
CONCLUSION AND PERSPECTIVES	145
Experimental Section	153

INTRODUCTION

Nanoparticles represent one of the main axes of the development of nanosciences and nanotechnologies. The high surface-to-volume ratio and the peculiar properties that matter can exhibit when in such a fine division state represent the principal motivations of the academic and industrial interests for nanoparticles. Gold nanoparticles, with their localized surface plasmon resonance,¹ which is responsible for the ruby-red color of their suspension, are no exception and many potential applications in optics and imaging, catalysis as well as medicine have been, and are still, explored.^{2,3} Since the Turkevich's method of the mid-20th century,⁴ a multitude of protocols have been described in the literature to synthesize gold nanoparticles. They are quite generally based on three main ingredients: a gold precursor, such as HAuCl₄ or AuClPPH₃, a reducing agent, and a surface ligand, which stabilizes the nanoparticles, avoid their aggregation and make them compatible with the dispersion medium. By varying the reaction conditions and the capping ligands, precise control over the morphology, stability and properties of the nanoparticles can be achieved. Numerous ligands can be used to stabilize gold nanoparticles, for example, amines⁵, phosphines⁶ and citrates,⁴ among others. The most widely used ligands however remain thiols, which are known to form a strong bond with gold⁷ and confer a good stability to the nanoparticles. That is why they have traditionally been the ligand of choice in many studies and applications. Nevertheless, thiol-stabilized nanoparticles tend to be unstable in harsh and/or biological conditions, which can be potentially harmful for certain applications.^{8,9} Therefore, there is a need for new families of ligands, that would bound strongly to gold surface atoms, and for developing new efficient syntheses to access nanoparticles with such new ligands.

N-heterocyclic carbenes (NHCs) are a relatively new class of molecules. Indeed, the first NHCs were isolated in the early 1990's.¹⁰ They are neutral compounds, which contain a divalent carbon atom with a six-electrons valence shell. While generally very reactive when free, they can form stable complexes with various metals. They have been well studied in molecular chemistry. Indeed their complexes with metals can present catalytic activity¹¹ or medicinal properties¹² depending on the metal and NHC structure. In the past decade, NHCs have been increasingly used as versatile surface ligands in materials chemistry.¹³ Indeed, the first synthesis of NHC-stabilized gold nanoparticles dates back to 2009.¹⁴ Since then several other reports on NHC-stabilized metallic nanoparticles have been published,¹⁵⁻¹⁹ some of them showing the very good stability of such nanoparticles in harsh and /or biologically relevant conditions.²⁰⁻²² Several studies of NHC self-assembled monolayers on gold have also been carried out,

providing useful information on their bonding strength to metal and their superior stability compared to thiols.^{23,24}

As Lewis bases, NHCs are also able to form stable adducts with boranes (Lewis acids). Such NHC-boranes are generally air and moisture stable compounds, the reducing properties of which have already been reported in the literature.²⁵ Despite the absence of any previous report in the literature, the possibility to use them as dual reagents, able to reduce the metallic precursor and provide, at the same time, the NHC ligands, sounds very appealing for the development of a new synthesis of NHC-stabilized gold nanoparticles.

In this PhD work, the focus was on the development of new syntheses of NHC-stabilized gold nanoparticles, notably using NHC-BH₃ as innovative “2-in-1” reagents. Throughout this study, special care was taken to thoroughly characterize the obtained nanoparticles and confirm the presence of NHCs at their surface as stabilizing agent.

This manuscript is divided in four main chapters. The first one gives a quick general overview on gold nanoparticles and NHCs, before focusing on the syntheses of NHC-stabilized gold nanoparticles described in the literature. The second chapter describes the synthesis of NHC-stabilized gold nanoparticles from imidazolium salts and various gold precursors. The possibility to tune the size of the particles through the experimental conditions is also presented. The surface characterization, in particular by XPS, of the so-obtained nanoparticles is reported in details. The third chapter, starts with a quick overview of NHC-boranes in the literature, and then reports on the synthesis of NHC-stabilized gold nanoparticles from NHC-boranes. The surface characterization, mainly by XPS, of the particles prepared with this totally new route is reported and a preliminary discussion of its possible mechanism is given. The fourth and final chapter focuses on the synthesis of gold nanoparticles stabilized by another type of NHCs, known as mesoionic carbenes (MICs). These ligands, which derive from easily prepared 1,2,3-triazolium salts, have never been used in surface chemistry. The explored synthetic routes are then presented. They use either triazolium salts and an external reducing agent or “2-in-1” MIC-boranes. The surface characterization of these various MIC-stabilized gold nanoparticles is finally presented. This manuscript ends with some conclusions on the work performed and several perspectives based on preliminary results which explore the extension of the present work to other metals.

Bibliography (Introduction)

- (1) Louis, C.; Pluchery, O. *Gold Nanoparticles for Physics, Chemistry and Biology*, 2nd ed.; WORLD SCIENTIFIC (EUROPE), 2017.
- (2) Dreaden, E. C.; Alkilany, A. M.; Huang, X.; Murphy, C. J.; El-Sayed, M. A. The Golden Age: Gold Nanoparticles for Biomedicine. *Chem Soc Rev* **2012**, *41* (7), 2740–2779.
- (3) Daniel, M.-C.; Astruc, D. Gold Nanoparticles: Assembly, Supramolecular Chemistry, Quantum-Size-Related Properties, and Applications toward Biology, Catalysis, and Nanotechnology. *Chem. Rev.* **2004**, *104* (1), 293–346.
- (4) Turkevich, J.; Stevenson, P. C.; Hillier, J. A Study of the Nucleation and Growth Processes in the Synthesis of Colloidal Gold. *Discuss. Faraday Soc.* **1951**, *11*, 55–75.
- (5) Sun, Y.; Jose, D.; Sorensen, C.; Klabunde, K. Alkyl and Aromatic Amines as Digestive Ripening/Size Focusing Agents for Gold Nanoparticles. *Nanomaterials* **2013**, *3* (3), 370–392.
- (6) Pettibone, J. M.; Hudgens, J. W. Gold Cluster Formation with Phosphine Ligands: Etching as a Size-Selective Synthetic Pathway for Small Clusters? *ACS Nano* **2011**, *5* (4), 2989–3002.
- (7) Pensa, E.; Cortés, E.; Corthey, G.; Carro, P.; Vericat, C.; Fonticelli, M. H.; Benítez, G.; Rubert, A. A.; Salvarezza, R. C. The Chemistry of the Sulfur–Gold Interface: In Search of a Unified Model. *Acc. Chem. Res.* **2012**, *45* (8), 1183–1192.
- (8) Caragheorghopol, A.; Chechik, V. Mechanistic Aspects of Ligand Exchange in Au Nanoparticles. *Phys. Chem. Chem. Phys.* **2008**, *10* (33), 5029–5041.
- (9) Montalti, M.; Prodi, L.; Zaccheroni, N.; Baxter, R.; Teobaldi, G.; Zerbetto, F. Kinetics of Place-Exchange Reactions of Thiols on Gold Nanoparticles. *Langmuir* **2003**, *19* (12), 5172–5174.
- (10) Arduengo, A. J.; Harlow, R. L.; Kline, M. A Stable Crystalline Carbene. *J. Am. Chem. Soc.* **1991**, *113* (1), 361–363.
- (11) Marion, N.; Nolan, S. P. N-Heterocyclic Carbenes in Gold Catalysis. *Chem. Soc. Rev.* **2008**, *37* (9), 1776–1782.
- (12) Mercks, L.; Albrecht, M. Beyond Catalysis: N-Heterocyclic Carbene Complexes as Components for Medicinal, Luminescent, and Functional Materials Applications. *Chem. Soc. Rev.* **2010**, *39* (6), 1903–1912.
- (13) Zhukhovitskiy, A. V.; MacLeod, M. J.; Johnson, J. A. Carbene Ligands in Surface Chemistry: From Stabilization of Discrete Elemental Allotropes to Modification of Nanoscale and Bulk Substrates. *Chem. Rev.* **2015**, *115* (20), 11503–11532.
- (14) Hurst, E. C.; Wilson, K.; Fairlamb, I. J. S.; Chechik, V. N-Heterocyclic Carbene Coated Metal Nanoparticles. *New J. Chem.* **2009**, *33* (9), 1837–1840.
- (15) Lara Patricia; Suárez Andrés; Collière Vincent; Philippot Karine; Chaudret Bruno. Platinum N-Heterocyclic Carbene Nanoparticles as New and Effective Catalysts for the Selective Hydrogenation of Nitroaromatics. *ChemCatChem* **2013**, *6* (1), 87–90.
- (16) Lara, P.; Rivada-Wheelaghan, O.; Conejero, S.; Poteau, R.; Philippot, K.; Chaudret, B. Ruthenium Nanoparticles Stabilized by N-Heterocyclic Carbenes: Ligand Location and Influence on Reactivity. *Angew. Chem. Int. Ed.* **2011**, *50* (50), 12080–12084.
- (17) Asensio, J. M.; Tricard, S.; Coppel, Y.; Andrés, R.; Chaudret, B.; de Jesús, E. Synthesis of Water-Soluble Palladium Nanoparticles Stabilized by Sulfonated N-Heterocyclic Carbenes. *Chem. – Eur. J.* **2017**, *23* (54), 13435–13444.
- (18) Vignolle, J.; Tilley, T. D. N-Heterocyclic Carbene-Stabilized Gold Nanoparticles and Their Assembly into 3D Superlattices. *Chem. Commun.* **2009**, No. 46, 7230–7232.
- (19) Serpell, C. J.; Cookson, J.; Thompson, A. L.; Brown, C. M.; Beer, P. D. Haloaurate and Halopalladate Imidazolium Salts: Structures, Properties, and Use as Precursors for Catalytic Metal Nanoparticles. *Dalton Trans* **2013**, *42* (5), 1385–1393.

- (20) MacLeod, M. J.; Johnson, J. A. PEGylated N-Heterocyclic Carbene Anchors Designed To Stabilize Gold Nanoparticles in Biologically Relevant Media. *J. Am. Chem. Soc.* **2015**, *137* (25), 7974–7977.
- (21) Salorinne, K.; Man, R. W. Y.; Li, C.-H.; Taki, M.; Nambo, M.; Crudden, C. M. Water-Soluble N-Heterocyclic Carbene-Protected Gold Nanoparticles: Size-Controlled Synthesis, Stability, and Optical Properties. *Angew. Chem.* **2017**, *129* (22), 6294–6298.
- (22) Man, R. W. Y.; Li, C.-H.; MacLean, M. W. A.; Zenkina, O. V.; Zamora, M. T.; Saunders, L. N.; Rousina-Webb, A.; Nambo, M.; Crudden, C. M. Ultrastable Gold Nanoparticles Modified by Bidentate N-Heterocyclic Carbene Ligands. *J. Am. Chem. Soc.* **2018**, *140* (5), 1576–1579.
- (23) Crudden, C. M.; Horton, J. H.; Ebralidze, I. I.; Zenkina, O. V.; McLean, A. B.; Drevniok, B.; She, Z.; Kraatz, H.-B.; Mosey, N. J.; Seki, T.; Keske, E. C.; Leake, J. D.; Rousina-Webb, A.; Wu, G. Ultra Stable Self-Assembled Monolayers of N-Heterocyclic Carbenes on Gold. *Nat. Chem.* **2014**, *6* (5), 409–414.
- (24) Crudden, C. M.; Horton, J. H.; Narouz, M. R.; Li, Z.; Smith, C. A.; Munro, K.; Baddeley, C. J.; Larrea, C. R.; Drevniok, B.; Thanabalasingam, B.; McLean, A. B.; Zenkina, O. V.; Ebralidze, I. I.; She, Z.; Kraatz, H.-B.; Mosey, N. J.; Saunders, L. N.; Yagi, A. Simple Direct Formation of Self-Assembled N-Heterocyclic Carbene Monolayers on Gold and Their Application in Biosensing. *Nat. Commun.* **2016**, *7*, 12654.
- (25) Curran, D. P.; Solovyev, A.; Makhoulf Brahmi, M.; Fensterbank, L.; Malacria, M.; Lacôte, E. Synthesis and Reactions of N-Heterocyclic Carbene Boranes. *Angew. Chem. Int. Ed.* **2011**, *50* (44), 10294–10317.

CHAPTER I: STATE OF THE ART ON NHC-STABILIZED GOLD NANOPARTICLES

I.A. Gold nanoparticles

While the first rational synthesis of gold nanoparticles was described by Faraday in 1857,¹ they had been used for centuries before. Indeed “soluble gold”, usually a deep red solution, was used through the centuries to stain glass, ceramics, fabrics and also as medicine.² “Potable gold” solutions were used to treat diseases ranging from the plague and epilepsy to diarrhea and syphilis.³ Colloidal gold was used in the diagnosis of the latter up to the 20th century.⁴ While the term nanoparticle was coined much later, scientists of the times had a rough idea of what was happening. Indeed, in the 17th century, German chemist Johann Kunckel published a book on “drinkable gold” where he concluded that “gold must be present in such a degree of communitation that it is not visible to the human eye”.² A century later, a French dictionary stated under “*or potable*” that “drinkable gold contained gold in its elementary form but under extreme sub-division suspended in a liquid”.² Nowadays, a nanoparticle is defined as a particle “with one or more external dimensions is in the size range 1 nm-100 nm”.⁵

The most famous example of the use of colloidal gold in history probably remains the Lycurgus cup (Figure I.1). Indeed the cup, which contains a mix of silver and gold nanoparticles, appears green when looked at in reflected light (e.g. day light) but red in transmitted light (light shone through the cup). This shift in color, as well as the color of nanoparticles in solution, is due to a phenomenon called localized surface plasmon resonance (LSPR).



Figure I.1: Lycurgus cup in a) reflected and b) transmitted light.⁶

Localized surface plasmon resonance is often defined as the collective oscillation of valence electrons within the confines of a noble metal nanostructure, that is correlated with the electromagnetic field of the incoming light.^{2,7} This oscillation leads to an absorption within the UV-visible spectrum. The maximum absorption can be described by Mie's resolution of Maxwell equation for spherical particles with the equation:⁸

$$E(\lambda) = \frac{24\pi^2 Na^3 \varepsilon_{out}^{3/2}}{\lambda \ln(10)} \left[\frac{\varepsilon_i(\lambda)}{(\varepsilon_r(\lambda) + \chi \varepsilon_{out})^2 + \varepsilon_i(\lambda)^2} \right]$$

where a is the radius of the nanoparticle, N is the number of particles in the sensing area, ε_i and ε_r are the imaginary and real dielectric constants of the particle, and ε_{out} is the external dielectric, or local refractive index, which becomes very important for sensing applications, as any change in the refractive index shifts the peak maximum (λ_{max}). Finally, χ is the shape factor of the particle (=2 for a sphere, approximated for other shapes).

According to Mie theory, the plasmon resonance thus depends on the metal of the nanoparticles, their size, their shape and their environment. For example, gold and silver nanospheres of similar size will have plasmon resonance around 520 nm and 400 nm respectively.^{9,10} Larger nanoparticles usually exhibit a higher plasmon resonance wavelength.² Anisotropic nanoparticles often present several peaks corresponding to the axis along which the electrons can oscillate. For example, the UV-visible spectrum of gold nanorods will exhibit 2 absorption maximums: one at around 520 nm corresponding to the short axis and one around 600 to 900 nm (depending on the length of the nanorods) corresponding to the longitudinal axis.^{11,12} Finally, the sensitivity to the environment can be seen when ligands are exchanged on the surface of the nanoparticles. For example, when exchanging half of the dodecanethiol molecules on the surface of 5 nm gold nanoparticles by p-terphenylthiophenol, Goldmann *et al.* observed a shift of the plasmon resonance from 519 nm to 535 nm.¹³

These plasmon properties are often sought after in detection applications. Indeed, plasmonic nanoparticles have become a staple of Surface Enhanced Raman Spectroscopy (SERS) which takes advantage of the electromagnetic "hot spots" created at the edges of anisotropic nanoparticles (Figure I.2), when irradiated at the right wavelength, and can enhance the Raman signal of molecules up to 10^{14} times, enabling the detection of single molecules.^{14,15} Detection assays can also be carried out in solution based on the complexation of target moieties to the nanoparticles leading to their aggregation creating a shift in the UV-vis spectrum (Figure I.2).^{12,16}

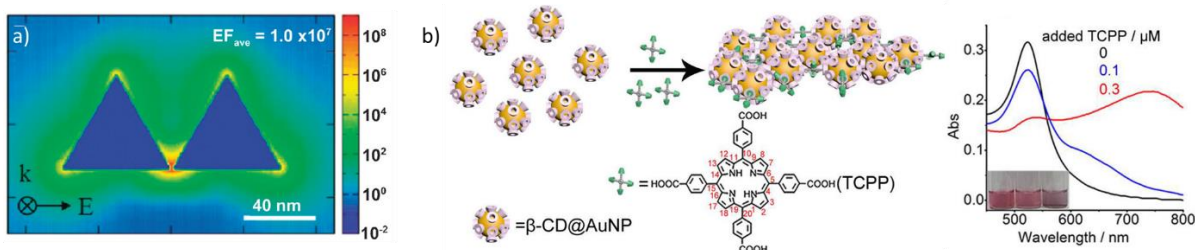


Figure I.2: a) Electromagnetic enhancement factor contours for a dimer of triangular prisms with a 2 nm gap¹⁴ and b) aggregation of cyclodextrine functionalized gold nanoparticles upon introduction of tetrakis (4-carboxyphenyl) porphyrin (TCPP).¹⁶

The plasmonic properties of gold nanoparticles are also sought after in medicine, where they could be used for detection as well as treatment. For example, it has been shown that gold nanoparticles can be functionalized by antibodies that specifically bind to tumoral markers which allows for the detection by dark-field microscopy of cancer cells.^{17,18} Gold nanoparticles are also used in photothermal therapy. Indeed, when irradiated at the right wavelength, gold nanoparticles heat up killing the nearby cells.¹⁸

Finally, as is the case of many metallic nanoparticles, gold nanoparticles have been used in catalysis. Indeed, due to their high surface area, metallic nanoparticles make good potential heterogeneous catalysts. The only drawback is that to remain stable in solution, most nanoparticles require ligands on their surface which can hinder the access of the targeted substrate to the metal itself. However, examples already exist in the literature of uses of gold nanoparticles in solution as catalysts in reactions as varied as the reduction of 4-nitrophenol to 4-aminophenol (Figure I.3),¹⁹ the aerobic oxidation of glucose²⁰ or polymerization of alkylsilanes to siloxane nanowires.²¹

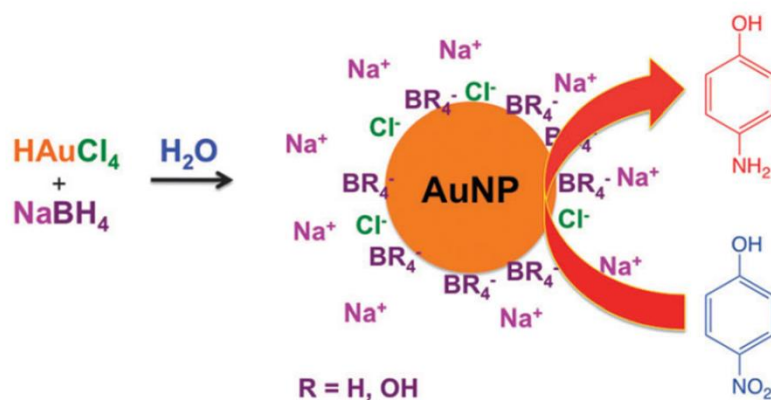


Figure I.3: Reduction of 4-nitrophenol by NaBH₄ catalyzed by gold nanoparticles.¹⁹

As briefly mentioned, some of those potential applications require different shapes, sizes or ligands on the surface of nanoparticles. As a result, many syntheses of gold nanoparticles have been described in

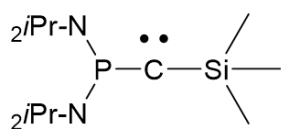
the literature. Syntheses can be achieved in a range of organic solvents,^{22,23} as well as in water²⁴ or biphasic systems.²⁵ A range of shapes can be obtained from small spheres, to rods,¹¹ stars,²⁶ bipyramids²⁷ or cages.²⁸ Finally, a range of ligands have been used to stabilize the nanoparticles, from ubiquitous thiols, to phosphines,²⁹ amines,³⁰ polymers,³¹ cetyltrimethylammonium bromide (CTAB),¹¹ citrates,²⁴ among others. These ligands play a crucial role in the stability of the obtained nanoparticles as well as their dispersibility in different solvents. For example, CTAB, which stabilizes the NPs mainly by electrostatic repulsion, is used for water soluble NPs. On the other hand, other ligands, such as dodecanethiol, which stabilizes the NPs by sterical repulsion, is suitable for apolar solvents due to its long alkyl chain.

In applications where a strong bond is necessary to stabilize the NPs, thiols are often the ligand of choice. Indeed, there is a lot of different structures commercially available and their affinity for gold is well known.³²

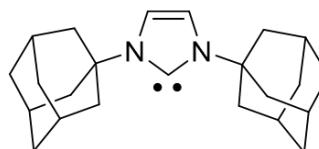
However, thiol stabilized NPs are known to be unstable in harsh conditions (extreme pH, high temperatures) and even in biological medium due to the presence of thiols (such as glutathione) which are able to displace the thiols on the surface of the NPs.^{33,34}

I.B. N-heterocyclic carbenes

The goal of our research project is to synthesize gold nanoparticles stabilized by N-heterocyclic carbenes (NHCs). NHCs are often described as “heterocyclic species containing a carbene carbon and at least one nitrogen within the ring structure”.³⁵ Carbenes are neutral compounds containing a divalent carbon atom with a six-electron valence shell. Due to their incomplete valence shell they used to be considered as highly reactive species, too sensitive to be isolated. However the first spectroscopically characterized carbene, stabilized by adjacent phosphorus and silicon substituents, was described by Bertrand *et coll.* in 1988.³⁶ The first “bottleable” NHC was synthesized only a few years later by Arduengo *et al.* (Scheme I.1).³⁷ The NHC is stabilized by the bulk of the adamantane substituents, which prevents dimerization of the carbene (according to the Wanzlick equilibrium),³⁸ but also by the electronic effects of the adjacent nitrogen atoms. Indeed, the π -donating properties of the nitrogen atoms compensate the electronic deficiency of the carbenic center, while their sigma-electron withdrawing properties stabilize the lone pair of the carbene.³⁵ The cyclic nature of the NHC also favors the singlet state by forcing the carbene carbon into a bent, sp^2 -like, arrangement.



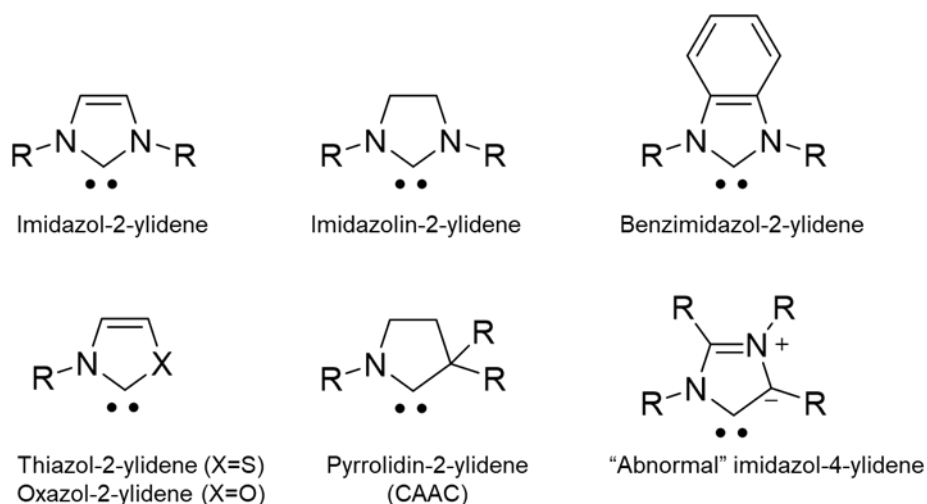
Bertrand *et coll.*, 1988



Arduengo *et al.*, 1991

Scheme I.1: Bertrand's and Arduengo's carbenes.^{36,37}

The presence of 2 adjacent N atoms are not absolute prerequisite to the stability of NHCs however. Indeed, NHCs where one of the nitrogen atoms is replaced by sulfur,³⁹ oxygen⁴⁰ or carbon⁴¹ have also been described. As well, as "remote" or "abnormal" NHCs where the imidazole ring is deprotonated in the C5 position (Scheme I.2). These changes in the ring structure usually give different electronic properties to the carbenes and thus different reactivities. The rest of this section however will focus on NHCs of the imidazol-2-ylidene type unless otherwise specified. Such NHCs present a wide range of available structures. Indeed, examples in the literature exist of asymmetric NHCs as well as NHCs functionalized on the aromatic backbone.



Scheme I.2: Some possible structures of NHCs.

Their nomenclature is often shortened as the N-substituent (methyl, isopropyl, phenyl, etc.) followed by the ring type (imidazole or benzimidazole). For example, in this thesis, 1,3-dimethylimidazol-2-ylidene will be abbreviated diMe-Imd, while 1,3-bis(2,6-diisopropylphenyl)imidazol-2-ylidene will be abbreviated diDipp-Imd and so on.

NHCs are nucleophilic species that act as sigma-donors and bind to a wide range of metallic and non-metallic species. Indeed, examples of NHC complexes exist for all transition metals⁴² as well as for a range of main group elements.⁴³

Coordination of NHCs to metals actually came earlier than their isolation as both Wanzlick and Ofele synthesized a NHC mercury and a NHC chrome complex respectively,^{44,45} in 1968. But Arduengo's work definitely sparked the interest of a wider scientific community. First thought to be very similar to phosphines, NHCs have actually shown a chemistry of their own. Indeed, as NHCs are typically more electron donating than phosphines they tend to form shorter and stronger bonds with metals.³⁵

NHC-metal complexes are often used in catalysis. A well-known example is Grubbs second generation catalyst, a NHC-Ru complex, used in olefin metathesis reactions.⁴⁶ NHC-gold complexes are no exception and have already been used in a range of reactions^{47,48} including the hydroamination of unactivated alkynes⁴⁹ where they showed enhanced catalytic activity when compared to sterically hindered biphenylphosphine-gold species.

NHC-gold complexes have also shown potential applications in the medical field. For example, a study by Iacopeta *et al.* showed that a gold-NHC complex exhibited better activity against cancer cell proliferation than cis-platin, without altering the viability of non-cancer cells.⁵⁰

I.C. Gold nanoparticles stabilized by N-heterocyclic carbenes

Even if NHCs have been studied in molecular chemistry for almost 3 decades, their use in materials chemistry came much later. Indeed, the first mention of NHC coordinated to metallic nanoparticles came in 2005 when Finke *et al.*, using a D/H exchange NMR study,⁵¹ suggested that a small portion of NHCs might be bound to the surface of the nanoparticles. Since then, NHCs have been coordinated to a range of metallic nanoparticles including Pt,⁵² Pd,⁵³ Ru,⁵⁴ Ag⁵⁵ and Au,⁵⁶⁻⁵⁸ among others. NHCs have also been studied for their organization on bulk metallic surfaces, mostly on gold⁵⁹⁻⁶² but also on silver,⁵⁹ copper^{59,60} and more recently Mg.⁶³

NHC-stabilized gold nanoparticles are expected to be more stable than their thiol stabilized counterparts. Indeed, a study of NHC self-assembled monolayer (SAM) on gold⁶¹ measured the desorption energy of NHCs to be $158 \pm 10 \text{ kJ.mol}^{-1}$ while the desorption energy of thiols was measured at 126 kJ.mol^{-1} . Other studies^{62,64,65} showed that NHC SAMs on gold are stable to a wide range of aggressive conditions. Indeed, they remained stable in boiling THF, boiling water, acidic and basic pH (from 2 to 12) and when stored in water for over a month. They also remained mostly intact when treated with 1% H₂O₂ or 1% NH₂OH for 24h. NHCs SAMs also presented good electrochemical stability (from 1V to -0.4V against Ag/AgCl), as well as stability to ultra sounds (up to 10 min) and temperature (no desorption at 365K).

Overall NHC SAMs presented much better stability than their thiol counterparts which are known to be unstable in ambient conditions over time.⁶⁶ Moreover, when NHCs were introduced on dodecyl sulfide (DDS) and dodecanethiol (DDT) SAMs, they were able to displace all of the thioether and about 50% of the thiol. However, when DDS and DDT were introduced on NHC SAMs no displacement occurred and no sulfur could be detected by XPS (Figure I.4).

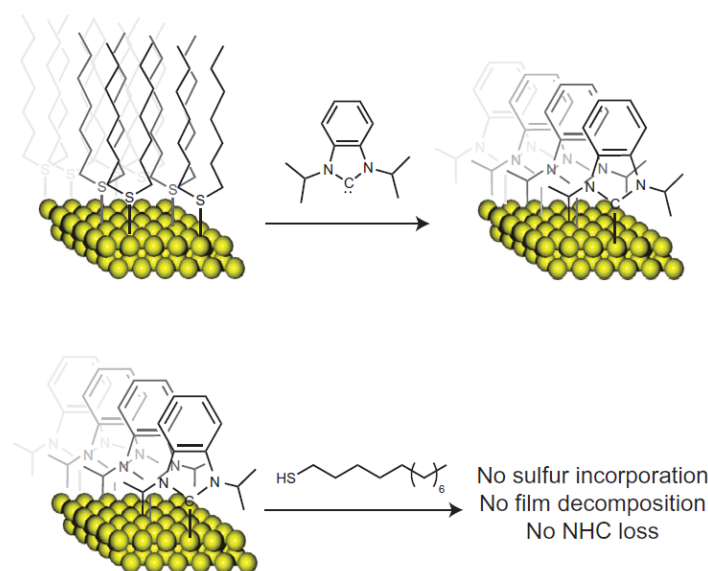


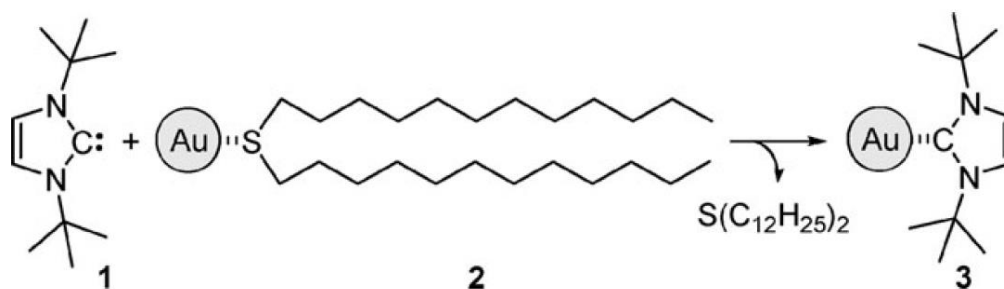
Figure I.4: Incorporation of NHCs on DDS SAM but no incorporation of DDT on NHC SAM.⁶²

While studies on SAMs offer a good rationalization for the use of NHCs as gold nanoparticles ligands, the first synthesis of NHC AuNPs⁵⁸ actually predates the first study on SAMs⁶⁷ by 2 years.

Three main synthetic pathways have been described to obtain NHC stabilized gold nanoparticles. The first one is based on the exchange by NHCs of sacrificial ligands on the surface of already formed NPs. The second is the reduction of NHC-gold(I) complexes. The third strategy is the successive deprotonation and reduction of a gold(III) (benz)imidazolium complex.

I.C.1. Ligand exchange

The first ever example of NHC-stabilized gold nanoparticles was described by Hurst *et al.* in 2009.⁵⁸ Their methodology relies on ligand exchange (Scheme I.3). Indeed, they synthesized gold nanoparticles stabilized by thioethers, which are weakly bound to the nanoparticles surface, using benzene or toluene as a solvent. When 1,3-ditertbutylimidazol-2-ylidene (ditBu-Imd) was introduced the nanoparticles precipitated within 12h and could only be redispersed in polar solvents. The obtained nanoparticles presented the same diameter as before the exchange (2.6 ± 0.5 nm).



Scheme 1.3: Synthesis of NHC-stabilized gold nanoparticles by ligand exchange.⁵⁸

The synthesis had to be carried out in a dry box due to the sensitivity of NHCs to moisture but once the exchange was performed the obtained nanoparticles could be handled in air. The exchange was confirmed by X-ray photoelectron spectroscopy; a technique routinely used to determine the chemical state of an analyzed surface, while able to give a precise elementary composition of the analyzed material. They found that the peak corresponding to sulfur (S2p) present for the thioether-functionalized NPs disappeared after the exchange, while the peak corresponding to nitrogen (N1s) appeared.

The NHC-stabilized NPs were stable for months in solid form, but degraded in a matter of hours (ca. 12) when in solution. MS and NMR analyses of the solution showed the presence of the imidazolium as well as NHC-Au-X (X=Cl or Br) and [Au(NHC)₂]⁺ complexes. Unfortunately, in this seminal work no information was given on the oxidation state of gold at the nanoparticle surface and a possible quantification of gold(I) in the sample.

The synthesis can be extended to other metals. Indeed, Pd nanoparticles were synthesized and exhibited the same behavior.

In 2014, Rodriguez-Castillo *et al.*⁶⁸ studied the influence of the NHC used on a similar ligand exchange reaction on gold nanoparticles. Their study focused on benzimidazol-2-ylidene with methyl or n-hexyl side chains which they also compared to dimethylimidazol-2-ylidene (diMe-Imd). They found that, similarly to Hurst *et al.*,⁵⁸ when benzimidazolium and sodium tert-butoxide were added to a solution of DDS-protected gold nanoparticles, they precipitated. However, when analyzing the obtained NPs by TEM, they found that they were almost half the size they were when coated with DDS (2.8 ± 0.6 nm instead of 5.8 ± 1.2 nm). Analysis of the NPs by ¹³C solid state NMR showed the complete disappearance of DDS and the presence of Au-NHC complexes not directly bound to the surface. After washing the NPs with acetonitrile, they were able to recover the [Au(NHC)₂]Cl complex in 45% yield. When reacted with [Au(NHC)₂]X, the AuNPs exhibit the same behavior as when reacted with NHCs. This would tend to suggest, according to the authors, stabilization by aurophilic interaction of the gold

complex with the surface, at least partially, as they do not mention the stability of the NPs after washing with acetonitrile.

The reaction conditions were modified and $[\text{Au}(\text{NHC})_2]^+$ was systematically formed despite changing the NHC from a benzimidazolylidene to diMe-Imd, or the base from sodium tert-butoxide to lithium triethylborohydride, or the sacrificial ligand from DDS to n-dodecylamine (also acting as a base) (Figure I.5).

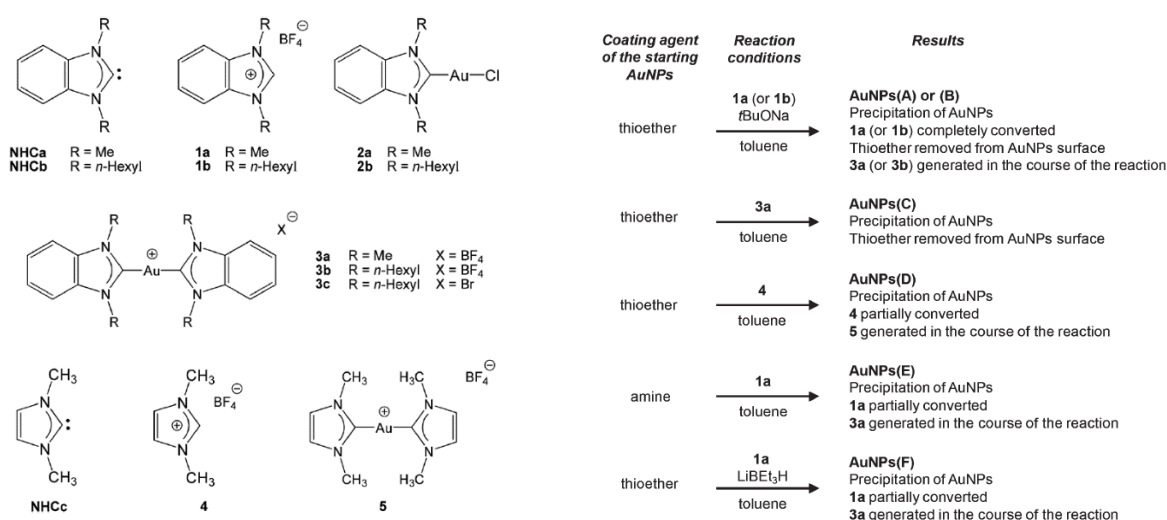


Figure I.5: Structures of the different ligands and summary of the different reaction conditions.⁶⁸

Unfortunately, they do not discuss in this study the size of the nanoparticles obtained from the different types of synthesis. Indeed, it has been showed in other studies (discussed below) that the steric bulk of the NHC used influences significantly the size of the particles, and, to the best of our knowledge, no other study compared different bases or sacrificial ligands. They also do not quantify how much ligand is formed in each case and it is thus impossible to compare to the 45% yield they obtained in the first synthesis.

They do however discuss it in a further study from 2016.⁶⁹ In the paper, they use the same protocol to synthesize nanoparticles using di-phenylimidazol-2-ylidene (diPh-Imd). When comparing the new results with their previous study, they show a clear influence of the side-group on the size of the obtained NPs (see Table I.1). Indeed, methyl and phenyl groups led to significant etching of the NPs and a decrease in size (from 5.8 ± 1.2 to 2.8 ± 0.6 and 3.4 ± 0.8 nm respectively) whereas n-hexyl group led to only a moderate size decrease (from 5.8 ± 1.2 to 5.1 ± 1.0 nm). Supposedly, the long alkyl chains interact better with each other leading to increased stabilization and decreased etching.

Table I.1: Nanoparticle size before and after exchange depending on N-substituents.⁶⁹

N-substituent	NPs size before exchange (nm)	NPs size after exchange (nm)
Methyl		2.8 ± 0.6
Phenyl	5.8 ± 1.2	3.4 ± 0.8
n-Hexyl		5.1 ± 1.0

As in their previous study, a significant amount of $[\text{Au}(\text{NHC})_2]^+$ complex was formed during the exchange. The focus of this study however was DFT calculations on the bonding of NHC to a gold surface or a gold cluster using two different methods (VASP or Gaussian).

When using the surface model, they found that NHCs prefer a perpendicular binding mode and react preferably with weakly bound gold atoms at the surface (known as adatoms). This result was confirmed by other DFT studies on SAMs.^{64,70} For the cluster model, they focused on a Au_{38} cluster. They found that the binding strength was stronger for the least coordinated gold atoms similarly to the adatoms of a gold surface. The electron donor properties of the NHC are highlighted by a partial negative charge on the cluster.

They finally propose a mechanism for the formation of gold-NHC complexes during the ligand exchange. According to their results, the binding of NHC to gold is more favorable than the binding of thioethers which leads to the gradual exchange. Even though, the strength of the Au-NHC bond should be enough to stabilize the NPs, the absence of secondary interactions between the ligands leads to a repositioning of the gold atom, surface reconstruction and thus the formation of surface defects such as adatoms. NHC-Au moieties might then diffuse in solution where they would react with remaining NHCs in solution leading to the formation of $[\text{Au}(\text{NHC})_2]^+$ complexes and the erosion of the Au surface.

This seems to be confirmed by a study of Glorius *et coll.*⁷¹ on SAMs of 3 different NHCs : 1,3-dimethylimidazol-2-ylidene (diMe-Imd), 1,3-dimesitylimidazol-2-ylidene (diMes-Imd) and 1,3-diisopropylimidazol-2-ylidene (di*i*Pr-Imd).

While the strength of the bond between gold and NHC seems unfavorable to mobility, STM analysis showed that NHCs were bound to adatoms which were able to move along the surface in a ballbot-type motion. Despite this mobility, the SAM remains stable at high temperature. Measurements at low temperature indicate a free rotation around a single bond between the NHC carbon and an Au atom. DFT calculations showed the strong effect of diMe-Imd on the surface as it “pulls” the gold atom it is linked to away from the surface. Indeed, the formation of an adatom in the absence of NHC has a free

energy barrier ten times higher than in the presence of NHCs. Molecular dynamics calculations showed that the Au atom is easily extracted from the surface to form an adatom but the transient vacancy is simultaneously filled by an Au atom of the second layer (Figure I.6). The adatom formation is irreversible but creates no vacancies on the surface. Similar calculation on thiols did not exhibit the same phenomenon indicating a different mechanism for the mobility of thiol-based SAMs.

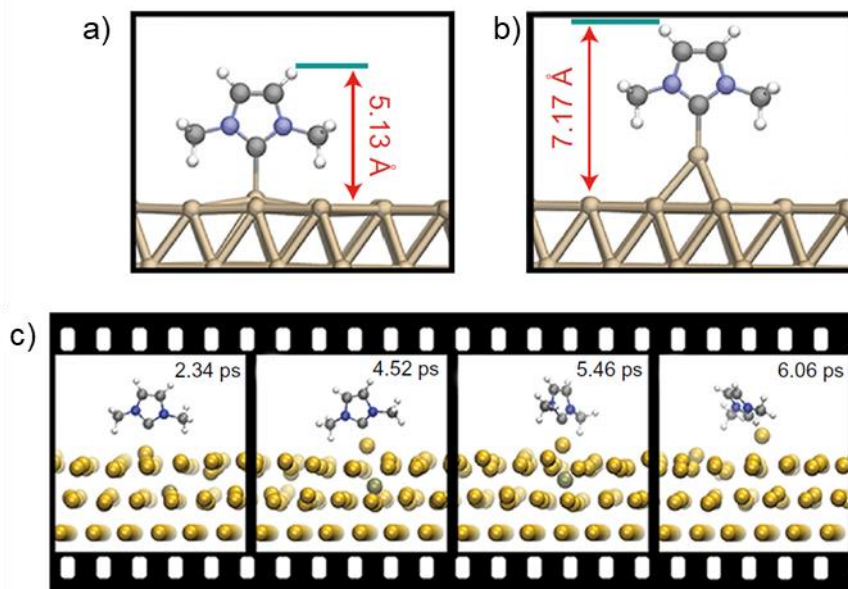


Figure I.6: Geometric structures of diMe-Imd on Au(111) without (a) and with (b) an additional Au adatom as determined from DFT optimization. c) Snapshots from a simulation of diMe-Imd on Au(111) illustrate the extraction of an Au atom from the top layer and the concerted migration of an Au atom in the second layer (dark-shaded ball) to fill the vacancy in the top layer.⁷¹

The bonding energy of *di*iPr-Imd and *di*Mes-Imd are higher than for diMe-Imd due to non-bonding interactions of the aromatic side groups with the surface. *di*iPr-Imd pulls the Au atom 0.2 Å further than *di*Mes-Imd which interacts more strongly with the surface. As a result, *di*iPr-Imd is more likely to form the adatom required for surface mobility. The formation of the adatom seems to be governed by a balance between electronic and steric effects.

DiMe-Imd is also capable of forming dimeric and trimeric NHC complexes which are formed following an equilibration after the initial formation of the monolayer. The formation appears to be surface-assisted. These complexes could easily diffuse into solution explaining the presence of $[\text{Au}(\text{NHC})_2]^+$ in most NPs syntheses.

The dependence of side substituents for the organization on the surface was also confirmed by another study⁶⁰ that found that while NHC with isopropyl substituent stand upright on the surface, methyl or

ethyl substituted NHCs lie flat on the surface. They also found that NHCs that bind upright desorb cleanly while flat-lying NHCs decompose and leave adsorbed organic residue.

Prolonged exposure to diMe-Imd leads to an increasing amount of upright NHCs but not all flat-lying NHCs are eliminated pointing to a coexistence of upright and flat-lying species.

The influence of NHC substituents was also confirmed for NPs. Indeed, in 2014, Glorius, Ravoo *et coll.*⁷² published a study focusing on the synthesis of palladium nanoparticles using NHCs with long chains on the backbone and methyl groups on the nitrogen. They assumed that small or flexible substituents on the nitrogen atoms would prevent repulsion between the Pd surface and the NHCs while the long chains would form a protective monolayer (Figure I.7).

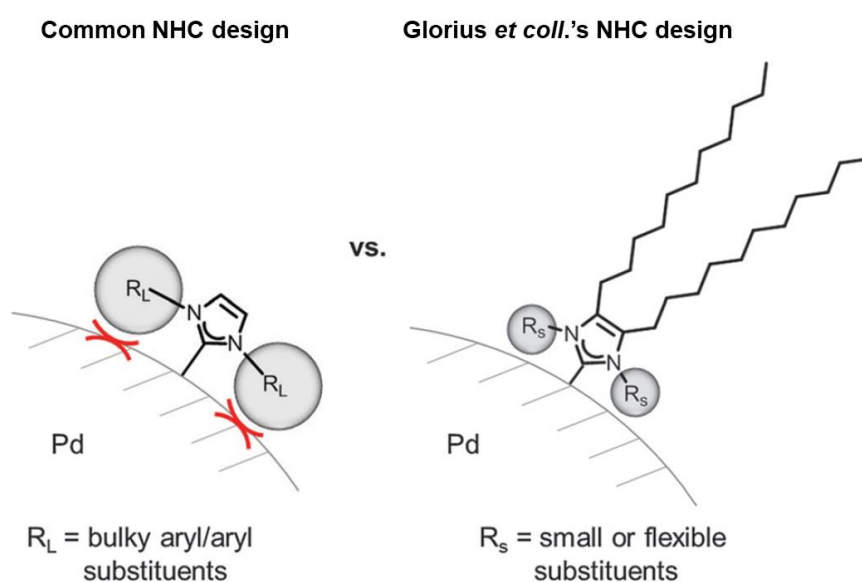


Figure I.7: Comparison of different NHC designs.⁷²

The obtained NPs are stable for months, can be handled in air and are of the same size as the thioether protected NPs. They found that when using NHCs without long chains on the backbone, the exchange would occur but the obtained nanoparticles would quickly aggregate over time or upon exposure to air. When using a bulkier N-substituent (*i*Pr instead of Me), the NPs were also unstable regardless of the presence of long chains on the backbone.

They mention in the article that they also managed to perform the exchange of thioether-protected gold nanoparticles and that the obtained NPs are stable. When looking at the supplementary information however one can see that the NHC-protected AuNPs are smaller than the thioether-protected ones (3.9 ± 0.7 and 5.0 ± 1.6 nm respectively). Unfortunately, they do not seem to have studied those NPs further and there is no indication of the presence of NHC-Au complexes in the sample. However, given the etching and the previous examples, one can assume there probably was.

It is also interesting to note that while Hurst *et al.*⁵⁸ detected the presence of Pd⁺ complexes in their synthesis, Glorius *et coll.* do not while both seem to have Au⁺ complexes. This seems to indicate that the formation of M⁺ complexes does not only depend on the NHC used but also on the metal itself.

In 2015, the same group, inspired by the work of Chaudret *et coll.*⁵² which synthesized water-soluble platinum nanoparticles using sulfonated NHCs, synthesized NHCs bearing sulfonate or carboxylate groups in order to obtain water-soluble Pd and Au NPs.⁷³ They used a biphasic system of hexane and DMF to perform the exchange between DDS and the NHCs (Figure I.8). The obtained NPs were stable in water for months and could be reversibly aggregated by adjusting the pH of the solution.

Similarly to their previous study, Pd NPs exhibited no change in size upon exchange but Au NPs did. Indeed, the DDS protected AuNPs were of 8.5 ± 1.7 nm in diameter whereas the NHC protected NPs ranged from 4.1 ± 1.5 to 4.9 ± 1.7 nm depending on the ligand. The decrease in size is due, as in the previous examples, to NHC-Au complexes which can be detected by NMR and ESI-MS. Once purified by dialysis, the AuNPs remained stable and showed no size changes.

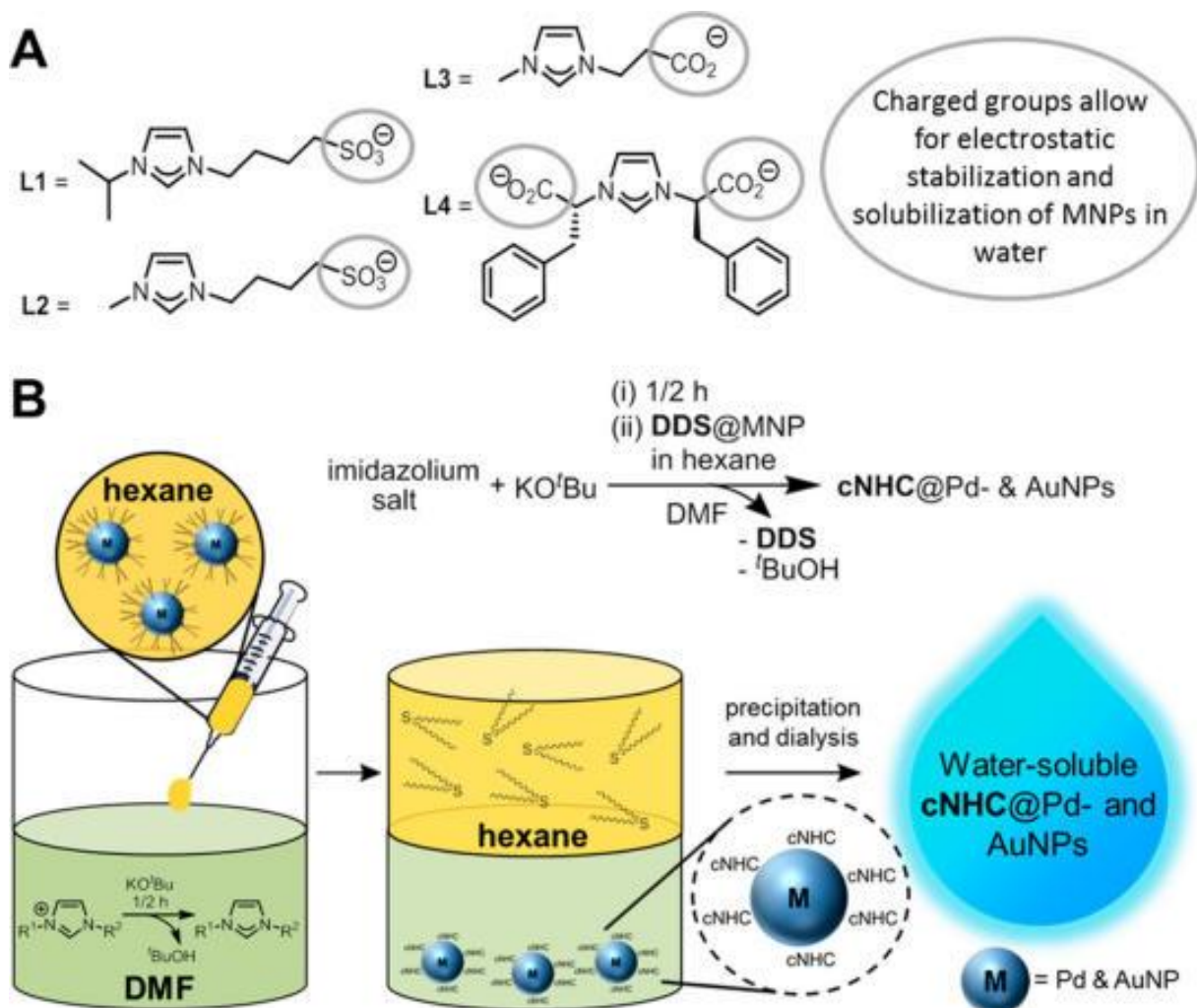


Figure I.8: Synthesis of water soluble metallic nanoparticles by ligand exchange in biphasic medium.⁷³

According to these examples, etching is a recurrent issue in ligand exchange reactions. However, a few exceptions can be found. First of all, while Hurst *et al.* do describe Au-NHC complexes, they observe no etching of their nanoparticles. Another example is a study published by Cao *et al.*⁷⁴ in which they synthesized NHC-functionalized AuNPs to use as a catalyst in carbon dioxide reduction. Not only did they find that the NHC-functionalized NPs had a significantly improved faradic efficiency compared to similar carbon supported naked NPs (83% instead of 53%), they also found that no etching occurred during the ligand exchange between oleylamine and NHCs. Indeed, the nanoparticles retain a size of approximately 7 nm. This seems to be in direct contradiction with the other examples presented above, especially given the fact that the NHC used has bulky mesityl N-substituents and no long alkyl chains to provide stability. Another study by Crudden *et coll.*,⁷⁵ comparing ligand exchange and complex reduction methods (described in more details below), found no etching either. The thing those syntheses have in common is the use of free NHC to perform the exchange instead of introducing imidazolium salts and a base. It is unclear why this leads to less gold being leached in solution.

I.C.2. NHC-gold complex reduction

The second method to obtain NHC-stabilized gold nanoparticles was also published in 2009. It is based on the reduction of NHC-Au-Cl complexes to yield stable nanoparticles. Interestingly, two papers described the same technique weeks from each other. A first paper published by Huang *et al.*,⁷⁶ which focused on the synthesis of NHC-Au(I) complexes and their possible uses as liquid crystals, and only presents the synthesis of nanoparticles in a brief paragraph. Moreover, they assumed that the obtained nanoparticles were stabilized by imidazoliums (without characterizing the surface). The other paper,⁵⁷ by Vignolle and Tilley, however, focused on the synthesis of NHC-stabilized gold nanoparticles. Therefore, they are usually credited as the pioneers of this technique.

In their paper, Vignolle and Tilley first synthesize nanoparticles by reducing 1,3-di(isopropyl)imidazol-2-ylidene gold chloride (*di*i*Pr-Imd-AuCl*) with KBET_3H at room temperature in THF (Figure I.9). They obtain 2.2 ± 0.5 nm NPs which, due to the nature of the ligand, cannot be purified. They thus switched to an NHC with C_{14} alkyl chains as N-substituents. By using the same reaction conditions, they obtain 6.8 ± 1.8 nm nanoparticles, which goes to show, as with the ligand exchange protocol, the importance of the NHC used. The obtained NPs proved stable for several months in apolar solvents. The size and morphology of the NPs can also be influenced by the solvent and reducing agent used. Indeed, when using Et_2O and 9-BBN, the obtained nanoparticles presented narrower polydispersity and were less spherical with a rhombic shape. MS analysis of the crude solution showed the presence of $[\text{Au}(\text{NHC})_2]^+$ complex and NMR analysis of the NPs presented broad peaks, suggesting that the NHC is on the NP surface.

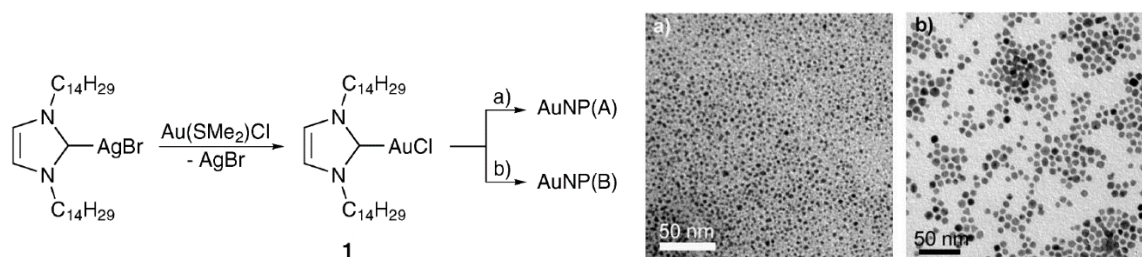
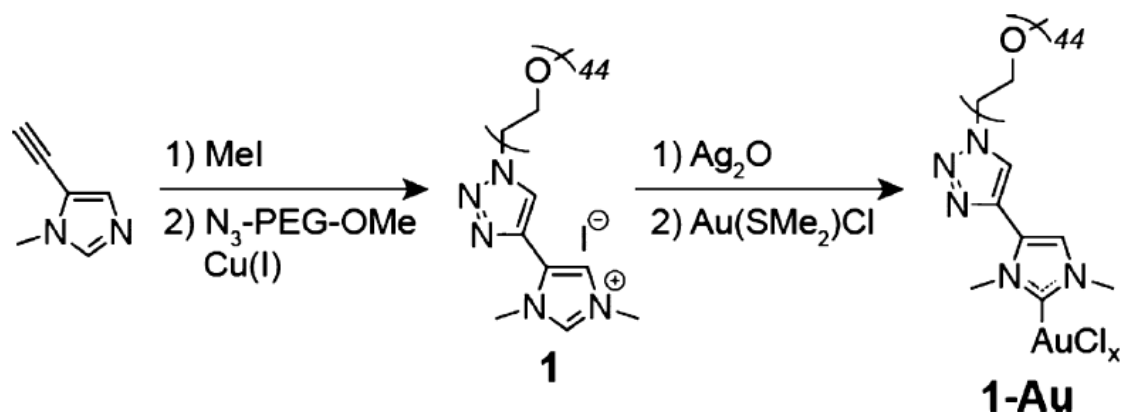


Figure I.9: Synthesis of NHC-stabilized gold nanoparticles by reduction of NHC-AuCl complex by a) KBt_3H in THF and b) 9-BBN in Et_2O .⁵⁷

In the following years, this type of synthesis, using an external reducing agent to reduce NHC-AuCl complexes to gold NPs dispersed in a more or less polar solvent, has proved the most popular to obtain NHC-coated AuNPs.

A lot of the work carried out on this type of synthesis aimed to change the NHC to give it “interesting” properties. One of the most sought-after property is water-solubility. Indeed, as seen above, gold nanoparticles have potential applications in the medical field. However, most of those applications require them to be water-soluble.

In 2015, MacLeod *et al.*⁷⁷ described the synthesis of poly ethylene glycol (PEG) functionalized AuNPs starting from the corresponding PEG-NHC-AuCl_x ($x=1$ or 3) complex and $\text{tBuNH}_2\text{BH}_3$. The complex was synthesized by methylation of 5-ethynyl-1-methyl-1H-imidazole and then functionalization with poly ethylene glycol via click chemistry. The functionalized imidazolium was then reacted successively with an excess of Ag_2O and AuClSMe_2 (2.5 eq each) to afford the gold complex PEG-NHC-AuCl_x (Scheme I.4). A mixture of Au^{I} and Au^{III} complexes was obtained, which proved impossible to purify but could be differentiated using NMR by comparing the signals to the spectrum of a purified tri ethylene glycol NHC-Au^I complex.



Scheme I.4: Synthesis of the PEG-NHC-AuCl_x ($x=1$ or 3) complex.⁷⁷

The obtained nanoparticles have an average diameter of 4.2 ± 0.7 nm. Similar spectra were obtained by IR analysis of the complex and the NPs, suggesting the integrity of the ligand on the surface. Moreover, a key imidazolium vibrational band at 1576 cm^{-1} was absent of the NPs spectrum. As a result, the authors claim functionalization by NHCs.

The particles were stable in water for at least 3 months. They also investigated the stability of the NPs in a range of harsher conditions. The NPs remained stable several hours in extreme temperatures (95°C or -78°C) and for weeks at $\text{pH}=4$ and up, but slowly degraded over the course of a few weeks in more acidic pH. The NPs remained stable for at least 6 hours in solutions with biologically relevant concentrations of NaCl and stayed well dispersed in acetic acid and phosphate buffers with minimal aggregation. They also remained stable when exposed to fetal bovine serum (at 26 and 37°C). They showed minimal aggregation when exposed to glutathione but aggregated fully and released NHC-Au complexes after 26h of exposure to 2-mercaptoethanol. The NPs are also stable up to 24h in 1.8M aqueous H_2O_2 .

In 2017, Crudden *et coll.*⁷⁸ synthesized water-soluble AuNPs using benzimidazolylidenes functionalized by a carboxylate group (Figure I.10). The synthesis of the NHC-Au(I) complex readily yielded NHC-AuCl and $[\text{Au}(\text{NHC})_2]^+$. They thus investigated both as precursors to gold nanoparticles. They found that while NHC-AuCl formed NPs immediately upon reaction with NaBH_4 , reduction occurred more slowly for $[\text{Au}(\text{NHC})_2]^+$. After 5h of reaction, they found that both precursors yielded similar NPs as evidenced by gel electrophoresis analysis. However, as $[\text{Au}(\text{NHC})_2]^+$ was easier to synthesize it was used as a precursor in the remainder of the study. They found that the size of the nanoparticles could be tuned, from 2.0 ± 0.4 nm to 3.3 ± 0.4 nm, depending on the reaction time. The longer the reaction time, the larger the obtained nanoparticles were. Yet growth appeared to be homogeneous as NPs retained similar size dispersion even with increased reaction times. If HAuCl_4 was added as a source of unligated gold, the nanoparticles formed immediately and were similar in size to the ones obtained from NHC-AuCl (as determined by gel electrophoresis and TEM) and had similar NHC: Au ratios according to TGA analysis (10:90 for NPs starting from NHC-AuCl and 15:85 for NPs using additional HAuCl_4).

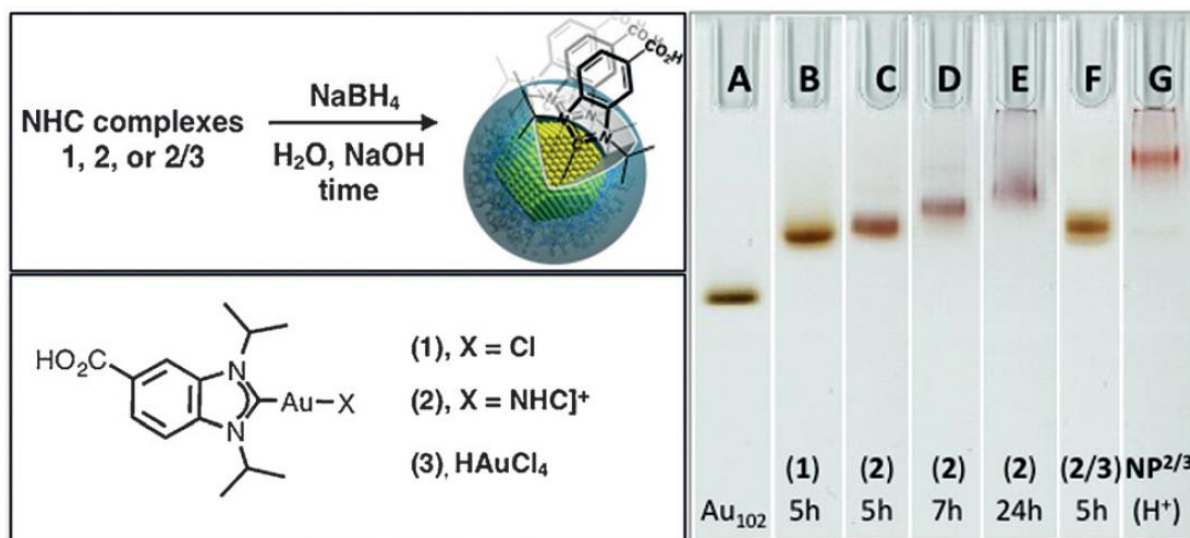


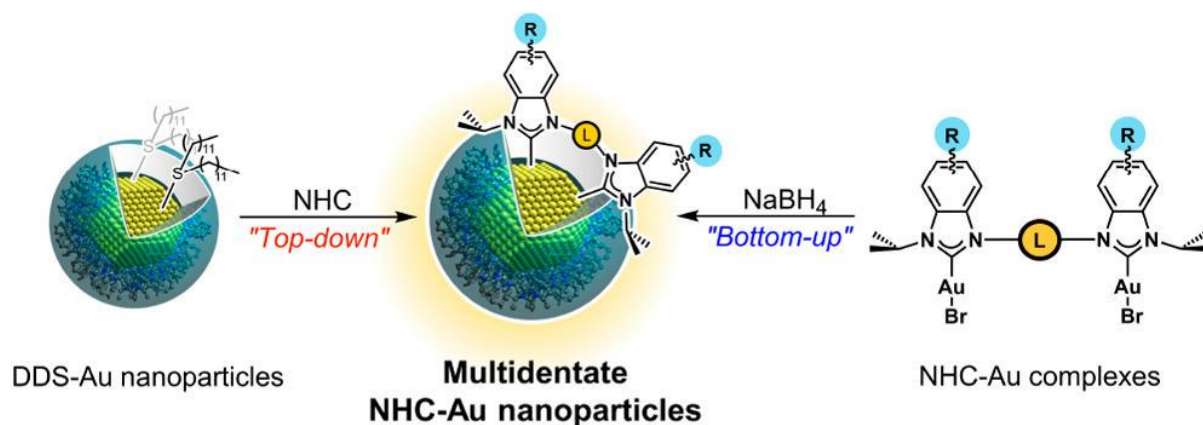
Figure I.10: Synthesis of water soluble NHC-stabilized gold nanoparticles.⁷⁸

NHC coordination was confirmed by XPS, notably by the observation of a N1s peak at 401 eV which corresponds to NHC coordination to the surface according to previous work from their group.⁶² Nanoparticles were stable for at least a month in pH 8 and 10. In acidic pH (pH=2), they precipitated but could be redissolved once the pH was adjusted to 10 and the cycle could be repeated at least 5 times. In protonated form, NPs are soluble in organic solvent. In alcohols (MeOH, EtOH, *i*PrOH), they aggregated irreversibly within 1-2 days. In MeCN or DMF however they evolve to larger particles which can be dissolved in water at a basic pH and isolated. Nanoparticles remained stable in saline solution (150 mM) for several days with only a moderate increase in polydispersity after a week (2%). Finally, exposure to glutathione led to etching of the nanoparticles but larger particles “resisted” better.

The same year, they described the synthesis of amphiphilic nanoparticles stabilized by an amphiphilic NHC,⁷⁹ 1-dodecyl,3-triethylene glycol-benzimidazol-5-ylidene, a benzimidazolylidene substituted with a C₁₂ alkyl chain and a triethyl ethylene glycol (TEG) chain. By reducing the NHC-AuBr complex with NaBH₄ in THF they obtained 4.1 ± 1.1 nm NPs stabilized by NHCs (as confirmed by N1s XPS). They found that the NPs could be aggregated in a controllable and reversible manner in H₂O:EtOH mixtures, because of the insolubility of C₁₂ chains in polar solvents. In hexane, however, there was a mixture of aggregates and discrete NPs due to the slight solubility of TEG in the solvent.

Different research groups modified the NHC structure in order to modify the stability/properties of obtained NPs.

For example, Crudden *et coll.*⁷⁵ synthesized bidentate NHC ligands in order to synthesize more stable nanoparticles. They synthesized particles by using both a top down (ligand exchange) and a bottom up (NHC-Au^I complex) approach to synthesize the NPs (Figure I.11).



- ✓ Soluble in organic solvents
- ✓ High thermal stability
- ✓ Stable against dodecanethiol

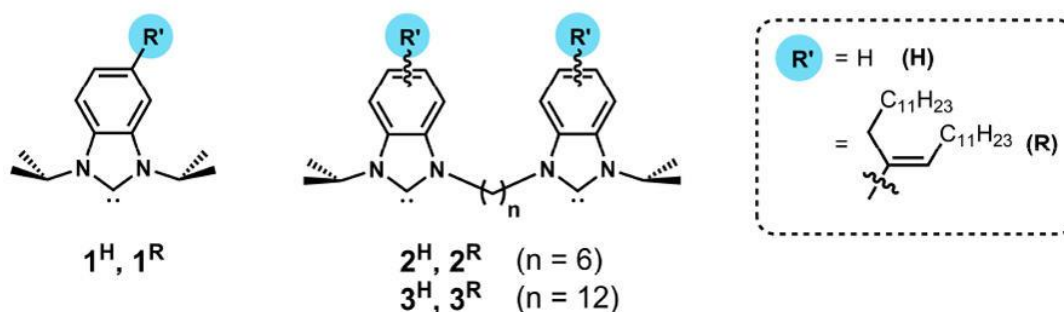


Figure I.11: Top down and bottom up synthesis of bidentate NHC stabilized gold nanoparticles.⁷⁵

They found that in general smaller particles resulted from the bottom-up approach than the top-down method but presented lower ligand density. When using the ligand exchange procedure, they found no significant change in size or morphology of the NPs (no etching). The correct and complete functionalization was confirmed by XPS, where the disappearance of the S2p peak and the appearance of a N1s peak at 401 eV was observed.

NHC alkylated on the aromatic ring led to more stable NPs than their non-alkylated counterparts. Indeed, the non-alkylated particles aggregated within a week whereas the others remained stable. When exposed to thiols (DDT), the NPs synthesized by top down method using bidentate NHCs remained stable and no sulfur was detected by XPS. The bottom up NPs proved more sensitive and decomposed in 2 days.

The same year, Serpell *et coll.*⁸⁰ developed AuNPs stabilized by chiral NHCs derived from histidine. Histidine is a well-known chiral amino acid which can be readily converted into imidazolium. Starting

from commercial L and D Boc protected histidines, they obtained the corresponding NHC-Au-Cl complexes which they reduced with ${}^t\text{BuNH}_2\text{BH}_3$ in THF to obtain AuNPs. By ${}^{13}\text{C}$ NMR analysis, they observed a shift of the carbene peak from 171 to 184 ppm and an absence of signal at 137 ppm corresponding to the free ligand. They interpret this as the confirmation of the presence of NHC at the surface of the NPs and the absence of complex in solution.

The size of the obtained NPs depended on the L or D nature of the starting ligand. Indeed, when using the D-histidine slightly polydisperse NPs of 4.0 ± 1.4 nm were obtained, whereas when using the L-histidine a bimodal distribution was obtained with a mixture of 1.9 ± 0.4 and 6.4 ± 1.1 nm NPs (Figure I.12). After size selection by centrifugation both samples contained similar monodisperse NPs (5.3 ± 0.8 and 5.0 ± 0.6 nm respectively). The NPs were stable over 48 hours, after which they showed a bit of aggregation.

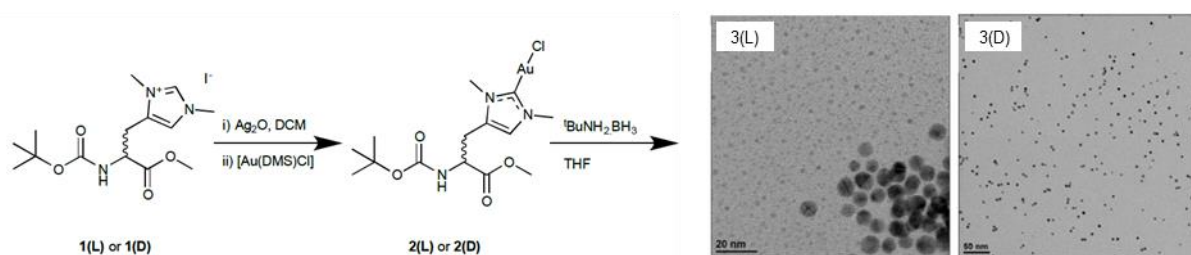


Figure I.12: Synthesis of histidine based NHC-AuCl complex and TEM images of corresponding nanoparticles.⁸⁰

The optical activity of the NPs was analyzed by circular dichroism. L and D NPs present opposing/symmetrical spectra while neither the imidazolium nor Au complex exhibited a circular dichroism signal. The NPs appeared to fix the histidine ligands in a certain conformation that gave rise to optical activity associated with supramolecular ordering rather than singular molecular chirality. Attempts to deprotect the amine by adding concentrated HCl in solution lead to irreversibly aggregated NPs. This is not surprising given the absence of long alkyl chains and/or charged ligands to stabilize the NPs.

However, had they been successful, further functionalization would probably have been possible as shown by works on SAMs. NHC-SAMs functionalized by Br,⁶⁵ methylstyrene,⁸¹ CN,⁶⁵ COOMe⁶⁵ and OH⁸² have been synthesized and some could be further modified by a polymer brush,⁸¹ ferrocene,⁶² a lipid bilayer⁸² or biologically relevant molecules such as dextran⁶⁶ and streptavidin.⁸³

I.C.3. Imidazolium gold complex reduction

The 3rd and last synthetic method to obtain NHC stabilized AuNP described in the literature is the deprotonation and then reduction of an imidazolium gold(III) complex.

Serpell *et al.*⁵⁶ first described this type of synthesis in 2013 where they successfully synthesized Au and Pd-NHC NPs. The starting complexes are easily obtained by biphasic anion exchange between the imidazolium salts and either HAuCl₄ or K₂PdCl₄. In this study they compared bis n-propyl, bis n-hexyl and bis tert-butyl imidazolium salts of Au and Pd tetrahalogenate.

As with the ligand exchange procedure, Au and Pd present slightly different behaviors. Indeed, if reduced directly with NaBH₄, the bishexyl imidazolium palladate complex yielded stable nanoparticles while the aurate complex yielded bulk metal. Prior deprotonation of the imidazolium cation by NaH, before addition of NaBH₄, yielded NPs for both metals (Figure I.13).

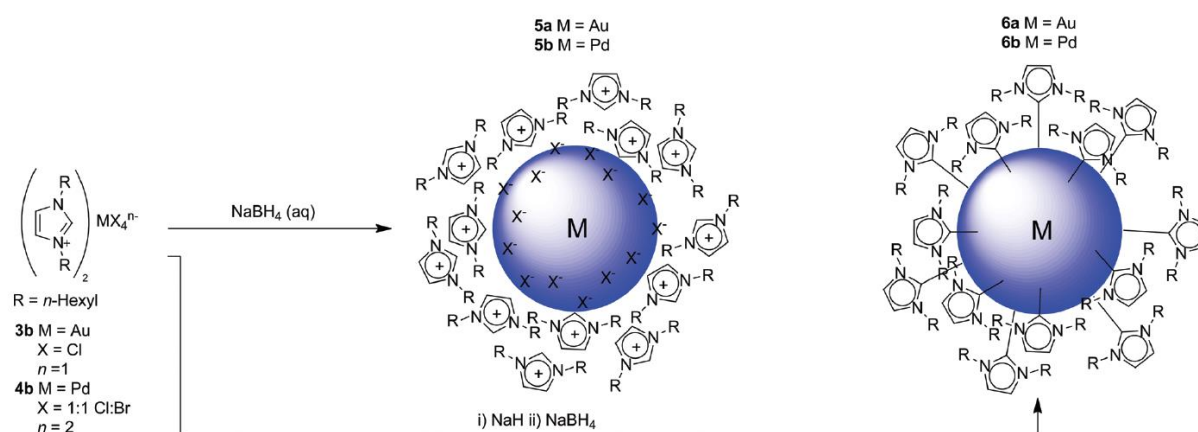


Figure I.13: Synthesis of imidazolium and NHC stabilized metallic nanoparticles.⁵⁶

¹H NMR analysis revealed that while a peak characteristic of imidazoliums was observable for the Pd NPs synthesized without NaH, it was not when NaH was used. Moreover, a broadening of signals was observed which is characteristic of coordinated ligands.

According to them, the fact that a strong base is needed to obtain stable AuNPs is one more indication that they are indeed stabilized by NHCs.

It also appears that the length/type of the side chains is once again important, as bis n-propyl and bis t-butyl imidazolium metallate salts failed to give stable NPs.

The work was picked up by Pileni *et coll.* in 2015,⁸⁴ in a paper studying the influence of the position of long alkyl chains on benzimidazolylidene ligands. They synthesized a series of ligand with long chains on the aromatic ring of the NHC, on the nitrogen atoms or both. Nanoparticles were obtained for all ligands synthesized (Figure I.14). Functionalization by NHCs was confirmed by XPS, with a carbon spectrum close to the corresponding NHC-AuCl complex but an absence of chlorine signal and the position of the N1s peak at 401 eV. By ¹H NMR, they observed the absence of a peak characteristic of benzimidazolium, but a spectrum close, yet not identical, to the one of NHC-AuCl and a broadening of the signals usually interpreted as the ligand being bound to the NP surface. This also suggests the

stabilization of the NPs by NHCs. They observed an effect on size depending on the ligand used (Figure I.14). Ligands **L**¹ and **L**², functionalized by long chains on the aromatic ring, gave the largest particles while ligand **L**³, functionalized by long chains on both the nitrogen and backbone, gave the smallest particles and those functionalized only on the nitrogen atoms, **L**⁴ and **L**⁵, were of intermediate size. They explain this difference in size by a difference in bulkiness of the ligands where steric repulsion lead to higher curvature radius. The obtained nanoparticles are able to assemble in supracrystals. The largest crystalline domains are obtained for the NPs with long chains as N-substituents only (**L**¹ and **L**²). The ligand which also has long chains on the aromatic backbone (**L**³) forms amorphous colloidal films. Interparticular distance suggests an interlocking of the long alkyl chain which would drive self-assembly.

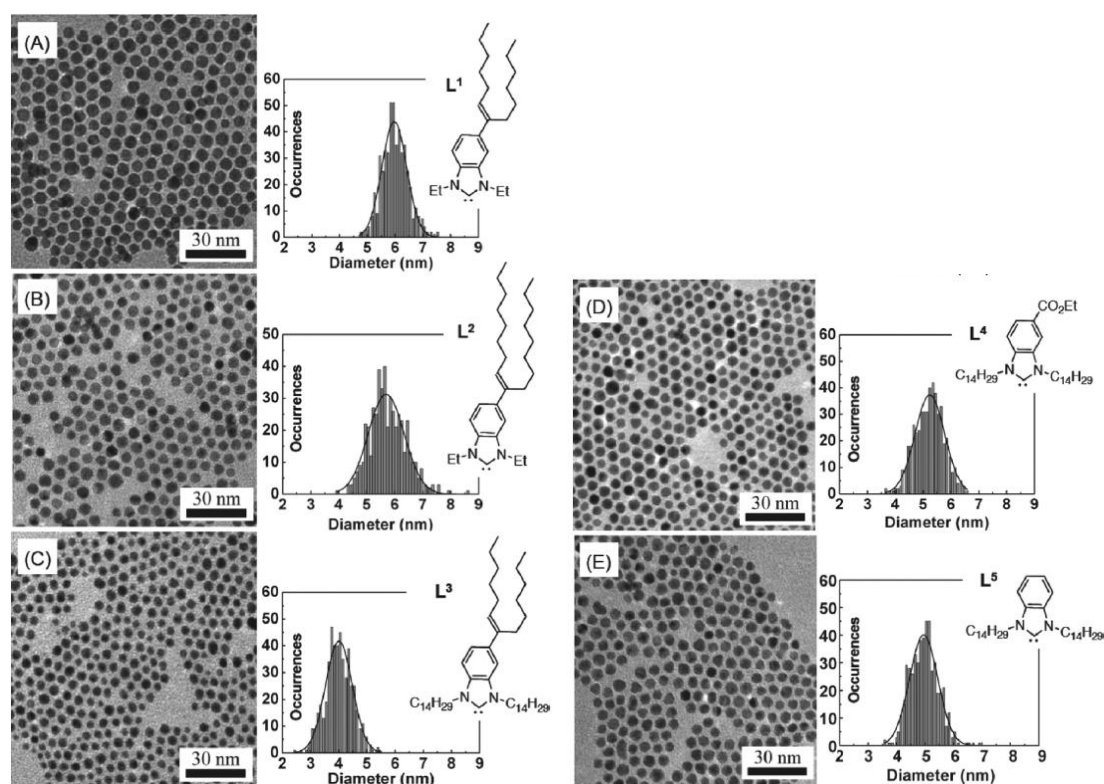


Figure I.14: TEM images and corresponding size distributions of gold nanoparticles stabilized by different NHC ligands.⁸⁴

In a follow-up paper,⁸⁵ they studied the stability of those NPs to oxygen plasma treatment compared to DDT protected NPs. They found that while DDT-AuNPs start coalescing after 60 to 80 sec exposure to oxygen plasma, NHC-AuNPs were unaffected by exposure up to 120 sec. When NHC-AuNPs were dried and exposed to dioxygen for a week, their UV-vis spectrum was similar once redissolved. NMR and MS analysis revealed the formation of a small quantity (15-20%) of Au(I) complexes. After analysis of DDT-AuNPs subjected to the same treatment, they found that only 35% of DDT remained bound

while half of what was released had been oxidized to DDS. These results clearly show a higher oxygen stability of NHC protected NPs compared to DDT-AuNPs.

I.D. Conclusion

To conclude, N-heterocyclic carbenes are relevant ligands for the stabilization of gold nanoparticles. Available in a wide range of structures, they provide remarkable stabilization due to the strong bond formed with the metal. NHC-stabilized gold nanoparticles can be synthesized by a few synthetic pathways but all have their advantages and drawback. For example, while in theory, the ligand exchange strategy enables the use of nanoparticles with a wide range of sizes and shapes, which syntheses have been described in the literature, performing the exchange requires the introduction of the free carbene if etching of the NPs is to be avoided. And free NHCs, while more stable than other carbenes, require stringent conditions to maintain their reactivity. Reduction of a NHC gold complex is a quick and easy way to obtain NHC-stabilized NPs but it requires the preliminary synthesis and isolation of the NHC-gold complex, and each time different complexes have to be synthesized to modify the properties of the NPs. Finally, the synthesis in two steps from imidazolium aurate salts enables an easier change of NHCs, as the salt is easier to synthesize than the NHC-Au complex, but could probably still be optimized.

Bibliography (Chapter I)

- (1) Faraday, M. X. The Bakerian Lecture. —Experimental Relations of Gold (and Other Metals) to Light. *Philos. Trans. R. Soc. Lond.* **1857**, *147*, 145–181.
- (2) Daniel, M.-C.; Astruc, D. Gold Nanoparticles: Assembly, Supramolecular Chemistry, Quantum-Size-Related Properties, and Applications toward Biology, Catalysis, and Nanotechnology. *Chem. Rev.* **2004**, *104* (1), 293–346.
- (3) Dykman, L. A.; Khlebtsov, N. G. Gold Nanoparticles in Biology and Medicine: Recent Advances and Prospects. *Acta Naturae* **2011**, *3* (2), 34–55.
- (4) Mellanby, J.; Anwyl-Davies, T. The Precipitation of Colloidal Gold by Cerebrospinal Fluid; the Diagnosis of Neuro-Syphilis. *Br. J. Exp. Pathol.* **1923**, *4* (3), 132–145.
- (5) *Commission Recommendation of 18 October 2011 on the Definition of Nanomaterial Text with EEA Relevance*; 32011H0696; 2011.
- (6) Image gallery: The Lycurgus Cup
http://www.britishmuseum.org/research/collection_online/collection_object_details/collection_image_gallery.aspx?assetId=36154001&objectId=61219&partId=1 (accessed Oct 22, 2018).
- (7) Hammond, J.; Bhalla, N.; Rafiee, S.; Estrela, P.; Hammond, J. L.; Bhalla, N.; Rafiee, S. D.; Estrela, P. Localized Surface Plasmon Resonance as a Biosensing Platform for Developing Countries. *Biosensors* **2014**, *4* (2), 172–188.
- (8) Willets, K. A.; Van Duyne, R. P. Localized Surface Plasmon Resonance Spectroscopy and Sensing. *Annu. Rev. Phys. Chem.* **2007**, *58* (1), 267–297.
- (9) Hutter, E.; Fendler, J. H.; Roy, D. Surface Plasmon Resonance Studies of Gold and Silver Nanoparticles Linked to Gold and Silver Substrates by 2-Aminoethanethiol and 1,6-Hexanedithiol. *J. Phys. Chem. B* **2001**, *105* (45), 11159–11168.
- (10) Sun, Y.; Xia, Y. Gold and Silver Nanoparticles: A Class of Chromophores with Colors Tunable in the Range from 400 to 750 Nm. *The Analyst* **2003**, *128* (6), 686–691.
- (11) Nikoobakht, B.; El-Sayed, M. A. Preparation and Growth Mechanism of Gold Nanorods (NRs) Using Seed-Mediated Growth Method. *Chem. Mater.* **2003**, *15* (10), 1957–1962.
- (12) Dreaden, E. C.; Alkilany, A. M.; Huang, X.; Murphy, C. J.; El-Sayed, M. A. The Golden Age: Gold Nanoparticles for Biomedicine. *Chem Soc Rev* **2012**, *41* (7), 2740–2779.
- (13) Goldmann, C.; Lazzari, R.; Paquez, X.; Boissière, C.; Ribot, F.; Sanchez, C.; Chanéac, C.; Portehault, D. Charge Transfer at Hybrid Interfaces: Plasmonics of Aromatic Thiol-Capped Gold Nanoparticles. *ACS Nano* **2015**, *9* (7), 7572–7582.
- (14) D. Sonntag, M.; M. Klingsporn, J.; B. Zrimsek, A.; Sharma, B.; K. Ruvuna, L.; Duyne, R. P. V. Molecular Plasmonics for Nanoscale Spectroscopy. *Chem. Soc. Rev.* **2014**, *43* (4), 1230–1247.
- (15) Nie, S.; Emory, S. R. Probing Single Molecules and Single Nanoparticles by Surface-Enhanced Raman Scattering. *Science* **1997**, *275* (5303), 1102–1106.
- (16) Zhao, Y.; Huang, Y.; Zhu, H.; Zhu, Q.; Xia, Y. Three-in-One: Sensing, Self-Assembly, and Cascade Catalysis of Cyclodextrin Modified Gold Nanoparticles. *J. Am. Chem. Soc.* **2016**, *138* (51), 16645–16654.
- (17) Sokolov, K.; Follen, M.; Aaron, J.; Pavlova, I.; Malpica, A.; Lotan, R.; Richards-Kortum, R. Real-Time Vital Optical Imaging of Precancer Using Anti-Epidermal Growth Factor Receptor Antibodies Conjugated to Gold Nanoparticles. *Cancer Res.* **2003**, *63* (9), 1999–2004.
- (18) Huang, X.; El-Sayed, I. H.; Qian, W.; El-Sayed, M. A. Cancer Cell Imaging and Photothermal Therapy in the Near-Infrared Region by Using Gold Nanorods. *J. Am. Chem. Soc.* **2006**, *128* (6), 2115–2120.
- (19) Deraedt, C.; Salmon, L.; Gatard, S.; Ciganda, R.; Hernandez, R.; Ruiz, J.; Astruc, D. Sodium Borohydride Stabilizes Very Active Gold Nanoparticle Catalysts. *Chem Commun* **2014**, *50* (91), 14194–14196.
- (20) Comotti, M.; Della Pina, C.; Falletta, E.; Rossi, M. Aerobic Oxidation of Glucose with Gold Catalyst: Hydrogen Peroxide as Intermediate and Reagent. *Adv. Synth. Catal.* **2006**, *348* (3), 313–316.

- (21) Prasad, B. L. V.; Stoeva, S. I.; Sorensen, C. M.; Zaikovski, V.; Klabunde, K. J. Gold Nanoparticles as Catalysts for Polymerization of Alkylsilanes to Siloxane Nanowires, Filaments, and Tubes. *J. Am. Chem. Soc.* **2003**, *125* (35), 10488–10489.
- (22) Kim, H.; Carney, R. P.; Reguera, J.; Ong, Q. K.; Liu, X.; Stellacci, F. Synthesis and Characterization of Janus Gold Nanoparticles. *Adv. Mater.* **2012**, *24* (28), 3857–3863.
- (23) Zheng, N.; Fan, J.; Stucky, G. D. One-Step One-Phase Synthesis of Monodisperse Noble-Metallic Nanoparticles and Their Colloidal Crystals. *J. Am. Chem. Soc.* **2006**, *128* (20), 6550–6551.
- (24) Turkevich, J.; Stevenson, P. C.; Hillier, J. A Study of the Nucleation and Growth Processes in the Synthesis of Colloidal Gold. *Discuss. Faraday Soc.* **1951**, *11*, 55–75.
- (25) Brust, M.; Walker, M.; Bethell, D.; Schiffrin, D. J.; Whyman, R. Synthesis of Thiol-Derivatized Gold Nanoparticles in a Two-Phase Liquid–Liquid System. *J. Chem. Soc. Chem. Commun.* **1994**, No. 7, 801–802.
- (26) Khoury, C. G.; Vo-Dinh, T. Gold Nanostars For Surface-Enhanced Raman Scattering: Synthesis, Characterization and Optimization. *J. Phys. Chem. C Nanomater. Interfaces* **2008**, *2008* (112), 18849–18859.
- (27) Liu, M.; Guyot-Sionnest, P. Mechanism of Silver(I)-Assisted Growth of Gold Nanorods and Bipyramids. *J. Phys. Chem. B* **2005**, *109* (47), 22192–22200.
- (28) Chen, J.; Saeki, F.; Wiley, B. J.; Cang, H.; Cobb, M. J.; Li, Z.-Y.; Au, L.; Zhang, H.; Kimmey, M. B.; Li; Xia, Y. Gold Nanocages: Bioconjugation and Their Potential Use as Optical Imaging Contrast Agents. *Nano Lett.* **2005**, *5* (3), 473–477.
- (29) Pettibone, J. M.; Hudgens, J. W. Gold Cluster Formation with Phosphine Ligands: Etching as a Size-Selective Synthetic Pathway for Small Clusters? *ACS Nano* **2011**, *5* (4), 2989–3002.
- (30) Sun, Y.; Jose, D.; Sorensen, C.; Klabunde, K. Alkyl and Aromatic Amines as Digestive Ripening/Size Focusing Agents for Gold Nanoparticles. *Nanomaterials* **2013**, *3* (3), 370–392.
- (31) Guo, S.; Wang, E. Synthesis and Electrochemical Applications of Gold Nanoparticles. *Anal. Chim. Acta* **2007**, *598* (2), 181–192.
- (32) Pensa, E.; Cortés, E.; Corthey, G.; Carro, P.; Vericat, C.; Fonticelli, M. H.; Benítez, G.; Rubert, A. A.; Salvarezza, R. C. The Chemistry of the Sulfur–Gold Interface: In Search of a Unified Model. *Acc. Chem. Res.* **2012**, *45* (8), 1183–1192.
- (33) Caragheorghopol, A.; Chechik, V. Mechanistic Aspects of Ligand Exchange in Au Nanoparticles. *Phys. Chem. Chem. Phys.* **2008**, *10* (33), 5029–5041.
- (34) Montalti, M.; Prodi, L.; Zaccheroni, N.; Baxter, R.; Teobaldi, G.; Zerbetto, F. Kinetics of Place-Exchange Reactions of Thiols on Gold Nanoparticles. *Langmuir* **2003**, *19* (12), 5172–5174.
- (35) Hopkinson, M. N.; Richter, C.; Schedler, M.; Glorius, F. An Overview of N-Heterocyclic Carbenes. *Nature* **2014**, *510* (7506), 485–496.
- (36) Igau, A.; Grutzmacher, H.; Baceiredo, A.; Bertrand, G. Analogous .Alpha.,.Alpha.-Bis-Carbenoid, Triply Bonded Species: Synthesis of a Stable .Lambda.3-Phosphino Carbene-.Lambda.5-Phosphaacetylene. *J. Am. Chem. Soc.* **1988**, *110* (19), 6463–6466.
- (37) Arduengo, A. J.; Harlow, R. L.; Kline, M. A Stable Crystalline Carbene. *J. Am. Chem. Soc.* **1991**, *113* (1), 361–363.
- (38) Denk, Michael K; Hatano, Ken; Ma, Martin. Nucleophilic Carbenes and the Wanzlick Equilibrium: A Reinvestigation. *Tetrahedron Lett.* **1999**, *40*, 2057–2060.
- (39) Arduengo, A. J.; Goerlich, J. R.; Marshall, W. J. A Stable Thiazol-2-Ylidene and Its Dimer. *Liebigs Ann.* **1997**, *1997* (2), 365–374.
- (40) Kelemen, Z.; Hollóczki, O.; Oláh, J.; Nyulászi, L. Oxazol-2-Ylidenes. A New Class of Stable Carbenes? *RSC Adv.* **2013**, *3* (21), 7970–7978.
- (41) Lavallo, V.; Canac, Y.; Präsang, C.; Donnadiou, B.; Bertrand, G. Stable Cyclic (Alkyl)(Amino)Carbenes as Rigid or Flexible, Bulky, Electron-Rich Ligands for Transition-Metal Catalysts: A Quaternary Carbon Atom Makes the Difference. *Angew. Chem. Int. Ed.* **2005**, *44* (35), 5705–5709.
- (42) Hahn F. Ekkehardt; Jahnke Mareike C. Heterocyclic Carbenes: Synthesis and Coordination Chemistry. *Angew. Chem. Int. Ed.* **2008**, *47* (17), 3122–3172.

- (43) Nesterov, V.; Reiter, D.; Bag, P.; Frisch, P.; Holzner, R.; Porzelt, A.; Inoue, S. NHCs in Main Group Chemistry. *Chem. Rev.* **2018**, *118*, 9678–9842.
- (44) Öfele, K. 1,3-Dimethyl-4-Imidazolinylyden-(2)-Pentacarbonylchrom Ein Neuer Übergangsmetall-Carben-Komplex. *J. Organomet. Chem.* **1968**, *12* (3), P42–P43.
- (45) Wanzlick, H.-W.; Schönherr, H.-J. Direct Synthesis of a Mercury Salt-Carbene Complex. *Angew. Chem. Int. Ed. Engl.* **1968**, *7* (2), 141–142.
- (46) Scholl, M.; Ding, S.; Lee, C. W.; Grubbs, R. H. Synthesis and Activity of a New Generation of Ruthenium-Based Olefin Metathesis Catalysts Coordinated with 1,3-Dimesityl-4,5-Dihydroimidazol-2-ylidene Ligands. *Org. Lett.* **1999**, *1* (6), 953–956.
- (47) Gatineau, D.; Goddard, J.-P.; Mouriès-Mansuy, V.; Fensterbank, L. When NHC Ligands Make a Difference in Gold Catalysis. *Isr. J. Chem.* **2013**, *53* (11–12), 892–900.
- (48) Marion, N.; Nolan, S. P. N-Heterocyclic Carbenes in Gold Catalysis. *Chem. Soc. Rev.* **2008**, *37* (9), 1776–1782.
- (49) Bender, C. F.; Widenhoefer, R. A. Room Temperature Hydroamination of N-Alkenyl Ureas Catalyzed by a Gold(I) N-Heterocyclic Carbene Complex. *Org. Lett.* **2006**, *8* (23), 5303–5305.
- (50) Iacopetta, D.; Mariconda, A.; Saturnino, C.; Caruso, A.; Palma, G.; Ceramella, J.; Muià, N.; Perri, M.; Sinicropi, M. S.; Caroleo, M. C.; Longo, P. Novel Gold and Silver Carbene Complexes Exert Antitumor Effects Triggering the Reactive Oxygen Species Dependent Intrinsic Apoptotic Pathway. *ChemMedChem* **2017**, *12* (24), 2054–2065.
- (51) Ott, L. S.; Cline, M. L.; Deetlefs, M.; Seddon, K. R.; Finke, R. G. Nanoclusters in Ionic Liquids: Evidence for N-Heterocyclic Carbene Formation from Imidazolium-Based Ionic Liquids Detected by ²H NMR. *J. Am. Chem. Soc.* **2005**, *127* (16), 5758–5759.
- (52) Baquero, E. A.; Tricard, S.; Flores, J. C.; de Jesús, E.; Chaudret, B. Highly Stable Water-Soluble Platinum Nanoparticles Stabilized by Hydrophilic N-Heterocyclic Carbenes. *Angew. Chem. Int. Ed.* **2014**, *53* (48), 13220–13224.
- (53) Asensio, J. M.; Tricard, S.; Coppel, Y.; Andrés, R.; Chaudret, B.; de Jesús, E. Synthesis of Water-Soluble Palladium Nanoparticles Stabilized by Sulfonated N-Heterocyclic Carbenes. *Chem. – Eur. J.* **2017**, *23* (54), 13435–13444.
- (54) Lara, P.; Rivada-Wheelaghan, O.; Conejero, S.; Poteau, R.; Philippot, K.; Chaudret, B. Ruthenium Nanoparticles Stabilized by N-Heterocyclic Carbenes: Ligand Location and Influence on Reactivity. *Angew. Chem. Int. Ed.* **2011**, *50* (50), 12080–12084.
- (55) Lee, C. K.; Vasam, C. S.; Huang, T. W.; Wang, H. M. J.; Yang, R. Y.; Lee, C. S.; Lin, I. J. B. Silver(I) N-Heterocyclic Carbenes with Long N-Alkyl Chains. *Organometallics* **2006**, *25* (15), 3768–3775.
- (56) Serpell, C. J.; Cookson, J.; Thompson, A. L.; Brown, C. M.; Beer, P. D. Haloaurate and Halopalladate Imidazolium Salts: Structures, Properties, and Use as Precursors for Catalytic Metal Nanoparticles. *Dalton Trans* **2013**, *42* (5), 1385–1393.
- (57) Vignolle, J.; Tilley, T. D. N-Heterocyclic Carbene-Stabilized Gold Nanoparticles and Their Assembly into 3D Superlattices. *Chem. Commun.* **2009**, No. 46, 7230–7232.
- (58) Hurst, E. C.; Wilson, K.; Fairlamb, I. J. S.; Chechik, V. N-Heterocyclic Carbene Coated Metal Nanoparticles. *New J. Chem.* **2009**, *33* (9), 1837–1840.
- (59) Li, J.; Zhang, B.; Médard, G.; Seitsonen, A. P.; Haag, F.; Allegretti, F.; Reichert, J.; Kuster, B.; Barth, J. V.; Papageorgiou, A. C. N-Heterocyclic Carbenes on the Close Packed Coinage Metal Surfaces: Bis-Carbene Metal Adatom Bonding Scheme of Monolayer Films on Au, Ag and Cu. *Chem. Sci.* **2017**, *8*, 8301–8308.
- (60) Larrea, C. R.; Baddeley, C. J.; Narouz, M. R.; Mosey, N. J.; Horton, J. H.; Crudden, C. M. N-Heterocyclic Carbene Self-Assembled Monolayers on Copper and Gold: Dramatic Effect of Wingtip Groups on Binding, Orientation and Assembly. *ChemPhysChem* **2017**, *18* (24), 3536–3539.
- (61) Crudden, C. M.; Horton, J. H.; Narouz, M. R.; Li, Z.; Smith, C. A.; Munro, K.; Baddeley, C. J.; Larrea, C. R.; Drevniok, B.; Thanabalasingam, B.; McLean, A. B.; Zenkina, O. V.; Ebralidze, I. I.; She, Z.; Kraatz, H.-B.; Mosey, N. J.; Saunders, L. N.; Yagi, A. Simple Direct Formation of Self-Assembled N-Heterocyclic Carbene Monolayers on Gold and Their Application in Biosensing. *Nat. Commun.* **2016**, *7*, 12654.

- (62) Crudden, C. M.; Horton, J. H.; Ebralidze, I. I.; Zenkina, O. V.; McLean, A. B.; Drevniok, B.; She, Z.; Kraatz, H.-B.; Mosey, N. J.; Seki, T.; Keske, E. C.; Leake, J. D.; Rousina-Webb, A.; Wu, G. Ultra Stable Self-Assembled Monolayers of N-Heterocyclic Carbenes on Gold. *Nat. Chem.* **2014**, *6* (5), 409–414.
- (63) Stephens, L.; Padmos, J. D.; Narouz, M. R.; Al-Rashed, A.; Li, C.-H.; Payne, N.; Zamora, M.; Crudden, C. M.; Mauzeroll, J.; Horton, J. H. The Structural and Electrochemical Effects of N-Heterocyclic Carbene Monolayers on Magnesium. *J. Electrochem. Soc.* **2018**, *165* (13), G139–G145.
- (64) Qi, S.; Ma, Q.; He, X.; Tang, Y. Self-Assembled Monolayers of N-Heterocyclic Carbene on Gold: Stability under Ultrasonic Circumstance and Computational Study. *Colloids Surf. Physicochem. Eng. Asp.* **2018**, *538*, 488–493.
- (65) DeJesus, J. F.; Trujillo, M. J.; Camden, J. P.; Jenkins, D. M. N-Heterocyclic Carbenes as a Robust Platform for Surface-Enhanced Raman Spectroscopy. *J. Am. Chem. Soc.* **2018**, *140* (4), 1247–1250.
- (66) Li, Z.; Narouz, M. R.; Munro, K.; Hao, B.; Crudden, C. M.; Horton, J. H.; Hao, H. Carboxymethylated Dextran-Modified N-Heterocyclic Carbene Self-Assembled Monolayers on Gold for Use in Surface Plasmon Resonance Biosensing. *ACS Appl. Mater. Interfaces* **2017**, *9* (45), 39223–39234.
- (67) Weidner, T.; Baio, J. E.; Mundstock, A.; Große, C.; Karthäuser, S.; Bruhn, C.; Siemeling, U. NHC-Based Self-Assembled Monolayers on Solid Gold Substrates. *Aust. J. Chem.* **2011**, *64* (8), 1177–1179.
- (68) Rodríguez-Castillo, M.; Laurencin, D.; Tielens, F.; van der Lee, A.; Clément, S.; Guari, Y.; Richeter, S. Reactivity of Gold Nanoparticles towards N-Heterocyclic Carbenes. *Dalton Trans.* **2014**, *43* (16), 5978–5982.
- (69) Rodríguez-Castillo, M.; Lugo-Preciado, G.; Laurencin, D.; Tielens, F.; van der Lee, A.; Clément, S.; Guari, Y.; López-de-Luzuriaga, J. M.; Monge, M.; Remacle, F.; Richeter, S. Experimental and Theoretical Study of the Reactivity of Gold Nanoparticles Towards Benzimidazole-2-Ylidene Ligands. *Chem. - Eur. J.* **2016**, *22* (30), 10446–10458.
- (70) Chang, K.; Chen, J. G.; Lu, Q.; Cheng, M.-J. Quantum Mechanical Study of N-Heterocyclic Carbene Adsorption on Au Surfaces. *J. Phys. Chem. A* **2017**, *121* (13), 2674–2682.
- (71) Wang, G.; Rühling, A.; Amirjalayer, S.; Knor, M.; Ernst, J. B.; Richter, C.; Gao, H.-J.; Timmer, A.; Gao, H.-Y.; Doltsinis, N. L.; Glorius, F.; Fuchs, H. Ballbot-Type Motion of N-Heterocyclic Carbenes on Gold Surfaces. *Nat. Chem.* **2017**, *9*, 152–156.
- (72) Richter, C.; Schaepe, K.; Glorius, F.; Ravoo, B. J. Tailor-Made N-Heterocyclic Carbenes for Nanoparticle Stabilization. *Chem. Commun.* **2014**, *50* (24), 3204–3207.
- (73) Ferry, A.; Schaepe, K.; Tegeder, P.; Richter, C.; Chepiga, K. M.; Ravoo, B. J.; Glorius, F. Negatively Charged N-Heterocyclic Carbene-Stabilized Pd and Au Nanoparticles and Efficient Catalysis in Water. *ACS Catal.* **2015**, *5* (9), 5414–5420.
- (74) Cao, Z.; Kim, D.; Hong, D.; Yu, Y.; Xu, J.; Lin, S.; Wen, X.; Nichols, E. M.; Jeong, K.; Reimer, J. A.; Yang, P.; Chang, C. J. A Molecular Surface Functionalization Approach to Tuning Nanoparticle Electrocatalysts for Carbon Dioxide Reduction. *J. Am. Chem. Soc.* **2016**, *138* (26), 8120–8125.
- (75) Man, R. W. Y.; Li, C.-H.; MacLean, M. W. A.; Zenkina, O. V.; Zamora, M. T.; Saunders, L. N.; Rousina-Webb, A.; Nambo, M.; Crudden, C. M. Ultrastable Gold Nanoparticles Modified by Bidentate N-Heterocyclic Carbene Ligands. *J. Am. Chem. Soc.* **2018**, *140* (5), 1576–1579.
- (76) Huang, R. T. W.; Wang, W. C.; Yang, R. Y.; Lu, J. T.; Lin, I. J. B. Liquid Crystals of Gold(I) N-Heterocyclic Carbene Complexes. *Dalton Trans.* **2009**, No. 35, 7121–7131.
- (77) MacLeod, M. J.; Johnson, J. A. PEGylated N-Heterocyclic Carbene Anchors Designed To Stabilize Gold Nanoparticles in Biologically Relevant Media. *J. Am. Chem. Soc.* **2015**, *137* (25), 7974–7977.
- (78) Salorinne, K.; Man, R. W. Y.; Li, C.-H.; Taki, M.; Nambo, M.; Crudden, C. M. Water-Soluble N-Heterocyclic Carbene-Protected Gold Nanoparticles: Size-Controlled Synthesis, Stability, and Optical Properties. *Angew. Chem.* **2017**, *129* (22), 6294–6298.
- (79) Narouz, M. R.; Li, C.-H.; Nazemi, A.; Crudden, C. M. Amphiphilic N-Heterocyclic Carbene-Stabilized Gold Nanoparticles and Their Self-Assembly in Polar Solvents. *Langmuir* **2017**, *33* (50), 14211–14219.

- (80) Young, A. J.; Serpell, C. J.; Chin, J. M.; Reithofer, M. R. Optically Active Histidin-2-Ylidene Stabilised Gold Nanoparticles. *Chem. Commun.* **2017**, 53 (92), 12426–12429.
- (81) Zhukhovitskiy, A. V.; Mavros, M. G.; Van Voorhis, T.; Johnson, J. A. Addressable Carbene Anchors for Gold Surfaces. *J. Am. Chem. Soc.* **2013**, 135 (20), 7418–7421.
- (82) Li, Z.; Munro, K.; Ebralize, I. I.; Narouz, M. R.; Padmos, J. D.; Hao, H.; Crudden, C. M.; Horton, J. H. N-Heterocyclic Carbene Self-Assembled Monolayers on Gold as Surface Plasmon Resonance Biosensors. *Langmuir* **2017**, 33 (49), 13936–13944.
- (83) Li, Z.; Munro, K.; Narouz, M. R.; Lau, A.; Hao, H.; Crudden, C. M.; Horton, J. H. Self-Assembled N-Heterocyclic Carbene-Based Carboxymethylated Dextran Monolayers on Gold as a Tunable Platform for Designing Affinity-Capture Biosensor Surfaces. *ACS Appl. Mater. Interfaces* **2018**, 10 (21), 17560–17570.
- (84) Ling, X.; Roland, S.; Pileni, M.-P. Supracrystals of N-Heterocyclic Carbene-Coated Au Nanocrystals. *Chem. Mater.* **2015**, 27 (2), 414–423.
- (85) Ling, X.; Schaeffer, N.; Roland, S.; Pileni, M.-P. Superior Oxygen Stability of N-Heterocyclic Carbene-Coated Au Nanocrystals: Comparison with Dodecanethiol. *Langmuir* **2015**, 31 (47), 12873–12882.

CHAPTER II: SYNTHESIS OF N-HETEROCYCLIC CARBENE-CAPPED GOLD NANOPARTICLES FROM IMIDAZOLIUM SALTS

II.A. Nanoparticles from imidazolium haloaurate salts and NaBH₄

For the first part of our work, we based ourselves on the synthesis developed by Serpell *et al.*¹ As stated in the previous chapter, they used a gold(III) imidazolium complex which is then deprotonated and reduced to obtain stable nanoparticles (Figure II.1).

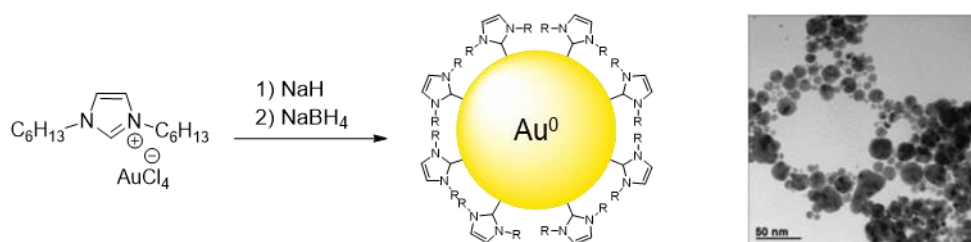


Figure II.1: Schematic representation of a synthesis starting from an haloaurate imidazolium complex and gold nanoparticles obtained by Serpell *et al.*¹

The two main goals of our study were to modify the synthesis in order to, hopefully, control the size (and maybe even the shape) of the nanoparticles and to confirm without ambiguity the presence of NHCs at the surface. Part of this work has already been the subject of a publication in Dalton Transactions.²

II.A.1. Imidazolium haloaurate salts

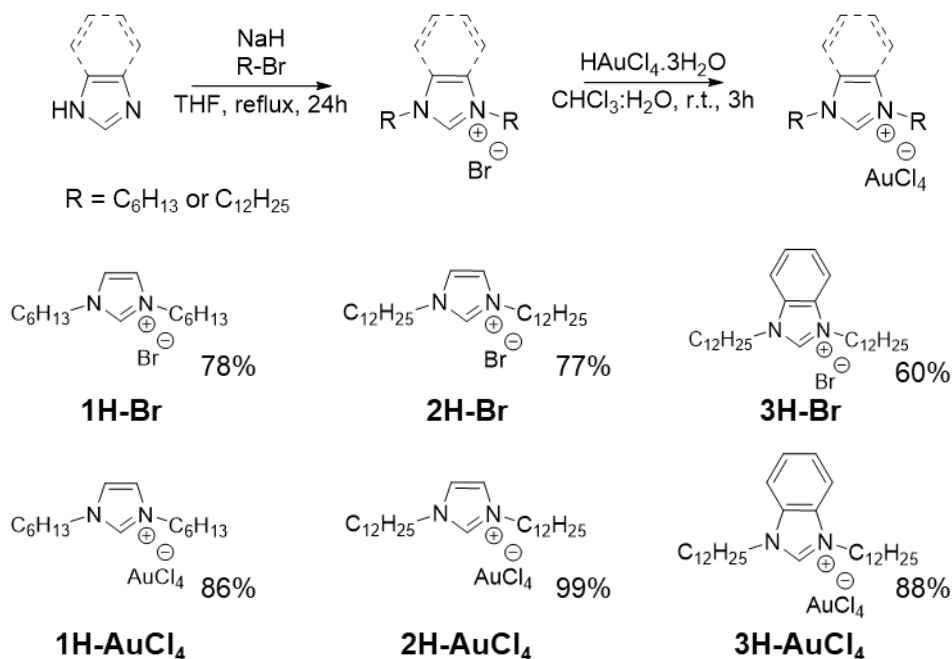
II.A.1.a. Synthesis

In order to study the influence of the ligand on the NPs synthesis, 3 (benz)imidazolium bromide salts were synthesized: 1,3-dihexylimidazolium bromide (**1H-Br**), 1,3-didodecylimidazolium bromide (**2H-Br**) and 1,3-didodecylbenzimidazolium bromide (**3H-Br**).

All were synthesized following a reported procedure.³ (Benz)imidazole was deprotonated in situ by NaH at 0°C in THF, the desired alkylbromide was then introduced in the reaction medium which was refluxed for 24h to obtain the bisalkylated product in good yields (up to 78%) (Scheme II.1).

1H-Br was obtained as a clear oil whereas **2H-Br** and **3H-Br** were obtained as white powders allowing for easier handling.

(Benz)imidazolium AuCl_4 complexes were synthesized from the corresponding (benz)imidazolium bromide and $\text{HAuCl}_4 \cdot 3\text{H}_2\text{O}$, by a biphasic anion metathesis, in good yields (Scheme II.1). Compounds were obtained as either a dark orange oil (**1H-AuCl₄**) or a dark orange powder (**2** and **3H-AuCl₄**).



Scheme II.1: Synthetic pathway to imidazolium salts and obtained imidazolium salts with corresponding yields.

II.A.1.b. Crystallographic analysis

X-ray quality crystals of **2H-AuCl₄** and **3H-AuCl₄** were obtained by slow diffusion of ethanol into a concentrated solution of the complexes in chloroform whereas **1H-AuX₄** was obtained as an orange oil.

Figure II.2 displays the structures of **2H-AuCl₄** and **3H-AuCl₄**. These structures have been deposited at Cambridge Crystallographic Data Centre (CCDC) under the references 1548811 and 1548812.² Complexes **2H-AuCl₄** and **3H-AuCl₄** both crystallize in a monoclinic system ($P2_{1/c}$ and $P2_{1/n}$ spaces respectively) with alternating anion and cation layers. This arrangement, which has already been described in the literature,¹ is probably due to the stacking of the long alkyl chains. The anionic layer presents, for both compounds, mixed species in which about a quarter of the halogen atoms are bromine which leads to a $\text{AuCl}_{4-x}\text{Br}_x$ ($x \sim 1$) composition. The bromine atoms come from the last step of the synthesis where **2H-Br** or **3H-Br** is reacted with $\text{HAuCl}_4 \cdot 3\text{H}_2\text{O}$. That is why in the rest of this manuscript, complexes **1H-AuCl₄**, **2H-AuCl₄** and **3H-AuCl₄** will be called **1H-AuX₄**, **2H-AuX₄** and **3H-AuX₄**.

Inside the anionic layer, the AuX_4^- ions have a square planar geometry with an average Au-X distance of 2.33 Å. The anions are well separated with a shortest Au-Au distance of 5.7710(2) Å for **2H-AuX₄** and 6.1637(1) Å for **3H-AuX₄**, which eliminates the possibility of aurophilic interactions.⁴

The Au...X interionic distance of 3.494(1) and 3.859(1) for **2H-AuX₄** and **3H-AuX₄** respectively corresponds to corner to face contacts as already reported in the literature for some compounds.^{1,5}

In both structures, ligands **2H** and **3H** are organized in a head-to-tail manner. Aliphatic chains present intermolecular hydrophobic interactions, the shortest C...C distance being 3.925(8) Å for **2H-AuX₄** and 3.63(1) Å for **3H-AuX₄**. These hydrophobic interactions are likely the main driving force of the crystallization.

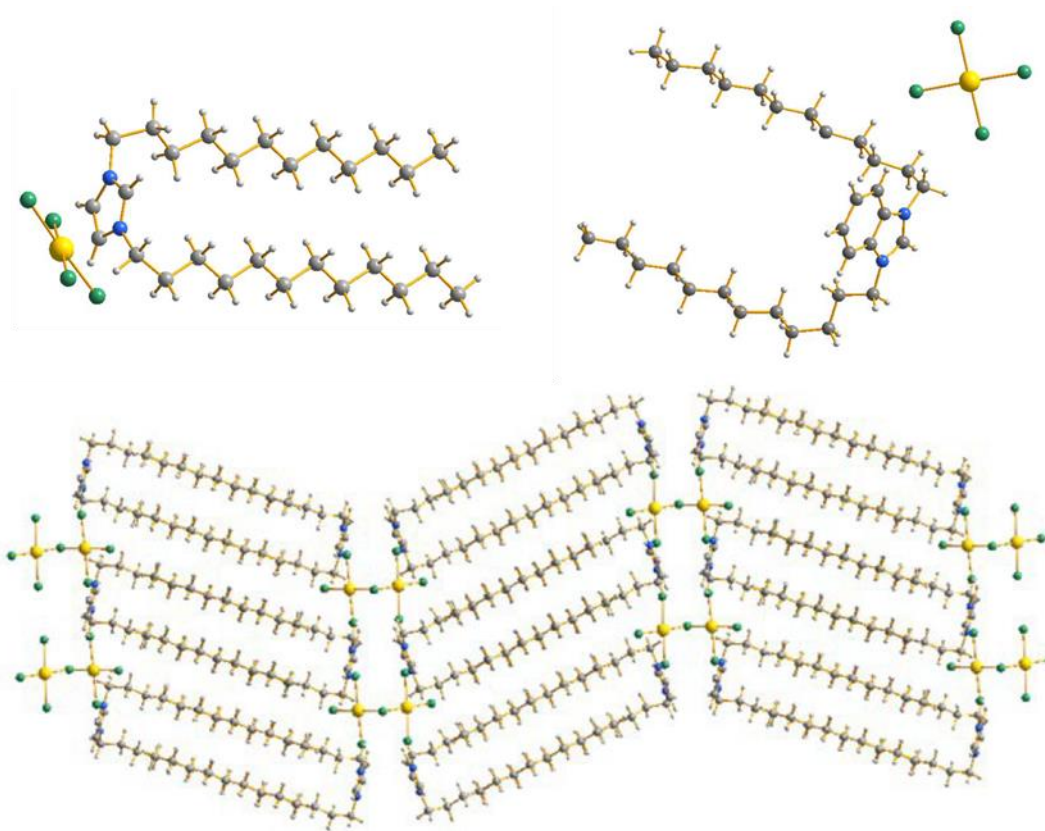


Figure II.2: Molecular structure of **2H-AuX₄** and **3H-AuX₄**, and extended structure of **2H-AuX₄** (color code: Au = yellow, Cl/Br = green, N = blue, C = grey, H = light grey).²

II.A.2. Nanoparticles synthesis

II.A.2.a. Synthesis with NaH

II.A.2.a.i. Effect of the ligand

Nanoparticles of 3.2 ± 0.8 nm in diameter were obtained when following the Serpell synthesis.¹ **1H-AuX₄** was dissolved in toluene, NaH was added at 0°C leading to a discoloration of the solution (from orange to transparent). Finally, an aqueous solution of NaBH₄ was injected and the solution turned bright red. When using **2H-AuX₄** instead of **1H-AuX₄**, nanoparticles of 4.8 ± 1.1 nm were obtained, while **3H-AuX₄** yielded 4.4 ± 1.2 nm nanoparticles (Figure II.3).

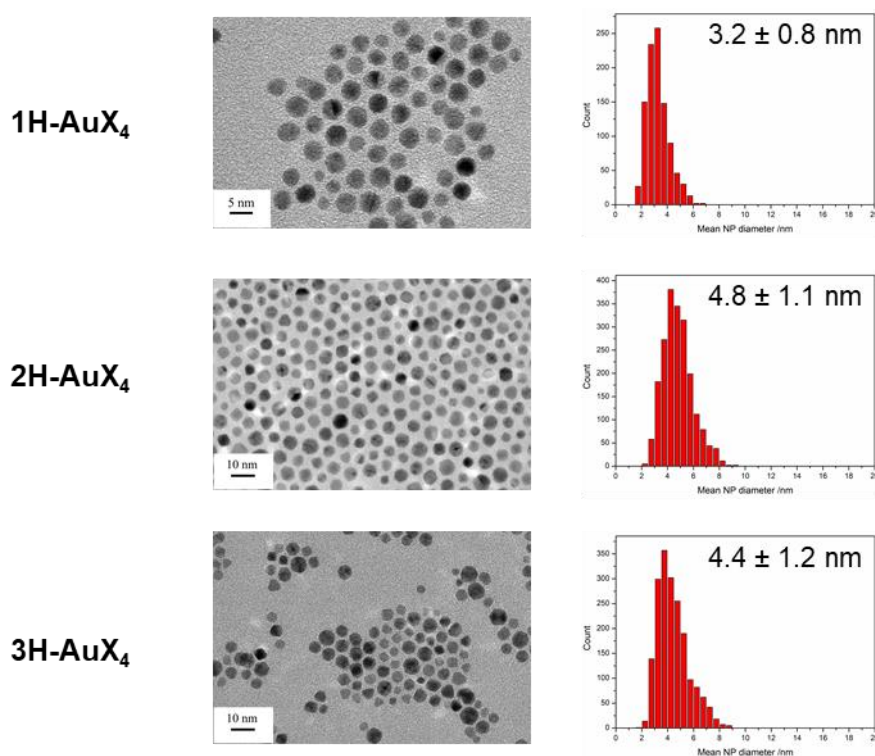


Figure II.3: Nanoparticles obtained from **1H-AuX₄**, **2H-AuX₄** and **3H-AuX₄** after successive addition of NaH and NaBH₄ (solvent toluene: H₂O), and corresponding distributions.

It can be noted that the nanoparticles, we obtained using the same ligand as Serpell *et al.* are much smaller and less polydisperse than the ones they described (16.6 ± 6.5 nm).¹

Also, using longer alkyl chains on the ligand yields larger nanoparticles. It can be suggested that longer chains are bulkier ligands and because of their bulkiness, less molecules find space at the surface leading to bigger nanoparticles.

II.A.2.a.ii. Effect of the ligand to gold ratio

Ligand to gold ratio is also known to have an influence on the size of gold nanoparticles and is a common strategy to control the size of nanoparticles.^{6,7} This is why excess (benz)imidazolium bromide was added to each type of synthesis (Figure II.4).

In the case of **2** and **3**, both with C₁₂ chains, the size of the nanoparticles decreased as expected (Table II.1). Indeed, increasing the quantity of available ligand led to the formation of smaller nanoparticles. This effect is well-known for citrate or thiols stabilized nanoparticles^{6,7} but it was the first time that it was evidenced for NHC-stabilized gold nanoparticles.

Additional **1H-Br**, on the other hand, led to slightly larger particles. It is unclear why.

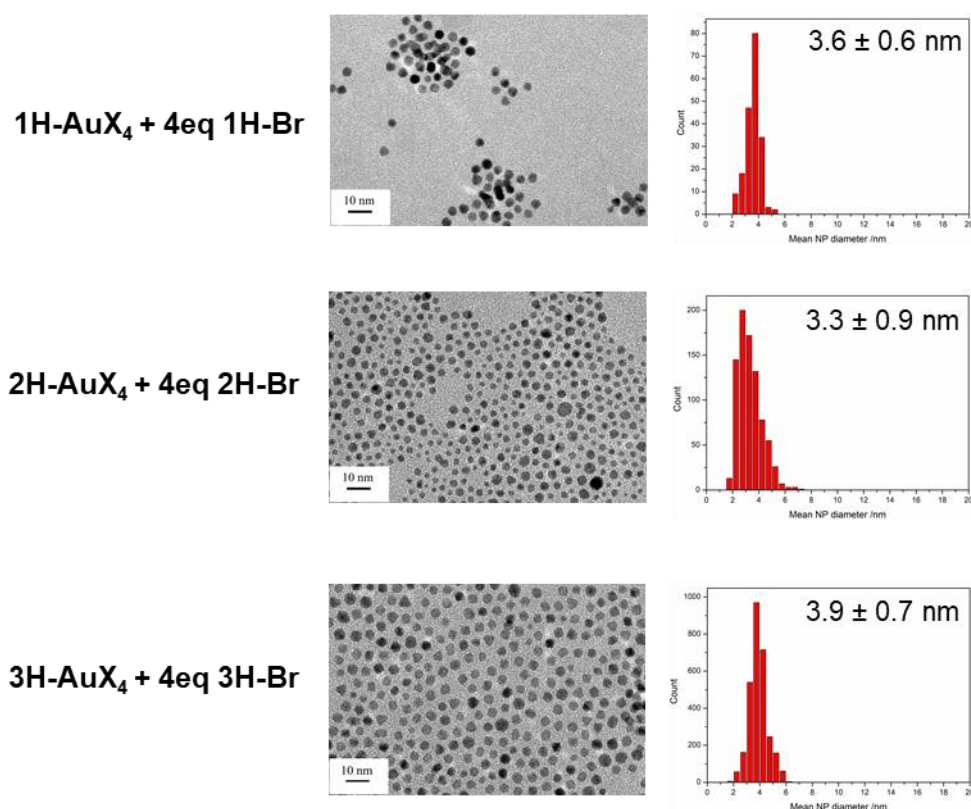


Figure II.4: Nanoparticles obtained from **1H-AuX₄**, **2H-AuX₄** and **3H-AuX₄**, and 4 equivalents of **1H-Br**, **2H-Br** and **3H-Br** respectively, after successive addition of NaH and NaBH₄ (solvent toluene: H₂O), and corresponding distributions.

Table II.1 : Average particle sizes (nm), as measured by TEM, for nanoparticles obtained with or without 4 equivalents of (benz)imidazolium bromide.

Precursors	NaH and NaBH ₄
1H-AuX₄	3.2 ± 0.8
1H-AuX₄ + 4 1H-Br	3.6 ± 0.6
2H-AuX₄	4.8 ± 1.1
2H-AuX₄ + 4 2H-Br	3.3 ± 0.9
3H-AuX₄	4.4 ± 1.2
3H-AuX₄ + 4 3H-Br	3.9 ± 0.7

II.A.2.b. Synthesis without NaH

Attempts were made to characterize, by ¹H NMR, the formation of the NHC in the first step. However, after addition of NaH, no deprotonation could be observed. As a result, we questioned the necessity of the first step and tested the synthesis in the absence of NaH. It can be noted that, in their paper, Serpell *et al.*¹ tested a synthesis without NaH starting from **1H-AuX₄** and did not obtain gold nanoparticles. However, when attempting the same synthesis from the corresponding palladium precursor, they obtained nanoparticles which, they concluded, were stabilized by imidazolium.

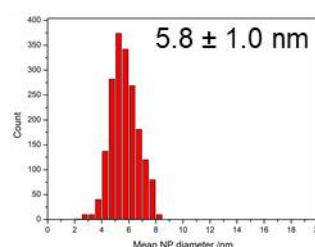
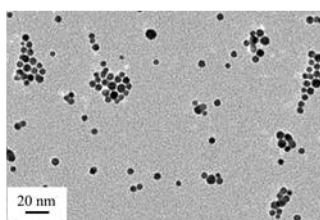
II.A.2.b.i. Effect of the ligand

When the synthesis was replicated, we did not obtain nanoparticles from **1H-AuX₄** without NaH either. However, when using only NaBH₄ on **2H-AuX₄** and **3H-AuX₄**, both gave stable nanoparticles (Figure II.5). The obtained NPs are of a larger diameter than with NaH (5.8 ± 1.0 nm and 4.9 ± 1.1 nm respectively). This means that the addition of a base is not necessary in the synthesis of nanoparticles starting from haloaurate salts, but it does have an influence on the size of the NPs. The binding mode of the ligand on the surface (covalent, electrostatic, etc.) will be further discussed in “Surface analysis” below.

1H-AuX₄

No NPs

2H-AuX₄



3H-AuX₄

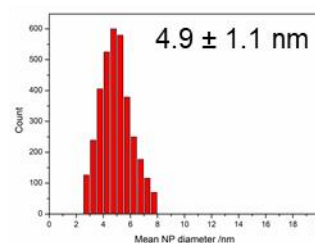
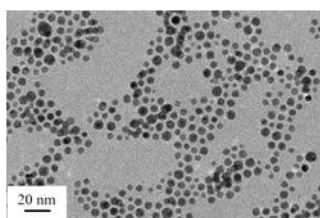


Figure II.5: Nanoparticles obtained from **1H-AuX₄**, **2H-AuX₄** and **3H-AuX₄**, after addition of NaBH₄ only (solvent toluene: H₂O), and corresponding distributions.

II.A.2.b.ii. Effect of the ligand to gold ratio

Once again, excess (benz)imidazolium bromide was added to each type of synthesis (Figure II.6). As was the case in the synthesis using NaH, adding **2H-Br** or **3H-Br** to an NaH-free synthesis yielded smaller NPs (from 5.8 ± 1.0 to 4.0 ± 0.9 nm and 4.9 ± 1.1 to 3.6 ± 0.8 nm respectively). In the case of **1H-Br**, the effect is even more dramatic as adding imidazolium bromide yielded stable particles (4.1 ± 1.0 nm) when there was no NPs without it.

It can be noted that for **1** and **2**, the synthesis using only NaBH₄ systematically yielded larger particles than the one using NaH regardless of the presence of imidazolium bromide or not (Table II.2). On the other hand, for **3**, when adding an excess of **3H-Br**, the obtained nanoparticles are slightly smaller for the NaH-free synthesis. Once again, the reason for this difference in behavior is unclear.

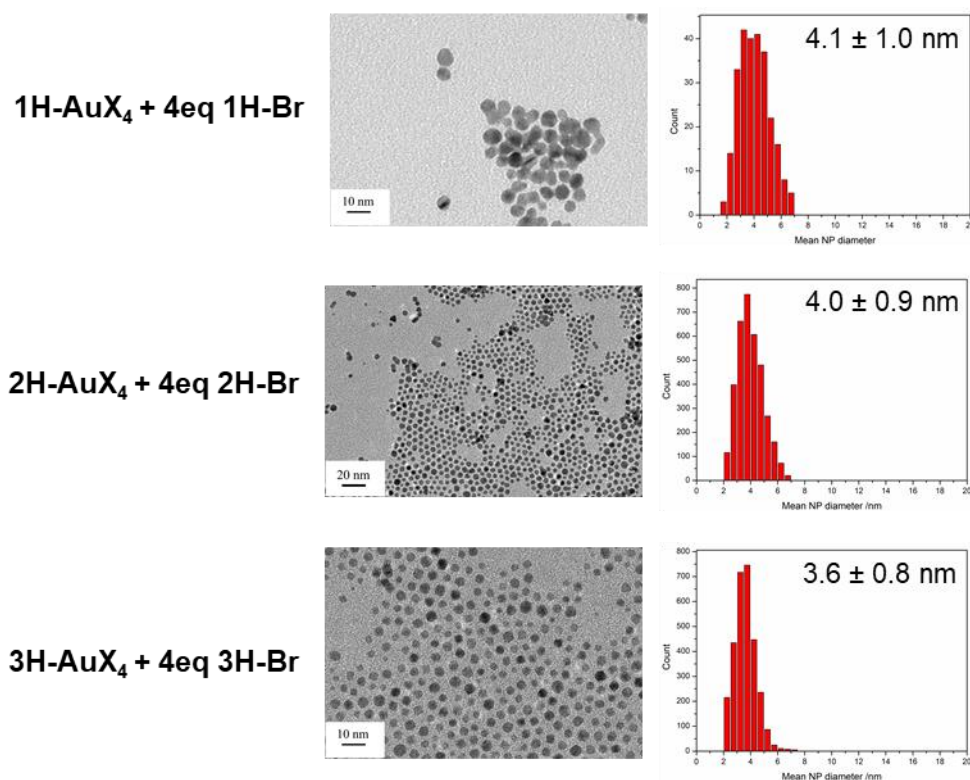


Figure II.6: Nanoparticles obtained from **1H-AuX₄**, **2H-AuX₄** and **3H-AuX₄**, and 4 equivalents of **1H-Br**, **2H-Br** and **3H-Br** respectively, after addition of NaBH₄ only (solvent toluene: H₂O), and corresponding distributions.

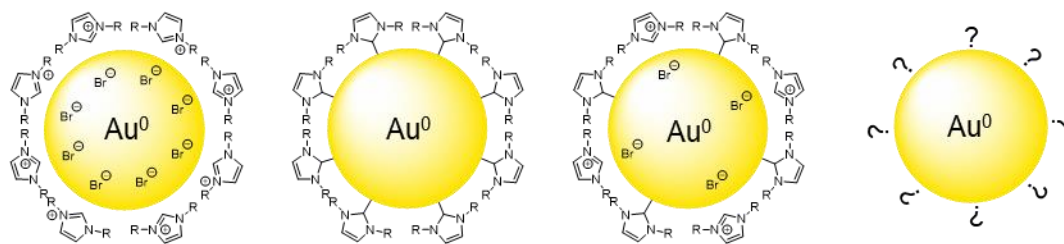
Table II.2: Average particle sizes (nm), as measured by TEM, for nanoparticles obtained with or without NaH and with or without 4 additional equivalents of (benz)imidazolium bromide.

Precursors	NaH and NaBH ₄	NaBH ₄ only
1H-AuX₄	3.2 ± 0.8	Not stable
1H-AuX₄ + 4 1H-Br	3.6 ± 0.6	4.1 ± 1.0
2H-AuX₄	4.8 ± 1.1	5.8 ± 1.0
2H-AuX₄ + 4 2H-Br	3.3 ± 0.9	4.0 ± 0.9
3H-AuX₄	4.4 ± 1.2	4.9 ± 1.1
3H-AuX₄ + 4 3H-Br	3.9 ± 0.7	3.6 ± 0.8

II.A.3. Surface analysis

In their analysis, Serpell *et al.*¹ concluded that since NaH was necessary to obtain stable nanoparticles, the stabilizing ligands had to be carbenes. And they concluded, in the case of palladium, that imidazoliums were the stabilizing ligands if NaH wasn't used. However, we found that addition of a strong base was not necessary to give stable gold nanoparticles. This begs the question: what is at the surface of our nanoparticles? Are there only imidazoliums stabilizing by electrostatic interaction? Are

there only N-heterocyclic carbenes covalently bound to the surface suggesting that sodium borohydride is enough of a base to deprotonate imidazolium molecules? Is it a mix of both interaction? Or is it another type of stabilization entirely? (Scheme II.2)



Scheme II.2: Possible stabilization modes of the nanoparticles.

In order to answer these questions, we characterized the purified nanoparticles by mass spectrometry, IR spectroscopy, NMR and XPS.

II.A.3.a. MS analysis

The nanoparticles were precipitated with ethanol and centrifuged. Then the supernatant was analyzed by mass spectrometry (MS, ESI⁺) (Figure II.7). The presence of [Au(NHC)₂]⁺ was evidenced.

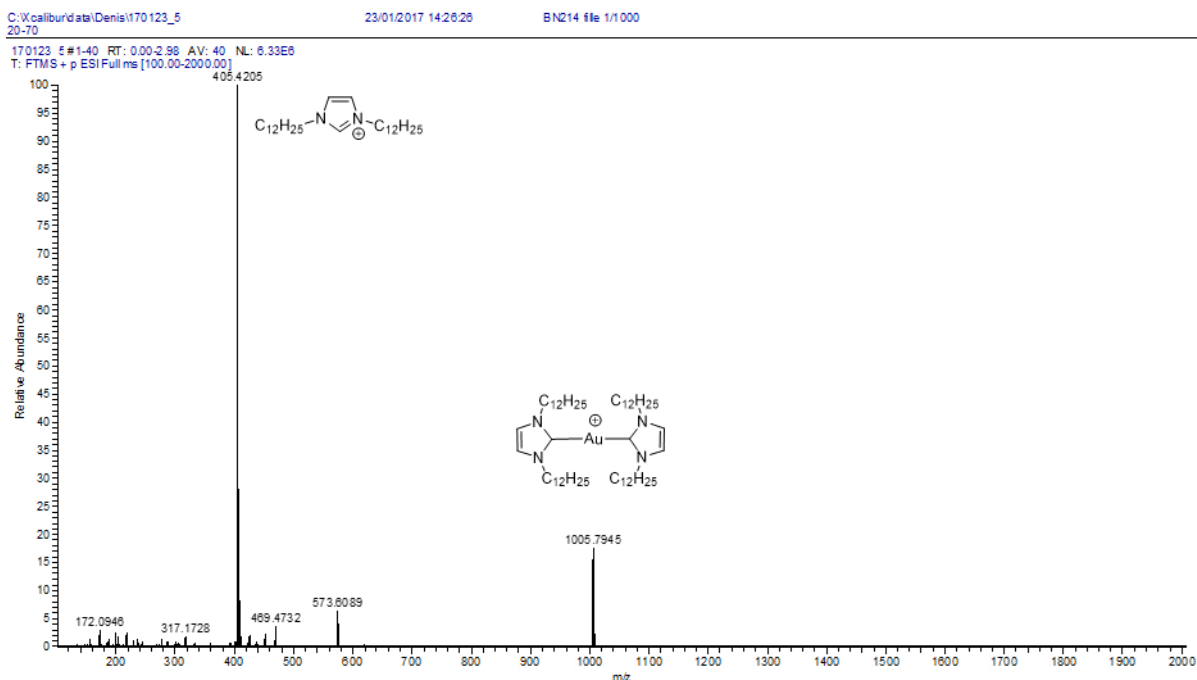
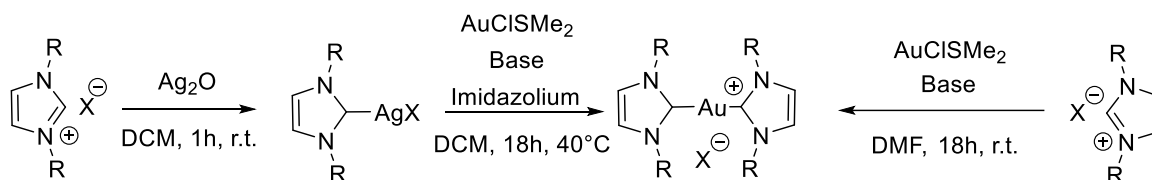


Figure II.7: Mass spectrum (ESI⁺) of a NPs synthesis supernatant.

In this complex, the NHC is covalently bound to the gold atom. It is usually synthesized by transmetalation from a silver complex and addition of a free carbene generated in situ,⁸ but examples can be found in the literature of deprotonation in situ of 2 equivalents of imidazolium before addition

of gold⁹ (Scheme II.3). However, in our synthesis no clear base is present; only imidazolium, gold and NaBH₄. As a result, we think that sodium borohydride is enough of a base to form this complex, which could be one of the intermediates in the synthesis of gold nanoparticles. Indeed, as seen in Chapter I, Crudden *et coll.* were able to synthesize AuNPs starting from such a [Au(NHC)₂]⁺ complex. The formation of this complex is also a strong indicator that NHCs are generated at some point during the synthesis and thus could be at the surface of the NPs.



Scheme II.3: Usual synthesis pathways for [Au(NHC)₂]⁺X⁻.

II.A.3.b. NMR analysis

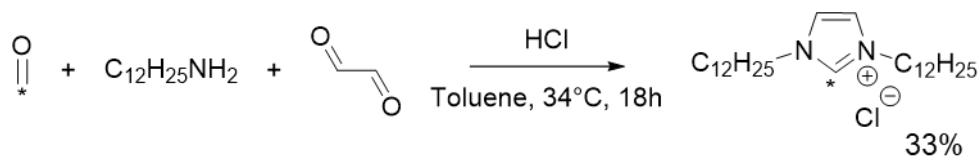
II.A.3.b.i. Liquid state NMR

The centrifuged nanoparticles were concentrated and analyzed by liquid ¹H NMR. No signal corresponding to the proton of the free imidazolium was observed. However, no signal was detected in the 8 to 4 ppm region where we would normally see the signal for the protons on the aromatic backbone and in alpha of the nitrogen atoms. This is most likely due to the broadening of the signal when molecules are close to the NP surface, due to the lower rotational mobility of the ligands when attached to the surface, and their distribution on the NP's surface. As a result, liquid NMR was inconclusive.

II.A.3.b.ii. Solid state NMR

Attempts were also made to characterize the NPs by solid state NMR, as it had already been used in the literature to show functionalization by NHCs of metallic NPs.^{10–13}

In order to have a better signal, a ¹³C marked imidazolium at the C2 position was synthesized. 100 mg of 100% ¹³C marked paraformaldehyde were mixed with 400 mg of regular paraformaldehyde in order to obtain an isotope enrichment of 20%. It was then mixed in a one pot reaction with glyoxal, dodecylamine and hydrochloric acid (Scheme II.4). After evaporation of the solvent, the product, through several precipitation processes, was obtained pure as a white powder in 33% yield (2.5 g of product).



Scheme II.4: Synthetic pathway to the marked imidazolium.

The marked imidazolium was then successfully used to synthesize nanoparticles which were centrifuged and dried. Unfortunately, technical issues made the solid-state NMR analysis impossible. Indeed, due to an absence of rotation of the rotor, no signal could be obtained. Our hypothesis is that the long alkyl chain gave a slightly oil like character to the sample that made it unsuitable for analysis.

II.A.3.c. IR analysis

IR analysis was also carried out on the centrifuged nanoparticles and compared to the IR spectra of **2H-AuX₄** and **2H-Br** (Figure II.8).

We observe a few differences when comparing the FTIR spectra of the precursors and the nanoparticles. The spectra of **2H-Br** and **2H-AuX₄** correspond to data available in the literature¹⁴ and are nearly identical, except for 2 bands which present a slight shift (from 1636 to 1616 cm^{-1} and from 773 to 757 cm^{-1}). However, the nanoparticles spectrum is very different as a new band appears at 1410 cm^{-1} and bands at 1616 and 1563 cm^{-1} are no longer visible. Those bands are located in the $\nu(\text{C}=\text{N})$ and $\nu(\text{C}=\text{C})$ stretching region of the aromatic cycle of the imidazolium. These differences have already been observed in the literature¹⁵ and have been suggested to confirm the NHCs' formation and their coordination to the gold surface. Moreover, we can stress that the $\nu(\text{C}-\text{H})$ stretching vibration, located around 3270 cm^{-1} , which corresponds to the imidazolium proton, is not visible on any of the 3 samples probably due to its expected very low intensity.

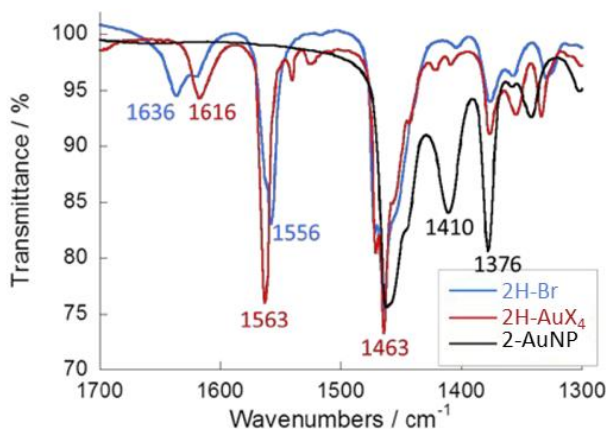


Figure II.8: IR spectra of **2H-Br** (blue trace), **2H-AuX₄** (red trace) and gold nanoparticles prepared from **2H-AuX₄** (black trace).

II.A.3.d. XPS analysis

While IR and MS gave indications that NHCs could be at the surface, the determining analysis was X-ray photoelectron spectroscopy.

X-ray photoelectron spectroscopy (XPS) was used to study the carbon-gold interaction at the nanoparticles' surface. XPS spectra are obtained by irradiating a material (placed in a high vacuum chamber) with a beam of X-rays while simultaneously measuring the kinetic energy and number of electrons that escape from the analyzed surface (up to 10 nm depth). As a result, XPS is a technique able to determine the chemical state of an analyzed surface, while giving a precise elementary composition. This technique is routinely used as a characterization tool in several fields (sensor, corrosion, catalysis). In the case of nanoparticles, XPS can be used to determine not only the integrity of the ligand on the metallic surface but also its binding mode. This makes XPS an interesting technique for the characterization of nanoparticles and could give a number of information: elementary composition of ligand and NPs, integrity of the ligand and nature of the bond. However, complete and accurate characterization of NPs sample remains challenging (peak widening, need to deposit NPs on a conductive surface).

XPS has already been used on palladium,¹⁶ platinum¹⁷ and gold^{18–20} nanoparticles stabilized by NHCs. The presence of the ligand was evidenced by the C1s and N1s photopeaks and the position of the latter confirmed the coordination of the carbene.^{18–20} However, none of these studies were able to give an elemental composition of the ligand, attesting to the difficulty that characterizing NPs to the full extent represents. Moreover, no clear evidence of a covalent carbon-metal bond was established.

XPS analysis was carried out on 2 samples: **2H-Br** and gold nanoparticles prepared from **2H-AuX₄** and 4 equivalents of **2H-Br** without NaH. The latter will be designated by **2-AuNP**. Each photopeak was carefully deconvoluted to study the possible presence of several components. Results are presented in Table II.3. For **2H-Br**, the photopeak Br3d can be divided into Br3d_{5/2} and Br3d_{3/2} at 67.4 and 68.3 eV respectively. In the case of **2-AuNP**, no peak is observed in the 185–210 and 65–72 eV regions which indicates an absence of bromine and chlorine in the sample and confirms the correct purification of the NPs.

For **2-AuNP**, the formation of metallic gold is evidenced by the Au4f signal composed of only 2 peaks at 84.0 and 87.6 eV, which correspond to spin orbit coupling Au4f_{7/2} and Au4f_{5/2} respectively. The binding energy of Au4f_{7/2} and difference between the two components (3.6 eV) is characteristic of metallic gold (Au⁰).²¹

Table II.3: XPS data (binding energy: BE, assignment and composition) for **2H-Br** and **2-AuNP**.

		BE (eV)	Assignment	Composition [at.%] ^a	Calculated stoichiometry	Expected stoichiometry
2H-Br	C1s	285.0	Aliph. C	72.5	21.7	22
	C1s	286.0	Aliph. C-N	7.2	2.2	2
	C1s	286.5	N-HC=CH-N	7.3	2.2	2
	C1s	287.2	N ₂ -C-H	3.6	1.1	1
	N1s	401.6		6.1	1.8	2
	Br3d _{5/2}	67.4		3.3	1.0	1
2-AuNP	C1s	285.0	Aliph. C	68.5	21.9	22
	C1s	286.0	Aliph. C-N	5.4	2.0	2
	C1s	286.4	N-HC=CH-N	5.4	2.0	2
	C1s	284.1	N ₂ -C-Au	2.8	1.0	1
	N1s	400.2		5.1	2.1	2
	Au4f	84 - 90				

^a Extracted from the fit

Fitting the C1s photopeak of **2H-Br** requires 4 contributions, all with the same FWHM (full-width at half maximum) (Figure II.9). Each contribution is characteristic of a chemical environment: at 285.0 and 286.0 eV are the aliphatic carbons (C-C and C-N respectively), at 286.5 and 287.2 eV are located the carbons for the aromatic heterocycle (C-CN and N₂-C-H respectively).^{22,23} It is important to note that the stoichiometry derived from this fit corresponds very well to what is expected from the molecular formula of **2H-Br** and so does the overall carbon, nitrogen, bromine composition (Table II.3).

For **2-AuNP**, the C1s spectrum was fitted with 5 components. Components 1, 2 and 3 correspond to those found for **2H-Br** and are attributed to C-C aliphatic, C-N aliphatic and C-N aromatic environments. A fourth component was found at 284.1 eV accompanied by the extinction of the component at 287.2eV (N₂-C-H in **2H-Br**). This contribution, already observed for gold and iron surfaces^{24,25} can be attributed to the N₂-C-Au bond. This all confirms the absence of the imidazolium and the formation of the carbene. The relative intensities of each component fits the atomic composition of the ligand well and so does the overall carbon/nitrogen composition. It is worth noting that no boron (which could have come from the reducing agent) was observed. We can thus exclude the possibility of a N₂-C-B environment.

The fifth C1s component, at 288.5 eV, can be attributed to the $\pi \rightarrow \pi^*$ transition characteristic of a shake-up peak (also known as a satellite peak) coming from the photoelectron excitation of the heterocycle ring. In our case, the satellite peak is only observed for **2-AuNP** suggesting an enhancement by plasmon effect (plasmon loss satellite).²⁶

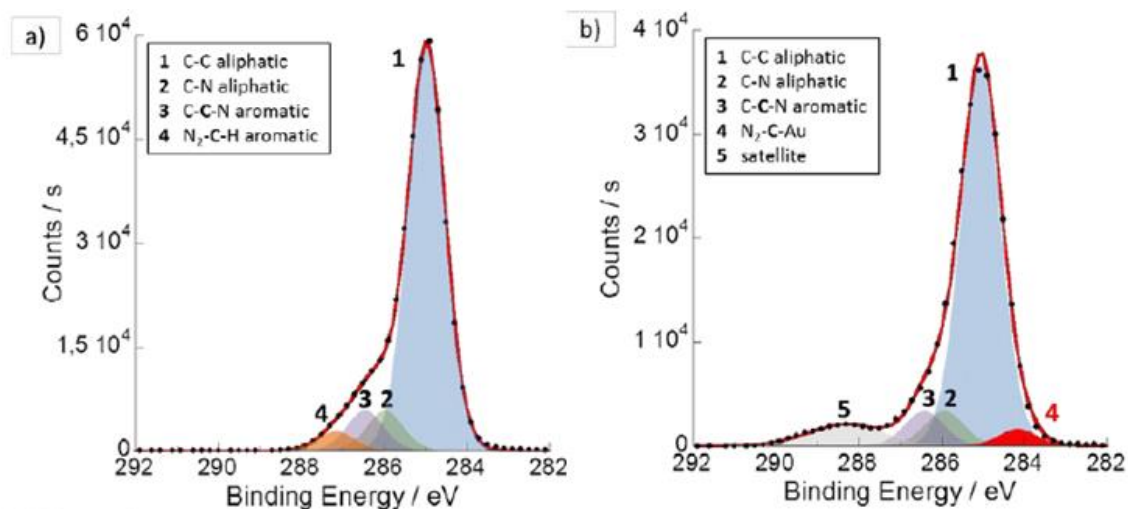


Figure II.9: C1s XPS spectra and their corresponding fits for a) the imidazolium precursor **2H-Br** and b) gold nanoparticles **2-AuNP**.²

The N1s photopeak of **2H-Br** is symmetrical and presents only 1 component at 401.6 eV as expected when looking at its molecular environment (Figure II.10). The N1s spectrum of **2-AuNP** also presents 1 component only but with a clear shift towards lower binding energies. Such a shift was already observed for nanoparticles stabilized by NHCs.^{16,17,19} This shift corresponds to a loss of charge on the heterocycle coming from the conversion of a positively charged imidazolium into a neutral NHC covalently bound to the surface. NHCs are thus the only species present on the nanoparticles' surface.

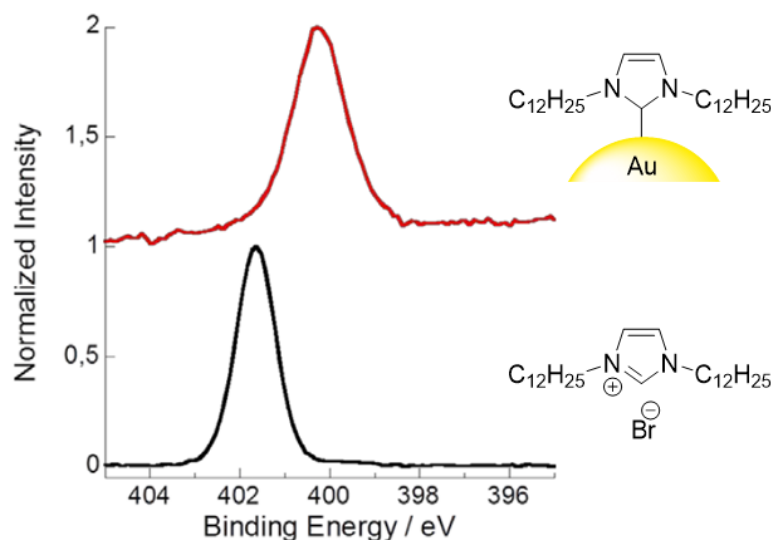


Figure II.10: N1s XPS spectra for the imidazolium bromide **2H-Br** (bottom trace) and gold nanoparticles **2-AuNP** (top trace).²

To conclude, XPS confirms the formation of NHCs in a NaH-free synthesis. Indeed, NaBH₄, added in excess, could be basic enough to deprotonate the (benz)imidazolium as suggested in the literature.²⁷ Finally, this, to the best of our knowledge, is the first example of an XPS C1s signal associated with a N₂-C-Au environment at the surface of gold nanoparticles.

II.B. Nanoparticles from imidazolium haloaurate salts and tBuNH₂BH₃

II.B.1. Synthesis of the nanoparticles

Now it was established that gold nanoparticles were stabilized by NHC even in the absence of a “proper” base, we decided to change the reducing agent. tBuNH₂BH₃, which is a milder reducing agent, was chosen. It is soluble in organic solvents, as opposed to NaBH₄, which allows for homogeneous synthesis.

Unexpectedly, tests carried out in the presence of NaH yielded very different results than for the synthesis using NaBH₄. Indeed, adding NaH before the reduction step by tBuNH₂BH₃ led solely to the formation of bulk material, this implies that the deprotonation step is not the only decisive one in the nucleation/growth mechanism of the nanoparticles.

As a result, the following tests were carried out in the absence of NaH. The effect of the ligand/Au ratio was also studied. Figure II.11 presents the TEM images and size distribution of the obtained nanoparticles for ratios of **2H-AuX₄:2H-Br** ranging from 1:0 (**2H-AuX₄** only) to 1:6. All syntheses were carried out at 55°C with 10 min of stirring. The size of the as obtained nanoparticles is strongly linked to the addition of **2H-Br**. When using only **2H-AuX₄**, NPs are large, very polydisperse (24 ± 7 nm) and of various shapes. They get smaller, more spherical and monodisperse with an increasing quantity of **2H-Br**. It appears that at least 1 equivalent of **2H-Br** is necessary to obtain reasonable polydispersity (~25%). When using 6 equivalents of imidazolium, the NPs reach 5.8 ± 1.1 nm in size. As such, it seems that when using tBuNH₂BH₃, the ligand/Au ratio can be used to influence the obtained NPs size in a 6-12 nm range.

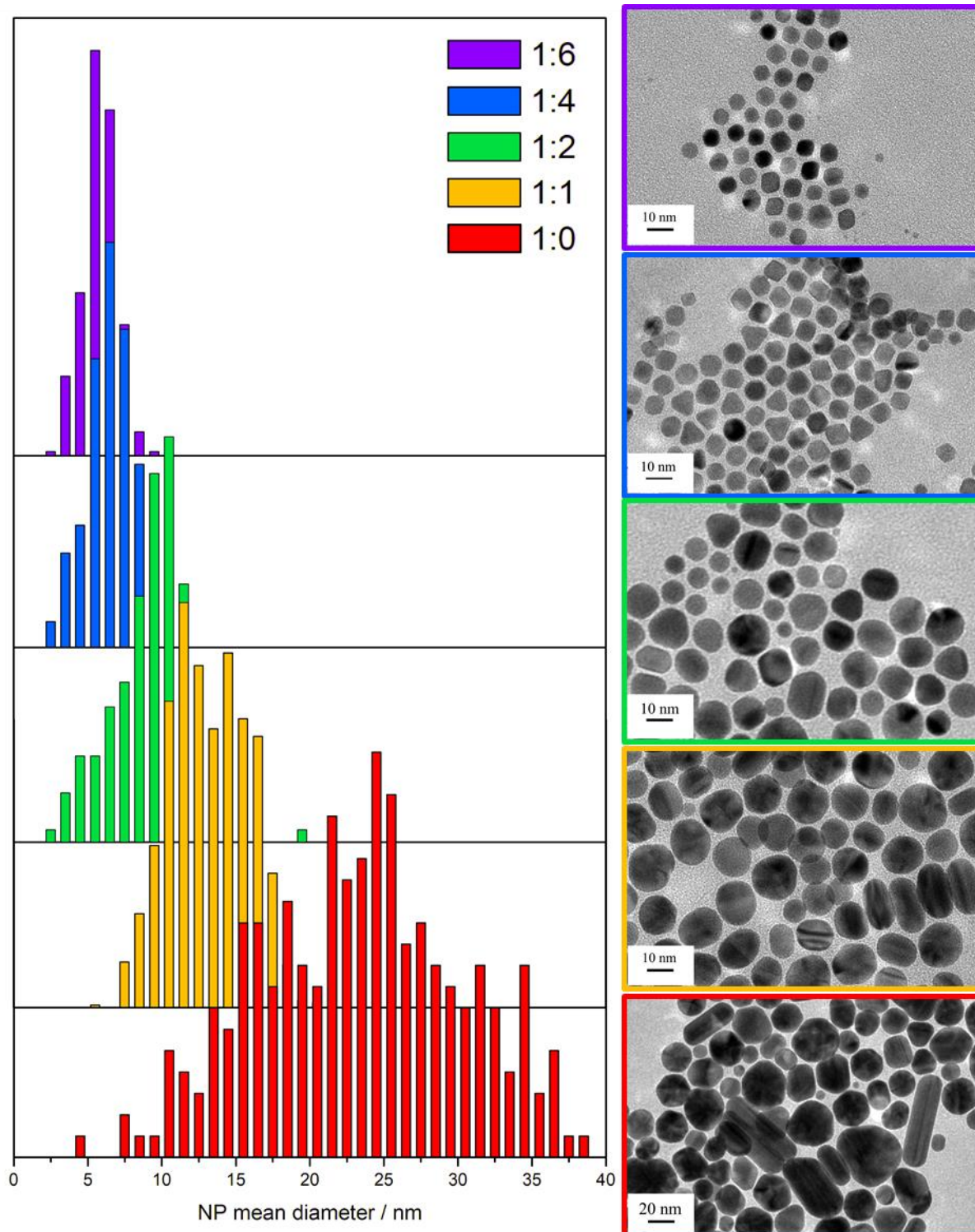


Figure II.11: TEM images and corresponding size distributions of gold nanoparticles obtained from to 1H-AuX_4 and various amount of 1H-Br (from 0 to 6 eq.) with $\text{tBuNH}_2\text{BH}_3$ as reducing agent (10 min. stirring at 55°C in toluene).

II.B.2. XPS analysis

XPS analysis was carried out on the nanoparticles obtained for the 1:6 **2H-AuX₄**: **2H-Br** synthesis. As was the case for samples using NaBH₄, no bromine, chlorine or boron were detected and the gold spectrum is characteristic of gold(0). This time however the nitrogen photopeak presents 2 components (Figure II.12). One at 399.9 eV which accounts for 81% of the peak and corresponds to a covalent interaction between NHC and the gold surface. The second, at 402.2eV, accounts for only 19% of the signal. Its position in the higher binding energies suggests the presence of a charge on the cycle. The presence of this charge indicates that deprotonation did not occur and that interaction is more likely to be electrostatic (and thus slightly weaker). However, as the major contribution corresponds to a covalent interaction, we can say that the vast majority of the stabilization comes from NHCs, and that tBuNH₂BH₃ is enough of a base to deprotonate imidazoliums. There are however remnants of other interactions suggesting that the stabilization mechanism may not be exactly the same when using NaBH₄ or tBuNH₂BH₃. For example, the amine of tBuNH₂BH₃ could interact with the gold surface at the beginning of the synthesis preventing a complete stabilization by NHCs.

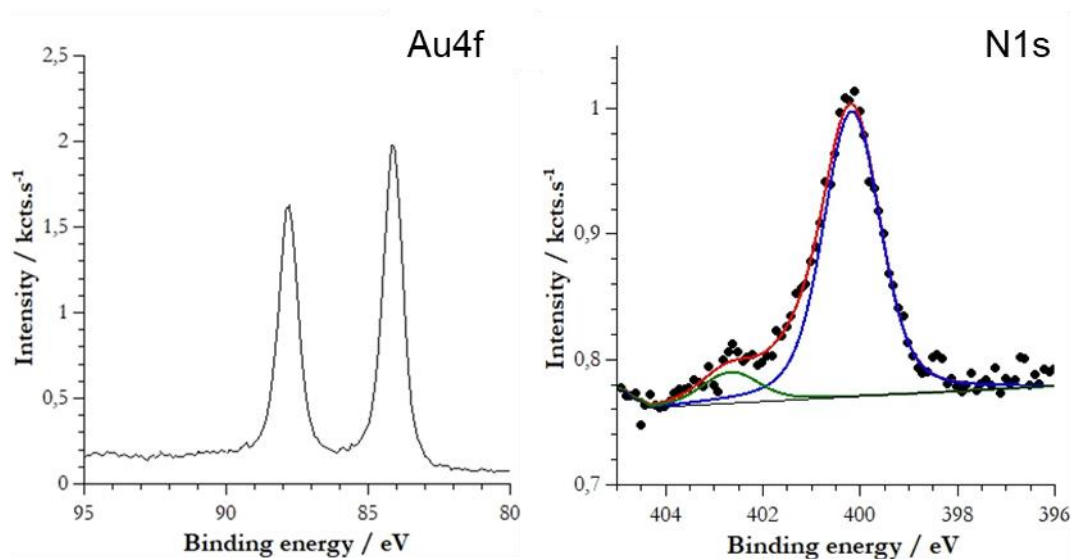


Figure II.12: Au4f and N1s XPS spectra of gold nanoparticles synthesized from **2H-AuX₄**, 6 eq of **2H-Br** and tBuNH₂BH₃ (in toluene).

II.C. Nanoparticles from AuCl and unfunctionalized imidazolium salts

II.C.1. Using NaBH₄ as a reducing agent

After seeing that the synthesis of NHC-capped NPs could be achieved without the addition of NaH to deprotonate the imidazolium, we decided to explore the synthesis further by using an even simpler gold precursor: AuCl. We hoped that the reduction of AuCl by NaBH₄ in the presence of imidazolium bromide would lead to stable, NHC-capped nanoparticles.

Upon addition of AuCl to a solution of imidazolium in toluene, the solution goes from colorless to orange, thus showing an interaction between the 2 reagents and the likely formation of an imidazolium AuClBr⁻ complex. Indeed, this type of complex have been described in the literature²⁸ and were obtained in quantitative yield by mixing an imidazolium bromide salt with AuClSMe₂ at room temperature. Upon addition of aqueous NaBH₄, the solution turns deep red and bubbles are formed, probably due to H₂ release upon reduction of Au(I) and the deprotonation of the imidazolium. The obtained nanoparticles are isotropic and 3.4 ± 0.8 nm in diameter when using 1 equivalent of imidazolium per gold. Increasing to 2 and 4 equivalents of imidazolium did not have a significant effect on the size (Figure II.13).

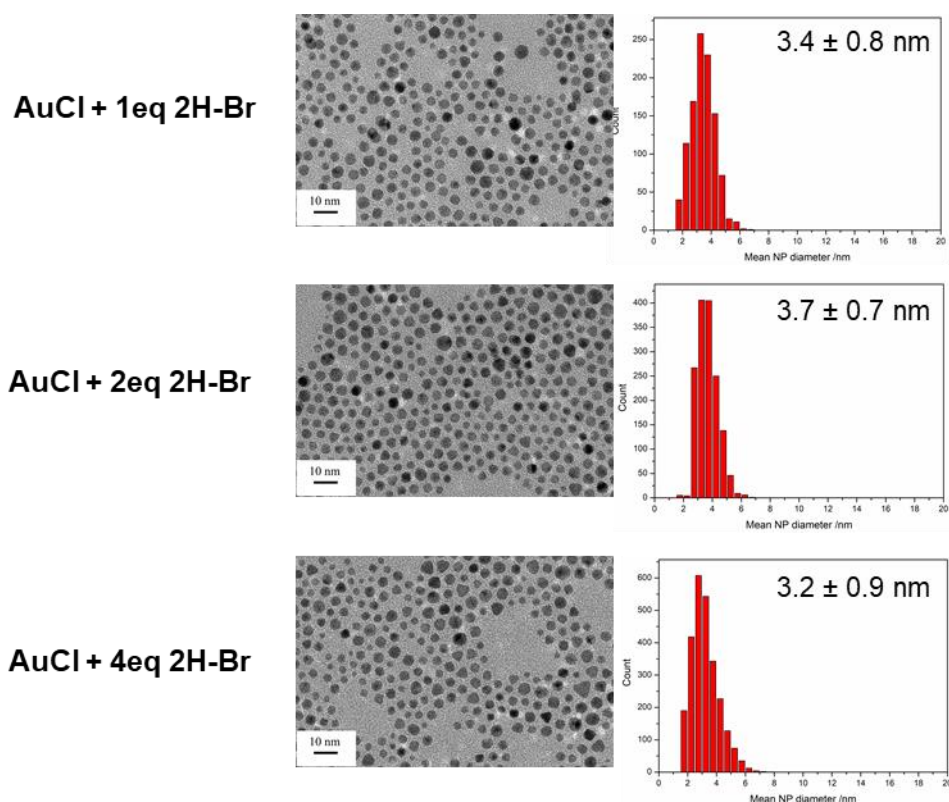


Figure II.13: TEM images of nanoparticles obtained from AuCl, 1, 2 or 4 equivalents of **2H-Br** and NaBH₄ (solvent toluene), and corresponding distributions.

Experiments carried out with 4 equivalents of **1H-Br** and **3H-Br** gave similar results with nanoparticles of 3.7 ± 0.8 nm and 4.4 ± 0.8 nm respectively (Figure II.14). It is worth noting that while **3H-Br** yielded smaller nanoparticles than **1H-Br** and **2H-Br**, when used in excess in an NaH-free synthesis starting from **3H-AuX₄**, when starting from AuCl it is not the case. This could hint to a different pathway for benzimidazoliums compared to imidazoliums where benzimidazoliums are more impacted by the change in oxidation state of the gold precursor.

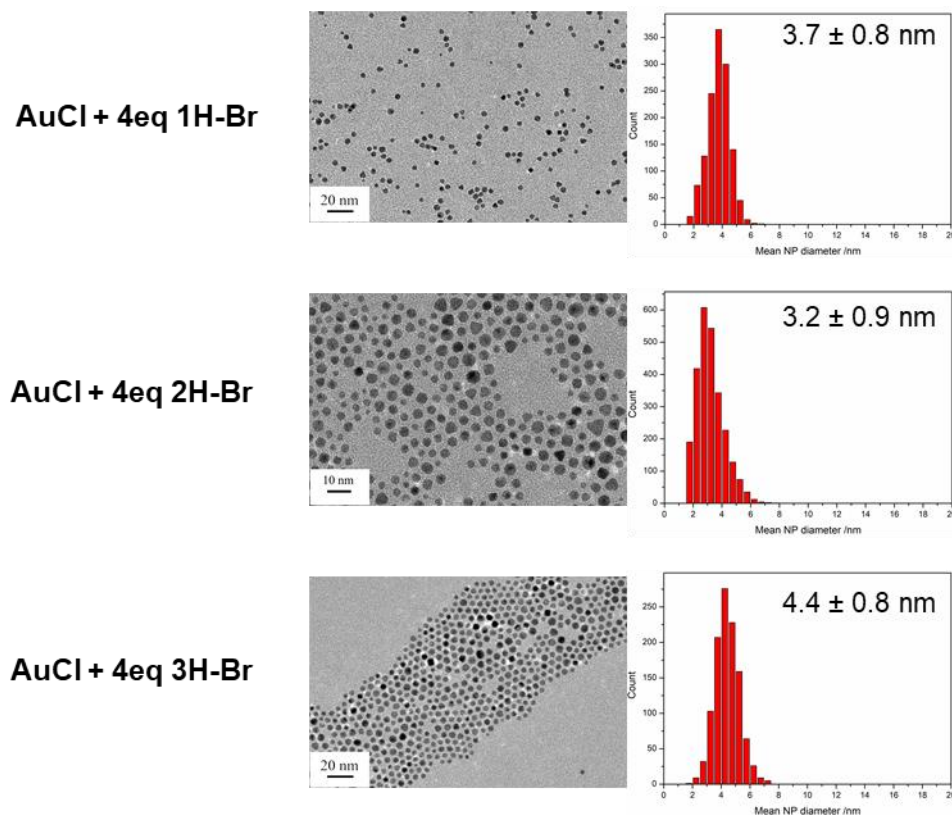


Figure II.14: TEM images of nanoparticles obtained from AuCl, 4 equivalents of **1H-Br**, **2H-Br** or **3H-Br** and NaBH₄ (solvent toluene), and corresponding distributions.

The addition of NaH to a **2H-Br** AuCl solution in toluene led to the formation of slightly larger NPs (4.3 ± 0.9 nm instead of 3.7 ± 0.9 nm) contrarily to what we observed for **2H-AuX₄** (Figure II.15). When increasing the amount of imidazolium (and corresponding NaH), the size of the nanoparticles increases also (contrarily to what could be observed before). As we don't know the exact formation mechanism of these nanoparticles it is unclear why more carbenes led to larger particles. One could hypothesize that those carbene get involved in the formation of $[\text{Au}(\text{NHC})_2]^+$ complexes leading to less ligand being able to stabilize the NPs leading in turn to larger nanoparticles.

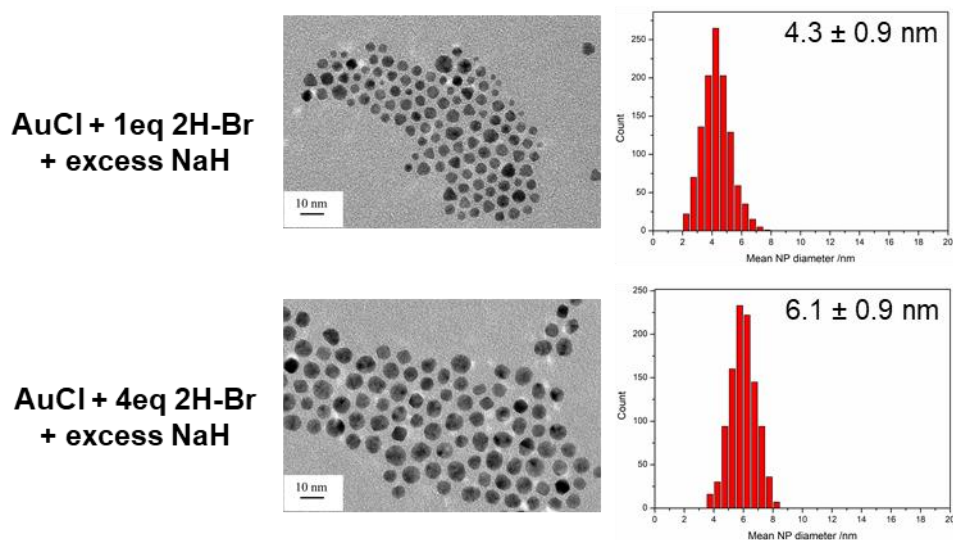


Figure II.15: TEM images of nanoparticles obtained from AuCl, 1 or 4 equivalents of **2H-Br**, NaH and NaBH₄ (solvent toluene), and corresponding distributions.

It is worth noting that examples of NHC-stabilized gold nanoparticles synthesized from a gold(I) precursor have already been reported in the literature. However, these protocols use previously synthesized NHC-AuX complexes (as seen in chapter I). Our protocol is the first to use AuCl and easily accessible (benz)imidazolium halides as our starting material. This synthesis probably follows a different pathway than the one starting from (benz)imidazolium haloaurates as evidenced by the different behaviors observed (notably regarding NaH and excess (benz)imidazolium addition). The difference probably stems from the different oxidation state which leads to different intermediate complexes which could potentially be involved in the reduction and/or formation of NPs.

II.C.2. Using tBuNH₂BH₃ as a reducing agent

As previously, changing the reducing agent to tBuNH₂BH₃ led to larger nanoparticles (6.8 ± 1.3 nm) (Figure II.16), which were characterized by XPS. As was the case with **2H-AuX₄**, there is no halides or boron detected and only gold(0). There are 2 components to the nitrogen photopeak (Figure II.16). One at 400.3 eV accounting for 80% of the signal and one at 401.9 eV accounting for the remaining 20%. Once again most of the stabilization of the NPs come from NHCs with a small contribution in the higher binding energies. This contribution suggests a charged species and thus an electrostatic interaction. This also shows that once again tBuNH₂BH₃ is enough of a base regardless of gold precursor.

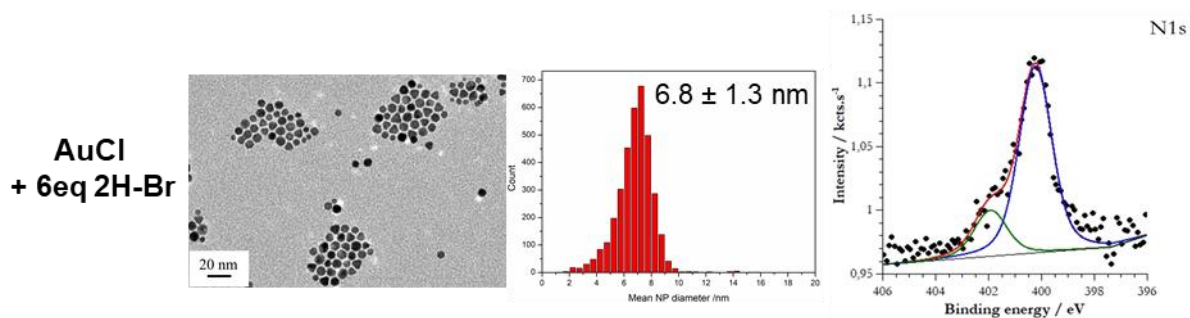


Figure II.16: TEM image of nanoparticles obtained from AuCl, 6 equivalents of **2H-Br** and tBuNH₂BH₃ (solvent toluene), corresponding distribution, and N1s XPS spectra of these gold nanoparticles.

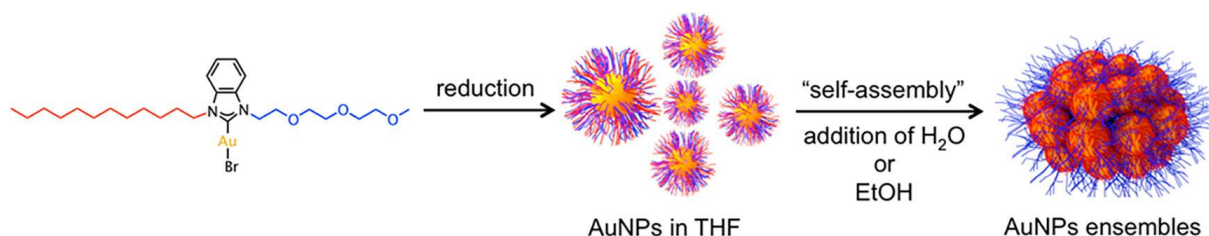
The analyzed nanoparticles were synthesized with an excess of **2H-Br** (6eq). Due to lack of time, no study on the influence of Au:**2H-Br** ratio was conducted.

II.D. Nanoparticle synthesis from functionalized imidazoliums

In this project, potential for future applications was never forgotten. Although many potential applications are possible, our focus narrowed on water-soluble and (post-)functionalizable nanoparticles.

II.D.1. Water-soluble imidazolium

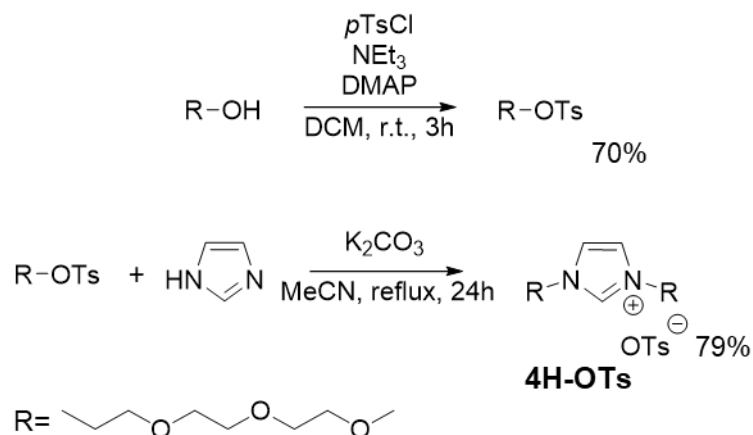
For the water-soluble imidazolium, we drew inspiration from a study by Cruden *et coll.*¹⁸ where they use an amphiphilic imidazolium-gold complex to synthesize amphiphilic nanoparticles that can aggregate in polar solvents (Scheme II.5).



Scheme II.5: Cruden *et coll.* synthesis of amphiphilic NHC-stabilized gold nanoparticles.¹⁸

We hoped that by using two triethylene glycol side chains instead of one, the water-affinity of the synthesized imidazolium would be greater and would lead to water-soluble nanoparticles. Moreover, it would serve as a proof of concept before moving forward with longer polyethylene glycol chains. Indeed, AuNPs functionalized with PEGs are known to circulate better in the body as they are less detected by the immune system.²⁹

The imidazolium was synthesized following a similar procedure to the one of Crudden *et coll.* (Scheme II.6).¹⁸ The terminal alcohol group of monomethylated triethylene glycol was functionalized with a tosyl group. The product was then reacted with imidazole to afford the imidazolium as a yellow viscous oil in 79 % yield. The obtained imidazolium, **4H-OTs**, proved soluble in water but also in organic solvents.



Scheme II.6: Synthetic pathway to water soluble imidazolium.

Using a water-soluble gold precursor, such as $\text{HAuCl}_4 \cdot 3\text{H}_2\text{O}$, directly leads to the formation of aggregates. As a result, **4H-OTs** was dissolved with AuCl in toluene which led to a slightly turbid orange solution. However, unlike with **2H-Br**, addition of aqueous NaBH_4 led to only aggregates at the solvents interface. We assume it's because the imidazolium preferably goes into the aqueous phase whereas the gold would remain mainly in the organic phase and/or because the deprotonation of imidazolium by sodium borohydride cannot occur in aqueous media.

By switching to $\text{tBuNH}_2\text{BH}_3$ as a reducing agent, the reaction could be carried out in a homogeneous system. Upon addition of the reducing agent, the AuCl + imidazolium solution turned transparent then deep red in a few seconds indicating the formation of gold nanoparticles. The obtained NPs have a mean diameter of 2.8 ± 0.7 nm and a plasmon resonance at 508 nm in toluene (Figure II.17). They can be transferred in water and remain stable long enough to record a UV-vis spectrum but they unfortunately do not remain stable over time. Indeed, they are visibly aggregated within a few hours.

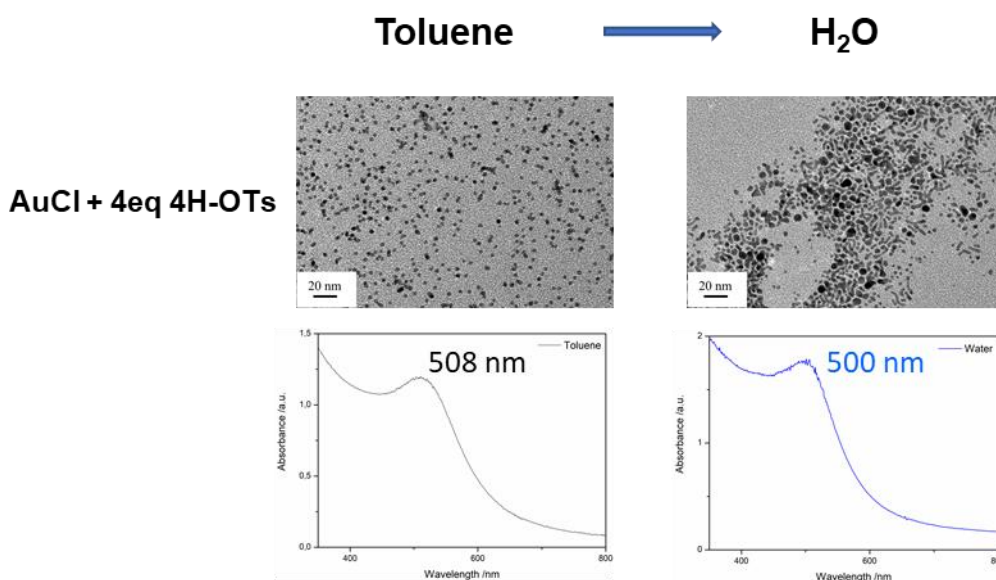


Figure II.17: TEM images of nanoparticles obtained from AuCl, 4 equivalents of **4H-OTs** and tBuNH₂BH₃, and corresponding UV-vis spectra.

Moreover, the behavior of the nanoparticles is not reproducible from sample to sample, as some samples transfer fully while others only transfer partially, and some remain stable for a few hours in water whereas others start aggregating almost instantaneously. The same behavior is observed when changing the gold precursor to AuClSMe₂ (3.6 ± 0.9 nm) or **4H-AuX₄** (2.9 ± 0.9 nm) (Figure II.18).

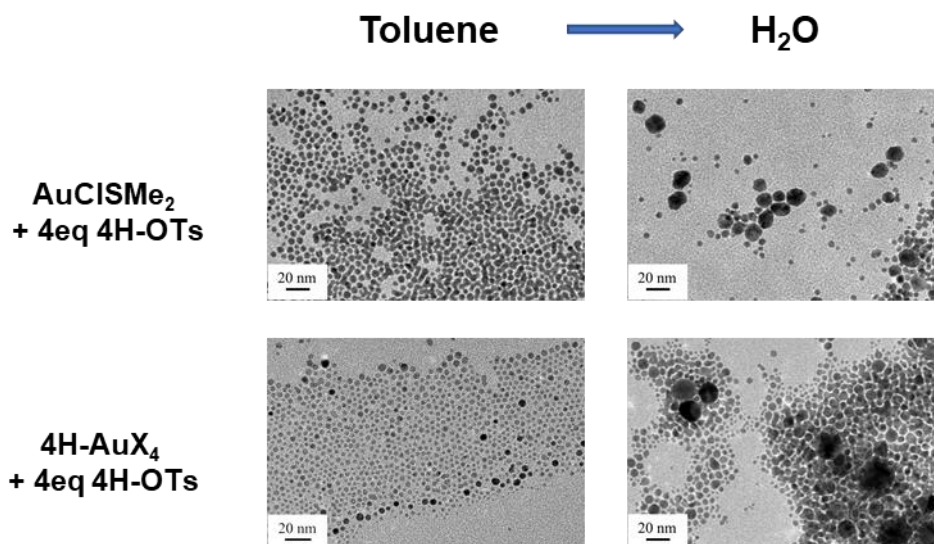


Figure II.18: TEM images of nanoparticles obtained from AuClSMe₂ and 4 equivalents of **4H-OTs** or **4H-AuX₄** and 4 equivalents of **4H-OTs** and tBuNH₂BH₃ in toluene.

The same protocol was applied in dichloromethane and also yielded NPs. However, the obtained nanoparticles (5.9 ± 1.1 nm in diameter) remain solely in the organic phase (Figure II.19). No transfer is observed.

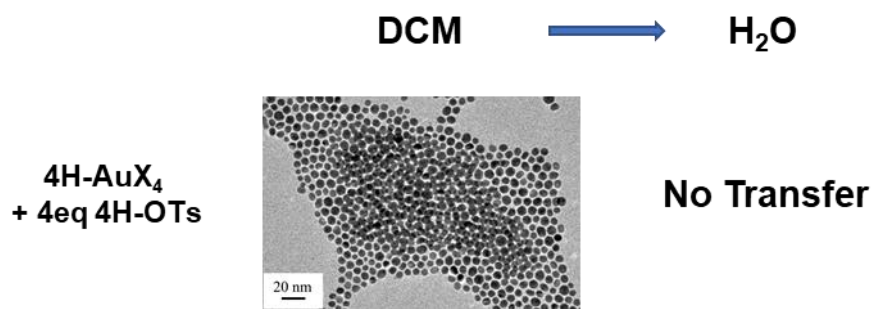


Figure II.19: TEM images of nanoparticles obtained from **4H-AuX₄** and 4 equivalents of **4H-OTs** and tBuNH₂BH₃ in DCM.

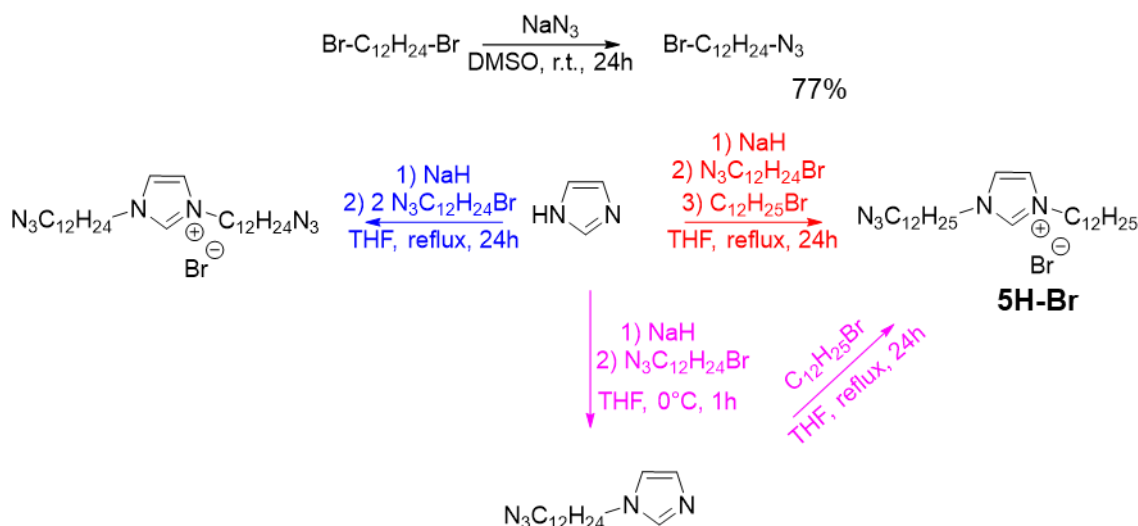
Due to the lack of reproducibility of the results and poor nanoparticle stability, the NPs were not characterized by XPS. However, it can be assumed that the nanoparticles are stabilized by NHCs. Indeed, there is no reason to assume that tBuNH₂BH₃ would be a strong enough base to deprotonate **2H-Br** but not **4H-OTs**. The poor stability in water is surprising, as NHC-SAMs^{30,31} and NHC stabilized AuNPs^{15,19} have been shown to be stable in water, and is thus unlikely to stem from the hydrolysis of the NHC-Au bond.

Even though **4H-OTs** proved insufficient in order to synthesize water soluble NPs, other imidazoliums can be considered. For example, one with longer PEG chains such as the one used by McLeod *et al.*,¹⁵ or one with an ionic group (for example sulfonate or carboxylate) as proposed by Crudden *et coll.*¹⁹ and Chaudret *et coll.*^{12,32}

II.D.2. Azide functionalized imidazolium

It has been shown in the literature that NHCs are compatible with click-chemistry.³⁰ Click chemistry is versatile and, by definition, uses mild conditions. One of the best-known examples of click-chemistry is the copper catalyzed [3+2] cycloaddition of alkynes and azides (CuAAC). That is why we were interested by an azide functionalized imidazolium, as the azide moiety would be available for post-functionalization of the nanoparticles.

The first step of the synthesis consisted in synthesizing 1,12-bromododecylazide side chain from 1,12-dibromododecane and sodium azide. Once reacted with imidazole, the obtained imidazolium would have 1 or 2 azide moieties available for (post)functionalization. Several synthetic pathways were envisioned and are presented in Scheme II.7.



Scheme II.7: Synthetic pathway to click-chemistry ready imidazolium. Blue = pathway 1a, red = pathway 1b, pink = pathway 2.

One-pot syntheses proved difficult to purify. Indeed, pathway 1a (Scheme II.7, blue), led to a mixture of mono and bis alkylated products which did not readily separate upon precipitation attempts. Pathway 1b (red) led to a mixture of imidazolium which, being salts, are difficult to purify by column chromatography.

Attempts to synthesize **5H-Br** in 2 steps by pathway 2 (pink) were unsuccessful as I was unable to obtain the pure monofunctionalized imidazole during the time of my PhD.

Nonetheless, experiments were carried out with the 85% pure imidazolium **5H-Br** (purity checked by NMR, 15% bis-azide imidazolium), synthesized by pathway 1b, to see if nanoparticles could be obtained. 1 equivalent of **5H-Br** was mixed with either 1 equivalent of AuClSMe₂ (in toluene, sample A) or 1 equivalent of HAuCl₄.3H₂O (dissolved in Toluene: CHCl₃ 9:1) (sample B) before addition of 10 equivalents of NaBH₄ (Figure II.20). Sample A turned bright red immediately whereas sample B started discoloring before turning red. Both samples were characterized by TEM and showed particles of 4.4 ± 1.4 nm for B and a mix of 3.3 ± 1.1 and 18.8 ± 2.6 nm particles in the case of A. However, the nanoparticles were not stable as sample B was completely transparent after 24h and sample A was severely discolored.

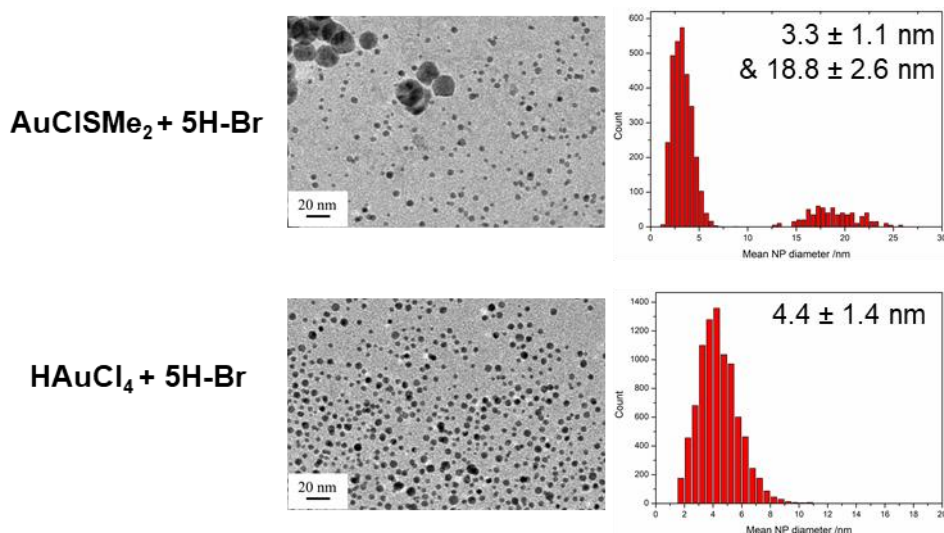


Figure II.20: TEM images of nanoparticles obtained from 1 equivalent of **5H-Br**, AuCISMe₂ or HAuCl₄.3H₂O, and NaBH₄, and corresponding distributions.

However, at this stage it is not possible to say if the nanoparticles are indeed stabilized by the carbene as the azide moiety on the imidazolium could also be reduced to NH₂ by NaBH₄. It is well known that amines can coordinate to gold and give nanoparticles.^{33,34} As the ligand was only 85% pure comparison between XPS spectra of imidazolium and NPs would not have given relevant information. Functionalization of the NPs could have been attempted. Indeed, if there was reaction of an alkyne with the azide moiety, it would prove that it is not bound to the surface. However, lack of reaction would not be definite proof of the opposite as unsuitable reaction conditions could be the culprit. As soon as the pure imidazolium is synthesized, further tests will be carried out.

II.D.3. C2-functionalized imidazoliums

Throughout this PhD, our main focus was on classical NHCs with (benz)imidazole-like structure, which could be deprotonated to form a stabilized carbene at the C2 position. However, an article³⁵ describing the synthesis of nanoparticles stabilized by an imidazolium functionalized in the C2 position (Figure II.21) shifted our focus.

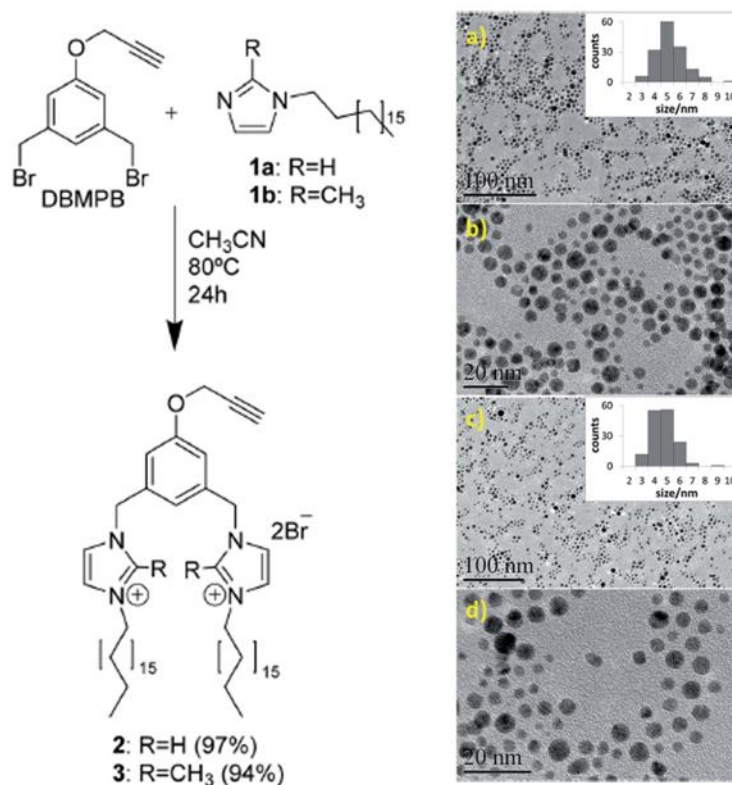
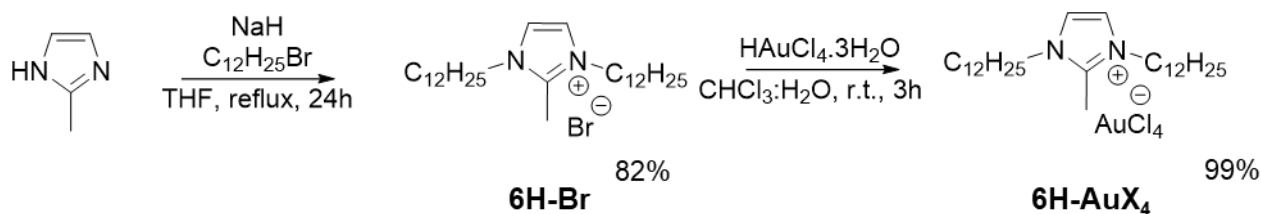


Figure II.21: Methylated imidazolium in the C2 position and nanoparticles obtained by Rodrigues *et al.*³⁵

In their paper, Rodrigues *et al.*³⁵ argue that since there is a methyl, and as they detect no Au(I) by XPS, no carbene were formed. As a result, they concluded that their gold nanoparticles had to be stabilized by imidazolium moieties. It is possible they were looking for Au-NHC complexes which are known to form during the synthesis of gold nanoparticles stabilized by NHCs (see Chapter I). Absence of these complexes, however, is not proof that NHC didn't form. Moreover, they measured 24 ligands per nm² by TGA which seems unlikely as studies on SAMs have measured a value of 4 ligands/nm². This suggests a poor purification of their NPs. Nevertheless, we decided to try using a similar methylated imidazolium to see if we would also obtain nanoparticles.

III.D.3.a. 2-methylimidazolium

The imidazolium **6H-Br** was synthesized by the same protocol as previously starting from 2-methylimidazole and was obtained as a white powder in 82% yield. The corresponding gold(III) precursor was also synthesized and obtained as an orange powder in quantitative yield (Scheme II.8).



Scheme II.8: Synthetic pathway to 2-methylimidazolium.

Attempts starting both from **6H-AuCl₄** and our AuCl + imidazolium synthesis yielded nanoparticles (3.5 ± 1.3 nm and 3.6 ± 0.8 nm respectively) (Figure II.22). It is worth noting that in the case of the AuCl synthesis, the obtained nanoparticles are of similar size to the ones obtained by the same protocol from **2H-Br**. Increasing the quantity of ligand to 5eq instead of 1 led to similar results as previously and the NPs size remained roughly the same at 3.8 ± 1.0 nm. Adding NaH in the synthesis from **6H-AuX₄** (without **6H-Br**) had no significant influence on the size of the NPs which were of 3.7 ± 1.0 nm (as opposed to 3.5 ± 1.3 nm without). However, for both the size of the obtained NPs are smaller than the ones obtained from **2H-Br**.

XPS analysis was carried out in order to determine the bonding mode of the ligand to the surface of the NPs.

Nanoparticles synthesized from both AuCl+**6H-Br** and **6H-AuX₄** (without NaH) were analyzed (Figure II.23). Both had a major component (90%) corresponding to a covalent interaction, at 399.9 eV and 400.0 eV respectively, and a minor component (10%), at 401.9 and 401.7 eV respectively, corresponding to a charged species. We have come to equate such components to an electrostatic interaction between the ligand and NPs. A covalent interaction is thus the driving force behind the stabilization of the nanoparticles. The covalent contribution is symmetrical, this would suggest a symmetrical bonding mode of the molecule and thus an attachment through the methyl.

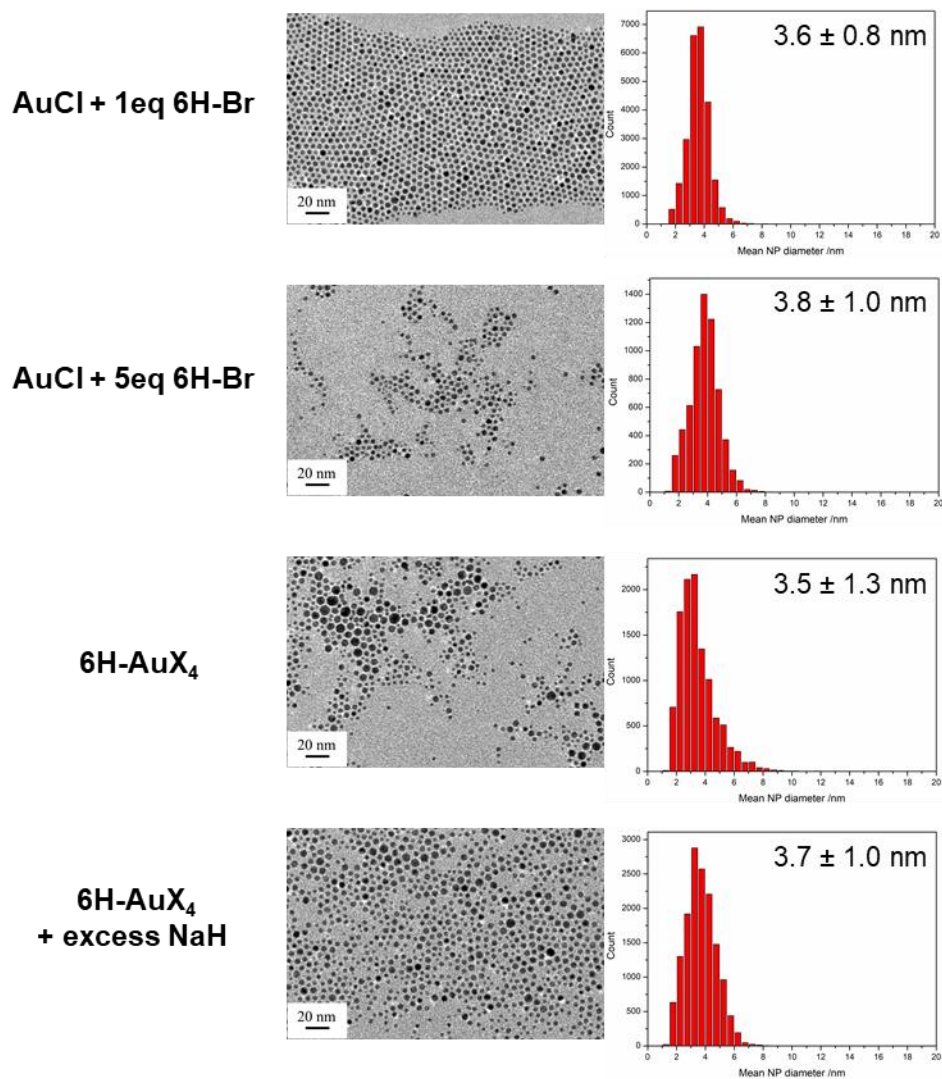


Figure II.22: TEM images and corresponding distributions obtained from 1 or 5 equivalents of **6H-Br**, AuCl and NaBH₄, and **6H-AuX₄** and NaBH₄ with or without NaH

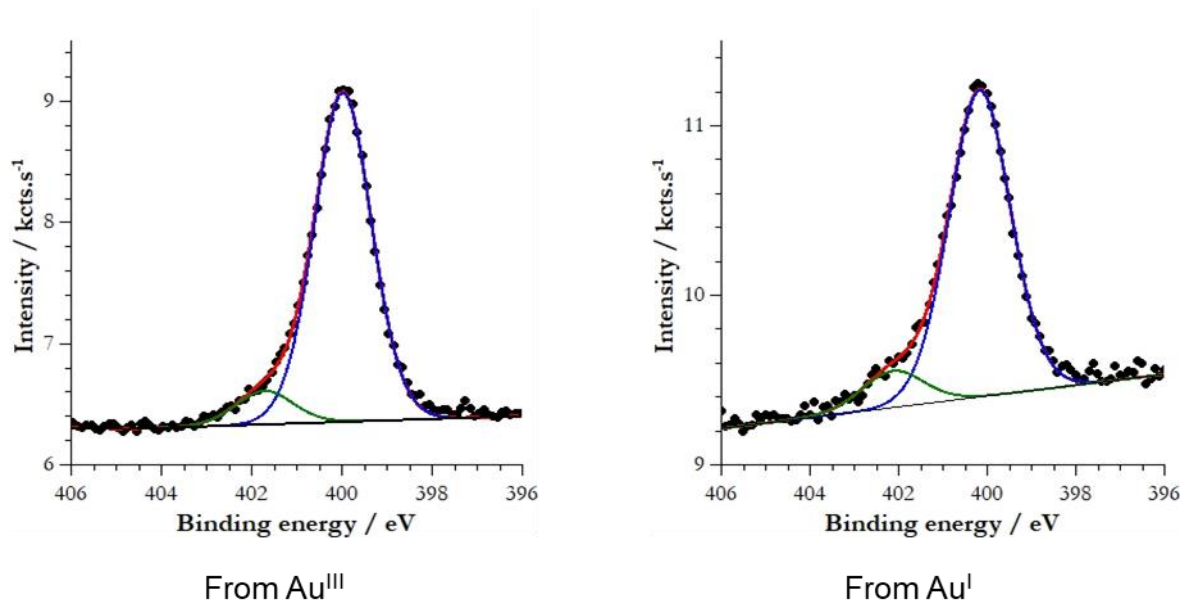
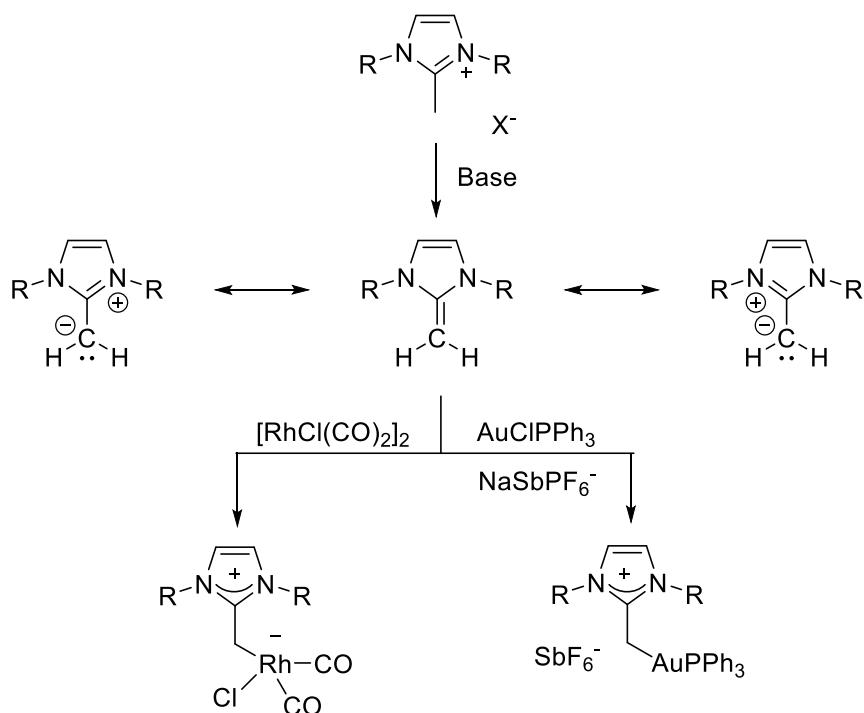


Figure II.23: N1s XPS spectra of nanoparticles obtained from **6H-AuX₄** without NaH and from AuCl and **6H-Br**.

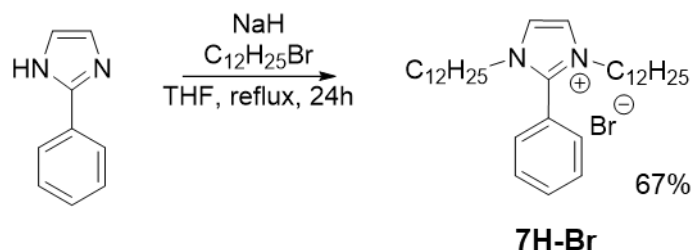
A stabilization through the methyl is not that surprising however when considering the fact that such methylated imidazoliums when deprotonated readily form N-heterocyclic olefins (NHO)³⁶ (Scheme II.9). Indeed, deprotonation at the methyl creates a carbanion which has a resonance structure as an NHO. Such NHOs have been shown to readily coordinate to gold and rhodium (Scheme II.9).³⁷ It is thus likely that our ligand would bind the same way to the nanoparticles' surface. This would explain the stability of the nanoparticles as well as the XPS results.



Scheme II.9: Formation of NHO from imidazoliums and resonance structures of NHO. ^{36,37}

II.D.3.b. 2-phenylimidazolium

Before getting the results from the XPS analysis and forming our hypothesis about NHOs, we looked for a quicker way to prove a stabilization by the methyl carbon. As a result, we synthesized a similar imidazolium but functionalized by a phenyl group on the C2 position: **7H-Br** (Scheme II.10). Our first hypothesis was that if the ligand coordinates through the methyl, the phenyl would prevent the formation of NPs as it is more difficult to deprotonate.



Scheme II.10: Synthetic pathway to **7H-Br**.

However, when the AuCl + imidazolium protocol was performed, nanoparticles were still obtained (Figure II.24). They were 3.0 ± 0.7 nm (or 3.6 ± 1.0 nm when repeated) in diameter and remained stable over time. In this case, it seems that the imidazolium would be deprotonated on the C4 position forming an abnormal NHC (see Chapter IV for more information). The abnormal carbene would thus be the stabilizing ligand.

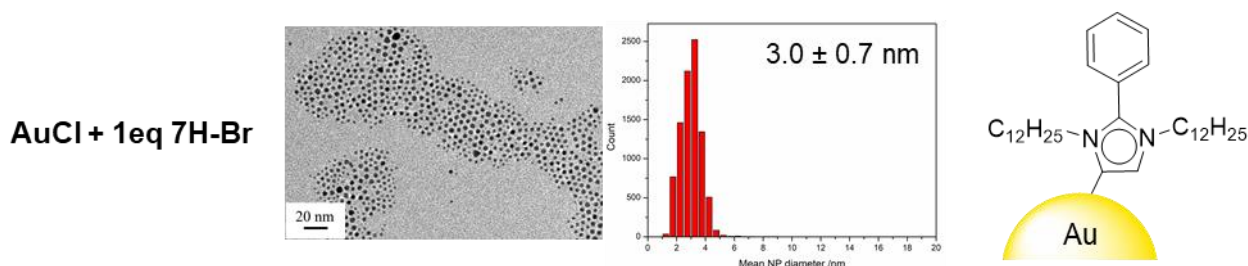


Figure II.24: TEM images of nanoparticles obtained from AuCl, 1 equivalent of **7H-Br** and NaBH₄ (solvent toluene: H₂O), corresponding distributions and representation of the bonding through the abnormal carbene.

It is worth noting that the nanoparticles proved harder to precipitate with ethanol when concentrated in toluene. This seems to further confirm the availability of the phenyl aromatic ring away from the surface of the NPs as they would interact preferably with an aromatic solvent like toluene.

The nanoparticles obtained from **7H-Br** were characterized by XPS (Figure II.25). The N1s spectrum showed 3 components, one (minor) towards the higher energies (402.6 eV) suggesting an electrostatic interaction. Some of this electrostatic component can be explained by insufficient washing of the NPs,

due to the difficulty of precipitation, as 2% of chloride is detected. This however does not account for the entirety of the electrostatic component. The other 2 components (at 400.2 and 399.7 eV) contribute equally to the signal. This indicates that the 2 nitrogen atoms are not chemically equivalent. Indeed, even if the ligand is neutral, the fact that one nitrogen atom is closer to the gold surface is likely to create a slight difference in charge, resulting in a slightly different binding energy. Our theory is that the contribution at 400.2 eV comes from the nitrogen adjacent to the carbene but it is difficult to say with certainty. This asymmetry in the signal is in line with the binding of the NHC through the C4 position as an abnormal carbene.

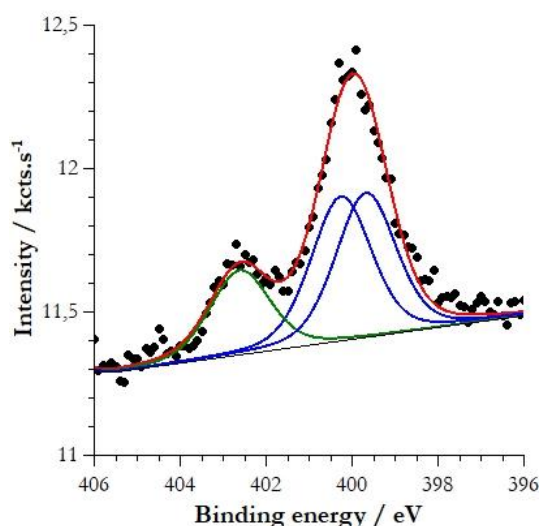


Figure II.25: N1s XPS spectra of nanoparticles obtained from AuCl and **7H-Br**.

II.D.3.c. C2 functionalized imidazoliums and tBuNH₂BH₃ as a reducing agent

Nanoparticle syntheses from C2-functionalized imidazoliums (**6H-Br** and **7H-Br**) were also attempted with tBuNH₂BH₃ as a reducing agent. Nanoparticles were obtained in both cases. However this time, NPs were significantly larger and less spherical (about 20 nm for **6H-Br** and 8.4 ± 1.5 nm for **7H-Br**)(Figure II.26). This is not surprising given the likelihood that tBuNH₂BH₃ is a weaker base than NaBH₄ and thus has more difficulty deprotonating the functionalized imidazoliums. Accordingly, less ligands would be available to coordinate to the surface.

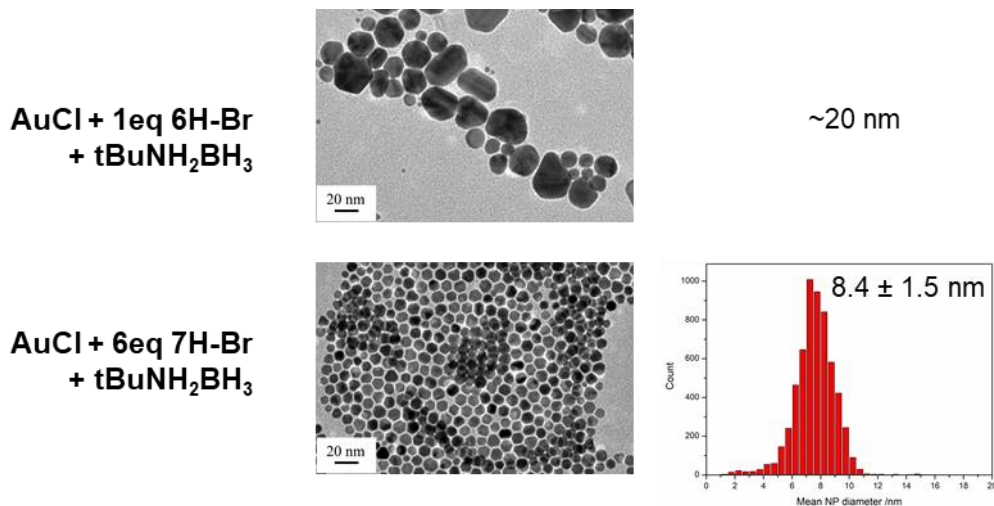


Figure II.26: TEM images of nanoparticles obtained from AuCl, 1 equivalent of **6H-Br** or 6 equivalents of **7H-Br** and tBuNH₂BH₃ (solvent toluene), and corresponding distributions.

The increased size of the nanoparticles is not surprising when looking at the N1s XPS spectra of the nanoparticles obtained from **6H-Br** or **7H-Br** and tBuNH₂BH₃ (Figure II.27). Indeed, the component attributed to electrostatic interactions significantly increases in both cases. In the case of **6H-Br** it even becomes the major component (with 60%) (although it is worth noting that due to experimental difficulties, the analyzed sample was synthesized using only 1 equivalent of **6H-Br** instead of 6, which could account for the difference with **7H-Br**).

Once again, the covalent contribution of the methylated NHC can only be fitted with one component. The mathematical resolution for **7H-Br** is a bit more ambivalent as its covalent component can be fitted with either 1 or 2 components. However, when fixing the distance between component to 0.5 eV (the same value than for NPs prepared with NaBH₄ (Figure II.25)), 2 identical contributions are obtained suggesting that once again **7** is an abnormal carbene bound through the backbone. This indicates that while tBuNH₂BH₃ is able to assist in the formation of NHC-stabilized gold nanoparticles, it may not be the best reducing agent to use in the case of C2 functionalized imidazoliums.

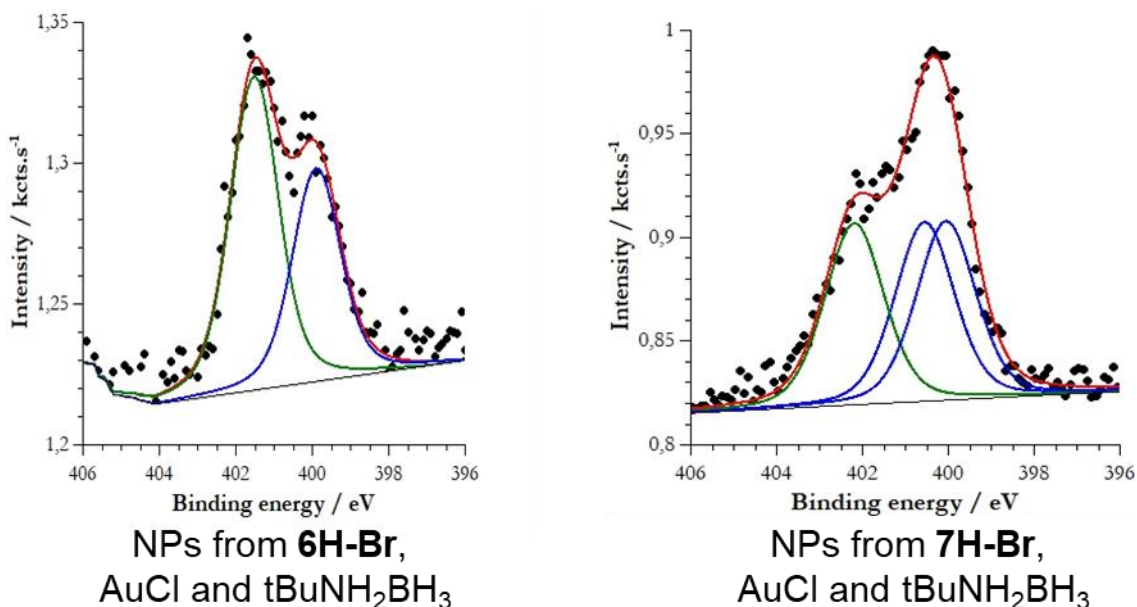


Figure II.27: XPS N1s spectra of nanoparticles synthesized from AuCl, 1 equivalent of **6H-Br** or 6 equivalents of **7H-Br** and tBuNH₂BH₃ in toluene.

II.E. Conclusion

To conclude, in this chapter we have seen that the synthesis of NHC-capped nanoparticles can be simplified compared to existing protocols. Indeed, we showed that there is no need for an additional base in the medium and that NaBH₄ and tBuNH₂BH₃ can act as both a reducing agent and a base. We have been able to tune the size of obtained nanoparticles by changing the ligand, quantity of ligand, reducing agent or gold precursor. We have been the first to synthesize NHC-capped gold nanoparticles starting from AuCl and (benz)imidazolium salts.

Extensive XPS studies have provided a clear proof of carbon-gold bond in the C1s spectrum for the first time on nanoparticles, and have also found that the N1s peak position and shape can be used to determine the binding mode of NHCs on the surface of nanoparticles.

Finally, we are the first to show that it is possible to synthesize gold nanoparticles stabilized by abnormal NHCs by extending our protocol to C2 functionalized imidazoliums.

This offers more options for functionalization or post-functionalization of the nanoparticles as further work in this area is considered.

Bibliography (Chapter II)

- (1) Serpell, C. J.; Cookson, J.; Thompson, A. L.; Brown, C. M.; Beer, P. D. Haloaurate and Halopalladate Imidazolium Salts: Structures, Properties, and Use as Precursors for Catalytic Metal Nanoparticles. *Dalton Trans* **2013**, 42 (5), 1385–1393.
- (2) Bridonneau, N.; Hippolyte, L.; Mercier, D.; Portehault, D.; Murr, M. D. E.; Marcus, P.; Fensterbank, L.; Chaneac, C.; Ribot, F. N-Heterocyclic Carbene-Stabilized Gold Nanoparticles with Tunable Sizes. *Dalton Trans*. **2018**, 6850–6859.
- (3) Dzyuba, S. V.; Bartsch, R. A. New Room-Temperature Ionic Liquids with C₂-Symmetrical Imidazolium Cations. *Chem. Commun.* **2001**, No. 16, 1466–1467.
- (4) Schmidbaur, H.; Raubenheimer, H. G.; Dobrzańska, L. The Gold-Hydrogen Bond, Au-H, and the Hydrogen Bond to Gold, Au...H-X. *Chem Soc Rev* **2014**, 43 (1), 345–380.
- (5) Hasan, M.; Kozhevnikov, I. V.; Siddiqui, M. R. H.; Steiner, A.; Winterton, N. Gold Compounds as Ionic Liquids. Synthesis, Structures, and Thermal Properties of N,N'-Dialkylimidazolium Tetrachloroaurate Salts. *Inorg. Chem.* **1999**, 38 (25), 5637–5641.
- (6) Goubet, N.; Richardi, J.; Albouy, P.-A.; Pileni, M.-P. Which Forces Control Supracrystal Nucleation in Organic Media? *Adv. Funct. Mater.* **2011**, 21 (14), 2693–2704.
- (7) Ji, X.; Song, X.; Li, J.; Bai, Y.; Yang, W.; Peng, X. Size Control of Gold Nanocrystals in Citrate Reduction: The Third Role of Citrate. *J. Am. Chem. Soc.* **2007**, 129 (45), 13939–13948.
- (8) Huang, R. T. W.; Wang, W. C.; Yang, R. Y.; Lu, J. T.; Lin, I. J. B. Liquid Crystals of Gold(I) N-Heterocyclic Carbene Complexes. *Dalton Trans*. **2009**, No. 35, 7121–7131.
- (9) Baker, M. V.; Barnard, P. J.; Berners-Price, S. J.; Brayshaw, S. K.; Hickey, J. L.; Skelton, B. W.; White, A. H. Cationic, Linear Au(I) N-Heterocyclic Carbene Complexes: Synthesis, Structure and Anti-Mitochondrial Activity. *Dalton Trans*. **2006**, No. 30, 3708–3715.
- (10) Rodríguez-Castillo, M.; Laurencin, D.; Tielens, F.; van der Lee, A.; Clément, S.; Guari, Y.; Richeter, S. Reactivity of Gold Nanoparticles towards N-Heterocyclic Carbenes. *Dalton Trans*. **2014**, 43 (16), 5978–5982.
- (11) Crespo, J.; Guari, Y.; Ibarra, A.; Larionova, J.; Lasanta, T.; Laurencin, D.; López-de-Luzuriaga, J. M.; Monge, M.; Olmos, M. E.; Richeter, S. Ultrasmall NHC-Coated Gold Nanoparticles Obtained through Solvent Free Thermolysis of Organometallic Au(I) Complexes. *Dalton Trans* **2014**, 43 (42), 15713–15718.
- (12) Baquero, E. A.; Tricard, S.; Flores, J. C.; de Jesús, E.; Chaudret, B. Highly Stable Water-Soluble Platinum Nanoparticles Stabilized by Hydrophilic N-Heterocyclic Carbenes. *Angew. Chem. Int. Ed.* **2014**, 53 (48), 13220–13224.
- (13) Lara, P.; Rivada-Wheelaghan, O.; Conejero, S.; Poteau, R.; Philippot, K.; Chaudret, B. Ruthenium Nanoparticles Stabilized by N-Heterocyclic Carbenes: Ligand Location and Influence on Reactivity. *Angew. Chem. Int. Ed.* **2011**, 50 (50), 12080–12084.
- (14) Abood, N. A.; AL-Askari, M.; Saeed, B. A. Structures and Vibrational Frequencies of Imidazole, Benzimidazole and Its 2-Alkyl Derivatives Determined by DFT Calculations. **2012**, 13.
- (15) MacLeod, M. J.; Johnson, J. A. PEGylated N-Heterocyclic Carbene Anchors Designed To Stabilize Gold Nanoparticles in Biologically Relevant Media. *J. Am. Chem. Soc.* **2015**, 137 (25), 7974–7977.
- (16) Martínez-Prieto, L. M.; Cano, I.; Márquez, A.; Baquero, E. A.; Tricard, S.; Cusinato, L.; Rosal, I. del; Poteau, R.; Coppel, Y.; Philippot, K.; Chaudret, B.; Cámpora, J.; Leeuwen, P. W. N. M. van. Zwitterionic Amidinates as Effective Ligands for Platinum Nanoparticle Hydrogenation Catalysts. *Chem. Sci.* **2017**, 8 (4), 2931–2941.
- (17) Rühling, A.; Schaepe, K.; Rakers, L.; Vonhören, B.; Tegeder, P.; Ravoo, B. J.; Glorius, F. Modular Bidentate Hybrid NHC-Thioether Ligands for the Stabilization of Palladium Nanoparticles in Various Solvents. *Angew. Chem. Int. Ed.* **2016**, 55 (19), 5856–5860.
- (18) Narouz, M. R.; Li, C.-H.; Nazemi, A.; Crudden, C. M. Amphiphilic N-Heterocyclic Carbene-Stabilized Gold Nanoparticles and Their Self-Assembly in Polar Solvents. *Langmuir* **2017**, 33 (50), 14211–14219.

- (19) Salorinne, K.; Man, R. W. Y.; Li, C.-H.; Taki, M.; Nambo, M.; Crudden, C. M. Water-Soluble N-Heterocyclic Carbene-Protected Gold Nanoparticles: Size-Controlled Synthesis, Stability, and Optical Properties. *Angew. Chem.* **2017**, *129* (22), 6294–6298.
- (20) Man, R. W. Y.; Li, C.-H.; MacLean, M. W. A.; Zenkina, O. V.; Zamora, M. T.; Saunders, L. N.; Rousina-Webb, A.; Nambo, M.; Crudden, C. M. Ultrastable Gold Nanoparticles Modified by Bidentate N-Heterocyclic Carbene Ligands. *J. Am. Chem. Soc.* **2018**, *140* (5), 1576–1579.
- (21) Moulder, J. F.; Stickle, W. F.; Sobol, P. E.; Bomben, K. D. *Handbook of X-Ray Photoelectron Spectroscopy: A Reference Book of Standard Spectra for Identification and Interpretation of XPS Data*; Chastain, J., Ed.; Physical Electronics Division, Perkin-Elmer Corporation, 1992.
- (22) Mercier, D.; Leconte, N.; Méthivier, C.; Suzenet, F.; Guillaumet, G.; Wuillaume, A.; Pradier, C.-M. Synthesis and Grafting of a BTP Derivative onto a Quartz Crystal Microbalance for Lanthanide Detection. *Phys. Chem. Chem. Phys.* **2010**, *12* (23), 6099–6106.
- (23) Lockett, V.; Sedev, R.; Bassell, C.; Ralston, J. Angle-Resolved X-Ray Photoelectron Spectroscopy of the Surface of Imidazolium Ionic Liquids. *Phys. Chem. Chem. Phys.* **2008**, *10* (9), 1330–1335.
- (24) Batra, A.; Kladnik, G.; Gorjizadeh, N.; Meisner, J.; Steigerwald, M.; Nuckolls, C.; Quek, S. Y.; Cvetko, D.; Morgante, A.; Venkataraman, L. Trimethyltin-Mediated Covalent Gold–Carbon Bond Formation. *J. Am. Chem. Soc.* **2014**, *136* (36), 12556–12559.
- (25) Boukerma, K.; Chehimi, M. M.; Pinson, J.; Blomfield, C. X-Ray Photoelectron Spectroscopy Evidence for the Covalent Bond between an Iron Surface and Aryl Groups Attached by the Electrochemical Reduction of Diazonium Salts. *Langmuir* **2003**, *19* (15), 6333–6335.
- (26) Petraki, F.; Papaefthimiou, V.; Kennou, S. The Electronic Structure of Ni-Phthalocyanine/Metal Interfaces Studied by X-Ray and Ultraviolet Photoelectron Spectroscopy. *Org. Electron.* **2007**, *8* (5), 522–528.
- (27) Gardner, S.; Kawamoto, T.; Curran, D. P. Synthesis of 1,3-Dialkylimidazol-2-ylidene Boranes from 1,3-Dialkylimidazolium Iodides and Sodium Borohydride. *J. Org. Chem.* **2015**, *80* (19), 9794–9797.
- (28) Collado, A.; Gómez-Suárez, A.; Martín, A. R.; Slawin, A. M. Z.; Nolan, S. P. Straightforward Synthesis of [Au(NHC)X] (NHC = N-Heterocyclic Carbene, X = Cl, Br, I) Complexes. *Chem. Commun.* **2013**, *49* (49), 5541–5543.
- (29) Jokerst, J. V.; Lobovkina, T.; Zare, R. N.; Gambhir, S. S. Nanoparticle PEGylation for Imaging and Therapy. *Nanomed.* **2011**, *6* (4), 715–728.
- (30) Crudden, C. M.; Horton, J. H.; Ebralidze, I. I.; Zenkina, O. V.; McLean, A. B.; Drevniok, B.; She, Z.; Kraatz, H.-B.; Mosey, N. J.; Seki, T.; Keske, E. C.; Leake, J. D.; Rousina-Webb, A.; Wu, G. Ultra Stable Self-Assembled Monolayers of N-Heterocyclic Carbenes on Gold. *Nat. Chem.* **2014**, *6* (5), 409–414.
- (31) Li, Z.; Munro, K.; Ebralize, I. I.; Narouz, M. R.; Padmos, J. D.; Hao, H.; Crudden, C. M.; Horton, J. H. N-Heterocyclic Carbene Self-Assembled Monolayers on Gold as Surface Plasmon Resonance Biosensors. *Langmuir* **2017**, *33* (49), 13936–13944.
- (32) Baquero, E. A.; Tricard, S.; Coppel, Y.; Flores, J. C.; Chaudret, B.; de Jesús, E. Water-Soluble Platinum Nanoparticles Stabilized by Sulfonated N-Heterocyclic Carbenes: Influence of the Synthetic Approach. *Dalton Trans.* **2018**, *47*, 4093–4104.
- (33) Sun, Y.; Jose, D.; Sorensen, C.; Klabunde, K. Alkyl and Aromatic Amines as Digestive Ripening/Size Focusing Agents for Gold Nanoparticles. *Nanomaterials* **2013**, *3* (3), 370–392.
- (34) Yang, G.; Chang, W.-S.; Hallinan, D. T. A Convenient Phase Transfer Protocol to Functionalize Gold Nanoparticles with Short Alkylamine Ligands. *J. Colloid Interface Sci.* **2015**, *460*, 164–172.
- (35) Rodrigues, M.; Russo, L.; Aguiló, E.; Rodríguez, L.; Ott, I.; Pérez-García, L. Au(I) N-Heterocyclic Carbenes from Bis-Imidazolium Amphiphiles: Synthesis, Cytotoxicity and Incorporation onto Gold Nanoparticles. *RSC Adv.* **2015**, *6* (3), 2202–2209.
- (36) Roy, M. M. D.; Rivard, E. Pushing Chemical Boundaries with N-Heterocyclic Olefins (NHOs): From Catalysis to Main Group Element Chemistry. *Acc. Chem. Res.* **2017**, *50* (8), 2017–2025.
- (37) Fürstner, A.; W, L. C.; Alcarazo. Coordination Chemistry of Ene-1,1-Diamines and a Prototype “Carbodicarbene.” *Angew. Chem. Int. Ed.* **2008**, *47* (17), 3210–3214.

CHAPTER III: SYNTHESIS OF N-HETEROCYCLIC CARBENE-CAPPED GOLD NANOPARTICLES FROM NHC-BORANES

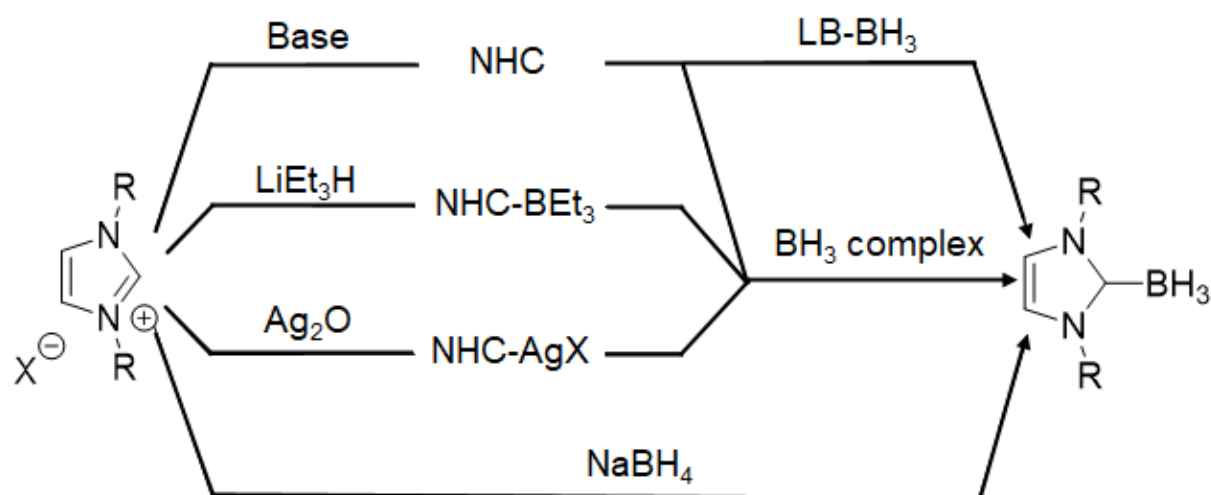
III.A. Bibliographic introduction on N-heterocyclic carbene boranes

NHC-boranes are Lewis adducts between NHCs (Lewis bases) and boranes (Lewis acids). Unlike free NHCs and boranes, they are known to be stable to air and moisture. They have already exhibited reducing properties (see below). As shown in the previous chapters, NHCs are good stabilizing agents for metallic nanoparticles. Our goal was thus to use NHC-boranes as a 2-in-1 reagent acting as both NHC sources and reducing agents.

While NHC-boranes present a wide range of available structures,¹ the following section will focus on those that present an imidazol-2-ylidene-BH₃ (NHC-BH₃) structure.

III.A.1. Synthesis of NHC-boranes

There are several routes to obtain NHC-boranes described in the literature and discussed below. They are summarized in Scheme III.1.



Scheme III.1: Different types of synthesis to obtain NHC-BH₃ (LB=Lewis base).

The first NHC-BH₃ was described by Kuhn *et al.* in 1993.² By reacting a range of NHCs with either BH₃.SMe₂ or BF₃.EtO₂ in THF at 0°C, they obtained NHC-BH₃ and NHC-BF₃ adducts. They found the adducts to be air stable and were able to obtain crystal structures.

In the following years, most syntheses of NHC-boranes followed a similar pathway by forming the carbene *in situ* by deprotonating an imidazolium salt with a base (NaHMDS,³ KHMDS,⁴ tBuOK,⁵ n-

BuLi,⁴...) at low temperatures (typically 0°C or -78°C) before introducing a borane complex (for example BH₃.SMe₂ or BH₃.THF). While this type of synthesis allows for the use of a wide range of imidazoliums and the corresponding NHCs structures, it requires strict anhydrous and inert conditions in order to preserve the reactivity of the NHC and borane moieties.

Over the years a few alternatives have been developed. For example, Makhlof Brahmi *et al.* developed a synthesis based on Lewis base exchange with amine and phosphine boranes and NHCs.⁵ While primary and secondary amines were not suited for the exchange, reactions carried out with tertiary amines (NMe₃, NEt₃), DMAP or pyridine, all performed better than the control reaction with BH₃.THF (70-93% yield compared to 40%). When comparing different NHC sources, they found that while most results were similar or better when using the amine borane, a few sterically hindered imidazoliums performed poorly compared to the control. This is probably due to the fact that BH₃ is less tightly bound and less sterically hindered when complexed to THF than to amines. They showed that the exchange could also be extended to some phosphines. Indeed, PPh₃.BH₃ yields similar results to NMe₃.BH₃ but only 30% conversion was obtained with PCy₃.BH₃ (Cy=cyclohexyl).

Yamaguchi *et al.* used LiBEt₃H as both a base to obtain the carbene and a Lewis acid source able to form NHC-BEt₃ complexes.⁶ When exposed to BH₃.THF, an exchange occurs, forming the NHC-BH₃ complex. The same thing is observed for BF₃.Et₂O. NHC-BEt₃ complexes thus act as NHC precursors probably due to the weaker Lewis acidity or higher steric bulk of BEt₃ compared to BH₃ and BF₃.

More recently, Yamaguchi *et coll.* designed another “protected” NHC source by using NHC-AgCl complexes⁷ in a base-free synthesis. Such complexes are readily formed when imidazolium is reacted with silver oxide.⁸ They are often used in transmetallation reactions to obtain NHC-M complexes with other metals.⁹⁻¹² They found that refluxing the silver complexes in THF with 2 equivalents of a NaBH₄ free solution of BH₃.THF (commercial solutions usually contain 0.5% of NaBH₄) yielded the best results (96% yield). The technique can be applied to a range of NHCs including sterically hindered 1,3-dimesitylimidazol-2-ylidene borane (diMes-Imd-BH₃) or benzimidazol-2-ylidenes or even some imidazolidines. It is interesting to note that they do not mention any reduction of silver. Indeed, in the literature, silver nanoparticles have been synthesized by the reduction of NHC-AgX complexes.^{8,13}

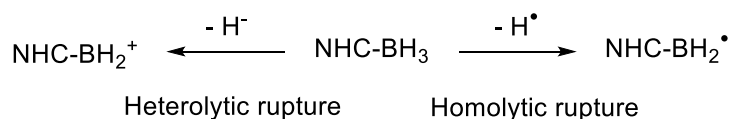
Gardner *et al.* used NaBH₄ as both a base and borane source.¹⁴ The reaction occurred in neat conditions at 105°C but refluxing in toluene yielded better results. Their best yield was obtained for 1,3-dimethylimidazol-2-ylidene borane (diMe-Imd-BH₃) with 53%. They were able to synthesize different boranes including 1,3-diisopropylimidazol-2-ylidene borane (diPr-Imd-BH₃) which required an excess of NaBH₄ to be added during the synthesis to obtain a 46% yield. Even if the reaction is promising due to the use of widely available reagents, the possibility to scale it up to 100 mmol and the possibility to carry it in ambient conditions (no need to exclude air and moisture), it quickly showed limitations.

Indeed, no reaction occurred when using a benzimidazolium or sterically hindered imidazolium and only 5% of a 2,4-dimethyl-1,2,4-triazol-3-ylidene (diMe-124Tri-BH₃) borane was recovered.

In the end, in a standard organic chemistry lab, the first type of synthesis remains accessible and presents the widest range of available structures for NHC-BH₃ complexes. This probably explains its popularity but the other types of synthesis could prove useful when looking for more specific type of structures, base-free syntheses or for laboratories ill-equipped to carry out sensitive reactions.

III.A.2. Uses of NHC-boranes in molecular chemistry

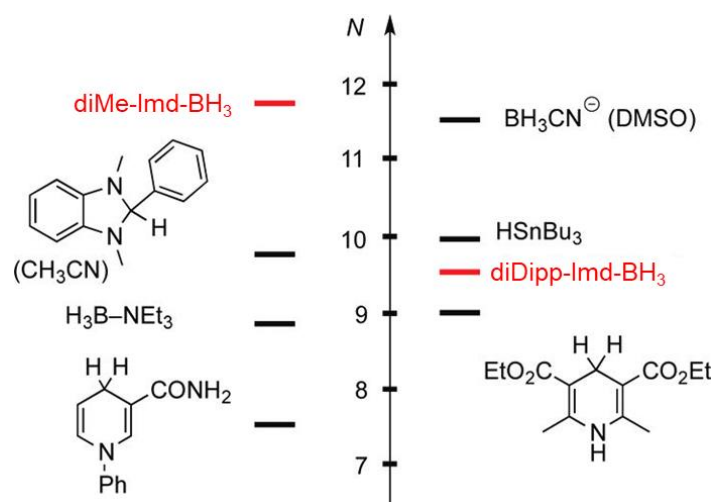
NHC-boranes are expected to behave as hydrogen donors^{1,15,16} either by heterolytic rupture giving a hydride and a borenium cation (NHC-BH₂⁺), or homolytic rupture giving H[•] and a boryl radical (NHC-BH₂[•]) (Scheme III.2). Both types have been studied in the literature and applied to a variety of substrates.



Scheme III.2: Two hydrogen donation types possible for NHC-BH₃.

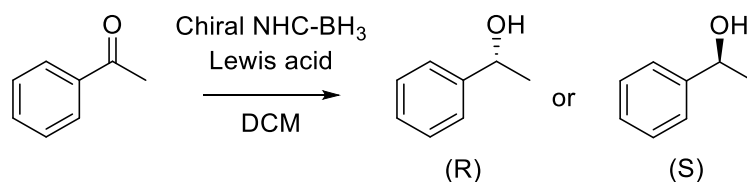
III.A.2.a. Heterolytic rupture

Horn *et al.* measured the nucleophilicity of diMe-Imd-BH₃ and 1,3-bis(2,6-diisopropylphenyl)imidazol-2-ylidene borane (diDipp-Imd-BH₃).¹⁵ They found that while neither borane could compare with BH₄⁻, diDipp-Imd-BH₃ was on par with neutral reference hydride donors, such as trialkylamine boranes and benzimidazolines, while diMe-Imd-BH₃ surpassed all of them and has a nucleophilicity closer to that of ionic BH₃CN⁻ (Scheme III.3). They also showed that diMe-Imd-BH₃ could react with C=N or C=C double bonds substituted with strong electron withdrawing groups. For example, they reduced iminium ions to the corresponding anilines in good yields even if NHC-BH₃ was introduced in default. The NHC-BH₃ could also be used to conduct one-pot reductive aminations starting from anilines or aldehydes, as they do not react with C=O bonds. NHC-BH₃ even prove to be more practical reagents as they are less toxic, more stable and more easily eliminated than conventional reagents for this type of reaction, such as sodium cyanoborohydride (NaBH₃CN), sodium triacetoxyborohydride (NaBH(OAc)₃) or amine boranes.



Scheme III.3: Nucleophilicity parameters (N) of some hydride donors (in CH_2Cl_2 if not otherwise noted).¹⁵

This type of reactivity has also been used in a range of reactions.^{17–20} For example, in the asymmetric reduction of ketones. Indeed in 2010, Lindsay *et al.* were the first to report the synthesis of chiral NHC-boranes. They were then able to use those chiral NHC-BH₃ in the asymmetric reduction of acetophenone (Scheme III.4).⁴

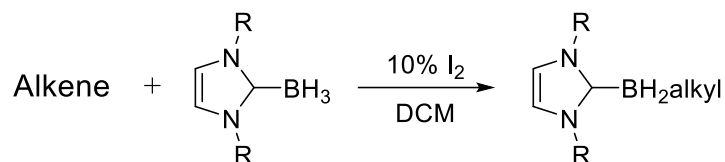


Scheme III.4: Asymmetric reduction of acetophenone by a chiral NHC-BH₃.⁴

They established proof of concept using 3,7-diisopropyl-THIBO borane (diiPr-THIBO-BH₃) at room temperature and 0°C yielding the *S* enantiomer in 14% enantiomeric excess (ee) (44% conversion) and 36% ee (10% conversion) respectively. They were able to increase the yield and ee (to 95% and 42%) by activating the ketone with a Lewis acid ($\text{Sc}(\text{OTf})_3$). However, they obtained the opposite enantiomer (*R* instead of *S*). By changing the functional groups of the NHC-BH₃ from *iPr* to *tBu*, the enantioselectivity was reversed again and they were able to obtain the *S* enantiomer in 75% ee (60% yield). By using NHC-9BBN instead of BH₃ they were able to increase the ee even higher to 84% by changing the Lewis acid to less sterically demanding $\text{BF}_3 \cdot \text{OEt}_2$. They tested their conditions on a scope of ketone substrates and most results compared favorably to the existing literature.

In theory, hydride abstraction from an NHC-borane will lead to a borenium ion (NHC-BH_2^+) but such ions are known to be unstable in solution.²¹ Their reactivity however can be studied using “borenium ion equivalents” such as $\text{LB-BH}_2\text{X}$ (LB= lewis base, X= good leaving group). This is what Pan *et al.* did in 2013 by using molecular iodine as an activator for the hydroboration of alkenes by NHC-BH₃ (Scheme III.5).²¹ NHC-boranes are typically inert to alkene hydroboration because of their stability, but they

found that by introducing molecular iodine in the reaction medium they formed NHC-BH₂I which acts as a catalyst. They tested diMe-Imd-BH₃ on a range of alkenes and found that the monohydroboration product was obtained in most cases. They showed that the synthesis could be extended to 1,5-cyclo-octadiene to form NHC-9BBN and even to intra molecular reaction using alkenyl NHC-boranes. They were also able to extend the reaction to a range of NHC-BH₃ with low steric hindrance. If the NHC-BH₃ was sterically hindered (such as diMes-Imd-BH₃ or diDipp-Imd-BH₃) no hydroboration product was detected as NHC-BH₂I was not consumed upon addition of the alkene.

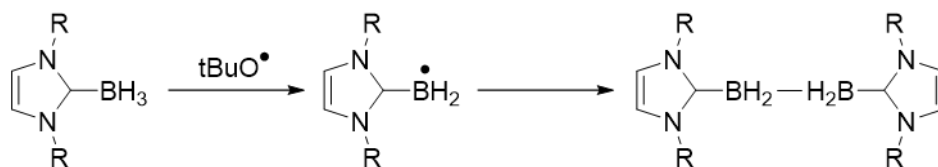


R = Me, *i*Pr, cyclohexyl

Scheme III.5: Iodine activated hydroboration of alkenes by NHC-BH₃.²¹

III.A.2.b. Homolytic rupture

The radical reactivity of NHC-BH₃ has also been extensively studied in the literature. DFT calculations¹⁶ have calculated the B-H bond dissociation energy (BDE) of NHC-BH₃ at 80 kcal.mol⁻¹. That is 20 kcal.mol⁻¹ lower than amine-boranes such as NH₃BH₃³ and 30 kcal.mol⁻¹ lower than BH₃ alone.¹⁶ This lowered BDE makes NHC-BH₃ good candidates for radical chemistry. EPR studies showed that tBuO[•] radicals removed H atoms from NHC-BH₃ to form NHC-BH₂[•] in a very rapid process (Scheme III.6)³. Radicals formed from imidazol-2-ylidene boranes were clearly observable by EPR while those obtained from benzimidazol-2-ylidene showed very weak signals if any. The radicals are roughly planar at the boron atom and the unpaired electron is delocalized into the NHC ring. They found that termination was extremely rapid and likely diffusion controlled. The decay process was followed by EPR. It most likely happens by irreversible dimerization (Scheme III.6), which is strongly influenced by the lateral substituents, as more hindered radicals dimerize more slowly than the others. The same study also found that while boryl radicals were able to abstract bromine atoms from various sources, chlorine atom abstraction was less efficient as only unhindered boryl radicals were able to abstract chlorine from allylic and benzylic chlorides.

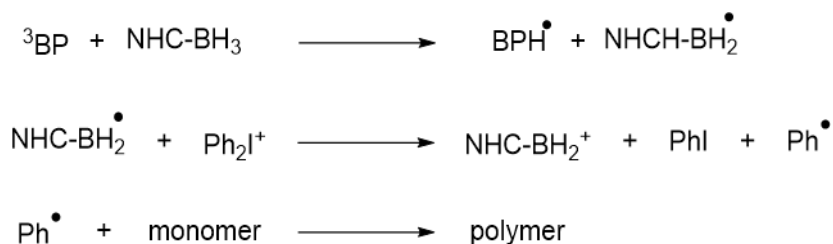


Scheme III.6: Formation and dimerization of NHC-BH₂[•].

Such radical reactivity has been exploited in a range of reactions throughout the years including the reduction of xanthates^{16,22} and alkyl halides,²³ hydroboration of alkynes²⁴ and imines,²⁵ among others.^{26,27}

NHC-boranes can also act as radical polymerization initiator. Tehfe *et al.*²⁸ investigated the use of 3 different NHC-BH₃ as co-initiators in the photopolymerization of trimethylolpropane triacrylate (TMPTA) with benzophenone as a photoactivator. The results were compared to triethyl amine borane and the reference co-initiator in this type of polymerization: ethyl-dimethylaminobenzoate (EDB). They found that while no NHC-BH₃ could match the commercial co-initiator, they all significantly improved the polymerization and were all better than reactions carried out with the amine borane or no co-initiator. Adding Ph₂IPF₆ increased the polymerization rate, for all NHC-BH₃, which resembled the one of EBD. One notable advantage is that NHC-BH₃/benzo/Ph₂IPF₆ mixtures were stable for at least a week whereas EBD mixtures degrade rapidly and have to be freshly prepared.

Investigation into the mechanism showed that benzophenone (in its triplet state) is an even better hydrogen abstractor than tBuO[•] and that the reaction corresponds to a pure hydrogen atom transfer with the triplet state of benzophenone reacting like an alkoxy radical. The increase in polymerization rate using Ph₂I⁺PF₆⁻ probably stems from the high rate constant for the oxidation of boryl radicals to borenium cations. The conversion releases a phenyl radical which initiates radical photopolymerization better than boryl radicals (Scheme III.7).



Scheme III.7: Radical polymerization initiation with NHC-BH₃ (³BP = benzophenone in the triplet state).²⁸

III.A.3. Uses of NHC-boranes beyond molecular chemistry

While the potential applications of NHC-boranes in molecular chemistry have been extensively studied, recently applications in other fields have been explored.

For example, in biology, where Pak *et al.*²⁹ showed in 2018, that a NHC-BH₃ functionalized with pyrene, acting as a fluorescence reporter, could be used to selectively detect HOCl in living cells (Figure III.1). Indeed, the NHC-BH₃ showed little to no change in fluorescence when reacted with a range of reactive oxygen species but its fluorescence decreased significantly in favor of the fluorescence of the reaction product (imidazolium) when OCl⁻ was introduced. They showed in NMR experiments that NHC-BH₃ had a kinetic selectivity for hypochlorite over peroxides that can be as high as 10⁸:1. Tests in solution

showed that the detection limit is of $3\mu\text{M}$ which is much lower than typical biological range of $20\text{--}400\ \mu\text{M}$. Finally experiments on living cells showed that fluorescence microscopy images of NHC-BH₃ directly reflect the presence of HOCl in the cells with minimal influence of cytotoxicity and photobleaching.

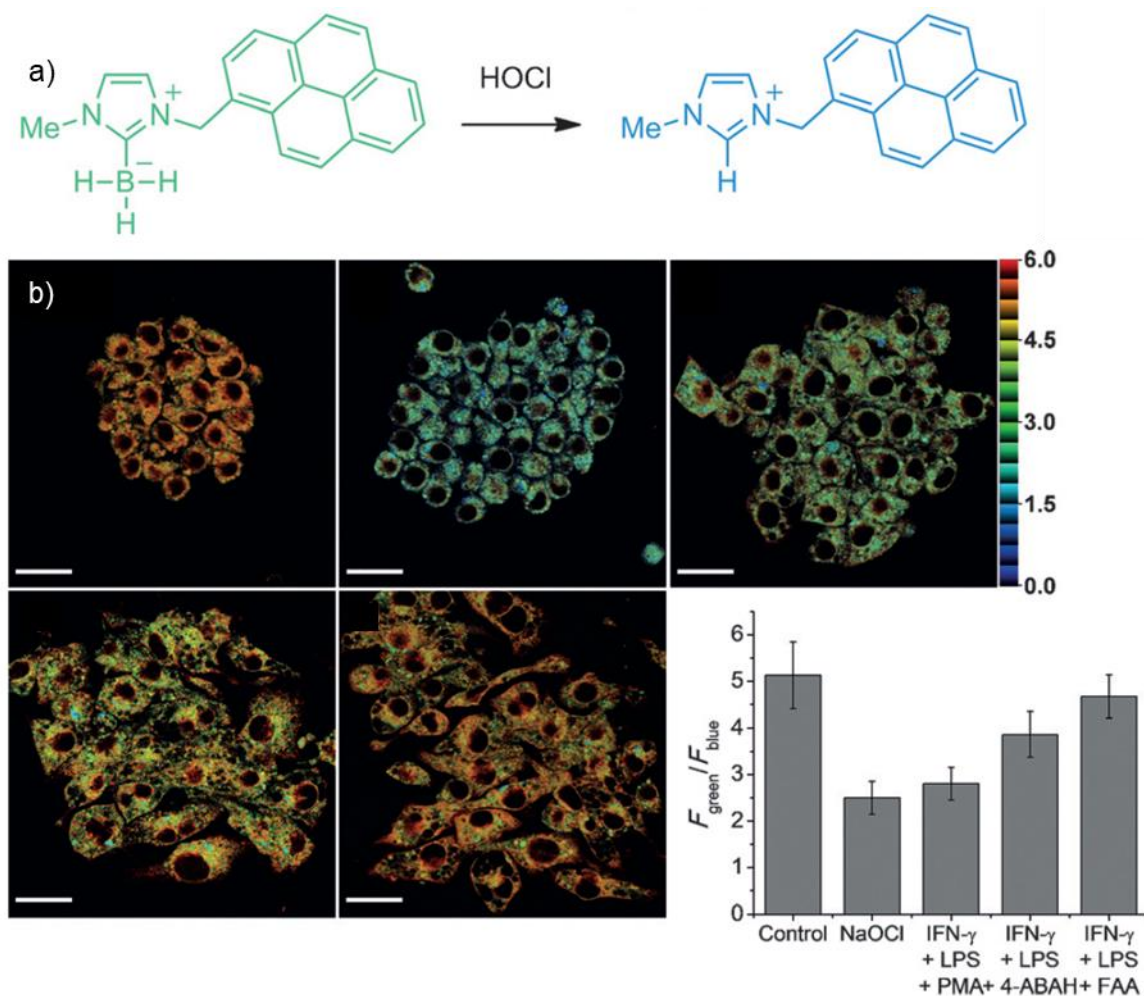


Figure III.1: a) NHC-BH₃ functionalized by fluorescence reporter and its reaction with HOCl, b) fluorescence microscopy images of cells incubated with NHC-BH₃ and average $F_{\text{green}}/F_{\text{blue}}$ intensity ratios of different samples.²⁹

NHC-BH₃ have also been tested as potential rocket fuel.³⁰ Indeed, the current rocket fuel of choice, hydrazine (and its derivatives), is highly toxic, volatile, carcinogenic and difficult to handle. In 2016, Huang *et al.* postulated that since NHC-BH₃ have reducing properties they should have a violent exothermic reaction with strong oxidizers, such as WFNA (white fuming nitric acid), which should lead to spontaneous combustion. They synthesized 6 different NHC-BH₃ with the synthesis of Gardner *et al.*¹⁴ by refluxing the corresponding imidazolium with NaBH₄ in toluene. All NHC-BH₃ exhibited hypergolic activity upon contact with WFNA. The shortest ignition time was exhibited by diMe-Imd-BH₃ with 2ms (compared to widely used hydrazine derivative at 4.7 ms) but its high melting point

(141°C) makes it an impractical candidate for liquid fuel. The second best candidate was 1-methy-3-allylimidazol-2-ylidene borane (MeAl-Imd-BH₃) which is liquid at room temperature, has high thermal and water stability, and exhibited an ignition time of 15 ms (Figure III.2) which is not as fast as hydrazine derivatives but still good regarding industry standards.

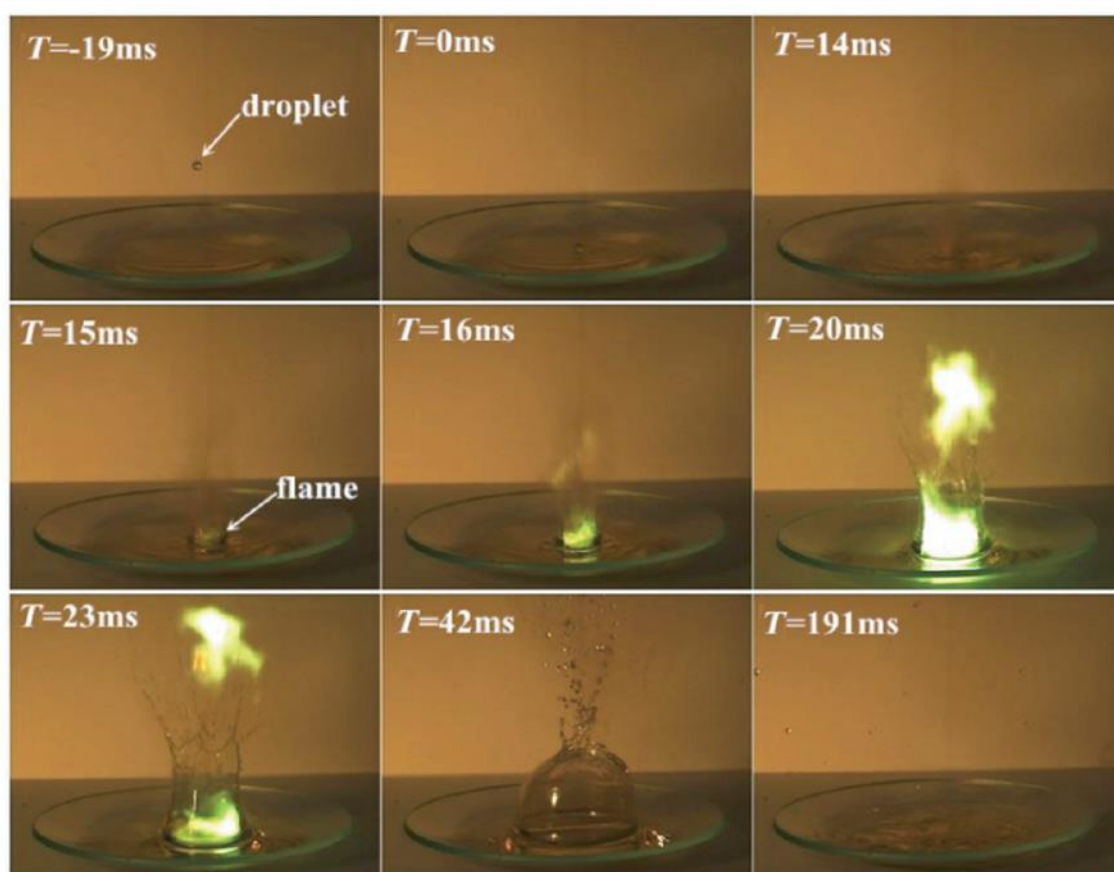
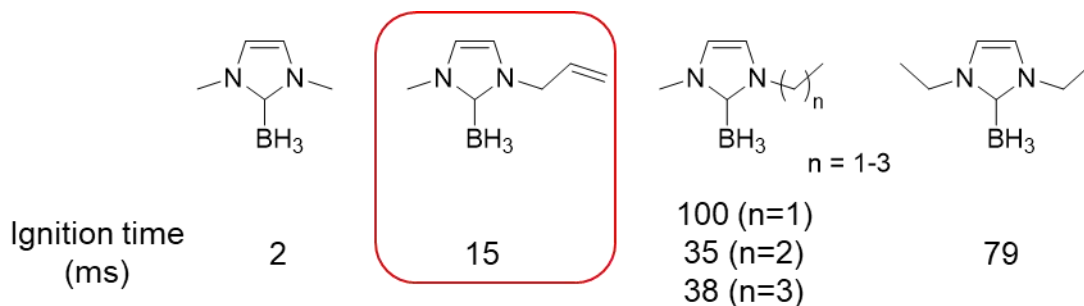


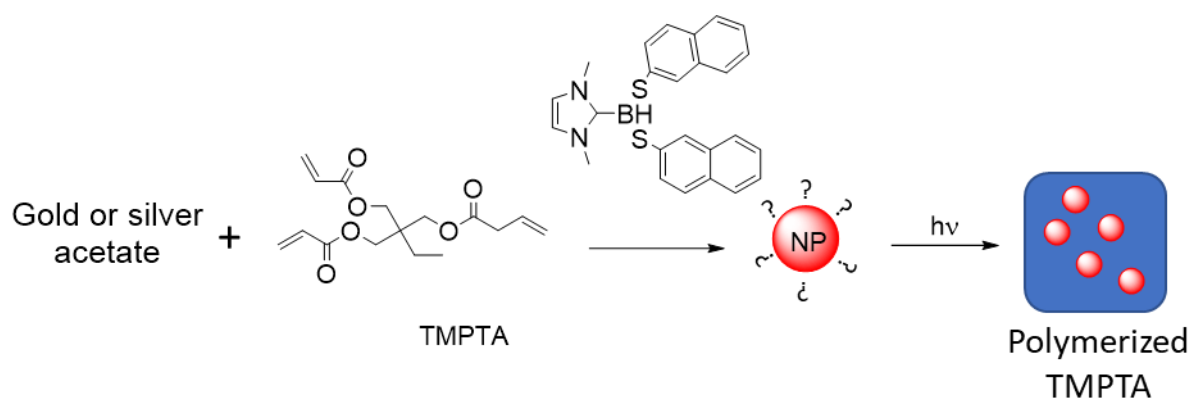
Figure III.2: Structures of NHC-boranes tested and high-speed camera photos of MeAl-Imid-BH₃ falling into 100% HNO₃.³⁰

NHC-boranes have also showed potential as reducing agents in the synthesis of gold and silver nanoparticles.³¹ Indeed Le Quemer presented, in his 2016 PhD dissertation, a synthesis of silane stabilized gold nanoparticles using diMe-Imd-BH₃ as a reducing agent. Using a Brust-like synthesis, they dissolved chloroauric acid in water and transferred it into the organic phase (toluene) using TOAB as a phase transfer agent. An excess of octylsilane and 2 equivalents of NHC-BH₃ were then successively

introduced. The reduction of the gold was indicated by a change of color of the solution. However, they found that using an excess of 2 equivalents of NHC-BH₃ led to mostly aggregated NPs, but lowering the amount of NHC-BH₃ to 0.6 and 0.4 eq gave a mixture of aggregates and discrete nanoparticles. Finally, lowering down the amount of NHC-BH₃ to 0.2 eq led to discrete NPs (no size given). It is unclear if all the gold in solution is reduced as it is not discussed. However, it seems unlikely that such a small quantity of reducing agent would reduce all the gold. Indeed, even if all 3 hydrides of the NHC-BH₃ are consumed only 0.6 eq of gold would be reduced.

In this study, their end goal was to encapsulate metallic nanoparticles in a polymer matrix. Their team had already shown the ability of 1,3-dimethylimidazol-2-ylidene bithionaphtylborane (Scheme III.8) to trigger the polymerization of trimethylolpropane triacrylate (TMPTA) upon light irradiation. After optimization of the conditions, they found the borane was able to form nanoparticles in MeCN starting from either gold or silver acetate. Once that was established, they mixed the metal precursor with TMPTA monomers in acetonitrile. The NHC-borane was added to form the nanoparticles before irradiating the solution to trigger polymerization effectively trapping the nanoparticles in the matrix (Scheme III.8).

It can be noted that even though they suggest a stabilization of the nanoparticles by thionaphtyls, they did not characterize the surface of the NPs. As a result, it is unclear what is at the surface.

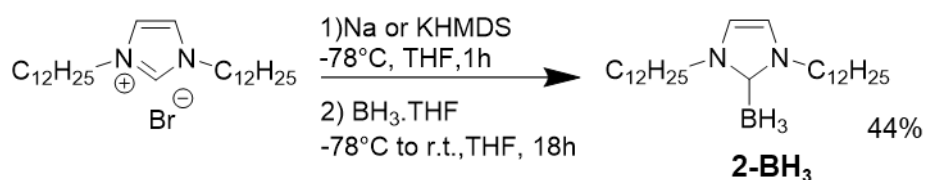


Scheme III.8: Synthesis of metallic NPs trapped in polymerized TMPTA by reduction of gold or silver acetate by an NHC-borane in the presence of TMPTA monomers.³¹

The last example came out after the beginning of our research project, yet it comforts the idea that NHC-boranes are enough to reduce gold into nanoparticles. The rest of this chapter will confirm these possibilities and will present the development of a gold nanoparticles synthesis using NHC-BH₃ not only as reducing agent but also as NHC sources to stabilize the nanoparticles. Characterization of the obtained nanoparticles will also be discussed.

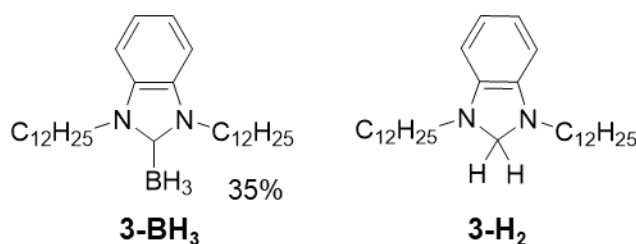
III.B. NHC-BH₃ synthesis

To ensure consistency, we synthesized our NHC-borane from the 1,3-didodecylimidazolium **2H-Br** used in Chapter II. The chosen protocol (Scheme III.9) is the most common in the literature and involves the *in situ* deprotonation of the (benz)imidazolium by a strong base (often Na or KHMDS) at -78°C before the addition of a BH₃ complex (in our case BH₃.THF). The reaction mixture is stirred overnight at room temperature then purified by flash chromatography. The NHC-borane adduct is readily obtained on a gram scale with a 44% yield. As other NHC-boranes of the literature, it is a white powder that is bench stable for months (even years).



Scheme III.9: Synthesis of **2-BH₃**.

The synthesis of the NHC-BH₃ from 1,3-didodecylbenzimidazolium **3H-Br** was also attempted following the same procedure. However, a byproduct is formed in almost the same quantity as the NHC-BH₃ itself (Scheme III.10). The byproduct has been identified as the hydride-reduced benzimidazolium (**3-H₂**). This led to a difficult purification and poor yield (35% at best). In the rest of this chapter “NHC-BH₃” will thus designate compound **2-BH₃**.



Scheme III.10: **3-BH₃** and byproduct formed during the synthesis.

III.C. Nanoparticles synthesis from gold precursor: AuClPPh₃

III.C.1. First attempts

It was decided to start from a gold(I) precursor. AuClPPh₃ was chosen as it is known to be soluble in organic solvents and is already used in the literature as a precursor in gold nanoparticles synthesis.³²

In an attempt to stay as close as possible to the conditions in Chapter 1, the first experiments were carried out in toluene. Upon addition of excess **2-BH₃** (6 eq) to a solution of AuClPPh₃, the solution started to slowly color to brown then pink and finally turned to dark purple after 18h of reaction. The obtained nanoparticles were characterized by UV-Vis spectroscopy and TEM (Figure III.3). They were of 5.4 ± 1.2 nm in diameter with a plasmon resonance at 570 nm. However, they were not stable and kept coalescing over a few days as evidenced by a blue shift of the plasmon band.

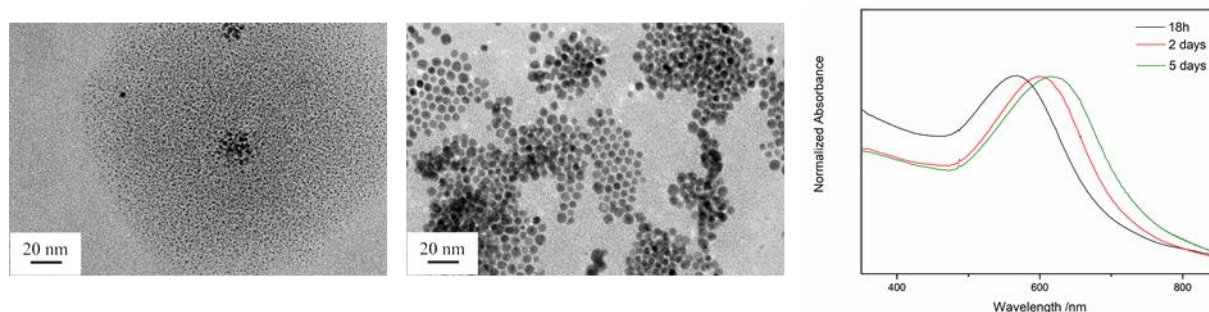


Figure III.3: TEM images of nanoparticles obtained after 6h and 18h of reaction (1eq AuClPPh₃ + 6eq **2-BH₃**) in toluene and UV-Vis spectra of the suspension.

As the reaction appeared slow, following it by *in situ* ¹H and ¹¹B NMR was attempted. However, after several hours, the only peaks that had shifted belonged to a small impurity present in the NHC-BH₃ batch used.

This impurity was isolated and characterized by NMR (Figure III.4) and mass spectrometry (ESI⁺, Scheme III.11). The ¹¹B NMR presents a broad singlet at -11.6 ppm that suggests the presence of boron in the impurity. The ¹H NMR spectrum (Figure III.4) presents peaks in the 4 to 0.5 ppm region only. This suggests a dearomatization of the heterocycle and a hydrogenation of the double bond. The peaks in the 2 to 0.5 ppm region seem to correspond to the aliphatic chains. Despite several 2D NMR experiments, a structure for this impurity could not be confirmed. Moreover, attempts to crystallize it were unsuccessful.

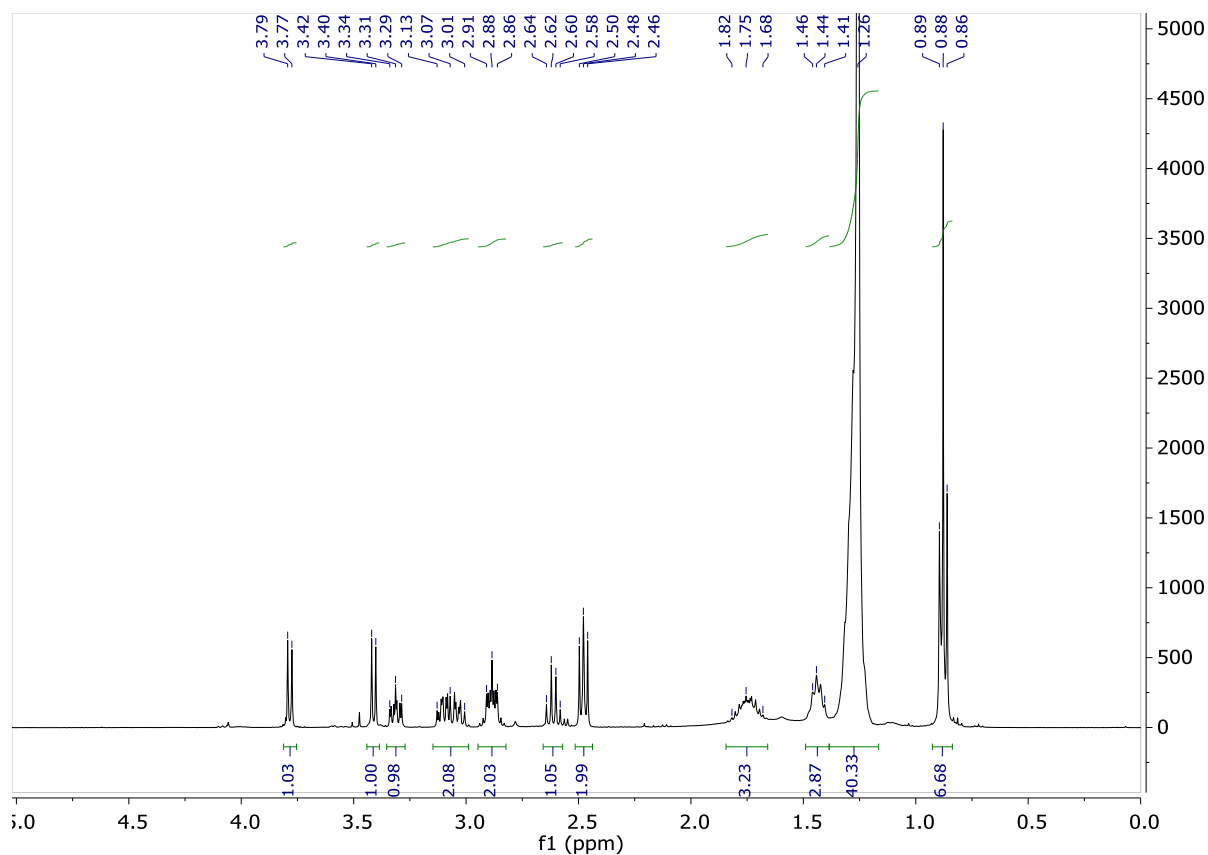
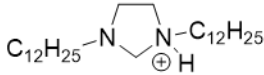
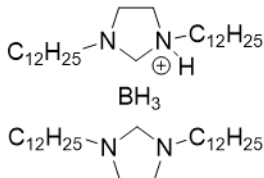
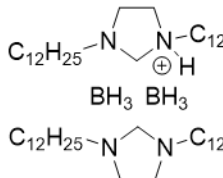


Figure III.4: ^1H NMR spectra of the isolated impurity in CDCl_3 .

When analyzing the impurity by mass spectrometry (ESI^+), 3 peaks at $m/z = 409.3679$, 831.8206 and 845.8528 are visible. The proposed atomic compositions corresponding to these masses are presented in Scheme III.11. It can be noted that the calculated m/z all differ by about 0.1 unit from the measurements. As the isotopic patterns correspond perfectly, this difference likely stems from the fact the spectra were recorded in low resolution. Tentative structures were drawn (Scheme III.11). They appear to correspond to a reduced form of the imidazolium which has been protonated at one nitrogen atom and is able to form stable adducts with the borane. Even though the way these adducts are formed and if they are stable remains unclear, the presence of BH_3 in the adducts suggests a potential reducing power.

Experimental <i>m/z</i>	409.3679	831.8206	845.8528
Proposed atomic compositions	$N_2C_{27}H_{57}$	$BN_4C_{54}H_{116}$	$B_2N_4C_{54}H_{119}$
Calculated <i>m/z</i>	409.4516	831.9288	845.9615
Tentative structures			

Scheme III.11: Peaks observed by MS (ESI⁺) analysis of the impurity, corresponding molecular composition and proposed structures.

Once isolated, a few mg (<5) of the impurity were added to a solution of AuClPPH₃ (1mg.mL⁻¹). As the molar mass of the impurity is unknown it is difficult to know the impurity to gold ratio.

The reaction slowly turned purple in a similar fashion as when using the contaminated NHC-BH₃. However, when 6 equivalents of the purified NHC-BH₃ were introduced in a AuClPPH₃ solution no reaction occurred. This confirms the role of the impurity in the formation of the gold nanoparticles.

It is possible to obtain a larger quantity of impurity by increasing the amount of BH₃.THF used in the NHC-BH₃ synthesis. Indeed, when using 1.05 equivalents of BH₃.THF, the mass of the isolated impurity is about 10% of the mass of the isolated NHC-BH₃. However, when using 1.5 equivalents of BH₃.THF, the mass of the isolated impurity is 5 times larger than the mass of the isolated NHC-BH₃. And the yield of the latter drops from 44% to 10%.

It is worth mentioning that no impurity is observed when using KHMDS as a base instead of NaHMDS. Thus, it can be assumed that sodium plays a crucial role in the formation of these species but it is unclear which role exactly. As our focus was on the synthesis of gold nanoparticles, no test using different bases were carried out.

As mentioned above, once purified the NHC-BH₃ no longer reacted with AuClPPH₃ in toluene. Increasing the quantity of NHC-BH₃ up to 20 equivalents proved ineffective, so did heating the solution as it led only to a slight reduction of the gold, exhibited by a purple coloration on the side of the vial.

III.C.2. Solvent screening

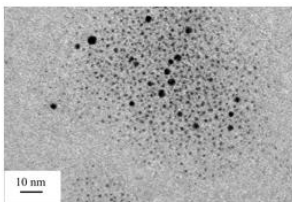
A solvent screening was undertaken to see if the formation of stable NPs from AuClPPh₃ and purified **2-BH₃** was possible in other solvents. The results are presented in Table III.1. In all cases a slight excess of NHC-BH₃ (3 to 5 equivalents for 1 of gold) was used.

AuClPPh₃ is insoluble in cyclohexane and diethyl ether. Heating was necessary to dissolve **2-BH₃** and/or AuClPPh₃ in ethyl acetate, acetonitrile, alcohols and DMSO (for the latter temperatures above 100°C were needed to dissolve NHC-BH₃ which would immediately precipitate upon cooling).

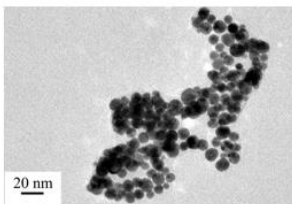
No reduction was observed in dichloromethane, chloroform and ethyl acetate. In THF, dioxane, acetonitrile and acetone, reduction occurred (as evidenced by a change in color of the solution from colorless to blue or purple) but was only partial (very slight coloration). Aggregated NPs were visible by TEM in the case of acetone. In toluene, partial reduction occurred on the side of the vial but only when heat was applied (T > 80°C). What seemed to be complete reduction was observed in DMSO and alcohols. The particles obtained in DMSO were very large and unstable. In the case of alcohols, clusters would be formed but would slowly evolve to form larger nanoparticles (Figure III.5) and finally a gold mirror on the side of the vial in a matter of days.

Table III.1: Solvents screened in the reaction of AuClPPh₃ and **2-BH₃**.

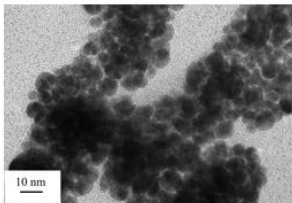
Solvent	Solubility NHC-BH ₃	Solubility AuClPPh ₃	Reduction
Propanol	Yes*	Yes*	Yes
Ethanol	Yes*	Yes*	Yes
DMSO	Yes**	Yes*	Yes*
Toluene	Yes	Yes	Partial *
THF	Yes	Yes	Partial
1,4-Dioxane	Yes	Yes	Partial
Acetonitrile	Yes*	Yes*	Partial
Acetone	Yes	Yes	Partial
Chloroform	Yes	Yes	No
Dichloromethane	Yes	Yes	No
Ethyl acetate	Yes*	Yes*	No
Diethyl ether	-	No	-
Cyclohexane	-	No	-



Propanol



DMSO



Acetone

* if heated above 50°C, **if heated above 100°C

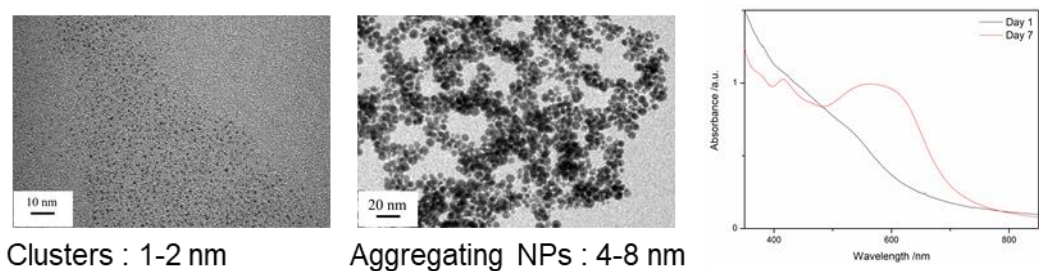
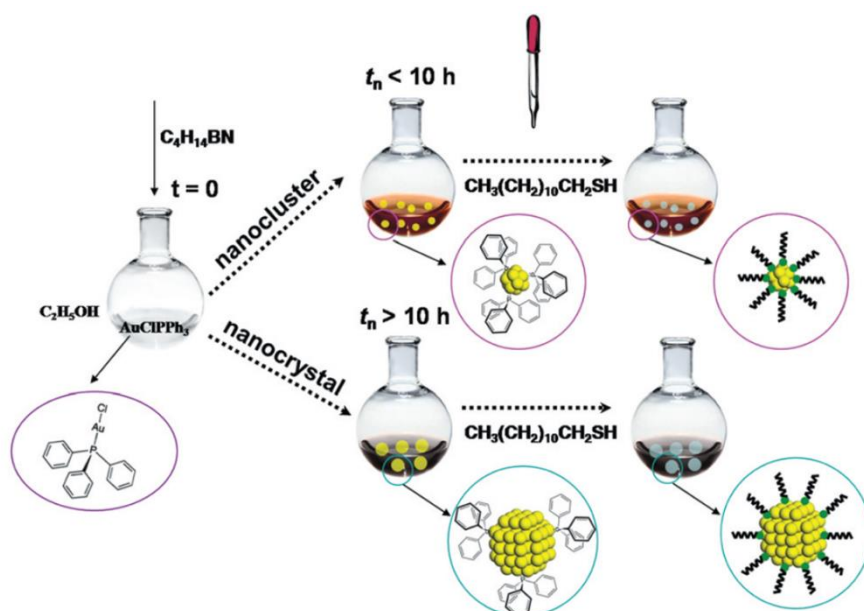


Figure III.5: TEM images and UV-Vis spectra of NPs (1 eq AuClPPH₃ and 6 eq **2-BH₃**) at day 1 and day 7 in ethanol.

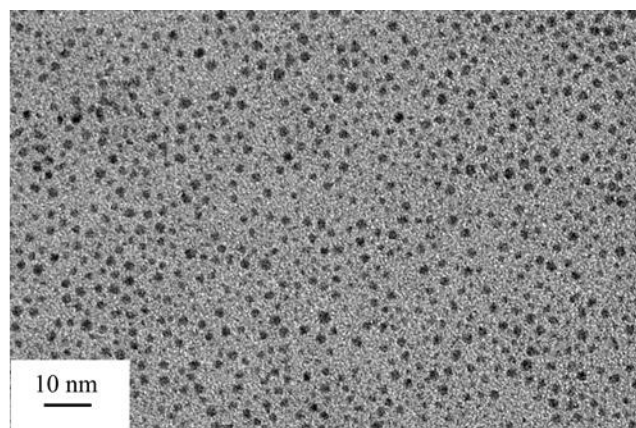
The success in ethanol was surprising as it is the solvent used to precipitate the nanoparticles of Chapter II and also because it is a protic solvent which seems incompatible with the existence of highly reactive carbenes.

A possibility is that the NHC-BH₃ is able to reduce AuClPPH₃ in alcoholic solvents but the phosphine remains on the surface and provides stabilization to the nanoparticles. After a time, the phosphine probably starts to leach off of the NPs leading to their slow aggregation. This theory seems to be confirmed by Li *et al.* (Scheme III.12).³³ Indeed, they describe a synthesis starting from AuClPPH₃ in ethanol and upon addition of a reducing agent (tBuNH₂BH₃ in their case) they obtain nanoclusters which then coalesce and grow into nanoparticles until their growth is halted by addition of thiols that bind to the surface.



Scheme III.12: Synthesis of gold nanoparticles from AuClPPH₃ and tBuNH₂BH₃ in EtOH.³³

Finally, this theory seemed to be confirmed by the addition of NaBH_4 to AuClPPh_3 in ethanol which yielded clusters similar to the ones obtained with NHC-BH_3 without any potential stabilizing agent present in the reaction medium (Figure III.6).



Clusters : 1-2 nm without NHC source

Figure III.6: TEM images of clusters obtained without a NHC source from AuClPPh_3 and NaBH_4 in ethanol.

III.D. Nanoparticles synthesis from gold precursor $\text{HAuCl}_4 \cdot 3\text{H}_2\text{O}$

As a result, AuClPPh_3 was dropped as gold precursor in favor of $\text{HAuCl}_4 \cdot 3\text{H}_2\text{O}$. $\text{HAuCl}_4 \cdot 3\text{H}_2\text{O}$ is highly soluble in water and often used as a gold precursor in aqueous synthesis of gold nanoparticles.³⁴⁻³⁷

Attempts to use a biphasic system of water and toluene, dichloromethane or chloroform, all led to the formation of a metallic gold layer at the interface of the 2 phases.

$\text{HAuCl}_4 \cdot 3\text{H}_2\text{O}$ is also soluble in chloroform up to a point (<100 mM) which allowed for a monophasic system.

A first attempt using 4 equivalents of NHC-BH_3 for 1 equivalent of gold yielded monodisperse spherical nanoparticles (of 5.8 ± 1.4 nm in diameter). However, reproducibility was quickly found to be an issue. Indeed, subsequent attempts led to the formation of nanoparticles ranging from slightly bigger (8.8 ± 2.2 nm) than the first attempt to a mixture of smaller and larger NPs to completely polydisperse NPs of different shapes (Figure III.7). Decreasing the temperature to 0°C or increasing it to 50°C yielded similar unreproducible results.

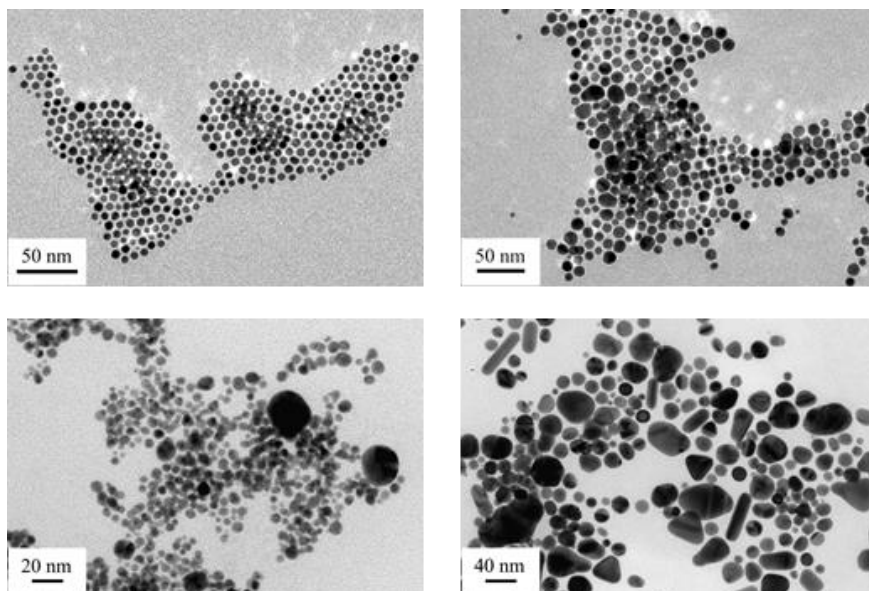


Figure III.7: TEM images of several attempts at synthesizing nanoparticles from $\text{HAuCl}_4 \cdot 3\text{H}_2\text{O}$ (1 eq) and 2-BH_3 (4 eq) in CHCl_3 .

Several hypotheses could be put forward for the difference in behavior: the use of a metallic spatula could have pre-reduced the gold precursor leading to inconsistent results, the amount of water molecules in the precursor is never constant and thus could lead to inconsistency in the gold to ligand ratio, the amount of water in the chloroform, which was used straight from the bottle, could also play a role. The acidity of chloroform could also be an issue.

We also found that $\text{HAuCl}_4 \cdot 3\text{H}_2\text{O}$ remains soluble and stable when a chloroform solution was diluted with a large amount of toluene. When reacted at different Au: NHC- BH_3 ratios with NHC- BH_3 dissolved in toluene, an effect of the ratio on the size was found (Figure III.8). Indeed, when the quantity of NHC- BH_3 was increased, the size of the obtained nanoparticles decreased. However, subsequent attempts were unable to reproduce the results.

Given the major reproducibility issues $\text{HAuCl}_4 \cdot 3\text{H}_2\text{O}$ was dropped as a precursor.

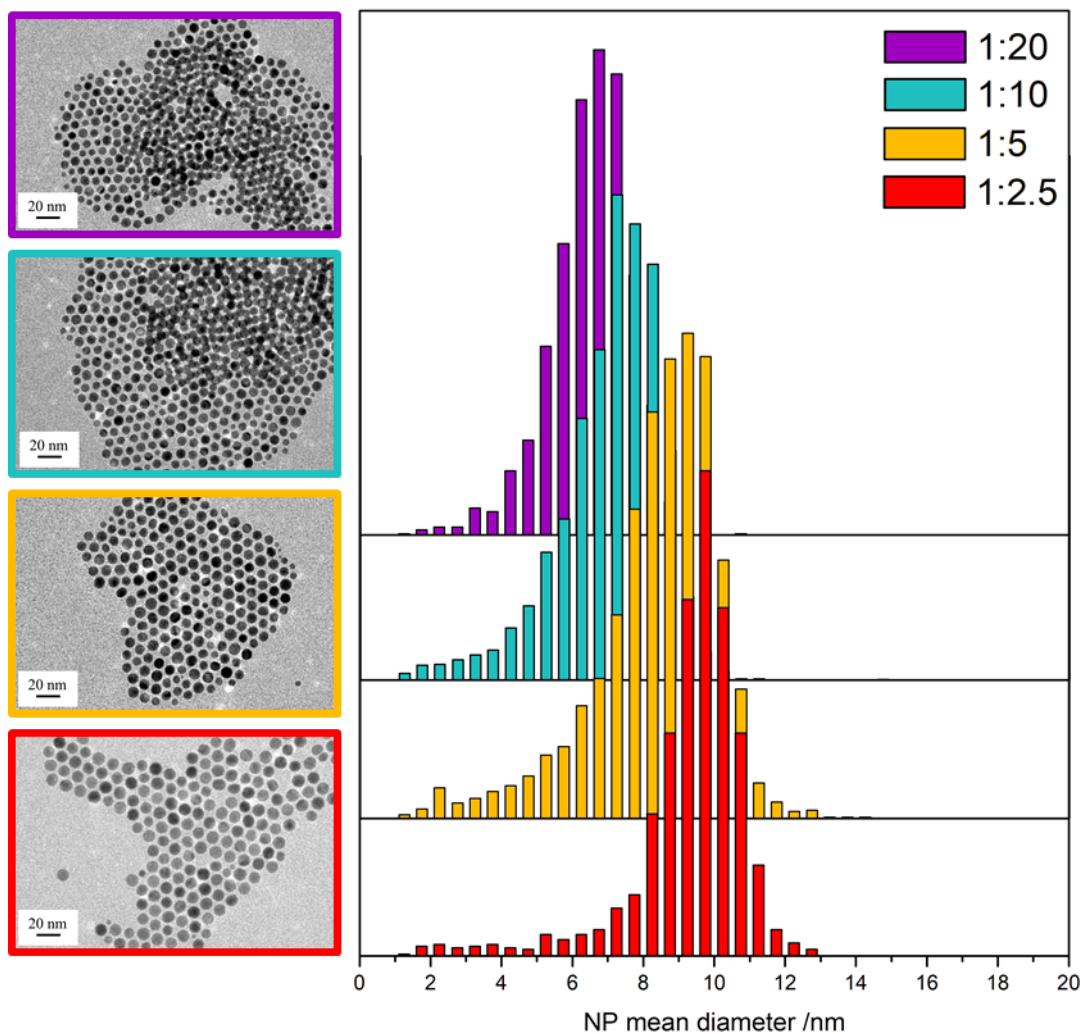


Figure III.8: TEM images and distribution of gold nanoparticles synthesized with different ratios of $\text{HAuCl}_4 \cdot 3\text{H}_2\text{O}$: **2-BH₃** in CHCl_3 : Toluene (1:9).

III.E. Nanoparticles synthesis from gold precursor AuClSMe_2

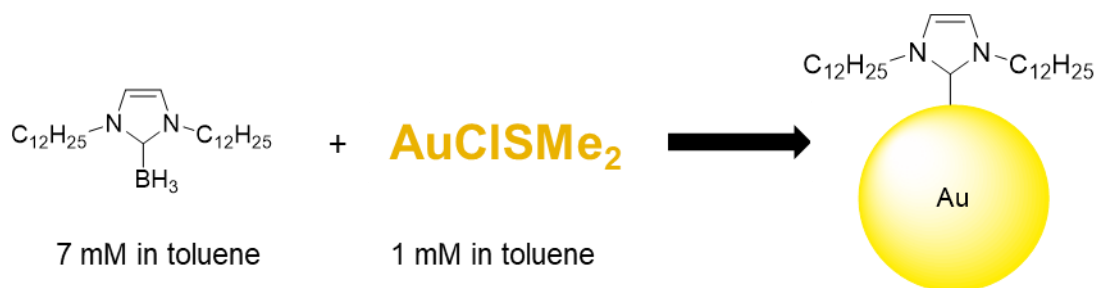
The previous studies led to a third gold precursor: AuClSMe_2 . AuClSMe_2 is routinely used in organometallic chemistry to synthesize gold chloride complexes due to its solubility in organic solvents (such as dichloromethane) and lability of dimethyl sulfide. It is, among other things, used in the synthesis of NHC-AuCl complexes.⁹

Once again, the synthesis was carried out in toluene. Due to the low solubility of the precursor in that solvent, a concentration of 1mM in gold was usually used and solutions were kept in the dark to prevent premature degradation (even though after a few hours the precursor degraded nevertheless forming a yellow halo on the side of the vial).

III.E.1. Reaction conditions effect

We found that the best conditions for the synthesis of gold nanoparticles in toluene were to mix equal volumes of a 1mM solution of AuClSMe₂ and a 7mM solution of **2-BH₃** (Scheme III.13). Upon addition of NHC-BH₃ into the gold solution, the reaction medium turned deep red within a few seconds.

Reaction conditions were then further explored to study their effect on the size and/or morphology of the obtained nanoparticles



Scheme III.13: Gold nanoparticles synthesis from **2-BH₃** and AuClSMe₂.

III.E.1.a. Solvent

A few solvents were screened. When dissolved in dichloromethane or chloroform, the mixing of the compounds led to a black bubbling solution meaning reduction to gold(0) but no NPs.

When introduced in the reaction medium as co-solvents, acetone, ethanol and THF all led to aggregated particles. In the case of THF a slow discoloration of the solution could be observed during 48h at which point it became completely clear. This discoloration suggests a disintegration of the aggregates into molecular gold complexes.

As a result, toluene was kept as the reaction solvent.

III.E.1.b. Water

NHCs are highly reactive species which are known to be moisture sensitive. Therefore, it can be assumed that the water-content of the solvent would impact the synthesis. The first attempts were carried out in toluene straight from the bottle. Before opening, such toluene already contains about 200 ppm of water, an amount that can easily double once opened.³⁸

Tests with bottled toluene, distilled toluene and distilled toluene shaken with water were carried out in order to study the influence of water in the reaction medium (Figure III.9).

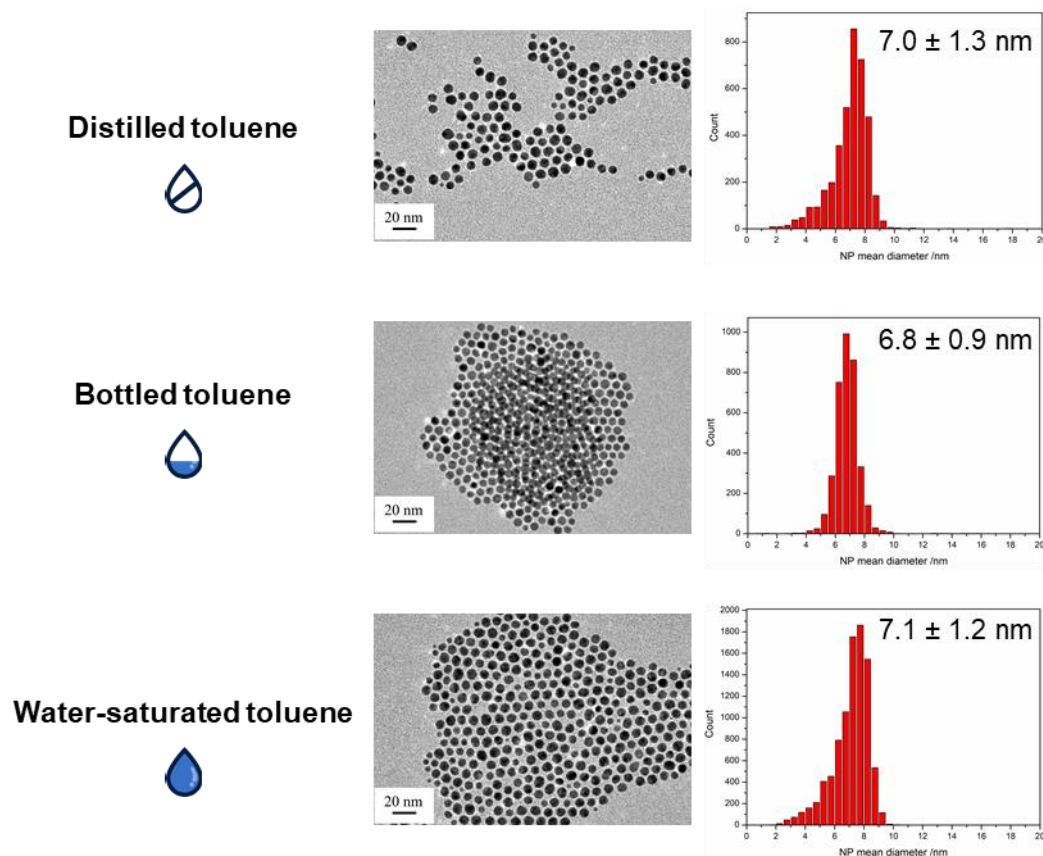


Figure III.9: TEM images and distribution of nanoparticles obtained in distilled, bottled and water-saturated toluene.

As exhibited in Figure III.9, all syntheses gave the same results with NPs at around 7 nm.

It is possible that the NHCs are already so close to gold when they are liberated, that they bind straight away with gold, and don't have time to diffuse and react with the water in solution. For example, this would be the case if reduction by the BH_3 moiety was the trigger to the release of the NHCs. It is also possible that there is such an excess of NHCs compared to gold that even if some liberated NHCs do react with water, the fraction needed to stabilize the NPs binds to gold before being able to be quenched.

III.E.1.c. Ligand to gold ratio

As seen in Chapter II, ligand to gold ratio is known to influence the size of obtained nanoparticles. As shown in Figure III.10, increasing the quantity of NHC- BH_3 decreased the size of the NPs, reaching a minimum of 5.1 ± 1.0 nm for a 1:28 ratio. Decreasing the ratio below 1:7, resulted in an increase in NP mean diameter as well as a loss in stability. Indeed, aggregates were formed along with NPs in suspension. The largest NPs of 10.8 ± 1.2 nm were obtained for a 1:3 ratio. Lower ratios (1:1 and 1:0,5)

led to an immediate reduction of gold as exhibited by a color change of the solution from colorless to dark blue but no dispersed nanoparticles were observed.

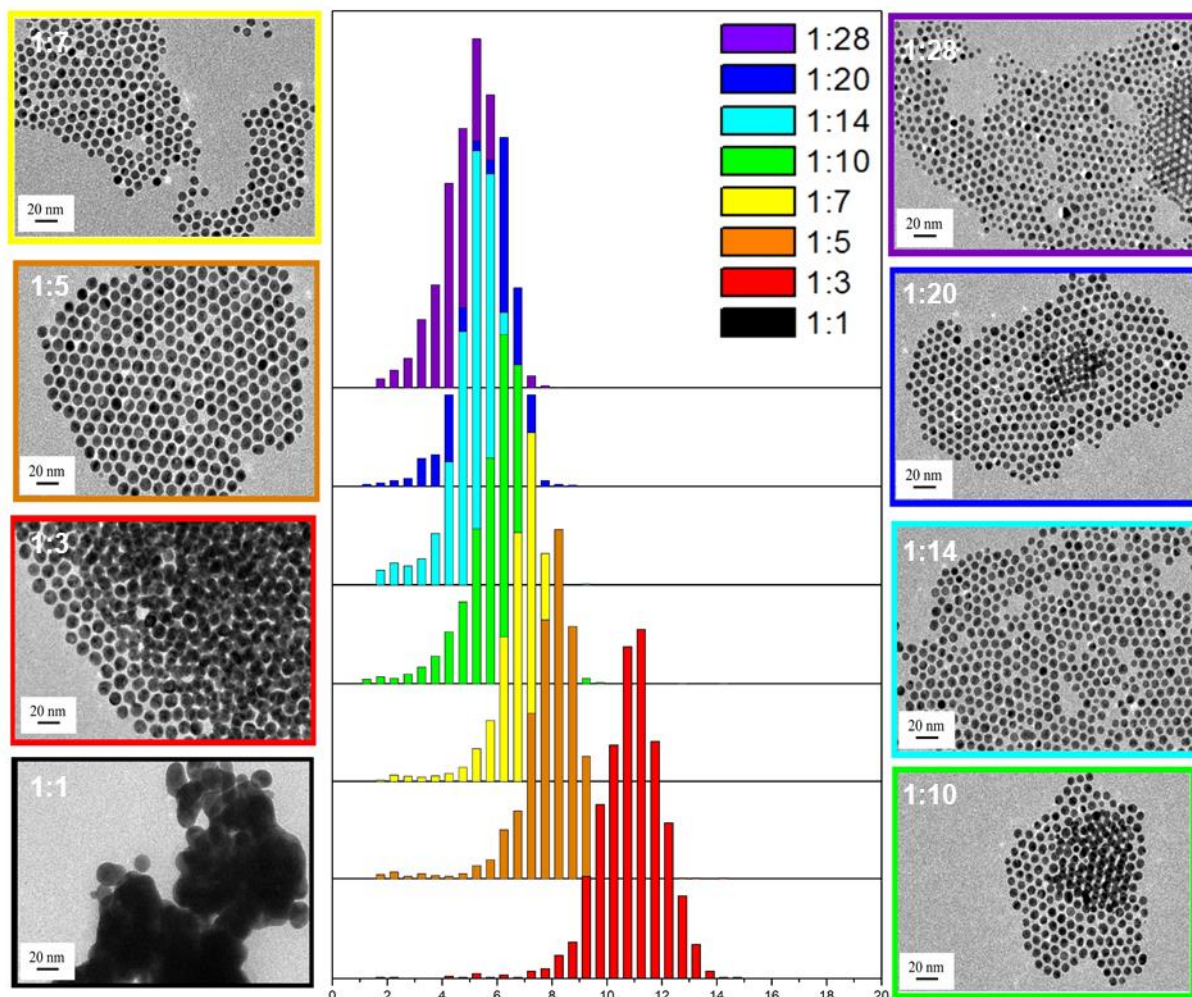


Figure III.10: TEM images and distributions of gold nanoparticles synthesized with different ratios of AuClSMe₂: 2-BH₃ in toluene.

III.E.1.d. Concentration

In order to increase the quantity of NPs synthesized from a single batch, we tried increasing the concentration of the gold precursor (Figure III.11). Solutions of 2 and 4 mM were prepared alongside the usual 1mM one. However, the low solubility of the complex led to its very slow dissolution. In fact, the dissolution was so slow that the solution started to degrade (as exhibited by a yellow halo on the side of the vial) before complete dissolution of AuClSMe₂.

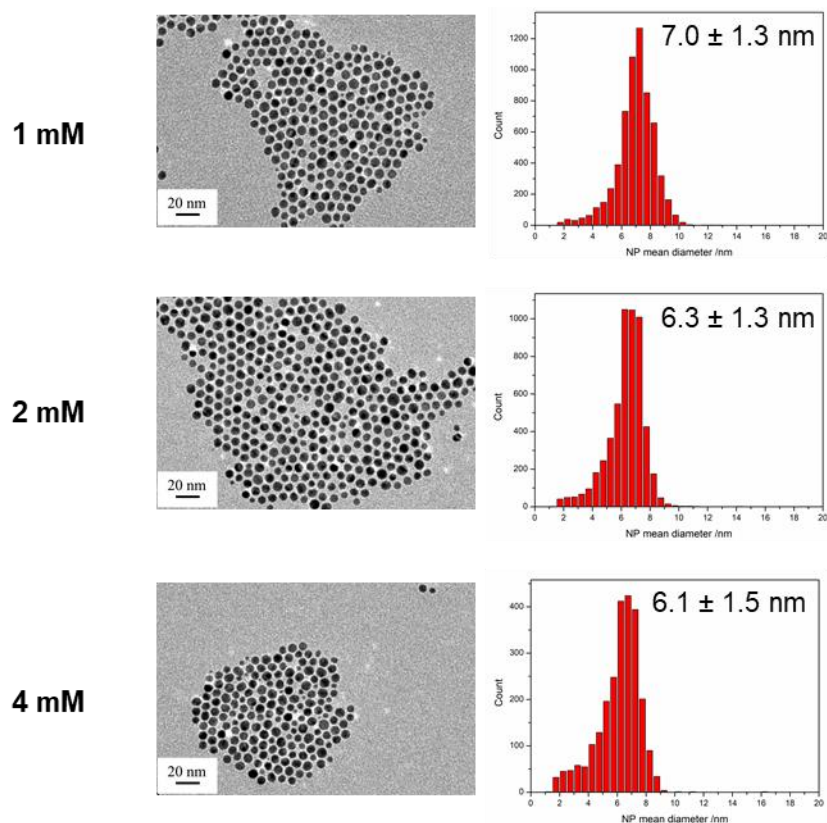


Figure III.11: TEM images and distributions of nanoparticles synthesized from different concentrations of AuClSMe₂ in toluene (1:7 Au:2-BH₃).

This is probably why higher concentrations led to smaller nanoparticles. Indeed, as gold deposited itself on the side of the vial, the concentration in solution was most likely lowered leading to a higher proportion of NHC-BH₃ compared to gold than originally planned. As a result, to avoid any premature degradation of the solution and to ensure the right concentration of precursor in solution, 1mM concentration remained the standard condition.

III.E.1.e. Stirring

Given the small quantity of solvent typically used (4mL), tests were usually carried out without additional stirring. Several stirring speeds were studied (Figure III.12) but no reproducible influence was found on the resulting nanoparticles, except for 1000 rpm which showed coalescing nanoparticles. Thus, no stirring remained the standard.

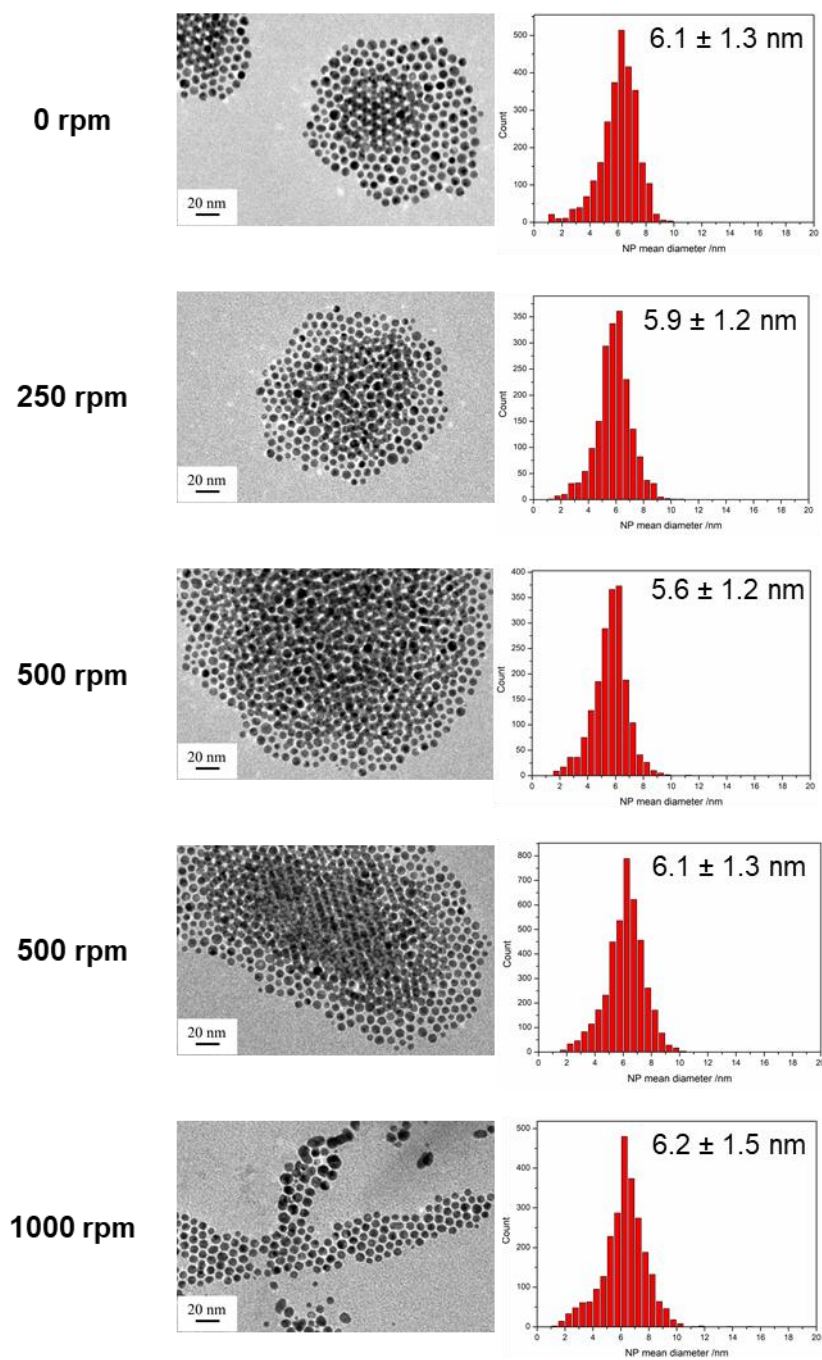


Figure III.12: TEM images and distributions of nanoparticles synthesized with different stirring speeds (1:10 Au:2-BH₃ in toluene).

III.E.1.f. Temperature

Temperature can have a significant effect on the synthesis of nanoparticles. By modifying the temperature, we hoped to be able to change the rate of formation of NPs and thus their size. The results are presented in Figure III.13.

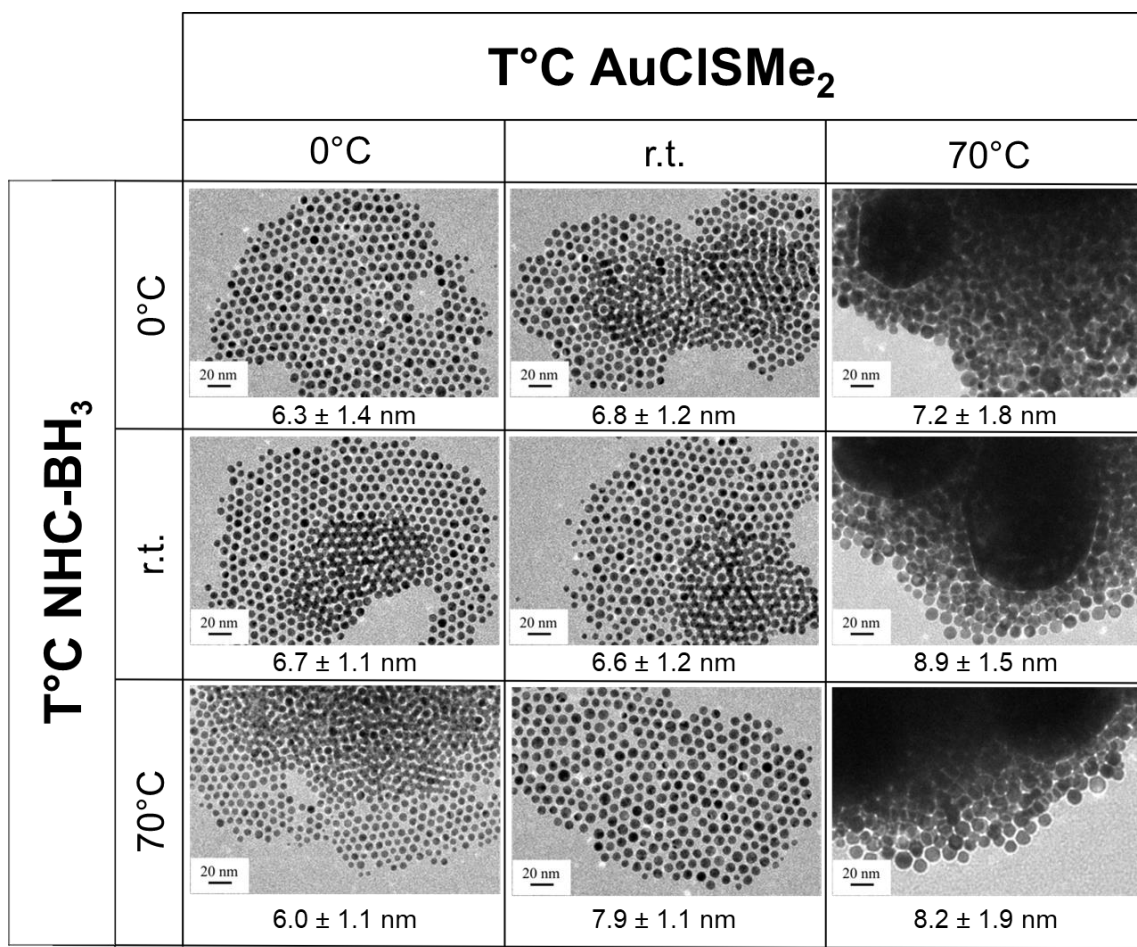


Figure III.13: TEM images and distributions of nanoparticles synthesized from solutions at different temperatures (1:7 AuClSMe₂: 2-BH₃ in toluene).

Increasing the temperature of the gold solution led to quick degradation of the solution and in turn yielded larger particles with observable “giant” particles of up to 150 nm. Other than that, no clear trend can be discerned when comparing cold and room temp gold precursor solutions reacted with cold, room temp or hot NHC-BH₃ solutions.

III.E.2. Surface characterization

The question remained the same as in Chapter II: what is on the surface of our nanoparticles? Is it NHCs, imidazoliums, a mixture of both or something else?

As in Chapter II, the NPs were purified by precipitation with EtOH and centrifugation before characterization.

III.E.2.a. MS

The supernatant of the centrifugated NPs was analyzed by Mass spectrometry (ESI⁺) (Figure III.14). The signal corresponding to the AuNHC₂ complex was present. As in Chapter II, it appears as a strong indication that the carbene is indeed released during the nanoparticle synthesis. The formation of free imidazolium can also be noted as none was introduced in the initial synthesis. It likely comes from the degradation of NHC-BH₃. It is unsure if this degradation happens directly in the reaction medium, during the purification process or during the mass analysis.

Signals corresponding to an adduct between NHC-BH₃ and sodium could also be observed.

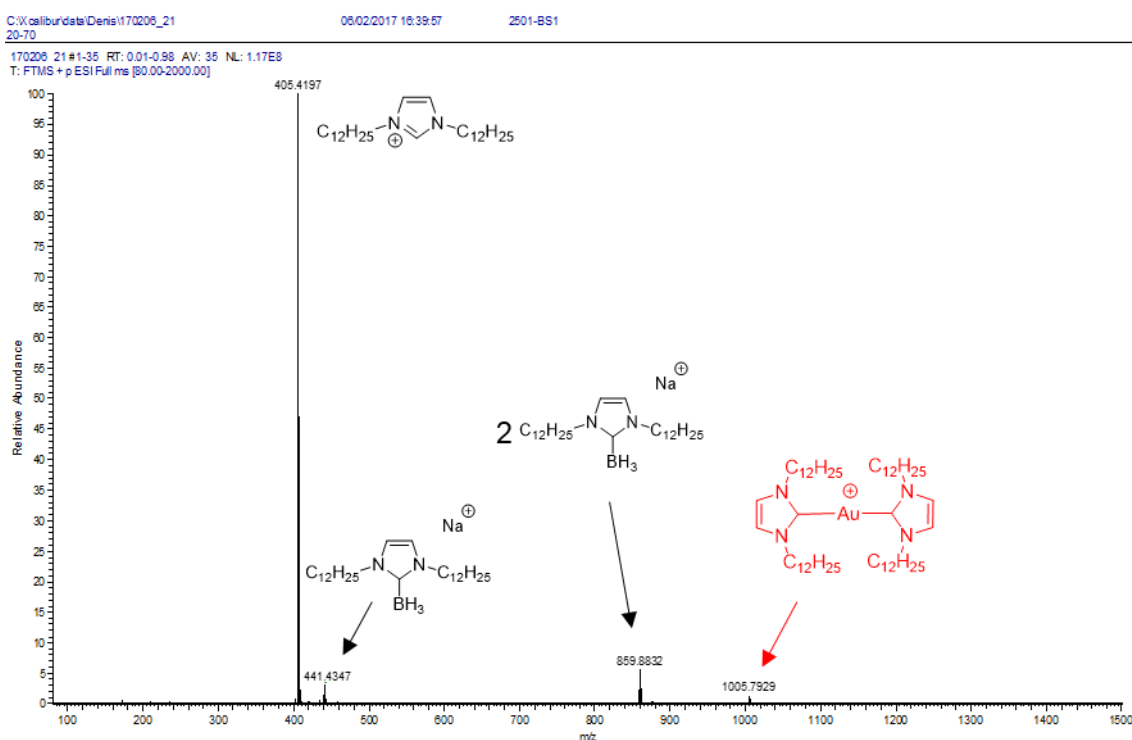


Figure III.14: Mass spectrum (ESI⁺) of the supernatant of centrifugated NPs (diluted in methanol).

III.E.2.b. NMR

The centrifugated NPs were dried, redispersed in deuterated toluene and analyzed by ¹H NMR. However, no signal was obtained probably due to the low concentration of NPs in the tube.

Following the reaction *in situ* by liquid NMR was attempted and will be discussed in “Mechanistic studies”.

Given the difficulties in obtaining a signal in the previous chapter, and the sheer amount of scale up it would require to obtain an appropriate sample, solid state NMR was not attempted. It can be noted however that ¹³C marked (20%) NHC-BH₃ in the C2 was obtained from marked imidazolium (see Chapter II) and can be used to synthesize nanoparticles.

III.E.2.c. XPS

Both the NHC-BH₃ and the NPs were analyzed by XPS. The general spectrum of the NHC-BH₃ showed the presence of carbon, nitrogen and boron. High-resolution spectra for C1s, N1s and B1s core levels enabled the assessment of the NHC-BH₃ composition which was in accordance with the expected composition of the molecule (Table III.2).

The same analysis of the gold NPs showed the presence of carbon, nitrogen and gold. The presence of metallic gold (84eV) as a single component and the simultaneous disappearance of boron on the B1s high resolution spectrum confirms the formation of nanoparticles. Once again, the C1s and N1s spectra are in accordance with the ligand composition attesting to the ligand integrity on the nanoparticles' surface.

Table III.2: C1s, N1s and B1s XPS data of **2-BH₃** and corresponding nanoparticles.

		BE (eV)	Assignment	Composition at%	Calculated stoichiometry	Expected stoichiometry
NHC-BH ₃	C1s	285.0	Aliph. C	75.1	22.5	22
	C1s	286.0	Aliph. C-N	7.0	2.1	2
	C1s	286.5	N-HC=CH-N	6.9	2.1	2
	C1s	284.3	N ₂ -C-B	3.4	1.0	1
	N1s	400.9	C-N-C	5.3	1.6	2
	B1s	187.4		2.3	0.7	1
AuNP	C1s	285.0	Aliph. C	68.5	22.8	22
	C1s	285.9	Aliph. C-N	5.4	1.8	2
	C1s	286.5	N-HC=CH-N	5.4	1.8	2
	C1s	283.9	N ₂ -C-Au	2.8	0.9	1
	N1s	400.4	C-N-C	5.1	1.7	2
	Au4f5/2	84.0				
	Au4f3/2	87.7		12.8		

The C1s photopeak deconvolution was carried out for the NHC-BH₃ and the nanoparticles (Figure III.15). A low energy component was found for both: at 284.3 eV corresponding to the C-B bond in NHC-BH₃, and 283.9 eV corresponding to the C-Au bond on the surface of nanoparticles as it cannot correspond to a C-B bond anymore since no boron was detected in the sample.

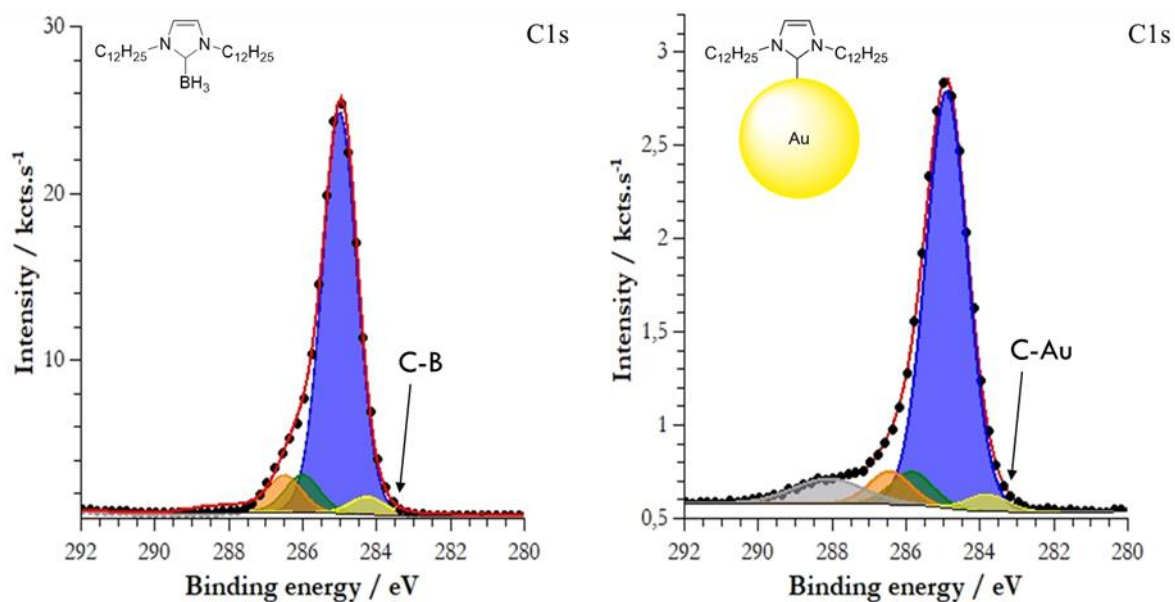


Figure III.15: Deconvoluted C1s XPS spectra of **2-BH₃** and corresponding nanoparticles (blue= aliphatic carbon, green = aliphatic C-N, orange = aromatic carbon, grey plasmonic shake-up peak).

The N1s spectra obtained for **2-BH₃** and the corresponding nanoparticles are presented in Figure III.16 along with the ones for the imidazolium and the NPs from Chapter II. The N1s energetic position for the NHC-BH₃ is shifted compared to the imidazolium (400.9 eV and 401.8 eV respectively) whereas the one for the nanoparticles is almost identical (400.3 eV compared to 400.2 eV in Chapter II). This lowering of the energy corresponds to a strengthening of the interaction between the carbenic carbon and its environment and is consistent with an evolution from a C-B to C-Au bond. This confirms the stabilization of the nanoparticles by NHCs.

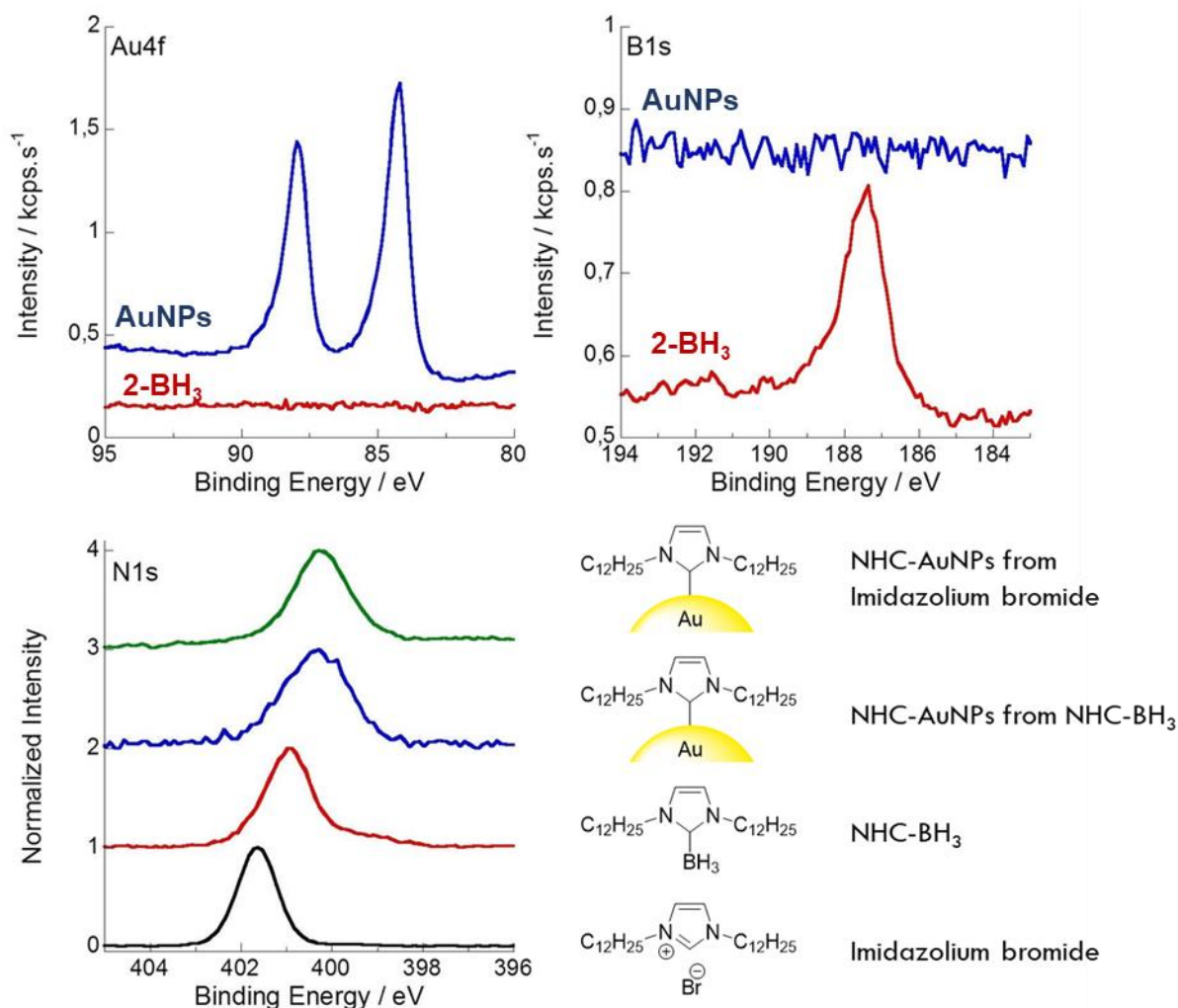


Figure III.16: Au4f, B1s, N1s XPS spectra of **2-BH₃** and corresponding gold nanoparticles and N1s spectra of **2H-Br** and corresponding nanoparticles.

III.E.3. Mechanistic study

Once the stabilization of the NPs by NHCs, and the role of NHC-BH₃ acting as a dual reducing agent and NHC-precursor, were established, we tried to understand the mechanism of their formation. Indeed, many things remain unclear: why and how does the NHC decoordinates from the borane to bind to gold? Does the reduction occur via hydride donation or a radical pathway? Does it occur before, after or simultaneously to the coordination of the NHC on gold? What happens to the BH₃ moiety?

III.E.3.a. NMR

As stated previously, we attempted to follow the reaction *in situ* by ¹H and ¹¹B solution NMR. Solutions of AuClSM₂ (1mM) and NHC-BH₃ (7mM) were prepared in toluene, then aliquots of the same volume

were collected from each solution, dried *in vacuo* and dissolved in deuterated toluene. Upon mixing, the solution turned red and was immediately transferred to an NMR tube and analyzed.

The main observable species, by ^1H NMR, was NHC-BH_3 with only a small new signal at 6.0 ppm (Figure III.17). It was then clear that only a small fraction of the NHC-BH_3 was used in the synthesis of the nanoparticles. Yet an excess was needed to obtain stable NPs.

The same experiment was carried out with a AuClSMe_2 :**2-BH₃** ratio of 1:1 instead of 1:7. Immediately the solution turned blue (which signals the formation of aggregates) and was analyzed by NMR. This time the new species was formed in larger proportions. Upon further addition of gold in the mixture, up to a $\text{Au}:\text{NHC-BH}_3$ ratio of 2:1, NHC-BH_3 seemed to completely disappear in favor of the new species (Figure III.17). For the latter, a broad singlet could be observed at -18 ppm by ^{11}B NMR and was corresponded to the new species. It can be noted that upon introduction of AuClSMe_2 , a peak corresponding to unligated SMe_2 (not shown) also appears at around 1 ppm in ^1H NMR. The new species has been identified as $\text{NHC-BH}_2\text{Cl}$. It is readily synthesized from NHC-BH_3 and HCl in dichloromethane.

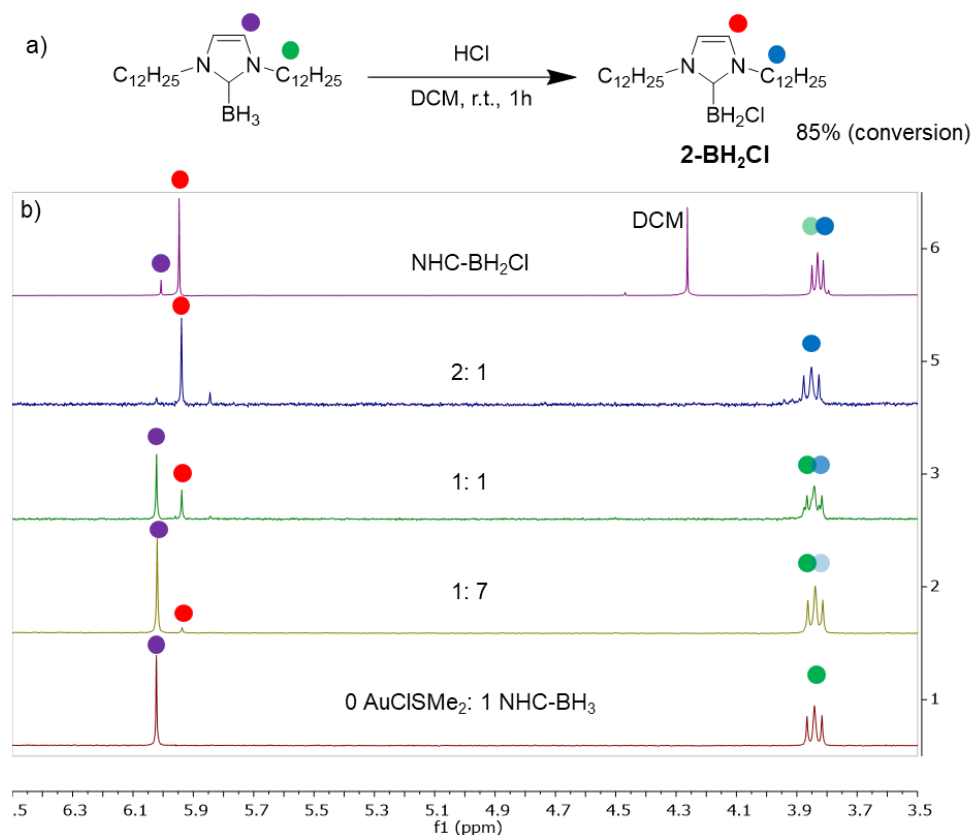


Figure III.17: a) $\text{NHC-BH}_2\text{Cl}$ synthesis and b) in-situ ^1H NMR of different $\text{Au}:\mathbf{2-BH}_3$ ratios and $\text{NHC-BH}_2\text{Cl}$ in tol-d_8 .

III.E.3.b. MS

NHC-BH₂Cl was also indirectly detected when the supernatant of a synthesis using 1 equivalent of NHC-BH₃, for 1 eq of AuClSMe₂, was analyzed by mass spectrometry (ESI⁺). The mass spectrum (Figure III.18) shows two signals of interest. One at 441.4347, which corresponds to an adduct of **2**-BH₃ and sodium, and one at 471.4454, which corresponds to an adduct of NHC-BH₂OCH₃ and sodium (theoretical m/z = 471.4461). As the mass spectrometry sample was diluted with methanol prior to analysis, it is our assumption that NHC-BH₂Cl reacted with methanol to form the detected species.

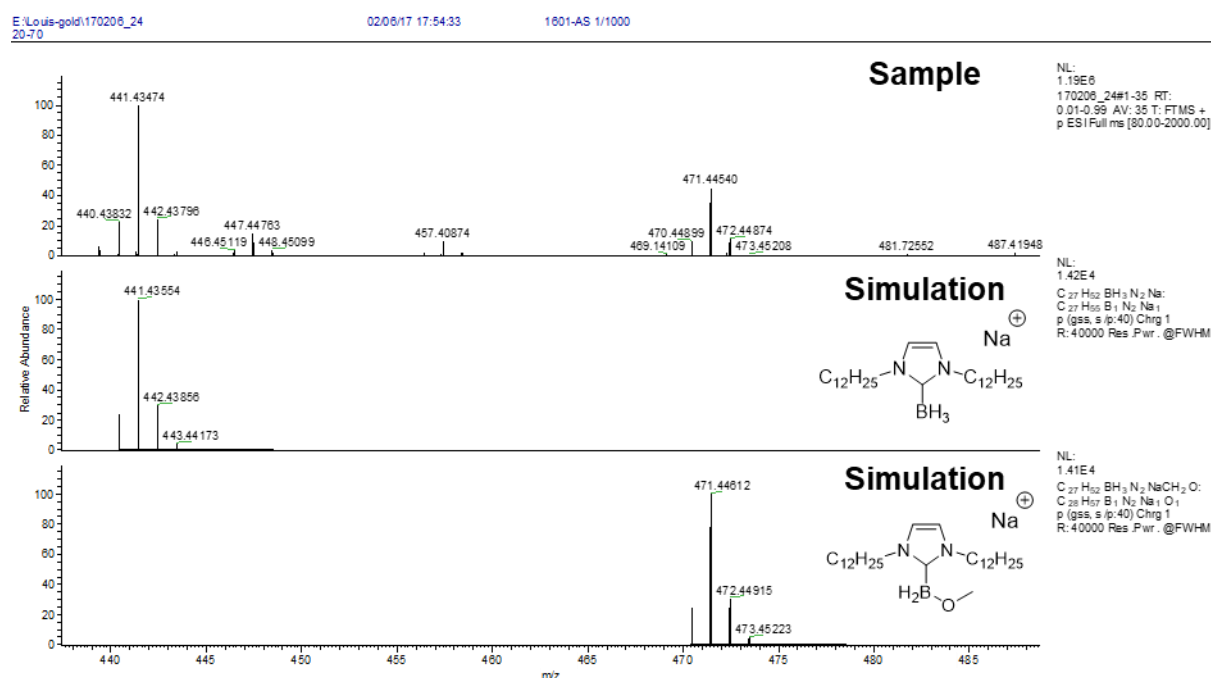


Figure III.18: Mass spectrometry spectrum (ESI⁺) of a 1:1 AuClSMe₂:**2**-BH₃ sample's supernatant diluted in methanol (top) and simulation of the corresponding structures.

After mass analysis by negative electrospray (ESI⁻) of a 1:1 crude solution, two species were identified (Figure III.19): [NHC-BH₂Cl₂]⁻ and [NHC-BH₂SMe₂Cl]⁻. The former seems to correspond to NHC-BH₂Cl ionized by Cl⁻. However, while the mass and isotopic patterns of the latter match well with the experimental signal it is unclear which moiety would bare the negative charge.

This confirms the formation of NHC-BH₂Cl as an intermediate in the reaction and even if not detected by ESI⁺.

23-Jan-2018

180123-19 (4.071) Cu (0.45); Is (0.70,0.10) C₂₇H₅₂N₂BH₂SCl₂H₆Cl

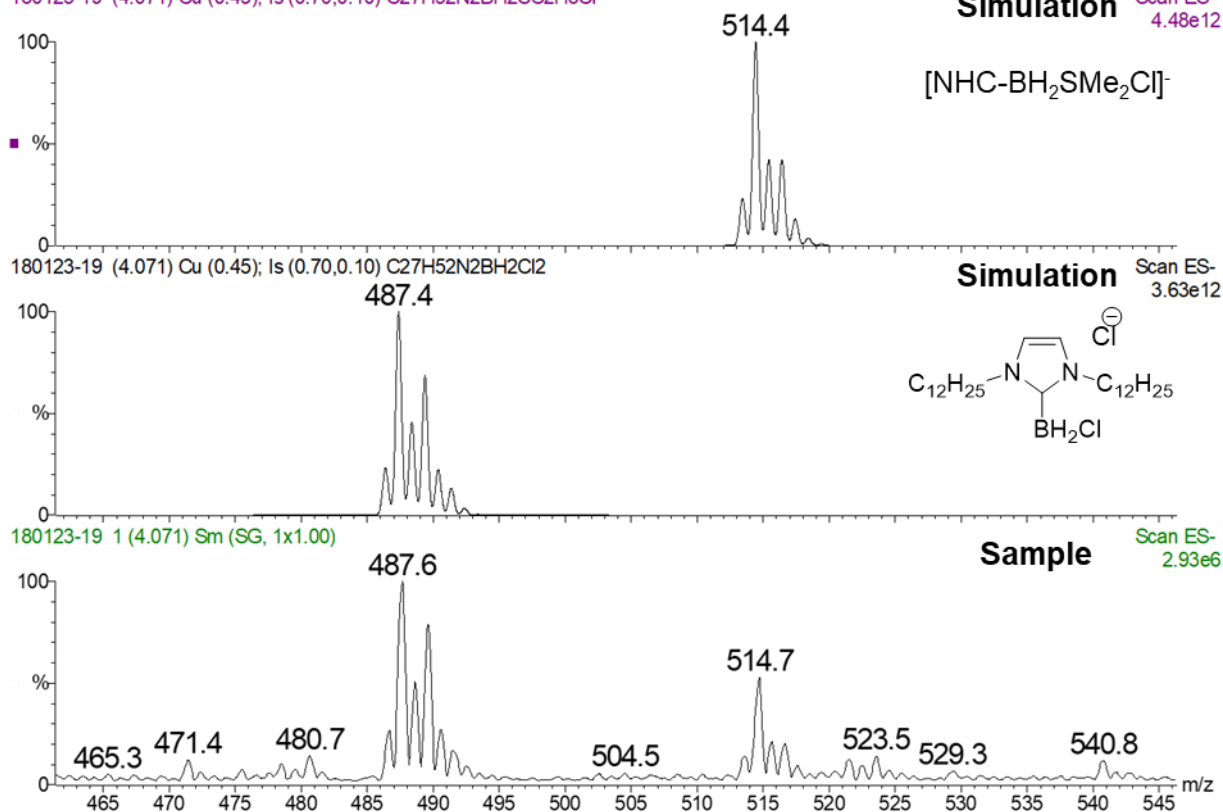


Figure III.19: Negative mass spectrometry spectrum (ESI) of a crude 1:1 Au:NHC-BH₃ sample diluted in dichloromethane bottom and simulation of the proposed corresponding species.

It can be noted however than when introduced into a gold solution, NHC-BH₂Cl did not appear to reduce gold as no change in color was observed.

III.E.3.c. Theoretical chemistry

As seen in the beginning of this chapter, NHC-boranes are known reducing agents that act via either hydride transfer or a radical pathway.¹ **2-BH₂Cl** could be generated by either one. In order to determine the most likely scenario, theoretical calculations were undertaken at the Density Functional Theory (DFT) level using the Gaussian 09 package of programs. Geometry optimizations were carried out using thePBE0 (PBE1PBE) hybrid functional, along with the def2-TZVP basis set for all atomic species. The nature of the minima of each optimized structure was verified by harmonic frequency calculations. These theoretical calculations were performed by Dr. Yves Gimbert (Sorbonne Université / Université Grenoble Alpes).

III.E.3.c.i. Hydride transfer

The first mechanism studied was the one involving a hydride transfer. The proposed mechanism is shown in Figure III.20. It should be noted that this is a tentative mechanism and many options can be envisioned.

First, a hydrogen from the NHC-BH₃ coordinates to gold leading to the decoordination of dimethyl sulfide. Dimethyl sulfide then comes back to coordinate to the boron atom inducing the release of a gold hydride. The chloride from this gold hydride coordinates to the boron atom, freeing once again dimethyl sulfide which binds back to the gold leading to the formation of NHC-BH₂Cl (observed by MS) and HAuSMe₂. The latter can then react with AuClSMe₂ to form a binuclear gold complex with a bridging hydrogen. This complex can then react further with NHC-BH₃ to form more exotic species which in the end transform into Au(NHC)₂ (observed by MS), NHC-Au-BH₄, NHC-Au-SMe₂ and Au(BH₄)₂. Due to the nature of calculations, attributing formal charges to complexes with certainty, and thus oxidation states to metals, is difficult. That is why none is explicitly written on the mechanism. However, with a few assumptions, one can try to attribute them. Assuming a negative charge on the gold hydride **5**, and a neutral charge on the other gold species, it appears that gold has an oxidation state of +I throughout the reaction up to the last step where **14** and **16** would have an oxidation state of 0 and **15** an oxidation state of +II. Gold(0) species are able to react with gold(I) species, according to the literature,⁴⁰ to form bigger clusters which are then able to react with each other to form even bigger clusters. These are likely the source of nucleation of nanoparticles. The fate of **15** is unclear but as a supposed gold(II) species it is not expected to be very stable.

The fact that species **7** and **4** were detected by MS (as seen above) lend some credibility to this mechanism. However, it is possible that the real mechanism is even more complex and involves several simultaneous reaction pathways. Indeed NHC-Au-Au-NHC hydride bridged species, not entirely unlike **10**, have been shown by Sadighi *et coll.*⁴¹ to precipitate into colloidal gold when reacted with nBuLi. So while this proposed mechanism explains the formation of NHC-BH₂Cl and gold(0) species, it is far from the only possible pathway.

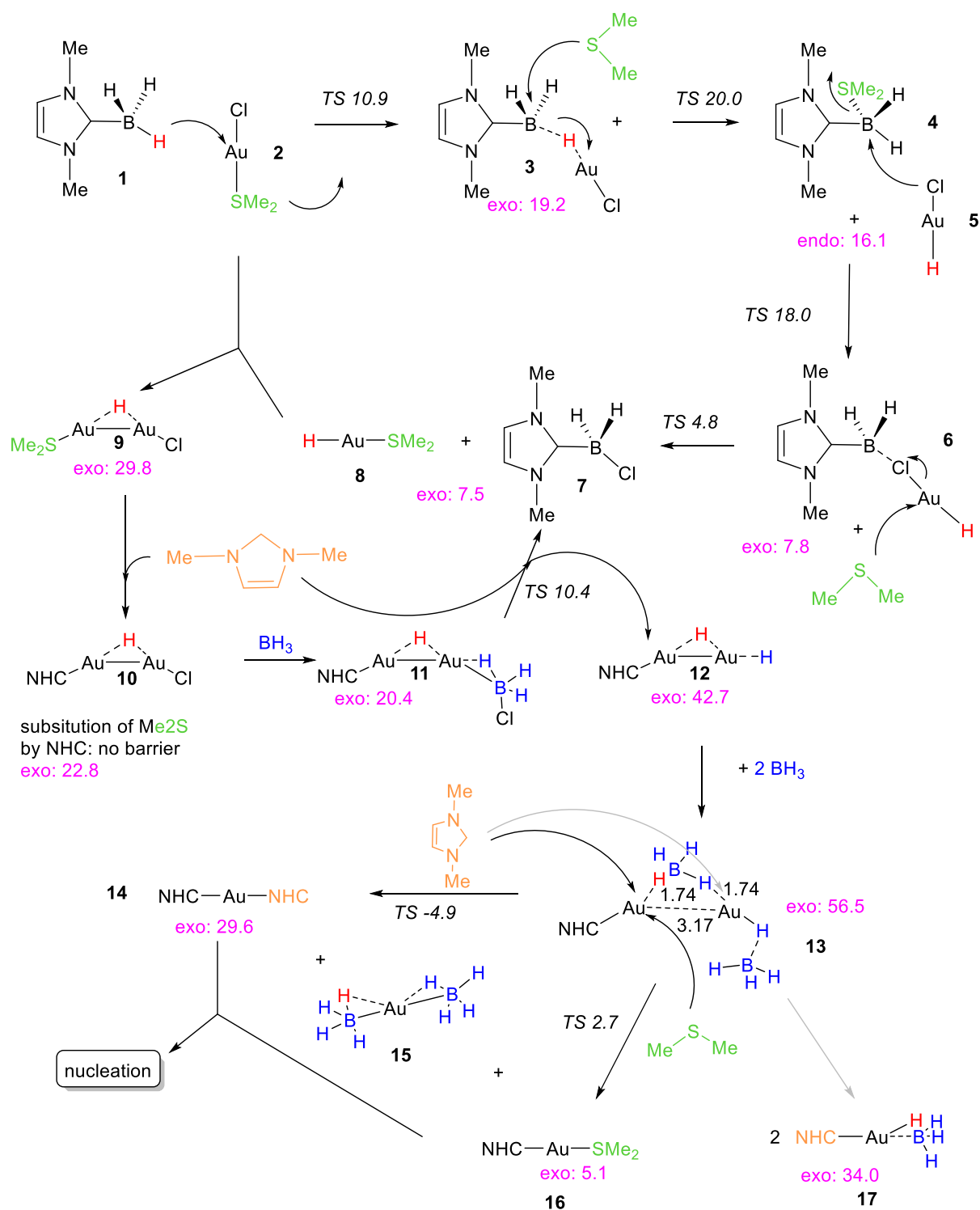


Figure III.20: Pathways for the formation of Au(0) species starting from NHC-BH₃ and AuClSMe₂ (energies in kcal·mol⁻¹).

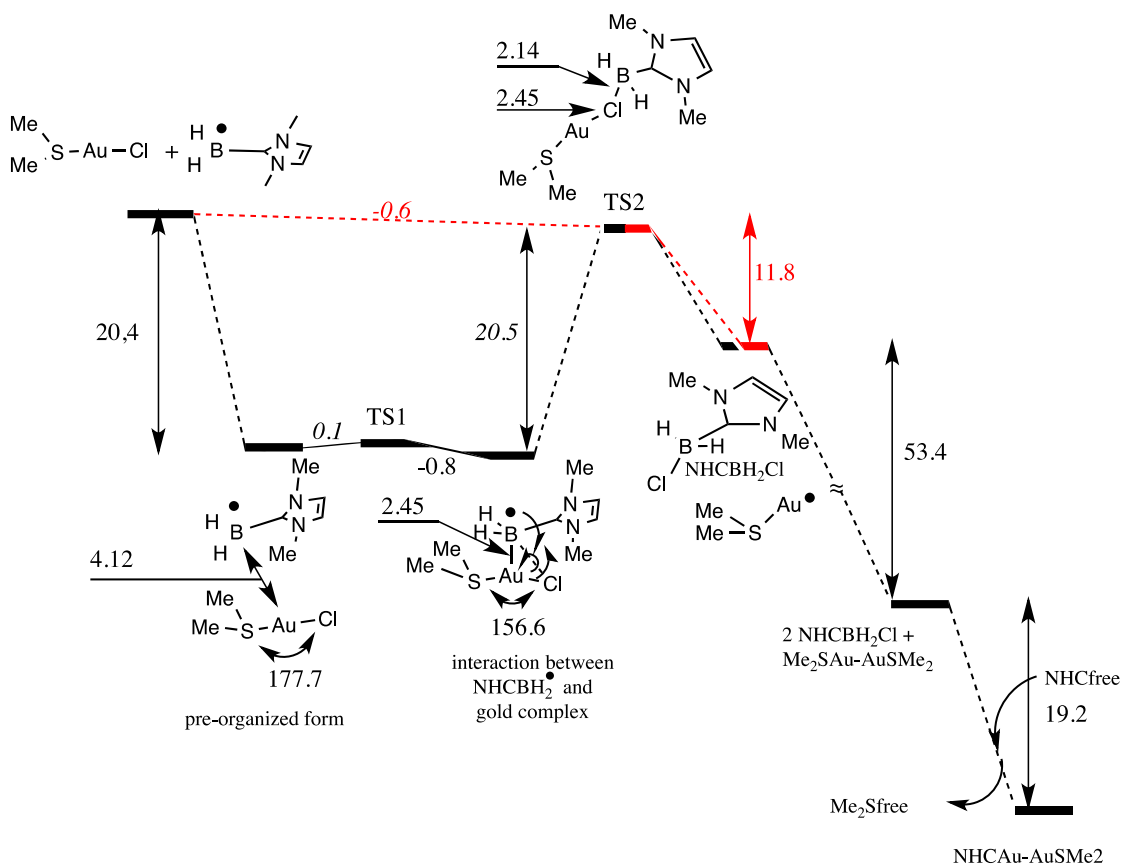
III.E.3.c.ii. Radical mechanism

We considered that under the experimental conditions used, it was possible to generate the radical species NHC-BH₂[•]. For example, traces of thiols in the gold precursor could act as radical initiators.

Indeed such N-heterocyclic carbene boryl radicals species are known⁴² and considered relatively short-lived. In presence of AuClSMe₂ gold complex, this NHC-BH₂[•] radical can react in various way according the literature: (i) by directly capturing Cl atom to give the compound NHCBH₂Cl (observed in the reactive middle) and Me₂SAu(0)[•], (ii) by being trapped first by the “AuCl” complex⁴³ before further reactions. These two possibilities have been investigated (Scheme III.14).

The first path (red) led to the formation of the compound NHCBH₂Cl and the radical [•]AuSMe₂, through a transition state (TS2) which was possible to determine, and is energetically slightly below the reagents (0.6 kcal.mol⁻¹). This transformation is exothermic by 11.8 kcal.mol⁻¹. The radical dimerizes very rapidly to give Me₂SAuAuSMe₂, a gold(0) complex strongly stabilized in energy (≈53 kcal.mol⁻¹). It is possible, on this complex, to replace a Me₂S group by an NHC, in a barrier-free process, exothermic by 19 kcal.mol⁻¹. The second path is relative to the ability of a chlorine gold complex to trap a radical. Corma *et al.*⁴³ have evidenced this possibility with benzyl radical and various gold complexes as such AuCl, AuCl₃, HAuCl₄.

We have been able to obtain a minimum of energy for a structure corresponding to a preorganization of the radical NHCBH₂[•] and AuClSMe₂ just before the interaction between them. The energy required to go, from the pre-organized form, to the form where the radical reacts on gold is almost zero (TS1, 0.1 kcal/mol), which effectively suggests that the process is barrier-less. Starting from this structure stabilized by interaction of the radical on Au, it is possible to transfer the Cl atom on the boron by a homolytic rupture of the Au-Cl bond, which implies exactly the same TS2 (activation energy this time of 20 kcal.mol⁻¹) as found during the direct transfer calculated in the first path.

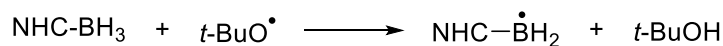
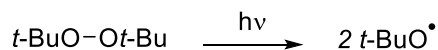


Scheme III.14: Pathways for the formation of Au(0) species starting from NHC-BH₂[•] radical and Cl-Au-SMe₂. Distances in Å, angles in °, energies in kcal.mol⁻¹.

III.E.3.d. EPR

In order to confirm a radical pathway, we decided to study the reaction by electron paramagnetic resonance (EPR). Our goal was first to generate the NHC-BH₂[•] radical in order to have a reference spectrum. Then, the radical, if stable enough, could be directly introduced in a gold solution to see what happened. Concurrently, having the reference spectrum would make it easier to detect the radical in an *in situ* reaction starting from NHC-BH₃ and AuClSMe₂.

Generation of a NHC-Boryl radical has been described in the literature:^{3,22} for instance, Ueng *et al.* reported that irradiating a solution of diDipp-Imd-BH₃ (**8-BH₃**, Figure III.21) in the presence of DTPB (di-tert-butyl peroxide) either in benzene or in tert-butyl benzene allowed for the detection of a short-lived boron centered radical (Scheme III.15 and Figure III.21).²²



Scheme III.15: Generation of NHC-BH₂[•] by hydrogen abstraction.

As the gold nanoparticles are generated in toluene, we slightly modified this literature procedure, by dissolving **2-BH₃** in toluene, added DTPB (di-tert-butyl peroxide) and irradiated the solution with an unfiltered mercury lamp.

However, no signal was detected despite the solution turning yellow, attesting that a reaction did occur.

Thus, we went closer to the original system. **8-BH₃** was dissolved in toluene and irradiated in the presence of DTPB. No signal was detected either. However, when the solvent was switched to benzene, in agreement with the literature, an EPR signal centered at 3330 G ($g=2.017$, Figure III.21) was detected which is very similar to the one reported for **8-BH₂[•]**.²²

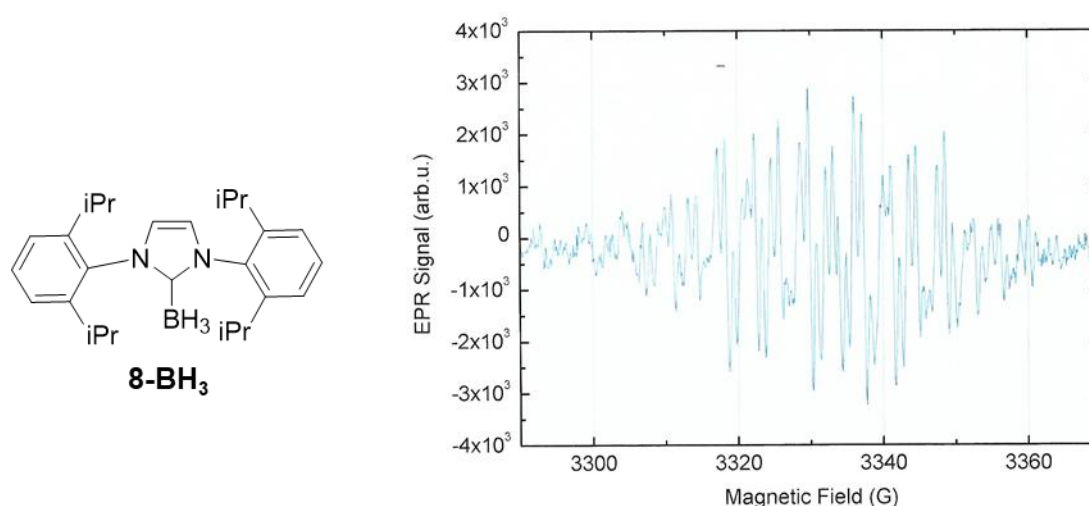


Figure III.21: **8-BH₃** structure and corresponding EPR spectrum.

Thus, in our conditions, toluene probably acted as a radical trap and reacted with DTPB before it was able to react with the borane.

We thus tried to generate **2-BH₃** in benzene, but again no signal was detected. Several attempts were made in order to shorten as much as possible the irradiation time before recording the spectrum but they were all unsuccessful.

It has been showed in the literature that NHC-BH₂[•] radicals bearing short alkyl groups on the nitrogen atoms are very transient.^{44,45} It is possible that **2-BH₂[•]** is transient as well, as unlike **8-BH₂[•]** it does not have neighboring aromatic rings to act as stabilizers. Due to this transient state, low temperatures and/or radical trapping experiments would be necessary in order to obtain a signal.

In a last attempt to confirm a radical mechanism, TEMPO was added to the reaction medium at a 9:10 ratio compared to **2-BH₃**. It was hoped that if formed, the radical would be scavenged by TEMPO and thus prevent the formation of gold nanoparticles. However, that was not the case, and nanoparticles

formed as usual. The same thing happened when adding an excess of BHT (butylated hydroxytoluene) in the medium. This suggests that either no radical is formed or that it reacts faster with gold than with TEMPO or BHT.

III.E.3.e. Discussion

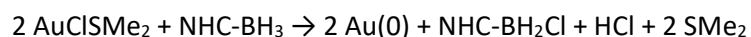
So far in this chapter, we have showed that stable gold nanoparticles could be prepared in toluene from AuClSMe₂ and NHC-borane with long alkyl chains such as **2-BH₃**. The nanoparticles size can be tuned in the range 11-5 nm through the **Au:2-BH₃** ratio. At least 7 equivalents NHC-BH₃ per Au seems necessary to avoid the formation of aggregates even if reduction of gold occurs with less than 1 equivalent of borane.

The characterization performed by XPS on the isolated nanoparticles indicates that the stabilizing ligands are NHC. Indeed, a characteristic shift was observed on the N1s spectrum and the integrity of the ligand on the surface was confirmed by the overall C/N ratio.

However, the pathway from the reagents to the final nanoparticles, as well as the mechanism that provides the NHC from the NHC-BH₃, remain unclear despite some attempts to gain insight into the process by theoretical calculations. Yet as the ion [Au(NHC)₂]⁺ has been observed by MS-ESI⁺, some NHC have to be generated in the medium.

The quantity of NHC that needs to be liberated may be minimal however. Indeed gold nanoparticles of around 7 nm in diameter have *ca.* 22% of their atoms on the surface. Studies on SAMs have found a ligand density around 4 NHC/nm². This would correspond to *ca.* 1 NHC for 3 gold atoms, and thus only *ca.* 7% of NHC relatively to gold would be necessary. Therefore, with a NHC-BH₃/Au starting ratio of 7, just 1% of the NHC-BH₃ would have to transform into NHC to generate enough surface ligands.

Concerning the reduction of Au(I) to Au(0), it appears that it can be achieved with only half an equivalent of NHC-BH₃. Moreover, according to ¹H and ¹¹B NMR, NHC-BH₂Cl was the only new derivative quantitatively evidenced. Thus, the reduction process could be globally written as follows:



Indeed, the liberation of SMe₂, unligated to gold, was also detected by ¹H NMR. The only remaining species to detect would be HCl.

III.E.4. Reproducibility issues

Despite being reproducible for several months, experiments suddenly stopped working. Instead of monodisperse nanoparticles, only aggregates were obtained. Meaning that the NHC-BH₃ was still performing as a reducing agent but not as a ligand, or not as well.

The main focus in this part was on reaction that worked vs. those that did not. As a result, most observations are based on the color of the solution. Indeed, as stated briefly in Chapter I, LSPR is responsible for the color of gold nanoparticles in solution and is determined mostly by the nature of the metal, the size and shape of the NPs and their environment (ligand and solvent). Since the metal, ligand and solvent remain constant throughout my tests, the only things that should affect the LSPR (and thus color of the solution) are the size, shape and aggregation of the nanoparticles.

A blue or black (often slightly turbid) solution means aggregates, deep translucent red is desired as it translates into monodisperse nanoparticles free of aggregates, brown means very small nanoparticles (often around or less than 3 nm), transparent means no gold reduction. Combinations of the different colors either means monodisperse nanoparticles of a slightly different diameter than the purely red ones (red-brown = smaller and purple = bigger) or in the case of purple it could also mean a mixture of aggregates and smaller dispersed nanoparticles (which can easily be determined by UV-Vis spectroscopy).

After testing several batches of NHC-BH₃ with different pots of gold precursor, it was concluded that the most recent batches were faulty. To this day it is unclear why, but as even a recrystallized batch of NHC-BH₃ did not work, we assume that something was present inside the working batches and not the faulty ones.

¹H and ¹¹B NMR of all the batches still available were carried out. While no differences were observed on the boron spectra, when looking in the baseline of ¹H NMR small peaks (< 2%) could sometimes be observed. However, no clear pattern was discernible and the peaks were too small to guess what species they could belong to.

As the problem was stabilization of our nanoparticles, we assumed that the unknown impurity could be an NHC precursor formed during the synthesis of the NHC-BH₃. Several hypotheses were formulated and are listed below.

III.E.4.a. Silica

The last working batch of NHC-BH₃ was synthesized in June 2017, the next batch was synthesized in February 2018 and was faulty, along with every batch after that. This corresponds to a change in silica gel precursor. Indeed, up to that point Davisil® silica produced by Grace was used. After that the lab switched to a silica gel with the same granulometry (40-63µm with 60Å porosity) but which is known to be slightly more acidic (pH 6-7) than the Davisil® silica (pH= 7.3). A new pot of silica was purchased from Carl Roth which is now in charge of reselling Grace's Davisil® silica in Europe.

Unfortunately, after purification on the new silica, the NHC-BH₃ that came out was also faulty.

A purification by precipitation instead of column chromatography was also attempted. However, while a nearly pure NHC-BH₃ readily recrystallizes from acetonitrile, the crude reaction mixture did not.

III.E.4.b. Byproduct from the NHC-BH₃ synthesis

When analyzing the crude of NHC-BH₃ syntheses by ¹H NMR a second species is often observed in various proportions (Figure III.22). The peaks are close in position to those of an imidazolium but do not present the characteristic peak at around 10 ppm. It is not impossible that some of this species would pass through column chromatography undetected and have a role in the NPs synthesis.

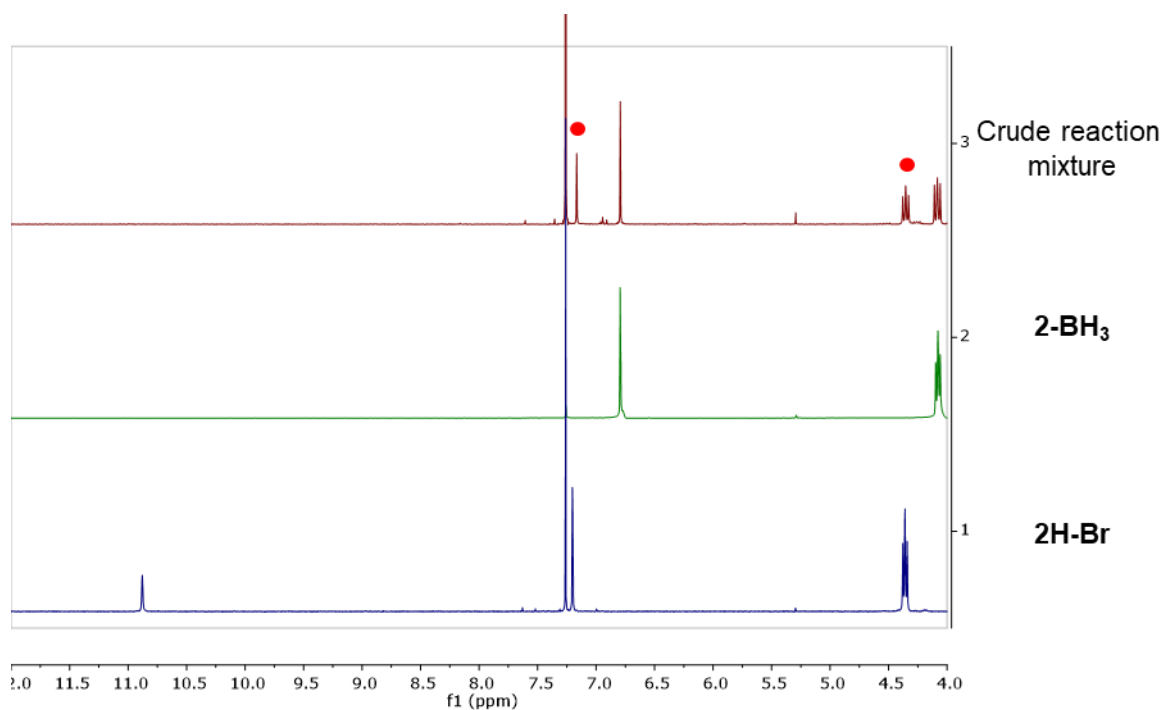


Figure III.22: ¹H NMR spectra of 2H-Br, 2-BH₃ and the crude reaction mixture of a 2-BH₃ synthesis (working batch) in CDCl₃. Red dots = byproduct signals.

A crude of an NHC-BH₃ synthesis was tested and yielded nanoparticles (as exhibited by a red solution). However, after rapid filtration on a silica plug, **2-BH₃** appeared very clean (¹H NMR) and did not give nanoparticles as expected. Moreover, a portion of the crude was stored in the same conditions as other batches of **2-BH₃** (in air, room temperature) and was tested again after a month. This time however no nanoparticles were obtained.

Finally, this species can be observed in crudes of working and faulty batches with no identifiable trend (Table III.3).

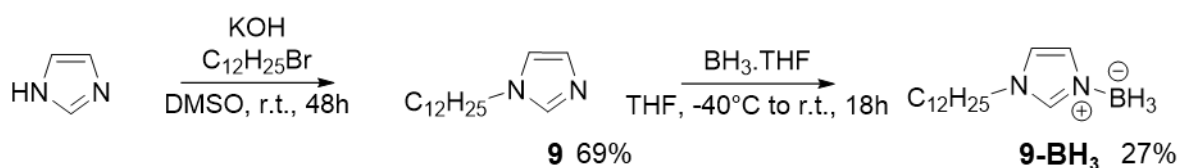
Table III.3: Ratio of byproduct per NHC-BH₃ determined by crude ¹H NMR of different batches.

Batch number	Ratio of byproduct in the crude for 1 NHC-BH ₃
LH88 (working)	0.69
LH123 (working)	0.51
LH206 (faulty)	0.33
LH234 (faulty)	1.79

III.E.4.c. Byproduct from the imidazolium synthesis

Mass spectrometry analysis comparing a faulty batch to a working one showed very few differences. However, a small peak corresponding to a monoalkylated borane (**9-BH₃**) could be seen a bit more clearly in the working batch than in the faulty one. This would mean the problem could originate from the synthesis of the imidazolium salt instead of the NHC-BH₃.

The monoalkylated imidazole and corresponding amine borane (**9-BH₃**) were synthesized (Scheme III.16). Imidazole was deprotonated by potassium hydroxide in DMSO and then reacted with a slight excess of bromododecane for 48h at room temperature. After purification by liquid phase extraction, the mono alkylated imidazole was reacted at low temperature with BH₃.THF to give the final product as an oil.

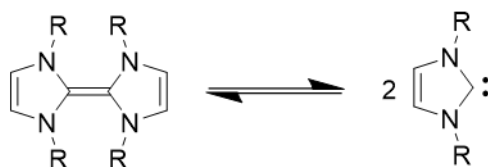


Scheme III.16: Synthesis of the amine borane **9-BH₃**.

Once isolated, neither addition of the imidazole, nor the amine borane helped in the NPs synthesis. (Even though the amine borane when used in large excess, does give nanoparticles albeit not stable over time, thus showing the poor stabilizing properties of **9**).

III.E.5.d. Dimer

Free NHCs are known to dimerize according to the Wanzlick equilibrium (Scheme III.17).⁴⁶ Such dimers are prepared in a glove box due to their reactive nature and the dimerization is usually prevented by bulky N-substituents. We thought that maybe a small portion of the NHC formed in situ during the synthesis of **2-BH₃** did dimerize, thus preventing the coordination of the BH₃ moiety. The dimer would then have to be stable enough to pass through silica gel chromatography unscathed.



Scheme III.17: Wanzlick equilibrium.

To verify this theory, the imidazolium salt was deprotonated with KHMDS in THF at -78°C , without introducing BH₃.THF, and then stirred overnight at room temperature. This, in theory, would form NHCs which would have nothing to coordinate to but each other, leading to the formation of dimers. Given that once the NHC-BH₃ is formed it is handled in air, we did not take any specific precaution in order to stick as closely as possible to our real reaction conditions.

The crude was analyzed by ¹H NMR in CDCl₃. The NMR spectrum of the crude looks like a mixture of several species. Column chromatography was carried out and two species were isolated.

Adding each species separately to a nanoparticle synthesis using a faulty batch of NHC-BH₃ did not yield nanoparticles. Indeed, reduction occurred and the blue color of the samples indicated the formation of only aggregates.

It can be noted that adding some of the crude reaction mixture to a similar synthesis did yield nanoparticles (as evidenced by a red-brown solution). However, when using this crude mixture directly on a gold solution, it turned purple. This indicates the formation of (large and/or partially aggregated) nanoparticles despite the absence of obvious reducing agent. It is thus possible that other species present in the crude (for instance KHMDS) may be responsible for its ability to form nanoparticles.

III.F. Conclusion

To conclude, gold nanoparticles synthesis was attempted from three different gold precursors. After optimization, AuClSMe₂ was found to be the best precursor. Different reaction conditions were tested and it was found that the reaction performed best at room temperature with no influence from the water content of the solvent or stirring speed. The ligand to gold ratio was found to be crucial to control the size of the gold nanoparticles. Indeed, increasing the amount of NHC-BH₃ decreases the size of the nanoparticles from ~11 nm to an apparent limit of 5 nm.

The nanoparticles were characterized by a range of techniques. XPS confirmed the stabilization of the NPs by NHCs. Studies were conducted to try to understand the mechanism. NHC-BH₂Cl was found to be a possible intermediate in the reaction. DFT calculations were carried out, but the exact reaction pathway remains unclear.

Finally, despite being reproducible for over a year, the synthesis ceased working. The problem was found to come from the batches of NHC-BH₃. Indeed, some batches were working while others were not. Our theory is that an impurity, acting as a sort of catalyst, is present in the working NHC-BH₃ batches. Several hypotheses were put forward; however, none seems to be the right one. It is possible that a combination of factors is responsible and more work is needed to solve the issue.

Bibliography (Chapter III)

- (1) Curran, D. P.; Solovyev, A.; Makhlof Brahmi, M.; Fensterbank, L.; Malacria, M.; Lacôte, E. Synthesis and Reactions of N-Heterocyclic Carbene Boranes. *Angew. Chem. Int. Ed.* **2011**, *50* (44), 10294–10317.
- (2) Kuhn, N.; Henkel, G.; Kratz, T.; Kreuzberg, J.; Boese, R.; Maulitz, A. H. Derivate Des Imidazols, VI. Stabile Carben-Borane. *Chem. Ber.* **1993**, *126* (9), 2041–2045.
- (3) Walton, J. C.; Brahmi, M. M.; Fensterbank, L.; Lacôte, E.; Malacria, M.; Chu, Q.; Ueng, S.-H.; Solovyev, A.; Curran, D. P. EPR Studies of the Generation, Structure, and Reactivity of N-Heterocyclic Carbene Borane Radicals. *J. Am. Chem. Soc.* **2010**, *132* (7), 2350–2358.
- (4) Lindsay, D. M.; McArthur, D. The Synthesis of Chiral N-Heterocyclic Carbene–Borane and –Diorganoborane Complexes and Their Use in the Asymmetric Reduction of Ketones. *Chem. Commun.* **2010**, *46* (14), 2474–2476.
- (5) Brahmi, M. M.; Monot, J.; Desage-El Murr, M.; Curran, D. P.; Fensterbank, L.; Lacôte, E.; Malacria, M. Preparation of NHC Borane Complexes by Lewis Base Exchange with Amine– and Phosphine–Boranes. *J. Org. Chem.* **2010**, *75* (20), 6983–6985.
- (6) Yamaguchi, Y.; Kashiwabara, T.; Ogata, K.; Miura, Y.; Nakamura, Y.; Kobayashi, K.; Ito, T. Synthesis and Reactivity of Triethylborane Adduct of N-Heterocyclic Carbene: Versatile Synthons for Synthesis of N-Heterocyclic Carbene Complexes. *Chem. Commun.* **2004**, No. 19, 2160–2161.
- (7) Ono, S.; Watanabe, T.; Nakamura, Y.; Sato, H.; Hashimoto, T.; Yamaguchi, Y. Synthesis of N-Heterocyclic Carbene Boranes via Silver N-Heterocyclic Carbene Complexes. *Polyhedron* **2017**, *137* (Supplement C), 296–305.
- (8) Lee, C. K.; Vasam, C. S.; Huang, T. W.; Wang, H. M. J.; Yang, R. Y.; Lee, C. S.; Lin, I. J. B. Silver(I) N-Heterocyclic Carbenes with Long N-Alkyl Chains. *Organometallics* **2006**, *25* (15), 3768–3775.
- (9) Huang, R. T. W.; Wang, W. C.; Yang, R. Y.; Lu, J. T.; Lin, I. J. B. Liquid Crystals of Gold(I) N-Heterocyclic Carbene Complexes. *Dalton Trans.* **2009**, No. 35, 7121–7131.
- (10) Arcau, J.; Andermark, V.; Rodrigues, M.; Giannicchi, I.; Pérez-García, L.; Ott, I.; Rodríguez, L. Synthesis and Biological Activity of Gold(I) N-Heterocyclic Carbene Complexes with Long Aliphatic Side Chains. *Eur. J. Inorg. Chem.* **2014**, *2014* (35), 6117–6125.
- (11) Drost, R. M.; Broere, D. L. J.; Hoogenboom, J.; de Baan, S. N.; Lutz, M.; de Bruin, B.; Elsevier, C. J. Allylpalladium(II) Histidylidene Complexes and Their Application in Z-Selective Transfer Semihydrogenation of Alkynes. *Eur. J. Inorg. Chem.* **2015**, *2015* (6), 982–996.
- (12) Castañón, E. B.; Kaposi, M.; Reich, R.; E. Kühn, F. Water-Soluble Transition Metal Complexes of Ruthenium(II), Osmium(II), Rhodium(III) and Iridium(III) with Chelating N-Heterocyclic Carbene Ligands in Hydrogenation and Transfer Hydrogenation Catalysis. *Dalton Trans.* **2018**, *47* (7), 2318–2329.
- (13) Ling, X.; Schaeffer, N.; Roland, S.; Pileni, M.-P. Nanocrystals: Why Do Silver and Gold N-Heterocyclic Carbene Precursors Behave Differently? *Langmuir* **2013**, *29* (41), 12647–12656.
- (14) Gardner, S.; Kawamoto, T.; Curran, D. P. Synthesis of 1,3-Dialkylimidazol-2-ylidene Boranes from 1,3-Dialkylimidazolium Iodides and Sodium Borohydride. *J. Org. Chem.* **2015**, *80* (19), 9794–9797.
- (15) Horn, M.; Mayr, H.; Lacôte, E.; Merling, E.; Deaner, J.; Wells, S.; McFadden, T.; Curran, D. P. N-Heterocyclic Carbene Boranes Are Good Hydride Donors. *Org. Lett.* **2012**, *14* (1), 82–85.
- (16) Ueng, S.-H.; Makhlof Brahmi, M.; Derat, É.; Fensterbank, L.; Lacôte, E.; Malacria, M.; Curran, D. P. Complexes of Borane and N-Heterocyclic Carbenes: A New Class of Radical Hydrogen Atom Donor. *J. Am. Chem. Soc.* **2008**, *130* (31), 10082–10083.
- (17) Chu, Q.; Makhlof-Brahmi, M.; Solovyev, A.; Ueng, S.-H.; Curran, D. P.; Malacria, M.; Fensterbank, L.; Lacôte, Emmanuel, E. Ionic and Organometallic Reductions with N-Heterocyclic Carbene Boranes. *Chem. - Eur. J.* **2009**, *15* (47), 12937–12940.
- (18) Taniguchi, T.; Curran, D. P. Silica Gel Promotes Reductions of Aldehydes and Ketones by N-Heterocyclic Carbene Boranes. *Org. Lett.* **2012**, *14* (17), 4540–4543.

- (19) Bolt, D. A.; Curran, D. P. 1-Butyl-3-Methylimidazol-2-ylidene Borane: A Readily Available, Liquid N-Heterocyclic Carbene Borane Reagent. *J. Org. Chem.* **2017**, *82* (24), 13746–13750.
- (20) Liu, T.; Chen, L.; Sun, Z. Asymmetric Reduction of *Tert*-Butanesulfinyl Ketimines by N-Heterocyclic Carbene Boranes. *J. Org. Chem.* **2015**, *80* (22), 11441–11446.
- (21) Pan, X.; Boussonnière, A.; Curran, D. P. Molecular Iodine Initiates Hydroborations of Alkenes with N-Heterocyclic Carbene Boranes. *J. Am. Chem. Soc.* **2013**, *135* (38), 14433–14437.
- (22) Ueng, S.-H.; Solovyev, A.; Yuan, X.; Geib, S. J.; Fensterbank, L.; Lacôte, E.; Malacria, M.; Newcomb, M.; Walton, J. C.; Curran, D. P. N-Heterocyclic Carbene Boryl Radicals: A New Class of Boron-Centered Radical. *J. Am. Chem. Soc.* **2009**, *131* (31), 11256–11262.
- (23) Ueng, S.-H.; Fensterbank, L.; Lacôte, E.; Malacria, M.; Curran, D. P. Radical Reductions of Alkyl Halides Bearing Electron Withdrawing Groups with N-Heterocyclic Carbene Boranes. *Org. Biomol. Chem.* **2011**, *9* (9), 3415–3420.
- (24) Shimoi, M.; Watanabe, T.; Maeda, K.; Curran, D. P.; Taniguchi, T. Radical Trans-Hydroboration of Alkynes with N-Heterocyclic Carbene Boranes. *Angew. Chem. Int. Ed.* **2018**, *57* (30), 9485–9490.
- (25) Zhou, N.; Yuan, X.-A.; Zhao, Y.; Xie, J.; Zhu, C. Synergistic Photoredox Catalysis and Organocatalysis for Inverse Hydroboration of Imines. *Angew Chem Int Ed* **2018**, *57*, 3990-3994.
- (26) Watanabe, T.; Geib, S. J.; Curran, D. P.; Taniguchi, T. N-Heterocyclic Carbene Boranes Are Hydrogen Donors in Masamune–Bergman Reactions of Benzo[3,4]Cyclodec-3-Ene-1,5-Diynes. *J. Org. Chem.* **2017**, *82* (24), 13034–13042.
- (27) Supranovich, V. I.; Levin, V. V.; Struchkova, M. I.; Korlyukov, A. A.; Dilman, A. D. Radical Silyldifluoromethylation of Electron-Deficient Alkenes. *Org. Lett.* **2017**, *19*, 3215–3218.
- (28) Tehfe, M.-A.; Makhlof Brahmi, M.; Fouassier, J.-P.; Curran, D. P.; Malacria, M.; Fensterbank, L.; Lacôte, E.; Lalevée, J. N-Heterocyclic Carbenes–Borane Complexes: A New Class of Initiators for Radical Photopolymerization. *Macromolecules* **2010**, *43* (5), 2261–2267.
- (29) Pak, Y. L.; Park, S. J.; Wu, D.; Cheon, B.; Kim, H. M.; Bouffard, J.; Yoon, J. N-Heterocyclic Carbene Boranes as Reactive Oxygen Species-Responsive Materials: Application to the Two-Photon Imaging of Hypochlorous Acid in Living Cells and Tissues. *Angew. Chem. Int. Ed.*, **2018**, *57*, 1567-1571.
- (30) Huang, S.; Qi, X.; Liu, T.; Wang, K.; Zhang, W.; Li, J.; Zhang, Q. Towards Safer Rocket Fuels: Hypergolic Imidazolylidene-Borane Compounds as Replacements for Hydrazine Derivatives. *Chem. – Eur. J.* **2019**, *25* (29), 10187–10193.
- (31) Le Quemener, F. Utilisation de NHC-Boranes Pour La Synthèse de Nanoparticules et l’amorçage de Photopolymérisation En Émulsion, Université de Lyon, 2016.
- (32) Zheng, N.; Fan, J.; Stucky, G. D. One-Step One-Phase Synthesis of Monodisperse Noble-Metallic Nanoparticles and Their Colloidal Crystals. *J. Am. Chem. Soc.* **2006**, *128* (20), 6550–6551.
- (33) Li, Y.; Liu, S.; Yao, T.; Sun, Z.; Jiang, Z.; Huang, Y.; Cheng, H.; Huang, Y.; Jiang, Y.; Xie, Z.; Pan, G.; Yan, W.; Wei, S. Controllable Synthesis of Gold Nanoparticles with Ultrasmall Size and High Monodispersity via Continuous Supplement of Precursor. *Dalton Trans.* **2012**, *41* (38), 11725–11730.
- (34) Turkevich, J.; Stevenson, P. C.; Hillier, J. A Study of the Nucleation and Growth Processes in the Synthesis of Colloidal Gold. *Discuss. Faraday Soc.* **1951**, *11*, 55–75.
- (35) Nikoobakht, B.; El-Sayed, M. A. Preparation and Growth Mechanism of Gold Nanorods (NRs) Using Seed-Mediated Growth Method. *Chem. Mater.* **2003**, *15* (10), 1957–1962.
- (36) Deraedt, C.; Salmon, L.; Gatard, S.; Ciganda, R.; Hernandez, R.; Ruiz, J.; Astruc, D. Sodium Borohydride Stabilizes Very Active Gold Nanoparticle Catalysts. *Chem Commun* **2014**, *50* (91), 14194–14196.
- (37) Azubel, M.; Kornberg, R. D. Synthesis of Water-Soluble, Thiolate-Protected Gold Nanoparticles Uniform in Size. *Nano Lett.* **2016**, *16* (5), 3348–3351.
- (38) Kirchnerová, J.; Cave, G. C. B. The Solubility of Water in Low-Dielectric Solvents. *Can. J. Chem.* **1976**, *54* (24), 3909–3916.

- (40) Barngrover, B. M.; Manges, T. J.; Aikens, C. M. Prediction of Nonradical Au(0)-Containing Precursors in Nanoparticle Growth Processes. *J. Phys. Chem. A* **2015**, *119* (5), 889–895.
- (41) Tsui, E. Y.; Müller, P.; Sadighi, J. P. Reactions of a Stable Monomeric Gold(I) Hydride Complex. *Angew. Chem. Int. Ed.* **2008**, *47* (46), 8937–8940.
- (42) Silva Valverde, M. F.; Schweyen, P.; Gisinger, D.; Bannenberg, T.; Freytag, M.; Kleeberg, C.; Tamm, M. N-Heterocyclic Carbene Stabilized Boryl Radicals. *Angew. Chem. Int. Ed.* **2017**, *56* (4), 1135–1140.
- (43) Aprile, C.; Boronat, M.; Ferrer, B.; Corma, A.; García, H. Radical Trapping by Gold Chlorides Forming Organogold Intermediates. *J. Am. Chem. Soc.* **2006**, *128* (26), 8388–8389.
- (44) Tehfe, M.-A.; Monot, J.; Brahmi, M. M.; Bonin-Dubarle, H.; Curran, D. P.; Malacria, M.; Fensterbank, L.; Lacôte, E.; Lalevée, J.; Fouassier, J.-P. N-Heterocyclic Carbene-Borane Radicals as Efficient Initiating Species of Photopolymerization Reactions under Air. *Polym Chem* **2011**, *2* (3), 625–631.
- (45) Subervie, D.; Graff, B.; Nerkar, S.; Curran, D. P.; Lalevée, J.; Lacôte, E. Difluorination at Boron Leads to the First Electrophilic Ligated Boryl Radical (NHC-BF₂). *Angew. Chem. Int. Ed.* **2018**, *57* (32), 10251–10256.
- (46) Denk, Michael K; Hatano, Ken; Ma, Martin. Nucleophilic Carbenes and the Wanzlick Equilibrium: A Reinvestigation. *Tetrahedron Lett.* **1999**, *40*, 2057–2060.

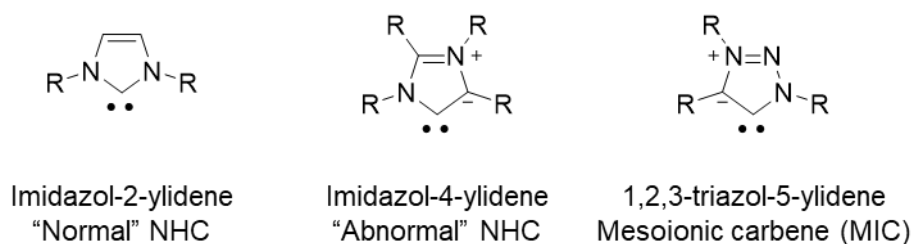
CHAPTER IV: SYNTHESIS OF MESOIONIC CARBENE-CAPPED GOLD NANOPARTICLES FROM TRIAZOLIUM SALTS AND MIC-BH₃

IV.A Mesoionic carbenes in the literature

As mentioned briefly in chapter I, imidazol-2-ylidene NHCs are not the only structure possible. Indeed, if an imidazolium is protected at the C2 position, for example by an alkyl or aryl group, the C4 or C5 position can be deprotonated to form what is often referred to as an “abnormal” or “mesoionic” carbene. The term “abnormal” simply refers to the difference between the imidazol-4-ylidenes and imidazole-2-ylidenes which are considered “normal”. The name mesoionic comes from the fact that, it is not possible to write a neutral structure for such carbenes. Indeed, a plus and minus charge have to be introduced on the structure (Scheme IV.1).

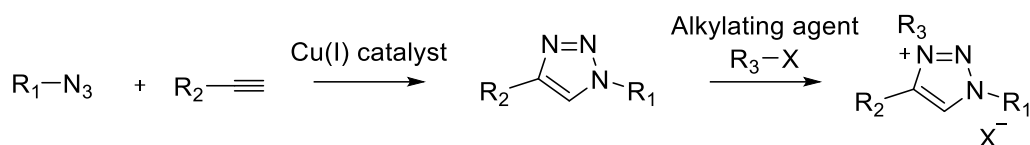
Normal NHCs are already strong neutral sigma donors but abnormal NHCs are expected to be even stronger due to the presence of only one nitrogen atom adjacent to the carbene.¹

While the first example of imidazol-4-ylidene was described in 2001,² a new class of abnormal/mesoionic carbenes was described in 2008 by Albrecht *et coll.*: 1,2,3-triazol-5-ylidenes.³ While both technically present a mesoionic character, in the rest of this chapter mesoionic carbene (MIC) will designate the triazolylidene type exclusively.



Scheme IV.1: Structures of imidazol-2-ylidene, imidazole-4-ylidene and 1,2,3-triazol-5-ylidene.

In the study by Albrecht *et coll.*,³ Pd and Ag complexes are obtained by direct metalation of a triazolium salt. The silver complex is unstable and decomposes within a few hours ($t_{1/2}$ ca. 20h at room temperature) but was successfully used in transmetalation reactions yielding Ru, Rh and Ir complexes. Triazolium salts are synthesized in 2 steps (Scheme IV.2). First the triazole ring is formed by copper(I) catalyzed click chemistry [3+2] cycloaddition (CuAAC) between an alkyne and an azide. This chemistry is well-developed and a wide range of triazoles have already been synthesized in high yields.^{4,5} The second step is the alkylation of the triazole in the N3 position yielding the 1,3,4 functionalized triazolium salt.



Scheme IV.2: Synthetic pathway to 1,3,4 functionalized 1,2,3-triazolium salts.

While it is possible to synthesize 1,2,4 functionalized triazolium salts, which would also yield MICs once deprotonated, their synthesis requires a different pathway. They have thus been less studied than the easily obtainable 1,3,4 functionalized triazolium salts and their corresponding carbenes, which the rest of this chapter will focus on.

The first free 1,2,3-triazol-5-ylidene was described in 2010 by Bertrand *et coll.*⁶ By deprotonating a triazolium salt with KHMDS, they obtained a MIC that could be characterized by X-ray diffraction and was stable for several days at -30°C. However, the MIC was only stable for a few hours at room temp and at 50°C it decomposed.

When investigating the donor properties of MICs, it was found that they were in between imidazol-2-ylidenes and imidazol-4-ylidenes, with the former being weaker donors and the latter stronger donors. As with normal NHCs, a range of MIC-M complexes (Pd,⁷ Ir,⁸ Fe,⁹ Ru,¹⁰...) were synthesized in the decade following their discovery and a majority of them were studied as catalysts. Gold-MIC complexes were no exception and examples exist^{11,12} of their use, for instance in the catalytic synthesis of oxazolines, which are a class of heterocyclic compounds that can be employed as precursors for the synthesis of a variety of bioactive compounds and as chiral auxiliaries in asymmetric synthesis.^{13,14}

Despite their similarity to normal NHCs, there is no example, to the best of our knowledge, of the use of MICs in materials chemistry. Because of their expected stronger binding properties, we decided to study the possibility of synthesizing MIC-stabilized gold nanoparticles by transposing the protocols used in Chapter II.

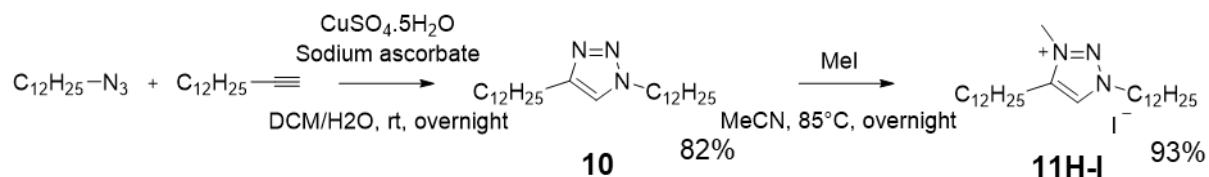
IV.B. Gold nanoparticles stabilized by MICs from triazolium salts

IV.B.1. Synthesis of the triazolium salts precursors

As with the NHCs, the first step was the synthesis of the triazolium salt. We decided on **11H-I** (Scheme IV.3) as we hoped that C₁₂ alkyl chains would promote nanoparticle stabilization (as was the case for imidazolium). **10** was synthesized (in 82% yield) by a copper(I) catalyzed cycloaddition between

tetradecyne and dodecyl azide. The latter was synthesized by addition of sodium azide to a solution of 1-bromododecane in DMSO and obtained in 78% yield.

The triazole **10** was then refluxed overnight in acetonitrile with iodomethane to afford the corresponding triazolium salt in 93% yield.



Scheme IV.3: Synthetic pathway to triazolium iodide salt **11H-I**.

However, when the synthesis of the triazolium AuCl_4 complex was attempted, by anion metathesis in $\text{H}_2\text{O}/\text{CHCl}_3$, a bright red solution was obtained.

Different reaction conditions were tested: solvent (DCM , CHCl_3 , $\text{DCM}/\text{H}_2\text{O}$ or $\text{CHCl}_3/\text{H}_2\text{O}$), gold precursor (HAuCl_4 or KAuCl_4) and amount of triazolium iodide (1 or 4 equivalents), but **11-AuX₄** could not be isolated. Each time the solution turned red, except for the latter (4 equivalents of triazolium) where it remained yellow.

The solutions in CHCl_3 starting from HAuCl_4 were characterized by TEM and in both cases small NPs were observed (2.6 ± 0.1 nm for 1 eq and 2.8 ± 0.7 nm for 4 eq). This type of nanoparticles usually results in a brown solution with no plasmon resonance visible by UV-vis spectrum.¹⁵ When characterized by UV-vis spectroscopy (Figure IV.1), the solution using 1 equivalent exhibited 2 peaks: one at 326 nm attributed to the triazolium AuCl_4 complex formed and one at 510 nm attributed to I_2 . The latter resulting from the reduction of gold by I^- . The solution using 4 equivalents exhibits 1 peak at 364 nm attributed to I_3^- ¹⁶ whose formation results from the reaction of I_2 with excess I^- . The presence of the oxidized form of I^- (I_2) in both samples suggests it acts as a reducing agent towards gold.

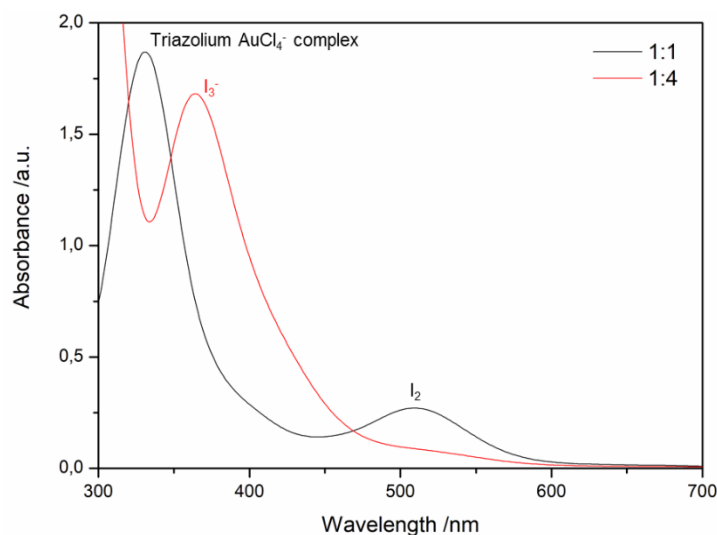
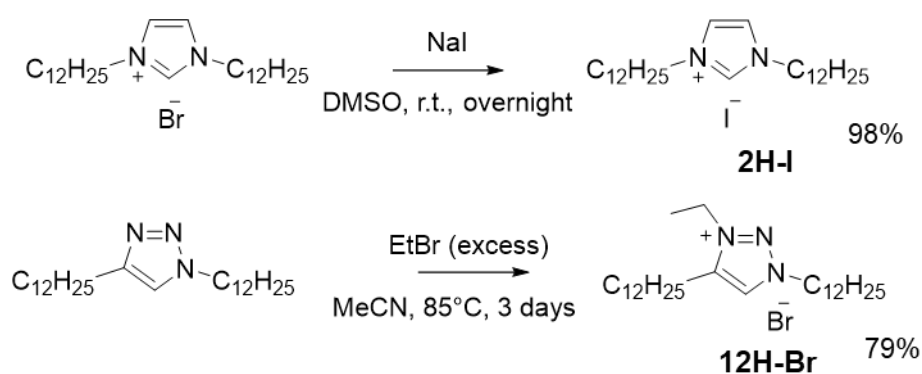


Figure IV.1: UV-vis spectra of samples 1:1 and 1:4 $\text{HAuCl}_4 \cdot 3\text{H}_2\text{O}:\mathbf{11H-I}$ (solvent: chloroform).

Indeed, it has been shown in the literature¹⁷ that iodide anions are able to produce nanoparticles from a gold(III) precursor. The iodide reduces the gold(III) into gold(I) (AuCl_2^-) which then disproportionates into gold(0) and gold(III).

Moreover, we found that by simply mixing $\text{HAuCl}_4 \cdot 3\text{H}_2\text{O}$ with KI in water a brown solution and yellow precipitate (most likely AuI) were obtained. Addition of CHCl_3 led to a pink organic phase confirming the presence of I_2 .

To test our theory on the role of the iodide counter ion acting as reducing agent, an imidazolium iodide (**2H-I**) and a triazolium bromide (**12H-Br**) were synthesized (Scheme IV.4). The imidazolium iodide was obtained by anion metathesis between the imidazolium bromide and sodium iodide in near quantitative yield. The triazolium bromide **12H-Br** was synthesized from **10** and bromoethane yielding an ethylated triazolium salt (instead of methylated). It is worth noting that in order to obtain the product in a good yield (79%), bromoethane had to be introduced in large excess (30 eq) and the reaction had to be carried out over 3 days instead of overnight.



Scheme IV.4: Synthetic pathways to imidazolium iodide **2H-I** and triazolium bromide **12H-Br**.

Imidazolium iodide yielded similar results to triazolium iodide. Indeed, when using 1 or 4 equivalents of imidazolium, nanoparticles were obtained (ca. 1 nm and 2.8 ± 0.4 nm respectively). The same species were observed by UV-vis spectroscopy (imidazolium AuCl_4 complex and I_2 for 1 eq and I_3^- for 4eq) (Figure IV.2). Whereas no reduction occurred with **12H-Br**.

This seems to confirm the role of the iodide counter ion in the reduction of gold into nanoparticles.

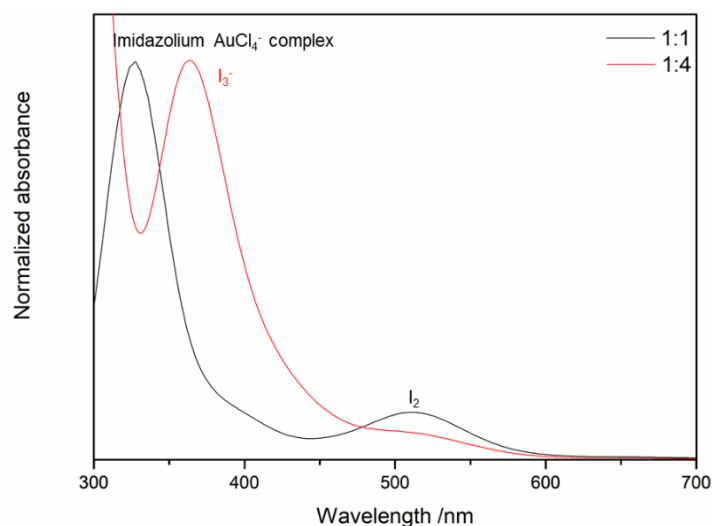


Figure IV.2: UV-vis spectra of samples 1:1 and 1:4 HAuCl₄.3H₂O:2H-I (solvent chloroform).

IV.B.2. Gold nanoparticle synthesis from triazolium salts

Addition of 10 equivalents of NaBH₄ to a solution of HAuCl₄ and **11H-I** led to a color change from orange to black and bubbling. After a few minutes the solution turned deep red. When excess of **11H-I** was used (4 eq instead of 1), the solution turned green, blue, purple black and finally red but no bubbling was observed. The solutions were washed with water to remove excess NaBH₄ and characterized by TEM. Both samples contained a mixture of different NPs.

For the 1:1 sample, the major population of nanoparticles were spherical and 14.1 ± 1.4 nm in diameter (Figure IV.3) but some smaller particles (3.5 ± 1.0 nm) and aggregates could also be observed. However, for the 1:4 sample, some clusters (1-2 μ m) were observed but the vast majority of NPs were much larger with an average diameter of 26.2 ± 3.4 nm and very faceted shapes (Figure IV.3). In both cases, the nanoparticles were unstable and precipitated in a few days.

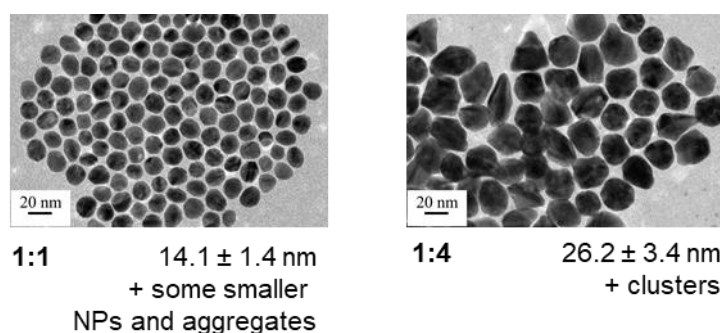


Figure IV.3: TEM images of AuNPs synthesized from 1 or 4 equivalents **11H-I**, HAuCl₄.3H₂O and 10 equivalents of NaBH₄ (solvent: toluene/H₂O).

In the literature,^{18,19} the presence of iodide ions and their concentration has been showed to strongly influence the shape of the obtained nanoparticles. Higher concentrations usually leading to more faceted structures as is the case here.

The same tests were carried out with triazolium bromide **12H-Br**. In both cases, a mixture of very small nanoparticles (1-2 nm) and larger and polydisperse nanoparticles (34 ± 9 nm for 1:1 and 16.0 ± 5.8 nm for 1:4) was obtained (Figure IV.4).

After centrifugation, the 1:1 sample presented 2 population of NPs at 5.4 ± 0.9 and 16.8 ± 2.1 nm. The nanoparticles are not very spherical and seem less stable in time than the ones obtained from **2H-Br** by a similar protocol.

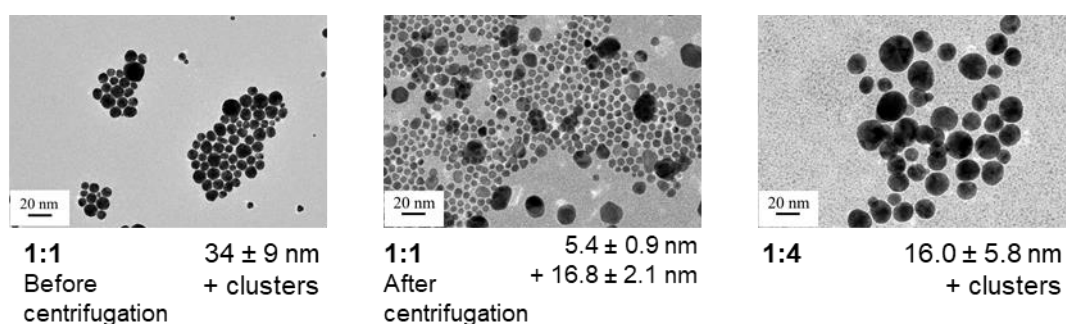


Figure IV.4: TEM images of AuNPs synthesized from 1 or 4 equivalents **12H-Br**, $\text{HAuCl}_4 \cdot 3\text{H}_2\text{O}$ and 10 equivalents of NaBH_4 (solvent: toluene/ H_2O).

A protocol using NaH was also tested for both triazoliums (**11H-I** and **12H-Br**). 4 equivalents of triazolium were mixed with 10 equivalents of NaH before addition of HAuCl_4 . In both cases, the solution turned orange before quickly discoloring.

After addition of NaBH_4 , the triazolium iodide sample turned different colors over the course of several hours (yellow, white, pink, white again) to finally settle on orange. TEM analysis of the sample showed small NPs of around 2nm in diameter.

On the other hand, the **12H-Br** sample turned red immediately and nanoparticles of 3.4 ± 0.6 nm were obtained. It is interesting to note that the nanoparticles are very similar in size and shape to the ones obtained with imidazolium bromide in the similar conditions (Figure IV.5).

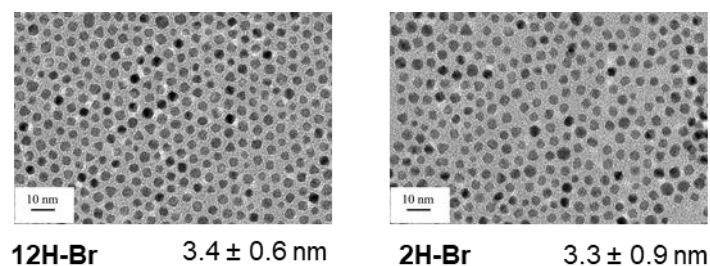


Figure IV.5: TEM images of AuNPs obtained from $\text{HAuCl}_4 \cdot 3\text{H}_2\text{O}$, 4 equivalents of **12H-Br** and 10 equivalents of NaH and NaBH_4 and from **2H-AuX₄**, 4 equivalents of **2H-Br** and 10 equivalents of NaH and NaBH_4 (solvent: toluene/ H_2O).

It thus appears that NaH is necessary to obtain monodisperse NPs from triazoliums. That does not seem surprising as MICs have a higher pK_a than their NHCs counterparts (~24 for triazoliums and between 21 and 23 for imidazoliums),¹ they are thus less prone to deprotonation. A difference in the kinetics of deprotonation could explain the difference in polydispersity. With a fast deprotonation step being key to obtain monodisperse nanoparticles.

IV.B.3. XPS analysis

Both triazolium iodide (**11H-I**) and bromide (**12H-Br**) were analyzed by XPS, along with the nanoparticles (**12-NP**) obtained from triazolium bromide (ratio 1 Au:4 **12H-Br**) and NaBH_4 . The nanoparticles analyzed were synthesized without NaH as we wanted to confirm the deprotonation of **12H-Br** by NaBH_4 .

Both N1s spectra (Figure IV.6) present three components: two present in the major peak at 402.6 and 401.7 eV for triazolium iodide and 402.6 and 401.9 eV for triazolium bromide and one minor at 399.8 eV for triazolium iodide and 399.6 eV for triazolium bromide. If all 3 nitrogen atoms were asymmetrical, they would present 3 different binding energies and a 1:1:1 distribution would be expected. The 2 major components for each triazolium presents a 2:1 ratio but the minor component was present in a different proportion depending on the triazolium. This seems to indicate that the major peaks correspond to the triazoliums but the minor component could belong to another species. Moreover, the 2:1 distribution we observe, suggests that 2 of the nitrogen atoms are symmetrical (or quasi-symmetrical) and thus present the same binding energy and one nitrogen atom would differ.

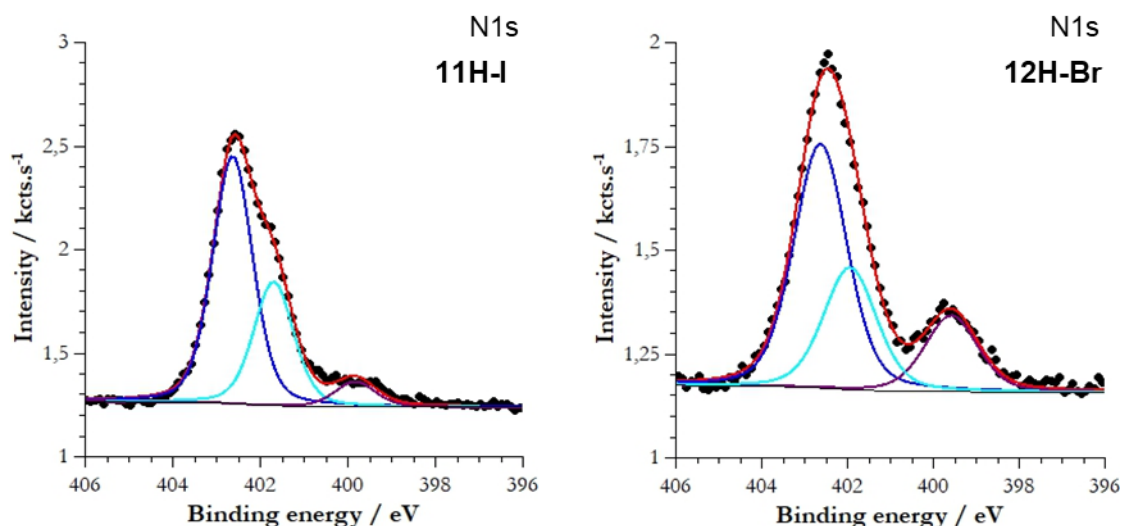


Figure IV.6: N1s XPS spectra of **11H-I** et **12H-Br**.

A closer look at the global spectrum of the sample showed the presence of copper. The copper most likely comes from the synthesis of the triazole **10** which is the base of both triazolium salts. As the presence of copper was not expected, the Cu2p spectrum was not recorded but the contamination in copper can be estimated at less than 1% of total atoms for both **11H-I** and **12H-Br**.

Copper remaining with the triazole probably formed a MIC-Cu complex during the synthesis of the triazolium. Indeed, direct metalation of NHCs has been shown to happen with copper.²⁰ Such a compound would explain the position of the contamination peak towards the lower binding energies. Indeed, examples of MIC-metal complexes seem to suggest a delocalization of the electrons on the ring^{1,3} and the formation of neutral complexes. The loss of charge of the cycle would be responsible for the position of the peak towards the lower binding energies.

The nanoparticles obtained from **12H-Br** (**12-NP**) were also characterized. No halides were detected and the gold spectrum exhibited only gold(0). This time the N1s spectrum (Figure IV.7) presented only 1 peak with 2 components at 401.2 and 400.3 eV accounting for 1 and 2 N respectively. It is worth noting that the shift of the N1s peak from **2H-Br** to **2-NP** was of 1.4 eV towards the lower binding energies. Here, the shift of the 1N component is of 0.7 eV while the shift of the 2N component is of 2.3 eV (towards lower binding energies for both). This results in an inversion of both components. At this stage we cannot attribute each component with certainty. However, we think that the 1N component corresponds to the central nitrogen and the 2N component to the 2 other nitrogen atoms. Indeed, the central nitrogen is less likely to be equivalent to one of the other 2. This remains however just a theory. Nonetheless, this global shift towards the lower binding energies suggests, as with NHCs, a loss of

charge on the cycle and a coordination of the MICs on the nanoparticles surface. All of this strongly suggests a deprotonation of **12H-Br** by NaBH_4 .

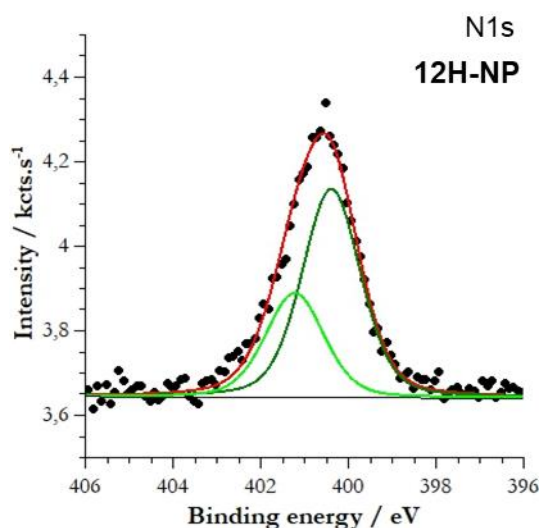


Figure IV.7: N1s XPS spectrum of **12-NP**.

It can be noted that some copper is still present in the NPs global XPS spectrum. This likely comes from the copper contamination of the triazoliums. It is possible that the copper got incorporated in the matrix. Indeed, AuCu alloy NPs exist and have already been synthesized in the literature.²¹

We have thus described the first synthesis of gold nanoparticles from triazolium salts. We have shown that syntheses using a brominated triazolium and a base yield the most monodisperse NPs. We have confirmed the stabilization of the synthesized nanoparticles by MICs (even in the absence of a base) for the first time. While copper was also detected, its role in the synthesis is unclear (if it has a role at all).

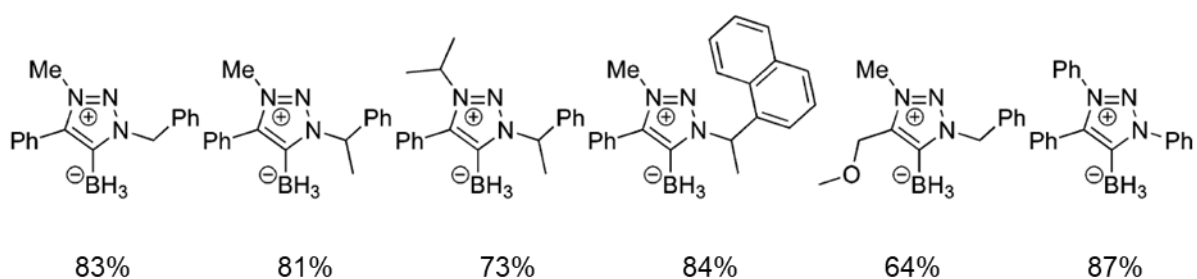
IV.C. Gold nanoparticles stabilized by MICs from MIC-BH₃

IV.C.1. MIC-BH₃ in the literature

To this date, and to the best of our knowledge, there is only one report of MIC-BH₃ in the literature. In 2013, Crudden *et coll.* described the synthesis of MIC-boranes starting from a variety of triazolium salts.²² By using reaction conditions similar to those used in the synthesis of NHC-BH₃, deprotonation at -78°C by KHMDS before introduction of BH₃.SME₂ and stirring overnight, they obtained a series of MIC-boranes in 64 to 87% yield (Scheme IV.5). They were able to obtain crystal structures for several

of the synthesized compounds. Finally, they used one MIC-BH₃ in the reduction of 4-bromoacetophenone and 4-bromobenzaldehyde. Similarly to NHC-BH₃,^{23,24} the reaction required the presence of a catalyst such as Sc(OTf)₃ or silica in order to activate the C=O double bond. While the yields are similar to those obtained with NHC-BH₃, part of the MIC-BH₃ was recovered intact when introduced in the same quantity as the substrate. When using only 0.3 eq of MIC-BH₃, they obtained the same yield as previously but did not recover any MIC-BH₃. This seems to suggest that all 3 hydrides of the borane are used in the reaction and that MIC-boranes are better reducing agent than NHC-boranes.

The increased hydricity of the MIC-BH₃ compared to NHC-BH₃ can be expected as MICs are better sigma donors than NHCs. The C-B bond is thus likely to be stronger which would weaken the B-H bond.



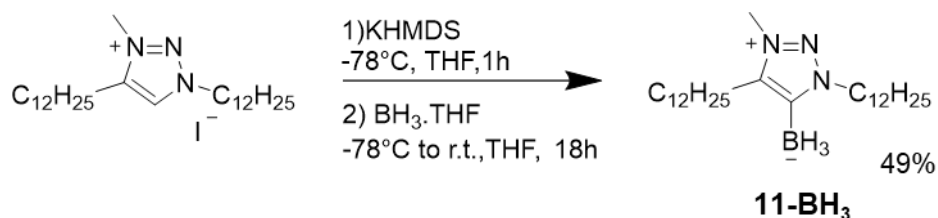
Scheme IV.5: MIC-boranes synthesized by Crudden *et coll.*²²

Since then only 2 other reports of MIC-boron species have been reported in the literature. MIC-borenum catalysts²⁵ reported by Crudden *et coll.* in 2015, which exhibit a reactivity similar to frustrated Lewis pairs in the hydrogenation of imines but in less stringent conditions and perform better overall than similar NHC-borenum complexes, as well as MIC-aryldihaloboranes and a MIC-diborane both reported by Arrowsmith *et al.* in 2017.²⁶

Attracted by the limited literature available for such compounds, we decided to try them in the synthesis of gold nanoparticles. Indeed, we thought interesting to study the difference in their reactivity and if eventually they would also give nanoparticles.

IV.C.2. Synthesis of MIC-BH₃

Synthesis of the MIC-BH₃ (**11-BH₃**) was carried out using the same protocol as for NHC-BH₃ (Scheme IV.6). **11H-I** was deprotonated by KHMDS in THF at -78°C, before addition of BH₃.THF and overnight stirring at room temperature. After purification by column chromatography, the MIC-BH₃ was obtained in 49% yield.



Scheme IV.6: Synthesis of MIC-borane **11-BH₃**.

IV.C.3. Gold nanoparticle synthesis using AuClSMe₂ as a precursor

Tests replicating the conditions used for NHC-BH₃ were carried out. Given the importance of the Au: NHC-BH₃ ratio in the previous chapter, the first series of tests was carried out with Au: MIC-BH₃ ratios ranging from 1:1 to 1:20 including intermediary ratios of 1:3, 1:5, 1:10 and 1:15.

Upon addition of MIC-BH₃, the solutions immediately turned blue signaling the formation of aggregates. However, after two hours all solutions had turned bright red. The shift in color happened faster for the samples containing the highest amounts of MIC-BH₃.

Samples for ratios 1:1, 1:5, 1:10 and 1:20 were analyzed by TEM after 24h of reaction. Unlike NHC-BH₃, there appears to be very little correlation between the ratio and the size of the obtained nanoparticles (Figure IV.8). Indeed, while samples 1:1, 1:10 and 1:20 all give NPs of around 3.8 nm in diameter, the 1:5 sample gives NPs of 4.9 ± 1.8 nm. These results are subject to caution however. Indeed, only one series of experiments was carried out and when ratios 1:1 and 1:10 were repeated individually, the obtained NPs had diameters of 6.5 ± 1.8 nm and 5.6 ± 1.5 nm respectively after the same reaction time. It is thus possible that the size obtained are simply not reproducible enough to conclude on the effect of ratios. This lack of reproducibility might stem from a non-reproducible kinetic factor.

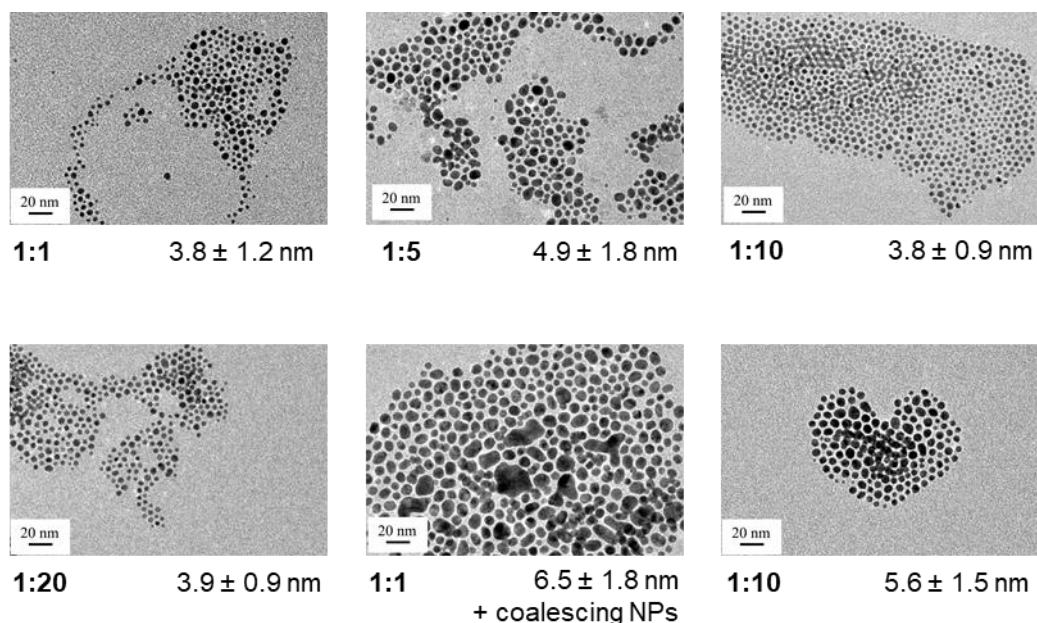


Figure IV.8: TEM images of gold nanoparticles starting from different Au:MIC-BH₃ ratios in toluene after 24h of reaction.

A sample with a 1:10 Au: MIC-BH₃ ratio was prepared and followed by UV-visible spectroscopy (Figure IV.9). Right after the injection (t=0), a broad peak is visible at 560 nm. Over time, the peak shifts towards the lower wavelengths (524 nm after 16h) and narrows. This indicates a narrowing of the size distribution of the nanoparticles and a decrease in size.

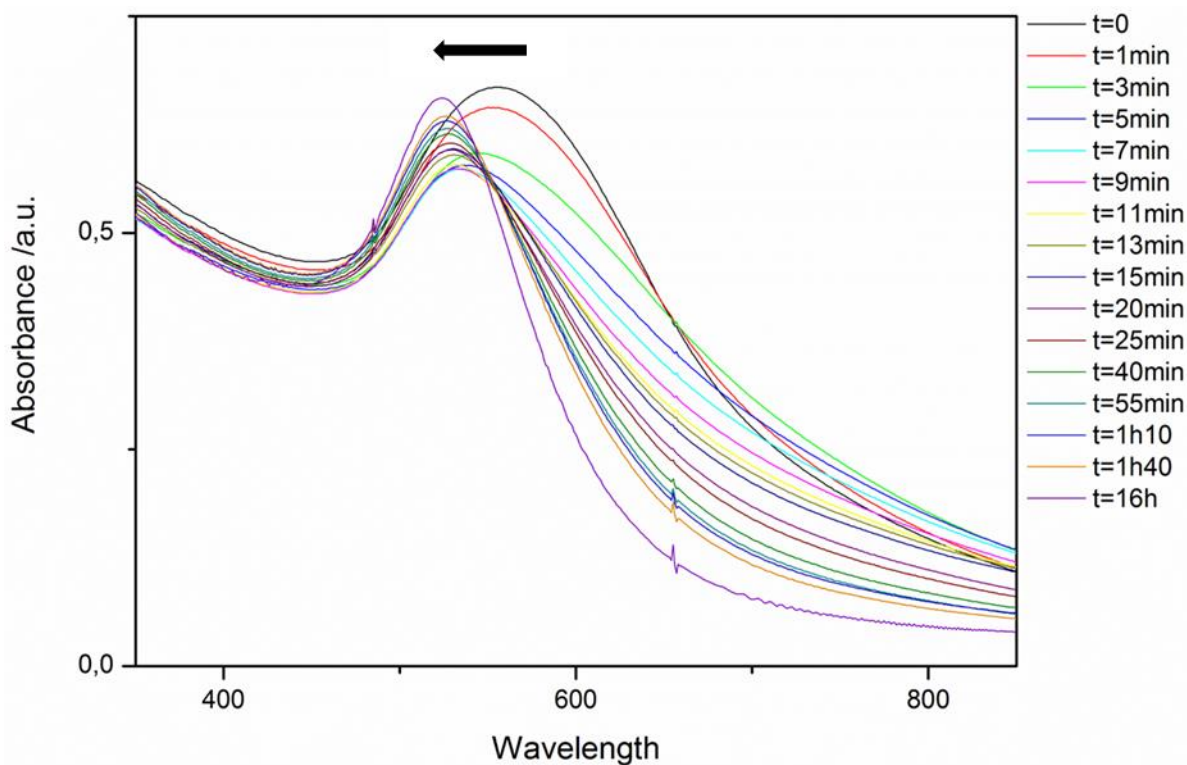


Figure IV.9: UV-visible spectra of a sample with a 1:10 Au: MIC-BH₃ ratio (in toluene) over time.

As exhibited by the UV-Vis spectra, the kinetics of the 1:10 sample are rather fast, a 1:1 sample (which transitions slower) was prepared to follow the reaction by TEM. Samples were prepared right after injection and after 3, 8, 24, and 48 hours of reaction (Figure IV.10).

As expected based on the color of the solution, the sample at $t=0$ presented only aggregates. After 3h of reaction, a mixture of aggregates and NPs of different sizes (from 2 to 15 nm) were observed. After 8h, discrete nanoparticles of 5.4 ± 1.5 nm were obtained but after 24h some NPs started coalescing, which increased the mean size of the NPs to 6.5 ± 1.8 nm. However after 48h, no large NPs were observed anymore and the mean size of the NPs dropped to 5.7 ± 1.7 nm. It seems however that the nanoparticles were unstable as after 6 weeks, large and polydisperse NPs of 8.1 ± 3.0 nm were obtained.

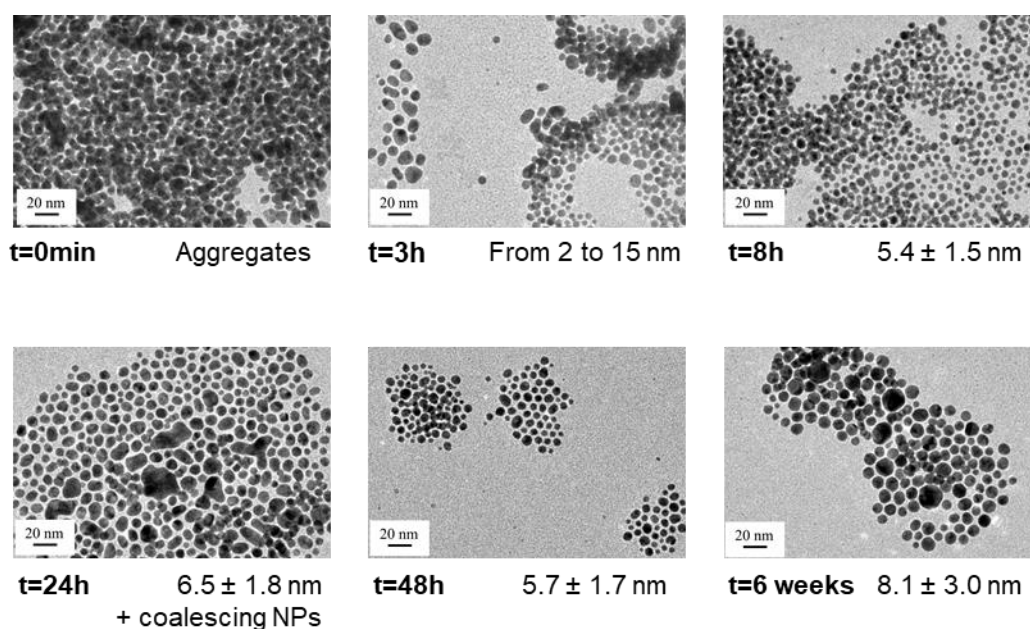


Figure IV.10: TEM images of a sample with a 1:1 Au:**11-BH₃** ratio (in toluene) over time.

The reaction was also followed by ^1H and ^{11}B NMR. As with NHC-BH₃ a new species appears, but it is not stable over time and seems to degrade into triazolium (Figure IV.11). Similarly to NHC-BH₃, only part of the MIC-BH₃ is consumed.

As with **2-BH₃** in Chapter III, **11-BH₃** was reacted with HCl in dichloromethane in order to form MIC-BH₂Cl and confirm the similarity of the reduction pathway. The minor product of the reaction corresponds to the unknown species formed during the reaction with gold. However, the major product is triazolium salt. It can be noted that when the same reaction was carried out with NHC-BH₃ only NHC-BH₂Cl and unreacted NHC-BH₃ were formed. It thus appears that MIC-BH₂Cl is less stable than its NHC counterpart, or MIC-BH₃ is more sensitive to acids as MICs are more basic than NHCs.

Another difference, is that the minor product, which corresponds to the species observed in situ, appears to be a protonated MIC-BH₂Cl. Indeed, the ¹¹B NMR spectrum presents a peak at -17 ppm which confirms the formation of MIC-BH₂Cl. However, ¹H NMR shows the presence of peak at 4.5 ppm that integrates for 1 with respect to the other protons. A plausible explanation is the protonation of MIC-BH₂Cl (probably on the N2 nitrogen atom). However, this would require more than the 1 equivalent of HCl introduced in solution. As of the time of writing, the formation of this species and the mechanism that leads to it remain unclear.

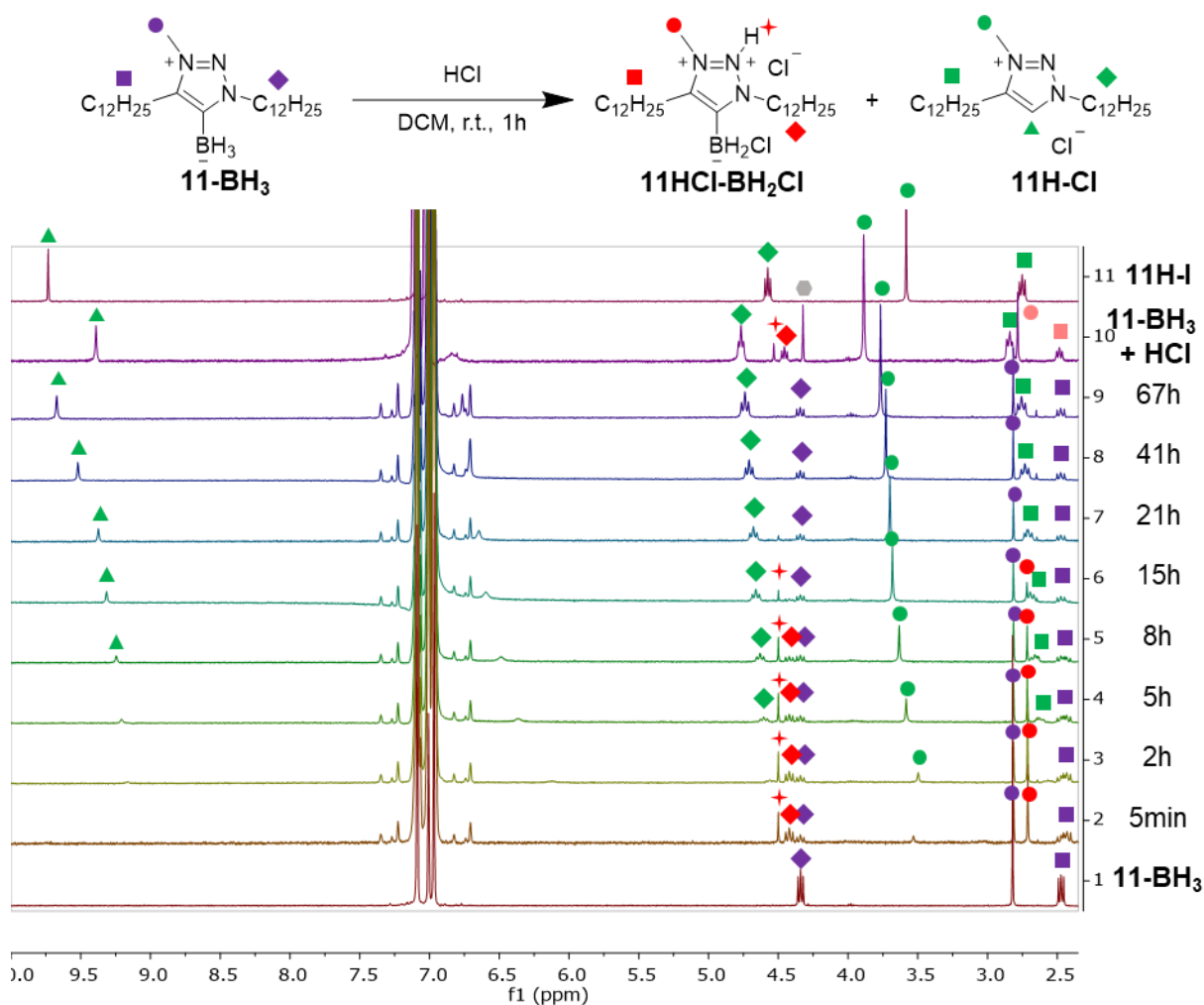


Figure IV.11: ¹H NMR in tol-d8 of **11-BH₃**, 1:1 AuClSMe₂:**11-BH₃** sample over time, synthesized MIC-BH₂Cl and **11H-I**. Grey dot= DCM signal.

This seems to suggest a similar reduction mechanism to the one of NHC-BH₃ but a different stabilizing action.

However, before more tests could be carried out the reaction stopped working. Indeed, regardless of the quantity of MIC-BH₃ introduced, the aggregates first formed never turned into discrete nanoparticles.

At the time, this change in reactivity was attributed to a possible degradation of the gold precursor. However, in light of the most recent results obtained with the NHC-BH₃, it is possible that a batch effect may have also been at play. At the time of writing, no systematic study comparing the different batches synthesized has been undertaken yet. Hopefully a parallel could be drawn between NHCs and MICs to better understand the issue.

IV.C.4. Gold nanoparticle synthesis using HAuCl₄.3H₂O as a precursor

Nanoparticle synthesis starting from **11-BH₃** and HAuCl₄.3H₂O was also attempted.

As with NHC-BH₃, a biphasic system led to a gold mirror at the interface regardless of the organic phase solvent (toluene or chloroform).

As a result, a solution of HAuCl₄.3H₂O in chloroform was diluted with toluene to afford the desired concentration and to perform the reaction in a monophasic system.

As first tests yielded strange results, the influence of the amount of chloroform in the solution was investigated. Three HAuCl₄.3H₂O solutions were prepared in order to obtain a final percentage of chloroform in the medium of 5%, 25% and 50% (Figure IV.12). The solution with 5% of chloroform yielded monodisperse nanoparticles of 5.7 ± 1.2 nm while solutions at 25 and 50% yielded a mixture of small and large nanoparticles. In the case of the solution with 50% chloroform, NPs were coalescing and aggregates could also be observed.

This clearly shows the influence of chloroform in the reaction medium and the less chloroform seems the best option. It is however unclear if this is due to the acidic nature of chloroform which could interfere with the carbenes or to different solvation properties that would alter the shape of the NPs.

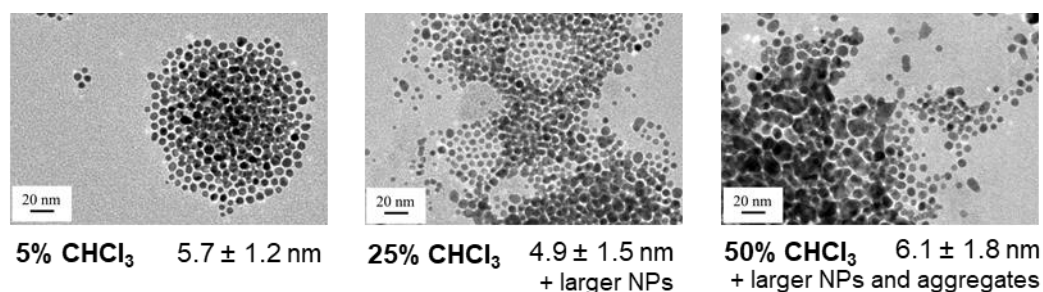


Figure IV.12: TEM images of 1:10 HAuCl₄.3H₂O:**11-BH₃** samples in toluene with varying amounts of chloroform.

The influence of the Au: MIC ratio was studied (Figure IV.13). While 1:5 NPs are always larger than 1:20 NPs, 1:10 NPs do not have an intermediate size and fall close to the 1:20 sample. However, at 0°C, the 1:10 ratio is closer in size to the 1:5 ratio.

Another effect of the lowered temperature is a better monodispersity of the NPs. Increasing the temperature to 50°C, on the other hand, yielded very polydisperse NPs.

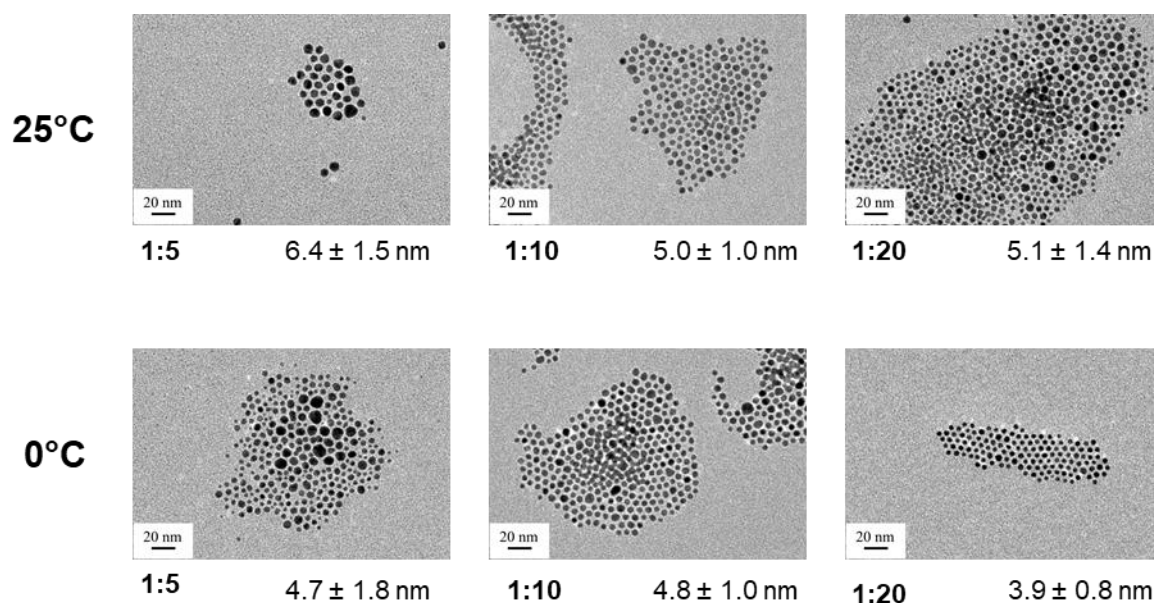


Figure IV.13: TEM images for different Au:11-BH₃ ratios depending on the temperature (in toluene). (solutions cooled independently before reaction at 0°C)

It is interesting to note that experiments could be repeated with only minor changes in size between samples, unlike with NHC-BH₃ which showed huge changes in size, shape and polydispersity of the NPs when using this gold precursor. It thus seems that MIC-BH₃ is better suited to a gold(III) precursor as opposed to NHC-BH₃ which is better suited to a gold(I) precursor.

IV.C.5. XPS analysis

The NPs obtained from ratio HAuCl₄:11-BH₃ 1:10 and 5% CHCl₃ (11-NP) were characterized by XPS along with 11-BH₃.

As with the triazoliums, copper contamination can be detected for 11-BH₃ and seems to account for less than 1% of the atoms of the sample. Once the contamination accounted for, the N1s component corresponding to the MIC-BH₃ can be decomposed into 2 components: at 402.5 and 401.5 eV which account for 2 and 1 N respectively (Figure IV.14). These values are very close to the ones obtained for 11H-Br (402.6 and 401.7 eV). This seems to confirm the mesoionic character of MIC-boranes which, unlike NHC-boranes, conserve a charge on the cycle.

As with NHC-BH₃, no boron is detected in the nanoparticles sample and the gold spectrum corresponds to gold(0) only. The N1s spectrum presents one peak with two components at 401.8 and 400.4 eV

accounting for 1 and 2 N respectively (Figure IV.14). It can be noted that these values are very close to the ones obtained for **10-NP**. As with the NPs obtained from triazolium this suggests a delocalization of the electrons on the ring and the coordination of MIC to the metal. As with **10-NP**, there is an inversion of 2N and 1N component. Indeed, the 1N component shifts by 0.3 eV towards the higher energies while the 2N component shifts by 2.1 eV towards the lower energies. It is still unclear, which nitrogen atoms contribute to which component. However, we can make the same assumption as for **10-NP**, that the central nitrogen atoms corresponds to the 1N component while the other 2 nitrogen atoms correspond to the 2N component.

Finally, the presence of copper in the nanoparticles cannot be excluded as it is detected in a small quantity. Yet, as with **10-NP**, its role in the NP formation is unclear.

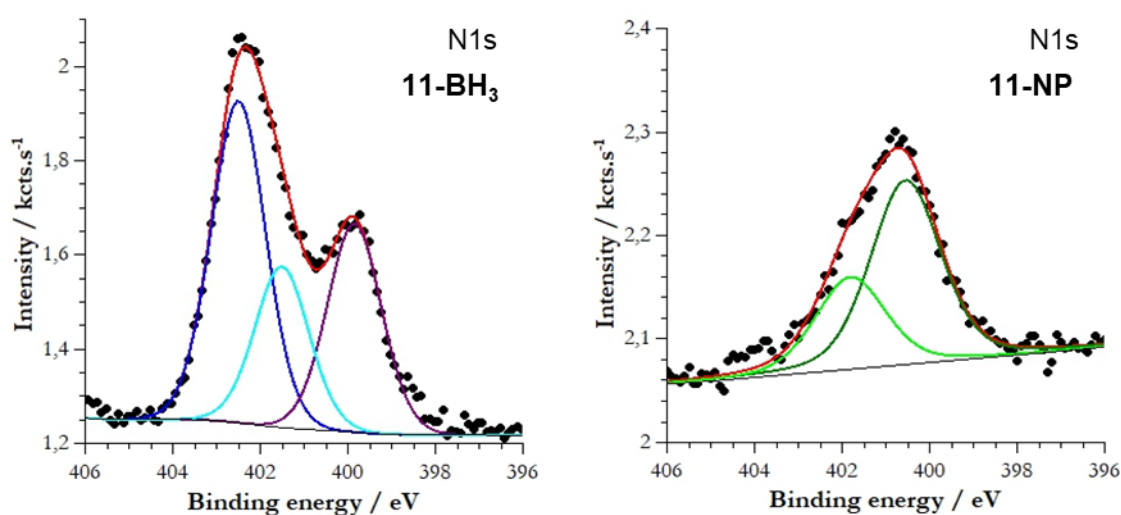


Figure IV.14: N1s XPS spectra of **11-BH₃** and corresponding nanoparticles (from HAuCl₄.3H₂O).

IV.D. Conclusion

To conclude, we have shown for the first time that gold nanoparticles can be synthesized both from triazolium salts and MIC-BH₃.

We have shown the possibility to use different triazolium salts and highlighted the influence of iodide in the reaction medium. While using NaBH₄ as both a reducing and deprotonating agent yields nanoparticles, the most monodisperse NPs are obtained when using NaH.

We have confirmed the stabilization of the NPs by mesoionic carbenes (even in the absence of NaH).

We have synthesized the first MIC-BH₃ with two long alkyl chains and successfully used it in the synthesis of gold nanoparticles starting from a gold(I) or gold(III) precursors. Some reproducibility issues were encountered with the gold(I) precursor AuClSM₂. In the synthesis, starting from the gold(III) precursor HAuCl₄.3H₂O, the amount of CHCl₃ was found to be crucial to obtain monodisperse

nanoparticles. The temperature was also found to have an effect as lowering the temperatures of the solutions yielded smaller nanoparticles. However, the relation between NPs size and Au:MIC ratio seems to be less straightforward than for NHCs. Finally, the stabilization by MICs of the nanoparticles from MIC-BH₃ was also confirmed by XPS.

While a copper-free synthesis could be desired to prevent any copper contamination (whose role is still unclear and may be minor), mesoionic carbenes are an attractive class of ligands. They possess a wide range of available structures, with tunable electronic properties, which are opening up new possibilities in the synthesis of carbene stabilized AuNPs.

Bibliography (Chapter IV)

- (1) Donnelly, K. F.; Petronilho, A.; Albrecht, M. Application of 1,2,3-Triazolylidenes as Versatile NHC-Type Ligands: Synthesis, Properties, and Application in Catalysis and Beyond. *Chem. Commun.* **2013**, 49 (12), 1145–1159.
- (2) Gründemann, S.; Kovacevic, A.; Albrecht, M.; Robert, J. W. F.; Crabtree, H. Abnormal Binding in a Carbene Complex Formed from an Imidazolium Salt and a Metal Hydride Complex. *Chem. Commun.* **2001**, 0 (21), 2274–2275.
- (3) Mathew, P.; Neels, A.; Albrecht, M. 1,2,3-Triazolylidenes as Versatile Abnormal Carbene Ligands for Late Transition Metals. *J. Am. Chem. Soc.* **2008**, 130 (41), 13534–13535.
- (4) Appukkuttan, P.; Dehaen, W.; Fokin, V. V.; Van der Eycken, E. A Microwave-Assisted Click Chemistry Synthesis of 1,4-Disubstituted 1,2,3-Triazoles via a Copper(I)-Catalyzed Three-Component Reaction. *Org. Lett.* **2004**, 6 (23), 4223–4225.
- (5) Feldman, A. K.; Colasson, B.; Fokin, V. V. One-Pot Synthesis of 1,4-Disubstituted 1,2,3-Triazoles from In Situ Generated Azides. *Org. Lett.* **2004**, 6 (22), 3897–3899.
- (6) Guisado-Barrios, G.; Bouffard, J.; Donnadieu, B.; Bertrand, G. Crystalline 1H-1,2,3-Triazol-5-Ylidenes: New Stable Mesoionic Carbenes (MICs). *Angew. Chem. Int. Ed.* **2010**, 49 (28), 4759–4762.
- (7) Keske, E. C.; Zenkina, O. V.; Wang, R.; Crudden, C. M. Synthesis and Structure of Palladium 1,2,3-Triazol-5-Ylidene Mesoionic Carbene PEPSI Complexes and Their Catalytic Applications in the Mizoroki–Heck Reaction. *Organometallics* **2012**, 31 (17), 6215–6221.
- (8) Mazloomi, Z.; Pretorius, R.; Pàmies, O.; Albrecht, M.; Diéguez, M. Triazolylidene Iridium Complexes for Highly Efficient and Versatile Transfer Hydrogenation of C=O, C=N, and C=C Bonds and for Acceptorless Alcohol Oxidation. *Inorg. Chem.* **2017**, 56 (18), 11282–11298.
- (9) Johnson, C.; Albrecht, M. Triazolylidene Iron(II) Piano–Stool Complexes: Synthesis and Catalytic Hydrosilylation of Carbonyl Compounds. *Organometallics* **2017**, 36 (15), 2902–2913.
- (10) Bolje, A.; Hohloch, S.; Urankar, D.; Pevec, A.; Gazvoda, M.; Sarkar, B.; Košmrlj, J. Exploring the Scope of Pyridyl- and Picolyl-Functionalized 1,2,3-Triazol-5-Ylidenes in Bidentate Coordination to Ruthenium(II) Cymene Chloride Complexes. *Organometallics* **2014**, 33 (10), 2588–2598.
- (11) Pretorius, R.; Fructos, M. R.; Müller-Bunz, H.; Gossage, R. A.; Pérez, P. J.; Albrecht, M. Synthesis and Catalytic Applications of 1,2,3-Triazolylidene Gold(I) Complexes in Silver-Free Oxazoline Syntheses and C–H Bond Activation. *Dalton Trans.* **2016**, 45 (37), 14591–14602.
- (12) Hettmanczyk, L.; Schulze, D.; Suntrup, L.; Sarkar, B. Mono- and Digold(I) Complexes with Mesoionic Carbenes: Structural Characterization and Use in Catalytic Silver-Free Oxazoline Formation. *Organometallics* **2016**, 35 (22), 3828–3836.
- (13) Barakat, A.; Al-Majid, A. M.; Al-Qahatany, F. M.; Islam, M. S.; Al-Agamy, M. H. M. Synthesis, Characterization and Antimicrobial Activity of Novel Pharmacophores Incorporating Imidazoline-Oxazoline Scaffold. *Bull. Korean Chem. Soc.* **2014**, 35 (2), 562–568.
- (14) Rawson, D. J.; Meyers, A. I. Highly Reactive Organolithiums (from “Freeman’s Reagent”) and Their Additions to Naphthalene Oxazolines. *Tetrahedron Lett.* **1991**, 32 (19), 2095–2098.
- (15) Lin, C.-A. J.; Yang, T.-Y.; Lee, C.-H.; Huang, S. H.; Sperling, R. A.; Zanella, M.; Li, J. K.; Shen, J.-L.; Wang, H.-H.; Yeh, H.-I.; Parak, W. J.; Chang, W. H. Synthesis, Characterization, and Bioconjugation of Fluorescent Gold Nanoclusters toward Biological Labeling Applications. *ACS Nano* **2009**, 3 (2), 395–401.
- (16) Wei, Y.-J.; Liu, C.-G.; Mo, L.-P. Ultraviolet absorption spectra of iodine, iodide ion and triiodide ion. *Guang Pu Xue Yu Guang Pu Fen Xi Guang Pu* **2005**, 25 (1), 86–88.
- (17) Das, A. K.; Raj, C. R. Iodide-Mediated Reduction of AuCl₄[–] and a New Green Route for the Synthesis of Single Crystalline Au Nanostructures with Pronounced Electrocatalytic Activity. *J. Phys. Chem. C* **2011**, 115 (43), 21041–21046.
- (18) Langille, M. R.; Personick, M. L.; Zhang, J.; Mirkin, C. A. Defining Rules for the Shape Evolution of Gold Nanoparticles. *J. Am. Chem. Soc.* **2012**, 134 (35), 14542–14554.
- (19) Millstone, J. E.; Wei, W.; Jones, M. R.; Yoo, H.; Mirkin, C. A. Iodide Ions Control Seed-Mediated Growth of Anisotropic Gold Nanoparticles. *Nano Lett.* **2008**, 8 (8), 2526–2529.

- (20) Furst, M. R. L.; Cazin, C. S. J. Copper N-Heterocyclic Carbene (NHC) Complexes as Carbene Transfer Reagents. *Chem. Commun.* **2010**, 46 (37), 6924–6925.
- (21) Andolina, C. M.; Dewar, A. C.; Smith, A. M.; Marbella, L. E.; Hartmann, M. J.; Millstone, J. E. Photoluminescent Gold–Copper Nanoparticle Alloys with Composition-Tunable Near-Infrared Emission. *J. Am. Chem. Soc.* **2013**, 135 (14), 5266–5269.
- (22) Crudden, C. M.; Eisenberger, P.; de Oliveira Freitas, L. B. Mesoionic Carbene–Boranes. *Organometallics* **2013**, 32 (22), 6635–6638.
- (23) Lindsay, D. M.; McArthur, D. The Synthesis of Chiral N-Heterocyclic Carbene–Borane and –Diorganoborane Complexes and Their Use in the Asymmetric Reduction of Ketones. *Chem. Commun.* **2010**, 46 (14), 2474–2476.
- (24) Taniguchi, T.; Curran, D. P. Silica Gel Promotes Reductions of Aldehydes and Ketones by N-Heterocyclic Carbene Boranes. *Org. Lett.* **2012**, 14 (17), 4540–4543.
- (25) Eisenberger Patrick; Bestvater Brian P.; Keske Eric C.; Crudden Cathleen M. Hydrogenations at Room Temperature and Atmospheric Pressure with Mesoionic Carbene-Stabilized Borenium Catalysts. *Angew. Chem. Int. Ed.* **2015**, 54 (8), 2467–2471.
- (26) Arrowsmith, M.; Böhnke, J.; Braunschweig, H.; Gao, H.; Légaré, M.-A.; Paprocki, V.; Seufert, J. Synthesis and Reduction of Sterically Encumbered Mesoionic Carbene-Stabilized Aryldihaloboranes. *Chem. – Eur. J.* **2017**, 23 (50), 12210–12217.

CONCLUSION AND PERSPECTIVES

Conclusion

During the last decade, N-heterocyclic carbenes (NHCs) have appeared as a promising and versatile family of capping ligands for the stabilization of metal nanoparticles and surfaces.¹ A wide library of available NHC structures offers the possibility of “on demand” functionalization. When it comes to gold, the stability they confer to nanoparticles has been shown to surpass the one of the widely used thiols, especially in harsh and/or biologically relevant conditions.

When this work started, three main pathways had been described in the literature to synthesize NHC-capped gold nanoparticles: ligand exchange on pre-formed nanoparticles², reduction of Au-NHC complexes³ or successive deprotonation (by NaH) and reduction (by NaBH₄) of imidazolium haloaurate complexes.⁴ Our main goal was to develop new syntheses of NHC-stabilized gold nanoparticles, with an emphasis on controlling their size.

The first part of this work revisited the route starting from (benz)imidazolium haloaurate. We showed that stable nanoparticles still formed even without adding a base before NaBH₄. Moreover, we were able to tune the size of the nanoparticles from 3 to 6 nm, through the use of additional (benz)imidazolium halide and depending on the presence of a base. Extensive XPS analysis of the obtained NPs confirmed their stabilization by NHCs covalently bound to the surface, suggesting that the reducing agent acts as a base as well. Switching the reducing agent from NaBH₄ to tBuNH₂BH₃, still without any NaH, yielded globally larger nanoparticles, whose size could be tuned from 5 to 12 nm by changing the amount of ligand used. XPS also confirmed the stabilization of those NPs by NHCs.

A new protocol was developed starting from commercially available AuCl and easily obtained imidazolium halide salts. Nanoparticles of *ca.* 3.5 nm were readily obtained by introducing NaBH₄ in a solution of 1,3-didodecylimidazolium bromide and AuCl. Unlike the previous synthesis, changing the amount of ligand did not modify the size of the nanoparticles. However, changing the ligand precursor to benzimidazolium halide, adding a base or changing the reducing agent to tBuNH₂BH₃, always led to the formation of larger NPs (from 4 to 7 nm). This work has recently been published (Bridonneau, Hippolyte *et al.*, Dalton Transactions, **2018**, 6850-6859).

This new protocol was also applied to imidazolium salts bearing a methyl or a phenyl group on their C2 position, *i.e.* unable to yield a “normal” NHCs. Yet, both imidazoliums yielded stable nanoparticles (*ca.* 3.5 nm). With a careful XPS analysis, we have been able to show that the methyl functionalized imidazolium binds to the nanoparticle through the terminal carbon of its methyl, while the phenyl

functionalized imidazolium yields an abnormal carbene, which binds to the nanoparticles surface through a carbon of the imidazole ring. To the best of our knowledge, it is the first time the binding of an abnormal carbene to a metallic surface is evidenced.

The second part of this work focused on the synthesis of NHC-stabilized gold nanoparticles with a brand-new approach based on NHC-borane Lewis adducts. Indeed, NHC-BH₃ are stable under ambient conditions and have already established reducing properties in organic chemistry. Our goal was thus to use them as “2-in-1” innovative reagents, able to serve as reducing agent and provide stabilizing ligands. Different experimental conditions were explored. It was found that the best option was to use AuClSMe₂, as gold precursor, toluene, as solvent, and 7 equivalents of NHC-BH₃. Interestingly, this synthesis occurred under ambient conditions and with no precautions, such as the exclusion of moisture. With this NHC-BH₃ based approach, the size of the nanoparticles could be tuned from 5 to 11 nm, just by changing the gold:NHC-BH₃ ratio. The stabilization of the nanoparticles by NHCs was confirmed by XPS. We found that while the stabilization of gold nanoparticles required several equivalents of NHC-BH₃, the reduction of gold only required 0.5 equivalent. The derivative NHC-BH₂Cl was also clearly evidenced as a reaction product. Attempts to unravel the reaction mechanism with theoretical chemistry were unsuccessful and no definitive pathway, either based on a transfer of hydride or involving radicals, could be determined. Finally, after several months without any problem we had to face reproducibility issues linked to faulty batches of NHC-BH₃. Several hypotheses were made to identify the problem. Unfortunately, at the time of writing, the problem has not been identified despite the investigation of several leads.

The last part of our work dealt with the synthesis of mesoionic carbene (MIC) stabilized gold nanoparticles. These ligands, based on triazolium rings, form a peculiar type of NHCs, also able to yield stable bonds with metals. These ligands, whose synthesis start by the very versatile copper catalyzed azide-alkyne click chemistry, are known to be stronger sigma donors than classical NHCs. In this part we followed two approaches: one with triazolium salts and one with MIC-BH₃. These latter reagents had only been described once before this work. We have shown that both triazolium salts and MIC-BH₃ can yield stable gold nanoparticles. However, several differences with imidazolium salts and NHC-BH₃ can be noted. For example, the most monodisperse nanoparticles from triazolium salts were obtained when NaH was introduced, whereas its presence had little effect on the size dispersion of nanoparticles obtained from imidazolium salts. Another difference is the fact that MIC-BH₃ reagent seems to yield the most reproducible results when HAuCl₄.3H₂O is used as gold precursor while, we encountered major reproducibility issues when using this precursor with NHC-BH₃.

The stabilization of gold nanoparticles by MICs was confirmed by XPS, for both those obtained from a triazolium salt and MIC-BH₃. To the best of our knowledge, this is the first time that mesoionic carbenes are used to stabilize metal nanoparticles.

Perspectives

This work has thus opened a lot of doors in the chemistry of carbene-stabilized gold nanoparticles. When considering future work, several axes could be explored: the understanding of the nanoparticles formation mechanism, the synthesis of new ligands in order to provide different properties to the nanoparticles, or the synthesis of nanoparticles based on other metals than gold.

Formation mechanism

At this stage the formation mechanism of nanoparticles obtained from either imidazolium salts and a reducing agent or NHC-BH₃ remains to be established. In the case of the former, a difference of mechanism between gold(III) and gold(I) precursors is likely. However, when the reducing agent is added, it is still unclear if an NHC-gold complex is formed before its reduction or if reduction occurs before the deprotonation of the imidazolium. If the generation of the NHC and the formation of an NHC gold complex are the first events, then the imidazolium-based route might not be so different from the synthesis that starts from NHC-AuX complexes.

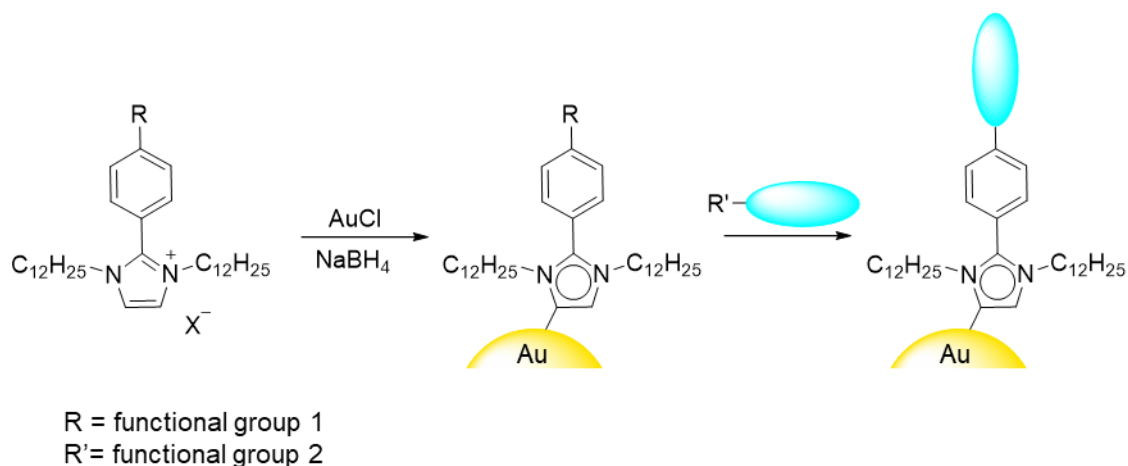
For NHC-BH₃ the question is not only on how are the NHCs released but also on the reduction mechanism and which event occurs first. However, the priority remains the comprehension of the problem leading to the reproducibility issues between batches. Indeed, if our theory is correct, and an impurity acts as a catalyst in the formation of nanoparticles, identifying this impurity could be the key to understanding the mechanism.

Ligand synthesis

Attempts were made to synthesize water-soluble and post-functionalizable imidazoliums in order to obtain water-soluble and post-functionalizable nanoparticles. However, during this PhD, those attempts were unsuccessful. In the case of water-soluble NHC-stabilized nanoparticles, several examples already exist in the literature and our next attempts should steer closer to those strategies that use charged NHCs.⁵⁻⁷

For post-functionalizable nanoparticles, several strategies could be envisioned. For example, the pathway described in Chapter II, using bromododecylazide, could be pursued and the reaction condition optimized to obtain the pure ligand. We could also decide on other functional groups or to place them on the heterocycle instead of on the N-substituents. For example, we could take advantage

of the coordination of **7** as an abnormal carbene and synthesize an analogous imidazolium with a functional group on the phenyl (Scheme C.1).



Scheme C.1: Example of strategy for the post-functionalization of gold nanoparticles.

Finally, we could also consider the synthesis of chiral NHCs. Indeed, they have been shown to organize on the surface of gold nanoparticles⁸ and could lead to the use of gold nanoparticles as chiral catalysts.

Other metals

There are many examples of NHC-stabilized metal nanoparticles. Indeed, examples have been described with Ru, Pt, Pd and Ir, among others. However, examples remain scarce for silver and, to the best of our knowledge, no example has been reported for copper. Moreover, as we have been the first to describe them, no other examples than gold exist from NHC-BH₃ or MICs.

As a result, preliminary studies were carried out on the synthesis of NHC-stabilized silver and copper nanoparticles. The results are described below.

Silver nanoparticles

From imidazolium or triazolium salts

A solution of azolium bromide (2 or 4 eq in DCM) was stirred with a solution AgNO₃ in water. This led to the precipitation of a white powder (AgBr). After 10min of stirring, NaBH₄ (in water) was injected leading to a brown coloration. After 24h, the solution was pale yellow and was showed to contain nanoparticles by TEM.

Using 2 equivalents of 1,3-dodecylimidazolium bromide (**2H-Br**) led to the formation of very large (40 – 60 nm) and polydisperse nanoparticles, whereas using 4 equivalents led to the formation of small nanoparticles of around 2 nm (Figure C.1).

Similarly using 2 equivalents of 1,4-didocely-3-ethyl-1,2,3-triazolium bromide (**12H-Br**) led to the formation of large and polydisperse NPs (23.2 ± 9.3 nm), whereas using 4 equivalents led to the formation of monodisperse nanoparticles of 3.6 ± 0.7 nm (Figure C.1).

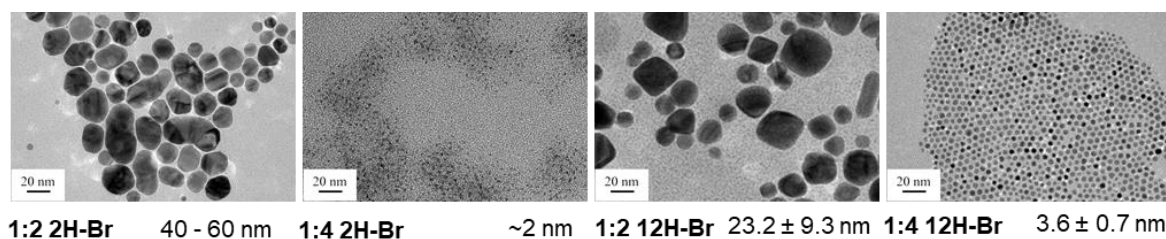


Figure C.1: TEM pictures of silver nanoparticles obtained from AgNO_3 and **2H-Br** or **12H-Br** at different ratios Ag:Azolium salt (solvent toluene: H_2O).

From NHC-BH₃ or MIC-BH₃

A solution of NHC-BH₃ or MIC-BH₃ (8mM) in toluene was stirred with a solution of AgNO_3 (1mM) in water. While, with gold, such biphasic systems led to the formation of a metallic gold film at the solvent interface, with silver, no immediate reduction was observed. Instead a slow coloration of the organic phase appeared over several hours. After 20h, a yellow organic phase was obtained and contained nanoparticles, as evidenced by TEM (Figure C.2).

The Ag:NHC-BH₃ ratio did not appear to change the size of the nanoparticles (Table C.1). However, increasing the amount of NHC-BH₃ accelerated the coloration of the solution (only 1h when using 1:20 Ag:NHC-BH₃). Increasing the concentration of the AgNO_3 solution (from 1mM to 10 mM) also increased the reaction rate and seemed to yield more monodisperse nanoparticles (Figure C.2).

It is important to stress that experiments with silver were carried out with NHC-BH₃ batches that worked or did not work with gold, without any noticeable difference.

Table C.1: Mean diameter of AgNPs obtained from AgNO_3 and NHC-BH₃ using different reagents ratios and concentrations.

Ag:NHC-BH ₃	1 : 5	1 : 8	1 : 10	1*:10	1:20
NPs diameter (nm)	7.3 ± 1.4	7.2 ± 1.4	8.9 ± 1.7	8.2 ± 0.9	8.1 ± 2.2

*= concentrated solution

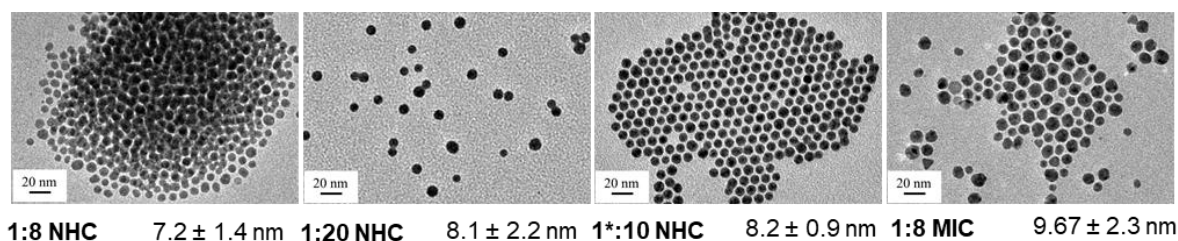


Figure C.2: Silver nanoparticles obtained from AgNO_3 and NHC- BH_3 or MIC- BH_3 at different ratios

(* = concentrated solution) (solvent toluene: H_2O).

Characterization of these nanoparticles by XPS remains to be done, but their isolation seems to be a real challenge that needs to be addressed first.

Copper nanoparticles

Copper nanoparticles were obtained by mixing a toluene solution of NHC- BH_3 (100mM) with a toluene solution of copper mesityl (100mM) ($\text{Cu}:\text{NHC}-\text{BH}_3$ 1:3) and heating for 2h30 at 110°C under inert atmosphere. The obtained NPs (11.6 ± 1.8 nm) (Figure C.3) are very sensitive to air and moisture and have to be handled and stored in a glovebox. Nevertheless, their characterization by XPS indicates a major component at 400.3 eV in the N1s spectrum, clearly in line with a covalently bound NHC at the copper NPs surface. The formation of NHC- BH_2Mes , reminding of the NHC- BH_2Cl observed with AuClSMe_2 , was also evidenced in this synthesis. This work was carried out in collaboration with Xavier Frogneux and Sophie Carencu from the Laboratoire de Chimie de la Matière Condensée de Paris (LCMCP) and a manuscript is about to be submitted.

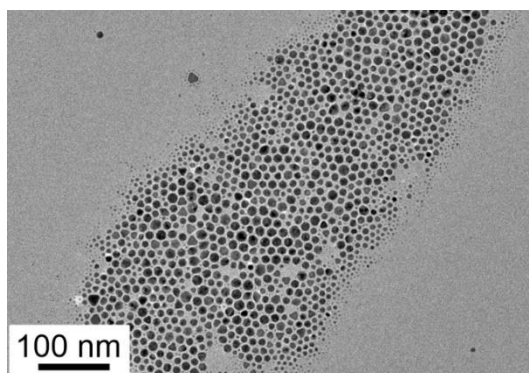


Figure C.3: Copper nanoparticles synthesized from copper mesityl and NHC- BH_3 in toluene.

These last results with silver and copper are really promising and clearly show that NHCs, including MICs, have a bright future in materials science. Of course, more work remains to be done on the first-ever reported syntheses using NHC- BH_3 or MIC- BH_3 , especially on their mechanisms, but these “2-in-1” innovative reagents offer great opportunities in the field of metal nanoparticles.

Bibliography (Conclusion)

- (1) Zhukhovitskiy, A. V.; MacLeod, M. J.; Johnson, J. A. Carbene Ligands in Surface Chemistry: From Stabilization of Discrete Elemental Allotropes to Modification of Nanoscale and Bulk Substrates. *Chem. Rev.* **2015**, *115* (20), 11503–11532.
- (2) Hurst, E. C.; Wilson, K.; Fairlamb, I. J. S.; Chechik, V. N-Heterocyclic Carbene Coated Metal Nanoparticles. *New J. Chem.* **2009**, *33* (9), 1837-1840.
- (3) Vignolle, J.; Tilley, T. D. N-Heterocyclic Carbene-Stabilized Gold Nanoparticles and Their Assembly into 3D Superlattices. *Chem. Commun.* **2009**, No. 46, 7230-7232.
- (4) Serpell, C. J.; Cookson, J.; Thompson, A. L.; Brown, C. M.; Beer, P. D. Haloaurate and Halopalladate Imidazolium Salts: Structures, Properties, and Use as Precursors for Catalytic Metal Nanoparticles. *Dalton Trans* **2013**, *42* (5), 1385–1393.
- (5) Baquero, E. A.; Tricard, S.; Flores, J. C.; de Jesús, E.; Chaudret, B. Highly Stable Water-Soluble Platinum Nanoparticles Stabilized by Hydrophilic N-Heterocyclic Carbenes. *Angew. Chem. Int. Ed.* **2014**, *53* (48), 13220–13224.
- (6) Salorinne, K.; Man, R. W. Y.; Li, C.-H.; Taki, M.; Nambo, M.; Crudden, C. M. Water-Soluble N-Heterocyclic Carbene-Protected Gold Nanoparticles: Size-Controlled Synthesis, Stability, and Optical Properties. *Angew. Chem.* **2017**, *129* (22), 6294–6298.
- (7) Ferry, A.; Schaepe, K.; Tegeder, P.; Richter, C.; Chepiga, K. M.; Ravoo, B. J.; Glorius, F. Negatively Charged N-Heterocyclic Carbene-Stabilized Pd and Au Nanoparticles and Efficient Catalysis in Water. *ACS Catal.* **2015**, *5* (9), 5414–5420.
- (8) Young, A. J.; Serpell, C. J.; Chin, J. M.; Reithofer, M. R. Optically Active Histidin-2-Ylidene Stabilised Gold Nanoparticles. *Chem. Commun.* **2017**, *53* (92), 12426–12429.

Experimental Section

Table of contents

General Remarks	153
Molecular synthesis.....	154
Chapter II.....	154
Chapter III.....	161
Chapter IV	164
Gold nanoparticles synthesis.....	167
Chapter II.....	167
Chapter III.....	169
Chapter IV	170
References.....	171

General Remarks

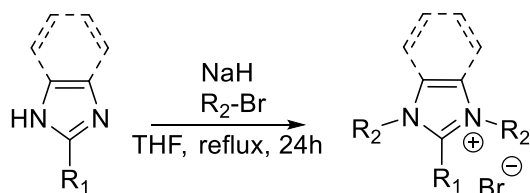
THF was distilled over sodium/benzophenone. Unless otherwise specified all other chemicals and reagents were purchased from commercial sources and used as received. ¹H NMR, ¹³C NMR and ¹¹B NMR spectra were recorded at room temperature on a Bruker Avance 300 MHz or Bruker Avance 400 MHz spectrometer. Shifts (δ) are given in parts per million (ppm) using the resonance of the solvent as a secondary reference.¹ Multiplicities are reported using the following abbreviations: s (singlet), d (doublet), t (triplet), q (quartet), p (quintuplet), m (multiplet), br (broad), Ar (aromatic) or a suitable combination. High resolution mass spectra were obtained using a mass spectrometer MicroTOF from Bruker with an electron spray ion source (ESI) and a TOF detector. UV spectra were recorded using Agilent 8453 UV-visible Spectrophotometer. TEM samples were prepared by dropping colloidal suspensions onto a copper grid coated with carbon film, and the solvent was allowed to evaporate in air. TEM images were obtained from a Tecnai Spirit G2 microscope operating at 120 kV associated with the Gatan software. Data size distribution histograms were obtained by measuring at least 500 particles per sample using ImageJ program. XPS spectra were recorded with a Thermo ESCALAB 250 X-Ray photoelectron spectrometer with a monochromatic Al-Ka X-Ray source ($h\nu=1486.6$ eV) operating at 10^{-10} Torr. The analyzer pass energy was 50 eV for survey spectra and 20 eV for high-resolution spectra. All spectra were calibrated versus binding energy (BE) of hydrocarbons (C1s at 285.0 eV). Spectra were recorded and analyzed using Thermo Advantage software. For curve fitting and decomposition, a Shirley-type background subtraction have been used and the shape of fitting curves was obtained by a 70% Gaussian / 30% Lorentzian distribution.

Molecular synthesis

Chapter II

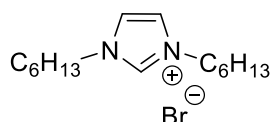
General procedure 1

Based on a slightly modified literature procedure²



In oven dried glassware, (benz)imidazole (1 eq) was dissolved in distilled THF and added dropwise to a solution of sodium hydride (1.1 eq) in distilled THF at 0°C under inert atmosphere. The ice bath was removed and the mixture was stirred for 1h at room temperature. After dropwise addition of the desired alkyl bromide (2 eq), the mixture was stirred at room temperature for at least 1h before being refluxed at 70°C (in air) for at least 24h until completion of the reaction (followed by ¹H NMR). Upon completion, the solvent was evaporated under reduced pressure. The residue was dissolved in dichloromethane and filtered. The filtrate was evaporated under reduced pressure, the residue was recrystallized from a dichloromethane and diethyl ether mixture at 4°C. After filtration, the precipitate was dried in vacuo to give the product as a white powder.

1,3-dihexylimidazolium bromide (**1H-Br**)

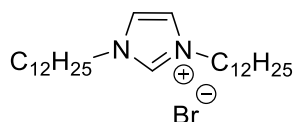


General procedure 1 was applied to imidazole (2g, 29.4 mmol) and 1-bromohexane (16.5 mL, 58.8 mmol) to afford the title compound as a clear oil (7.3 g, 78% yield).

¹H NMR (400 MHz, CDCl₃) δ 10.55 (1H, t, NCHN), 7.29 (2H, d, NCHCHN), 4.35 (4H, t, NCH₂C₅H₁₁), 1.92 (4H, p, NCH₂CH₂C₄H₉), 1.35-1.28 (12H, m, N(CH₂)₂C₃H₆CH₃), 0.86 (6H, t, N(CH₂)₅CH₃);

¹³C NMR (75 MHz, CDCl₃) δ 137.10 (NHCN), 122.13 (NHCCHN), 50.09 (NCH₂), 31.09, 30.29, 25.88, 22.38, 13.90 (CH₃).

1,3-didodecylimidazolium bromide (**2H-Br**)



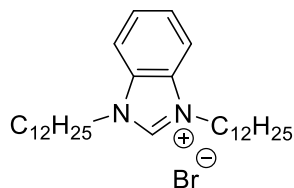
General procedure 1 was applied to imidazole (2.5 g, 36.7 mmol) and 1-bromododecane (17.7 mL, 73.5 mmol) to afford the title compound as a white powder (13.7g, 77% yield).

$^1\text{H NMR}$ (400 MHz, CDCl_3) δ 10.88 (1H, t, NCHN), 7.20 (2H, d, NCHCHN), 4.36 (4H, t, $\text{NCH}_2\text{C}_{11}\text{H}_{23}$), 1.92 (4H, p, $\text{NCH}_2\text{CH}_2\text{C}_{10}\text{H}_{21}$), 1.35-1.25 (36H, m, $\text{N}(\text{CH}_2)_2\text{C}_9\text{H}_{18}\text{CH}_3$), 0.88 (6H, t, $\text{N}(\text{CH}_2)_{11}\text{CH}_3$);

$^{13}\text{C NMR}$ (101 MHz, CDCl_3) δ 137.70 (NHCN), 121.78 (NHCCHN), 50.29 (NCH_2), 32.00, 30.44, 29.70, 29.60, 29.49, 29.43, 29.11, 26.37, 22.78, 14.22 (CH_3);

HRMS (ESI) calculated for $\text{C}_{27}\text{H}_{53}\text{N}_2^+$, m/z : 405.4203, found: 405.4197.

1,3-didodecylbenzimidazolium bromide (**3H-Br**)



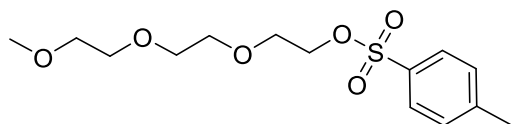
General procedure 1 was applied to benzimidazole (4 g, 33.9 mmol) and 1-bromododecane (16.3 mL, 67.7 mmol) to afford the title compound as a white powder (10.6 g, 60% yield).

$^1\text{H NMR}$ (400 MHz, CDCl_3) δ 11.57 (1H, s, NCHN), 7.67 (4H, m, C_6H_4), 4.62 (4H, t, $\text{NCH}_2\text{C}_{11}\text{H}_{23}$), 2.06 (4H, p, $\text{NCH}_2\text{CH}_2\text{C}_{10}\text{H}_{21}$), 1.44-1.24 (36H, m, $\text{N}(\text{CH}_2)_2\text{C}_9\text{H}_{18}\text{CH}_3$), 0.87 (6H, t, $\text{N}(\text{CH}_2)_{11}\text{CH}_3$);

$^{13}\text{C NMR}$ (75 MHz, CDCl_3) δ 142.93 (NHCN), 131.44, 127.18, 113.19, 47.79 (NCH_2), 31.98, 29.67, 29.58, 29.47, 29.40, 29.14, 26.65, 22.76, 14.20 (CH_3).

Mono methylated triethylene glycol tosylate

Based on a literature procedure³



Monomethylated triethylene glycol (4.9 mL, 30.5 mmol), NEt_3 (10.6 mL, 76 mmol) and DMAP (870 mg, 7.1 mmol) were dissolved in DCM (200 mL). p-Toluenesulfonyl chloride (6.6 g, 34.5 mmol) was added at 0°C. The reaction mixture was stirred at room temperature for 3h. The reaction mixture was washed with water (twice). The organic phase was dried over MgSO_4 and the solvent was evaporated under reduced pressure. Silica gel chromatography (eluent DCM to DCM/AcOEt 7/3) afforded the product

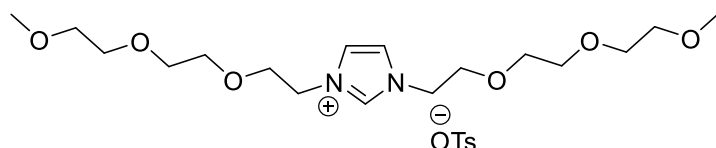
as a clear oil (6.8 g, 70%yield).

$^1\text{H NMR}$ (300 MHz, CDCl_3) δ 7.79 (d, 2H), 7.33 (d, 2H), 4.15 (m, 2H), 3.68 (m, 2H), 3.52 (m, 8H), 3.36 (s, 3H), 2.44 (s, 3H).

$^{13}\text{C NMR}$ (75 MHz, CDCl_3) δ 144.90, 133.15, 129.93, 128.10, 72.03, 70.87, 70.67, 69.35, 68.80, 59.15, 21.76.

1,3-ditriethyleneglycolimidazolium tosylate (**4H-OTs**)

Based on a modified literature procedure⁴



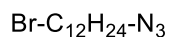
Imidazole (136 mg, 2 mmol), TEGOTS (1.33 g, 4.2 mmol) and K_2CO_3 (415 mg, 3 mmol) were charged in a sealed pressure tube with MeCN (7mL). The reaction was heated at 90°C for 24h. The solvent was evaporated under reduce pressure, the residue was dissolved in DCM and filtered. The filtrate was evaporated under reduced pressure, triturated in Et_2O and decanted. The supernatant was removed to afford the product as an oil (0.9 g, 84 %)

$^1\text{H NMR}$ (400 MHz, CDCl_3) δ 9.27 (t, 1H), 7.65 (d, 2H), 7.45 (d, 2H), 7.05 (m, 2H), 4.32 (m, 4H), 3.69 (m, 4H), 3.46 (m, 17H), 3.26 (s, 6H), 2.24 (s, 3H).

$^{13}\text{C NMR}$ (101 MHz, CDCl_3) δ 143.40, 139.25, 137.02, 128.53, 125.78, 122.75, 71.69, 70.13, 70.09, 70.01, 68.87, 58.76, 49.37, 21.14.

1,12-bromododecylazide

Based on a modified literature procedure⁵

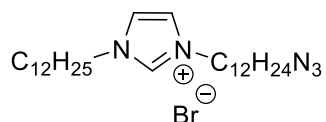


1,12-dibromododecane (5g, 15.2 mmol) was dissolved in DMSO (20 mL). NaN_3 (990 mg, 15,2 mmol) was added portion wise and the reaction mixture was stirred at room temperature for 24h. H_2O (80 mL) was added and the solution was extracted with Et_2O (3 times). The organic phase was dried over MgSO_4 and the solvent was removed under reduced pressure to afford the title compound as a clear oil (3.4 g, 77% yield).

$^1\text{H NMR}$ (400 MHz, CDCl_3) δ 3.40 (t, 2H), 3.25 (t, 2H), 1.85 (dt, 2H), 1.58 (m, 2H), 1.28 (m, 16H).

$^{13}\text{C NMR}$ (101 MHz, CDCl_3) δ 51.61, 34.11, 32.96, 29.58, 29.56, 29.52, 29.25, 28.96, 28.87, 28.29, 26.83.

1-dodecylazide-3-dodecylimidazolium bromide (**5H-Br**)



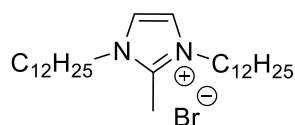
Imidazole (95 mg, 1.4 mmol) was dissolved in THF (4mL) and added dropwise to a solution of sodium hydride (60mg, 1.5 mmol) in THF at 0°C. The ice bath was removed and the mixture was stirred for 1h at room temperature. BrC12H25N3 (400 mg, 1.4 mmol) was added dropwise. The solution was stirred for 1h before addition of 1-bromododecane (0.3 mL, 1.4 mmol). The solution was then heated for 24h until completion of the reaction (followed by ¹H NMR). Upon completion, the solvent was evaporated under reduced pressure. The residue was dissolved in dichloromethane and filtered. The filtrate was evaporated under reduced pressure, the residue was triturated in Et₂O and the supernatant was removed to afford the product as a clear oil.

¹H NMR* (400 MHz, CDCl₃) δ 10.33 (t, 1H), 7.47 (d, 2H), 4.29 (t, 4H), 1.85 (p, 4H), 1.21 (m, 38H), 0.80 (t, 3H).

¹³C NMR* (101 MHz, CDCl₃) δ 136.96, 122.11, 50.04, 31.86, 30.32, 29.56, 29.48, 29.38, 29.29, 29.00, 26.23, 22.64, 14.08.

*only the signals corresponding to the compound are listed, but the spectrum also presented signals of impurities.

1,3-didodecyl-2-methylimidazolium bromide (**6H-Br**)

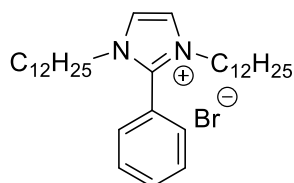


General procedure 1 was applied to 2-methylimidazole (1g, 12.2 mmol) and 1-bromododecane (5.9 mL, 24.4 mmol) to afford the title compound as a white powder (5g, 82% yield).

¹H NMR (300 MHz, CDCl₃) δ 7.52 (s, 2H), 4.24 (t, 4H), 2.80 (s, 3H), 1.82 (p, 4H), 1.24 (m, 36H), 0.87 (m, 6H).

¹³C NMR (75 MHz, CDCl₃) δ 142.82, 121.67, 49.27, 32.02, 29.96, 29.71, 29.63, 29.52, 29.45, 29.20, 26.54, 22.80, 14.24, 11.20.

1,3-didodecyl-2-phenylimidazolium bromide (**7H-Br**)

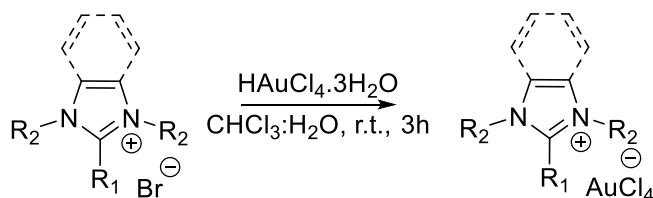


General procedure 1 was applied to 2-phenylimidazole (1.4 g, 10 mmol) and 1-bromododecane (4.8 mL, 20 mmol) to afford the title compound as an off-white powder (3.75 g, 67% yield). (AcOEt used for precipitation instead of Et₂O)

¹H NMR (400 MHz, CDCl₃) δ 8.00 (s, 2H), 7.59 (m, 5H), 4.05 (t, 4H), 1.70 (p, 4H), 1.15 (m, 36H), 0.81 (t, 6H).

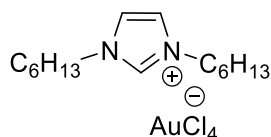
¹³C NMR (101 MHz, CDCl₃) δ 143.80, 132.82, 130.38, 130.04, 122.83, 121.25, 49.07, 31.86, 30.13, 29.55, 29.53, 29.43, 29.28, 29.25, 28.77, 26.14, 22.64, 14.08.

General procedure 2:



(Benz)imidazolium bromide (1 eq) was dissolved in chloroform (20 mL) and mixed with H[AuCl₄·3H₂O] (1 eq) in water (5 mL). After 3h of stirring at room temperature the organic phase was washed with water, dried with MgSO₄, the solvent was evaporated under reduced pressure. The product was dried in vacuo to afford the product as a yellow powder.

1,3-dihexylimidazolium tetrachloroaurate (**1H-AuX₄**)

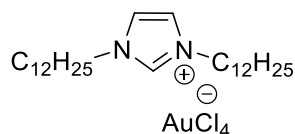


General procedure 2 was applied to **1H-Br** (40 mg, 0.1 mmol) to afford the title compound as an orange oil (62 mg, 86% yield).

¹H NMR (400 MHz, CDCl₃) δ 8.98 (1H, t, NCHN), 7.28 (2H, d, NCHCHN), 4.29 (4H, t, NCH₂C₅H₁₁), 1.94 (4H, p, NCH₂CH₂C₄H₉), 1.35-1.29 (12H, m, N(CH₂)₂C₃H₆CH₃), 0.90 (6H, t, N(CH₂)₅CH₃);

¹³C NMR (75 MHz, CDCl₃) δ 134.94 (NHCN), 122.77 (NHCCHN), 50.80 (NCH₂), 31.22, 31.13, 30.22, 30.09, 26.06, 22.49, 14.06 (CH₃).

1,3-didodecylimidazolium tetrachloroaurate (**2H-AuX₄**)

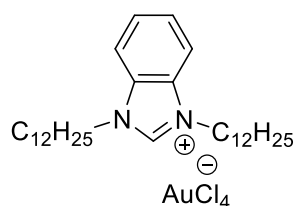


General procedure 2 was applied to **2H-Br** (160 mg, 0.33 mmol) to afford the title compound as an orange powder (240 mg, 99% yield).

¹H NMR (400 MHz, CD₂Cl₂) δ 8.71 (1H, t, NCHN), 7.35 (2H, d, NCHCHN), 4.25 (4H, t, NCH₂C₁₁H₂₃), 1.94 (4H, p, NCH₂CH₂C₁₀H₂₁), 1.37-1.29 (36H, m, N(CH₂)₂C₉H₁₈CH₃), 0.90 (6H, t, N(CH₂)₁₁CH₃);

¹³C NMR (75 MHz, CDCl₃) δ 135.19 (NHCN), 122.59 (NHCCHN), 50.94 (NCH₂), 32.05, 30.29, 29.75, 29.65, 29.52, 29.49, 29.10, 26.48, 22.83, 14.27 (CH₃).

1,3-didodecylbenzimidazolium tetrachloroaurate (**3H-AuX₄**)

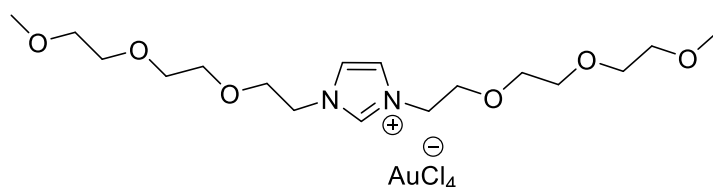


General procedure 2 was applied to **3H-Br** (426 mg, 0.8 mmol) to afford the title compound as an orange powder (557 mg, 88% yield).

¹H NMR (400 MHz, CDCl₃) δ 9.55 (1H, s, NCHN), 7.77 (4H, m, C₆H₄), 4.57 (4H, t, NCH₂C₁₁H₂₃), 2.09 (4H, p, NCH₂CH₂C₁₀H₂₁), 1.47-1.38 (36H, m, N(CH₂)₂C₉H₁₈CH₃), 0.90 (6H, t, N(CH₂)₁₁CH₃);

¹³C NMR (75 MHz, CDCl₃) δ 140.33 (NHCN), 131.56, 127.85, 113.52, 48.34 (NCH₂), 32.04, 29.74, 29.65, 29.59, 29.54, 29.47, 29.16, 26.81, 22.82, 14.26 (CH₃).

1,3-ditriethyleneglycolimidazolium tetrachloroaurate (**4H-AuX₄**)

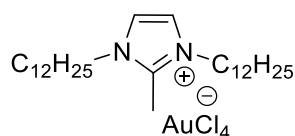


General procedure 2 was applied to **4H-OTs** (107 mg, 0.2 mmol) to afford the title compound as an orange oil (120 mg, 86% yield).

¹H NMR (400 MHz, CDCl₃) δ 9.77 (t, 1H), 7.54 (s, 2H), 4.51 (t, 4H), 3.91 (t, 6H), 3.63 (m, 16H), 3.37 (s, 6H).

¹³C NMR (101 MHz, CDCl₃) δ 137.28, 123.11, 72.01, 70.50, 69.01, 59.12, 50.03.

1,3-didodecyl-2-methylimidazolium tetrachloroaurate (**6H-AuX₄**)



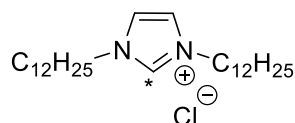
General procedure 2 was applied to **6H-Br** (127 mg, 0.25 mmol) to afford the title compound as an orange oil (190 mg, 99% yield).

¹H NMR (400 MHz, CDCl₃) δ 7.26 (s, 2H), 4.15 (t, 4H), 2.72 (s, 3H), 1.87 (p, 4H), 1.27 (m, 36H), 0.87 (t, 6H).

¹³C NMR (101 MHz, CDCl₃) δ 143.01, 121.65, 49.54, 32.05, 29.74, 29.63, 29.52, 29.47, 29.15, 26.63, 22.83, 14.27, 10.81.

20% ¹³C marked 1,3-dodecylimidazolium chloride

Based on a modified literature procedure⁶



100 mg (3.4 mmol) of ¹³C enriched (100%) were mixed with 400 mg (13.6 mmol) of non-enriched paraformaldehyde, dispersed in toluene and cooled to 0°C. A solution of dodecylamine (7.6 mL, 33 mmol) in toluene (4mL) was added over 20 min. After stirring for 5 min, 4mL of HCl in dioxane (4N) were added dropwise. The reaction was then heated to 34°C before dropwise addition of glyoxal (40% in water, 4.8 mL, 33 mmol). The solution was heated at 34°C overnight. The solvent was removed by distillation. The residue (tar-like substance) was triturated with Et₂O, decanted and the supernatant was removed. The process was repeated several times (15) before drying the obtained light brown paste under vacuum. The solid was dissolved in a heated Et₂O: DCM mixture before addition of a large excess of Et₂O and cooling down to 0°C for 30 minutes. After filtration, the product was obtained as a white powder (2.5 g, 33% yield)

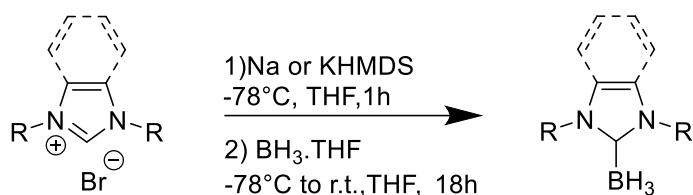
¹H NMR (400 MHz, CDCl₃) δ 10.98 (t, 1H), 7.20 (d, 2H), 4.35 (t, 4H), 1.90 (p, 4H), 1.29 (m, 36H), 0.87 (t, 6H).

¹³C NMR (101 MHz, CDCl₃) δ 138.79, 121.30, 50.34, 32.05, 29.73, 29.63, 29.52, 29.47, 29.15, 26.42, 22.83, 14.26.

Chapter III

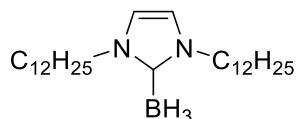
General procedure 3

Based on a modified literature procedure.⁷



In oven dried glassware and under inert atmosphere, (benz)imidazolium bromide (1 eq) was dissolved in distilled THF. NaHMDS or KHMDS (1M in THF, 1 eq) was added dropwise at -78°C. After 1h of stirring at -78°C, BH₃.THF (1M in THF, 1 eq) was added dropwise. The solution was kept in the cold bath for 30 minutes before being stirred at room temperature overnight. The solvent was evaporated under reduced pressure. The crude product was purified by silica chromatography to afford the title compound.

1,3-didodecylimidazol-2-ylidene borane (**2-BH₃**)



General procedure 3 was applied to **2H-Br** (2 g, 4.1mmol). Silica gel chromatography (eluent pentane/DCM 55/45) afforded the product as a white powder (750 mg, 44%yield).

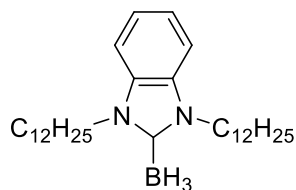
¹H NMR (400 MHz, CDCl₃): δ 6.80 (2H, s), 4.09 (4H, t), 1.77 (4H, p), 1.31-1.25 (36H, m), 0.88 (6H, t)

¹³C NMR (101 MHz, CDCl₃): δ 170.16, 118.80, 48.84, 32.04, 30.26, 29.75, 29.68, 29.62, 29.47, 29.32, 26.65, 22.81, 14.24

¹¹B NMR (96 MHz, CDCl₃): δ -37.3 (q)

HRMS (ESI) calculated for C₂₇H₅₂N₂BH₃Na⁺: *m/z*: 441.4356, found: 441.4347

1,3-didodecylbenzimidazol-2-ylidene borane (**3-BH₃**)



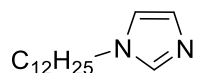
General procedure 3 was applied to **3H-Br** (428 mg, 0.8 mmol). Silica gel chromatography (eluent from pentane to pentane/Et₂O 100/2) afforded the product as a white powder (130 mg, 35% yield).

¹H NMR (300 MHz, CDCl₃) δ 7.38 (m, 4H), 4.40 (t, 4H), 1.84 (p, 4H), 1.25 (m, 36H), 0.88 (t, 6H).

^{13}C NMR (75 MHz, CDCl_3) δ 132.81, 123.60, 110.96, 45.90, 32.06, 29.76, 29.70, 29.64, 29.48, 29.42, 29.21, 26.99, 22.83, 14.25.

^{11}B NMR (96 MHz, CDCl_3) δ -36.9 (q).

1-dodecylimidazole (**9**)

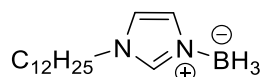


Imidazole (1g, 14.7 mmol) was dissolved in DMSO (6mL). KOH (1.65 g, 29.4 mmol) was added and the reaction mixture was stirred for 90 min. 1-bromododecane (2.9 mL, 12.2 mmol) was added dropwise under vigorous stirring and the reaction was stirred overnight. H_2O (60 mL) was added and the mixture was extracted 3 times with Et_2O . The organic phase was washed with water, then dried over MgSO_4 and the solvent was removed under reduced pressure to afford the title product as a clear oil (2g, 69%).

^1H NMR (400 MHz, CDCl_3) δ 7.42 (s, 1H), 7.02 (s, 1H), 6.87 (s, 1H), 3.88 (t, 2H), 1.73 (p, 2H), 1.25 (m, 18H), 0.84 (t, 3H).

^{13}C NMR (101 MHz, CDCl_3) δ 137.16, 129.36, 118.84, 47.11, 31.95, 31.13, 29.65, 29.57, 29.48, 29.38, 29.12, 26.61, 22.73, 14.15.

1-dodecylimidazole borane (**9-BH₃**)



In oven dried glassware and under inert atmosphere, **9** (500 mg, 2.1 mmol) was dissolved in distilled THF (6mL). $\text{BH}_3\cdot\text{THF}$ (1M in THF, 2.1 mL, 2.1 mmol) was added at -78°C and the reaction mixture was stirred overnight at room temperature. The solvent was evaporated under reduced pressure. Silica gel chromatography (eluent pentane: DCM 1:1 to DCM) afforded the product as a clear oil (140 mg, 27% yield).

^1H NMR (400 MHz, CDCl_3) δ 7.73 (s, 1H), 7.07 (s, 1H), 6.87 (t, 1H), 3.93 (m, 2H), 1.77 (m, 2H), 1.25 (m, 37H), 0.87 (t, 6H).

^{13}C NMR (101 MHz, CDCl_3) δ 136.19, 127.97, 119.73, 48.72, 32.01, 31.20, 30.62, 29.71, 29.69, 29.64, 29.59, 29.55, 29.44, 29.19, 29.06, 26.68, 26.47, 22.80, 14.23.

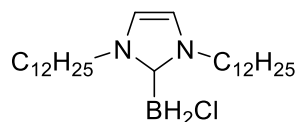
^{11}B NMR (128 MHz, CDCl_3) δ -18.8 (q)

General procedure 4

Based on a literature procedure⁸

A carbene-borane (1 eq) was dissolved in DCM (0.1 mmol/mL) before addition of dry HCl (1N in Et₂O, 1 eq). The solution was stirred for 1h at room temperature. The solvent was evaporated and the product characterized by NMR.

1,3-didodecylimidazol-2-ylidene chloroborane (**2-BH₂Cl**)



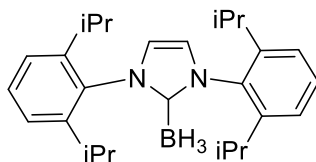
General procedure 4 was applied to **2-BH₃** (200mg, 0.5 mmol). NMR indicated an 85% conversion.

¹H NMR* (400 MHz, Tol-d8) δ 6.02 (s, 2H), 3.90 (t, 4H), 1.59 (p, 4H), 1.34 (m, 36H), 0.95 (t, 6H).

¹¹B NMR* (128 MHz, Tol-d8) δ -18.4 (bs).

*without peaks from unreacted **2-BH₃**

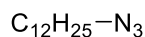
1,3-dimesitylimidazol-2-ylidene borane (**8-BH₃**)



Synthesized as described in the literature⁹

Chapter IV

1-dodecylazide



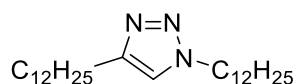
1-bromododecane (7.9 mL, 33 mmol) was dissolved in DMSO (50 mL). NaN_3 (2.47 g, 38 mmol) was added portion-wise and the reaction mixture was stirred overnight. H_2O (200mL) was added and the solution was extracted with Et_2O (3 times). The organic phase was dried over MgSO_4 and the solvent was removed under reduced pressure to afford the title compound as a clear oil (5.7 g, 78% yield)

$^1\text{H NMR}$ (400 MHz, CDCl_3) δ 3.25 (m, 2H), 1.59 (p, 2H), 1.27 (m, 18H), 0.87 (m, 3H).

$^{13}\text{C NMR}$ (101 MHz, CDCl_3) δ 51.66, 32.07, 29.78, 29.70, 29.64, 29.49, 29.31, 29.00, 26.88, 22.84, 14.27.

1,4-didodecyl-1,2,3-triazole (**10**)

Based on a modified literature procedure¹⁰



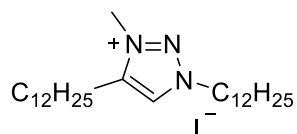
1-dodecylazide (2.5g, 11.4 mmol) and tetradecyne (3.1 mL, 12.5 mmol) were dissolved in DCM (20 mL). H_2O (15mL) and $\text{CuSO}_4 \cdot 5\text{H}_2\text{O}$ (424 mg, 1.7 mmol) were added successively. Sodium ascorbate (1.13 g, 5.7 mmol) was added portion-wise. The reaction mixture was stirred overnight, then extracted with DCM (3 times). The organic phase was washed with brine, dried over MgSO_4 and the solvent was evaporated under reduced pressure. Silica gel chromatography (eluent DCM to DCM:MeOH 100:5) afforded the title compound as an off-white powder (3.8g, 82% yield).

$^1\text{H NMR}$ (400 MHz, CD_2Cl_2) δ 7.30 (s, 1H), 4.28 (t, 2H), 2.66 (t, 2H), 1.86 (p, 2H), 1.64 (p, 2H), 1.27 (m, 36H), 0.88 (t, 6H).

$^{13}\text{C NMR}$ (101 MHz, CD_2Cl_2) δ 135.82, 128.52, 32.00, 29.76, 29.73, 29.69, 29.68, 29.60, 29.49, 29.44, 29.42, 29.33, 29.09, 26.59, 22.77, 13.96.

1,4-didocely-3-methyl-1,2,3-triazolium iodide (**11H-I**)

Based on a modified literature procedure¹¹



1,4-didodecyl-1,2,3-triazole (1g, 2.5 mmol) was charged in a sealed tube with iodomethane (0.5 mL, 7.4 mmol) and MeCN (5mL) under argon. The reaction was heated at 80°C overnight. After evaporation

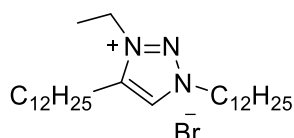
of the solvent under reduced pressure, the mixture was triturated with cold ethyl acetate and filtered. The product was obtained as an off-white powder (1.25g, 93% yield).

$^1\text{H NMR}$ (400 MHz, CDCl_3) δ 9.16 (s, 1H), 4.71 (t, 2H), 4.26 (s, 3H), 2.92 (m, 2H), 2.04 (p, 2H), 1.79 (m, 2H), 1.26 (m, 36H), 0.87 (t, 6H).

$^{13}\text{C NMR}$ (101 MHz, CDCl_3) δ 144.78, 129.61, 54.55, 38.35, 32.04, 29.76, 29.73, 29.70, 29.63, 29.59, 29.46, 29.29, 29.24, 29.01, 27.42, 26.32, 24.17, 22.82, 14.25.

HRMS (ESI) calculated for $\text{C}_{27}\text{H}_{54}\text{N}_3^+$: m/z : 420.4312, found: 420.4296

1,4-didodecyl-3-ethyl-1,2,3-triazolium bromide (**12H-Br**)

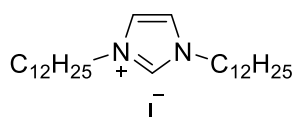


1,4-didodecyl-1,2,3-triazole (300 mg, 0.74 mmol) was charged in a sealed tube with bromoethane (1.7mL, 22.2 mmol) and MeCN (5mL) under argon. The reaction was heated at 80°C for 3 days. After evaporation of the solvent under reduced pressure, the mixture was triturated with cold ethyl acetate and filtered. The product was obtained as an off-white powder (300mg, 79% yield).

$^1\text{H NMR}$ (400 MHz, CDCl_3) δ 9.46 (s, 1H), 4.72 (t, 2H), 4.55 (q, 2H), 2.84 (t, 2H), 1.94 (p, 2H), 1.71 (p, 2H), 1.57 (t, 3H), 1.16 (m, 36H), 0.78 (t, 6H).

$^{13}\text{C NMR}$ (101 MHz, CDCl_3) δ 143.68, 129.73, 54.14, 46.86, 31.80, 29.53, 29.50, 29.41, 29.38, 29.24, 29.09, 29.04, 28.81, 27.56, 26.10, 23.55, 22.58, 14.28, 14.01.

1,3-dodecylimidazolium iodide (**2H-I**)



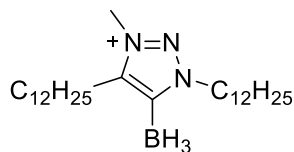
2H-Br (485 mg, 1 mmol) and NaI (300 mg, 2 mmol) were dissolved in acetone (10mL). The reaction mixture was stirred overnight at room temperature. The solvent was evaporated under reduced pressure. The residue was dissolved in DCM, solids were filtered off. The solvent was evaporated under reduced pressure to afford the title compound as an off-white powder (500 mg, 94% yield).

$^1\text{H NMR}$ (400 MHz, CDCl_3) δ 10.04 (t, 1H), 7.50 (d, 2H), 4.27 (d, 4H), 1.86 (p, 4H), 1.16 (m, 36H), 0.78 (t, 6H).

$^{13}\text{C NMR}$ (101 MHz, CDCl_3) δ 136.06, 122.36, 50.08, 31.78, 30.24, 29.49, 29.41, 29.30, 29.21, 28.90, 26.13, 22.56, 14.00.

1,4-didocetyl-3-methyl-1,2,3-triazol-5-ylidene borane (**11-BH₃**)

Inspired by the literature.¹¹



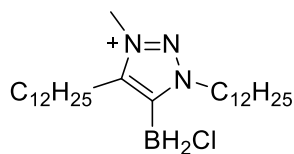
In oven dried glassware and under inert atmosphere, **11H-I** (1.8g, 3.3 mmol) was dissolved in THF (33mL). KHMDS (1M in THF, 3.5mL, 3.5 mmol) was added dropwise at -78°C. After 1h of stirring at -78°C, BH₃.THF (1M in THF, 3.3 mL, 3.3 mmol) was added dropwise. The solution was kept in the cold bath for 30 minutes before being stirred at room temperature overnight. The solvent was evaporated under reduced pressure. Silica gel chromatography (eluent: pentane/ DCM 1/1) afforded the title product as a white powder (700 mg, 49%).

¹H NMR (300 MHz, CDCl₃) δ 4.40 (t, 2H), 3.97 (s, 3H), 2.79 (t, 2H), 1.91 (m, 2H), 1.26 (m, 36H), 0.89 (t, 6H).

¹³C NMR (75 MHz, CDCl₃) δ 143.39, 51.05, 35.83, 32.06, 29.77, 29.69, 29.67, 29.58, 29.54, 29.49, 29.43, 29.21, 28.52, 26.61, 24.23, 22.83, 14.26.

¹¹B NMR (96 MHz, CDCl₃) δ -36.8 (q).

1,4-didocetyl-3-methyl-1,2,3-triazol-5-ylidene chloroborane (**11-BH₂Cl**)



General procedure 4 was applied to **11-BH₃** (43mg, 0.1 mmol). NMR indicated a full conversion with 2 products: triazolium **11H-Cl** and the title product.

¹H NMR (400 MHz, Tol-d₈) δ 9.41* (s, 1H), 4.78* (t, 2H), 4.55 (s, 0.5H), 4.47 (m, 1H), 3.90* (s, 3H), 2.86* (t, 2H), 2.80 (s, 1H), 2.50 (t, 1H), 1.98* (m, 2H), 1.76* (m, 2H), 1.39 (m, 52H), 0.99 (m, 8H).

¹¹B NMR (128 MHz, Tol-d₈) δ -18.4 (bs)

*peaks attributed to **11H-Cl**

Gold nanoparticles synthesis

Chapter II

- Synthesis from (benz)imidazolium haloaurate, NaH and NaBH₄

The (benz)imidazolium haloaurate (1eq) and the corresponding (benz)imidazolium bromide salt (0 to 4 eq) were dissolved in toluene (~10mL, [Au] = 5mM). A solution of NaH (60% oil, 1.5 eq/(benz)imidazolium) in toluene (5mL) was added dropwise at 0°C, causing discoloration of the initially orange solution. The mixture was stirred for 10-15 min before adding NaBH₄ (~10 eq.) freshly dissolved in water (3 mL). The solution turned red almost immediately indicating the formation of gold nanoparticles. After 10 min of stirring, the mixture was rinsed with ~25 mL of water to remove any remaining salts. The nanoparticles, dispersed in the organic layer, were precipitated with ~50 mL of ethanol and centrifuged (10 000 RPM for 30 min). Two more redispersion/precipitation cycles, with 3 mL of toluene and 50 mL of ethanol, were achieved before dispersing the nanoparticles in a small amount of toluene for storage, in order to ensure optimal redispersibility.

- Synthesis from (benz)imidazolium haloaurate and NaBH₄

The same protocol was applied except no NaH was added.

- Synthesis from (benz)imidazolium haloaurate and tBuNH₂BH₃

The (benz)imidazolium haloaurate (1eq) and the corresponding (benz)imidazolium bromide salt (0 to 6 eq) were dissolved in toluene (~10mL, [Au] = 5mM). tBuNH₂BH₃ (~10 eq.) was separately dissolved in toluene (5 mL) and both solutions thermalized for 5 min. tBuNH₂BH₃ was added leading to a gradual discoloration of the solution before a sharp change of color to dark red. The mixture was stirred for 10 min, before precipitating the Au nanoparticles in ethanol and resuspension in toluene for TEM analyses.

- Synthesis from AuCl, (benz)imidazolium salt and NaBH₄

AuCl (1eq) and (benz)imidazolium bromide were dissolved in toluene (~10mL, [Au] = 5mM), forming an orange solution. After approx. 10 min, a fresh aqueous solution of NaBH₄ (~10 eq.) was added, instantly producing a deep red solution, and allowed to react for another 15 min. Precipitation of the gold nanoparticles was carried out as for the previous syntheses.

- Synthesis from AuCl, (benz)imidazolium salt, NaH and NaBH₄

AuCl (1eq) and (benz)imidazolium bromide were dissolved in toluene (~10mL, [Au] = 5mM), forming an orange solution. After approx. 10 min, a solution of NaH (60% oil, 1.5 eq/(benz)imidazolium) in toluene (5mL) was added dropwise, causing a discoloration of the solution. After 10 further min, a fresh aqueous solution of NaBH₄ (~10 eq.) was added, instantly producing a deep red solution, and allowed to react for another 15 min. Precipitation of the gold nanoparticles was carried out as for the previous syntheses.

- Synthesis from AuClSMe₂, (benz)imidazolium salt and NaBH₄

The protocol as for AuCl was applied

- Synthesis from HAuCl₄.3H₂O, (benz)imidazolium bromide and NaBH₄

The protocol as for AuCl was applied.

Chapter III

- Synthesis from AuClPPh₃ and NHC-BH₃

AuClPPh₃ (1eq) and NHC-BH₃ (5eq) were dissolved separately in the desired solvent (~2.5mL each, [Au]=5mM). The NHC-BH₃ solution was then injected into the gold precursor solution.

- Synthesis from HAuCl₄.3H₂O and NHC-BH₃ in chloroform

HAuCl₄.3H₂O and NHC-BH₃ were dissolved separately in chloroform to obtain solutions of 1mM and 4mM respectively. 2mL of the NHC-BH₃ solution were injected into an equal volume the gold precursor solution, leading to a darkening of the solution (to black, purple or red) indicating a reduction of the gold precursor.

- Synthesis from HAuCl₄.3H₂O and NHC-BH₃ in toluene

HAuCl₄.3H₂O was dissolved in CHCl₃ to obtain a concentration of ~10 mM. This solution was then diluted in toluene to reach a 1mM concentration. NHC-BH₃ was dissolved in toluene to obtain the desired concentration (from 1 to 20 mM). 2mL of the NHC-BH₃ solution were injected into an equal volume the gold precursor solution, leading to a darkening of the solution (to black, purple or red) indicating a reduction of the gold precursor.

- Synthesis from AuClSMe₂ and NHC-BH₃ in toluene

AuClSMe₂ was dissolved in toluene to obtain a concentration of 1mM. NHC-BH₃ was dissolved in toluene to obtain the desired concentration (from 1 to 28 mM). 2mL of the NHC-BH₃ solution were injected into an equal volume the gold precursor solution, leading to a darkening of the solution (to black, purple or red) indicating a reduction of the gold precursor. TEM and UV samples were taken from the crude before precipitation of the nanoparticles with a large amount of ethanol (~25mL) and centrifugation at 10 000 rpm for 30 min. Two more redispersion/precipitation cycles were carried out before dispersing the nanoparticles in a small amount of toluene for storage, in order to ensure optimal redispersibility.

- Synthesis from AuClSMe₂ and NHC-BH₃ in water-saturated toluene

Prior to reaction, distilled toluene was stirred with water for 2h in air. The stirring was stopped and the organic phase was separated and used as solvent following the same protocol as described above.

Chapter IV

- Synthesis from AuCl, triazolium salt and NaBH₄

The same synthesis as for (benz)imidazolium was applied.

- Synthesis from AuCl, triazolium salt, NaH and NaBH₄

The same synthesis as for (benz)imidazolium was applied.

- Synthesis from HAuCl₄.3H₂O, triazolium salt and NaBH₄

The protocol as for AuCl was applied.

- Synthesis from AuClSMe₂ and MIC-BH₃ in toluene

The protocol as for NHC-BH₃ was applied.

- Synthesis from HAuCl₄.3H₂O and MIC-BH₃ in toluene

The protocol as for NHC-BH₃ was applied.

References

- (1) Fulmer, G. R.; Miller, A. J. M.; Sherden, N. H.; Gottlieb, H. E.; Nudelman, A.; Stoltz, B. M.; Bercaw, J. E.; Goldberg, K. I. NMR Chemical Shifts of Trace Impurities: Common Laboratory Solvents, Organics, and Gases in Deuterated Solvents Relevant to the Organometallic Chemist. *Organometallics* **2010**, *29* (9), 2176–2179.
- (2) Dzyuba, S. V.; Bartsch, R. A. New Room-Temperature Ionic Liquids with C₂-Symmetrical Imidazolium Cations. *Chem. Commun.* **2001**, No. 16, 1466–1467.
- (3) Gobbo, P.; Workentin, M. S. Improved Methodology for the Preparation of Water-Soluble Maleimide-Functionalized Small Gold Nanoparticles. *Langmuir* **2012**, *28* (33), 12357–12363.
- (4) Narouz, M. R.; Li, C.-H.; Nazemi, A.; Crudden, C. M. Amphiphilic N-Heterocyclic Carbene-Stabilized Gold Nanoparticles and Their Self-Assembly in Polar Solvents. *Langmuir* **2017**, *33* (50), 14211–14219.
- (5) Schena, A.; Johnsson, K. Sensing Acetylcholine and Anticholinesterase Compounds. *Angew. Chem. Int. Ed.* **2014**, *53* (5), 1302–1305.
- (6) Lara, P.; Rivada-Wheelaghan, O.; Conejero, S.; Poteau, R.; Philippot, K.; Chaudret, B. Ruthenium Nanoparticles Stabilized by N-Heterocyclic Carbenes: Ligand Location and Influence on Reactivity. *Angew. Chem. Int. Ed.* **2011**, *50* (50), 12080–12084.
- (7) Walton, J. C.; Brahmi, M. M.; Fensterbank, L.; Lacôte, E.; Malacria, M.; Chu, Q.; Ueng, S.-H.; Solovyev, A.; Curran, D. P. EPR Studies of the Generation, Structure, and Reactivity of N-Heterocyclic Carbene Borane Radicals. *J. Am. Chem. Soc.* **2010**, *132* (7), 2350–2358.
- (8) Curran, D. P.; Boussonnière, A.; Geib, S. J.; Lacôte, E. The Parent Borylene: Betwixt and Between. *Angew. Chem. Int. Ed.* **2012**, *51* (7), 1602–1605.
- (9) Ueng, S.-H.; Solovyev, A.; Yuan, X.; Geib, S. J.; Fensterbank, L.; Lacôte, E.; Malacria, M.; Newcomb, M.; Walton, J. C.; Curran, D. P. N-Heterocyclic Carbene Boryl Radicals: A New Class of Boron-Centered Radical. *J. Am. Chem. Soc.* **2009**, *131* (31), 11256–11262.
- (10) Creary, X.; Anderson, A.; Brophy, C.; Crowell, F.; Funk, Z. Method for Assigning Structure of 1,2,3-Triazoles. *J. Org. Chem.* **2012**, *77* (19), 8756–8761.
- (11) Crudden, C. M.; Eisenberger, P.; de Oliveira Freitas, L. B. Mesoionic Carbene–Boranes. *Organometallics* **2013**, *32* (22), 6635–6638.

Abstract - New syntheses of N-heterocyclic carbene-stabilized gold nanoparticles

Over the past decade, N-heterocyclic carbenes (NHC) have drawn considerable interest in the field of materials chemistry. Indeed, this relatively new class of ligands forms strong bonds with a wide range of metals and their structures and electronic properties can be tuned "at-will" through organic synthesis. This strong bond is of particular interest for gold nanoparticles. Indeed, gold nanoparticles have many potential applications, for example in sensors, catalysis or medicine, but those potential applications are sometimes hindered by a lack of stability of the surface ligand. A few syntheses of NHC-stabilized gold nanoparticles have already been described in the literature but each presents their own set of drawbacks. This thesis work has focused on the development of new syntheses of NHC-stabilized gold nanoparticles. First, by revisiting a literature procedure starting from imidazolium salts, we managed to develop a one-pot synthesis starting only from commercially available AuCl, NaBH₄ and easily synthesized imidazolium salts. A totally new synthesis was developed using NHC-boranes, which are stable Lewis adducts. Here, we reported for the first time their use as a 2-in-1 reagent, able to reduce the metallic precursor and provide the nanoparticles stabilizing ligands. Finally, we are the first to report a synthesis of gold nanoparticles stabilized by mesoionic carbenes (MIC). MICs are a sub-class of NHCs synthesized by well-known "click-chemistry", which present unique electronic properties. Throughout this work, special care was taken to characterize the nanoparticles, notably by XPS.

Keywords: Gold nanoparticles, synthesis, N-heterocyclic carbene, N-heterocyclic carbene-borane, mesoionic carbene, X-ray photoelectron spectroscopy.

Résumé - Nouvelles synthèses de nanoparticules d'or stabilisées par des carbènes N-hétérocycliques

Durant la dernière décennie, les carbènes N-hétérocycliques ont suscité un intérêt important dans le domaine de la chimie des matériaux. En effet, cette catégorie relativement récente de ligands forme des liaisons très fortes avec une diversité de métaux et leur structure, ainsi que leurs propriétés électroniques, peuvent être adaptées "à volonté" par le biais de la synthèse organique. Cette forte liaison est d'un intérêt particulier dans le domaine des nanoparticules d'or. En effet, celles-ci présentent de nombreuses applications potentielles, par exemple dans les capteurs, en catalyse ou médecine, mais ces applications sont parfois freinées par un manque de stabilité du ligand de surface. Quelques synthèses de nanoparticules d'or stabilisées par des NHCs ont déjà été décrites dans la littérature mais chacune présente quelques inconvénients. Ce travail de thèse s'est concentré sur le développement de nouvelles synthèses de nanoparticules d'or stabilisées par des NHC. D'abord, en revisitant une procédure existante à base de sels d'imidazoliums, ce qui a mené à une synthèse n'utilisant que les composés commerciaux : AuCl et NaBH₄ et des halogénures d'imidazolium, qui sont facilement obtenus. Une synthèse totalement nouvelle a ensuite été développée en utilisant des NHC-boranes qui sont des adduits de Lewis stables. Nous avons montré pour la première fois que les NHC-boranes peuvent être utilisés comme réactifs "2-en-1" dans la synthèse de nanoparticules d'or : comme réducteurs du précurseur d'or et comme source de NHC. Enfin, nous sommes les premiers à décrire la synthèse de nanoparticules d'or stabilisées par des carbènes mésoionique (MIC). Les MICs sont une sous-catégorie des NHCs qui sont préparés par « chimie click » et qui présentent des propriétés électroniques uniques. Tout au long de ce travail un intérêt particulier a été porté à la caractérisation des nanoparticules, notamment par XPS.

Mots clés : Nanoparticules d'or, synthèse, carbène N-hétérocyclique, carbène N-hétérocyclique borane, carbène mésoionique, spectrométrie photoélectronique X.